CANCER CELL-SPECIFIC INDUCTION OF ENDOPLASMIC RETICULUM STRESS BY SMALL MOLECULES FOUND IN THE SERUM

DOCTORAL (Ph.D.) THESIS

Dalma Scheffer

Supervisors: Tamás Czömpöly M.D., Ph.D. and Zoltán Rékási M.D., Ph.D.

Head of Doctoral School: Júlia Szekeres, M.D., Ph.D., D.Sc.

Program leader: Dóra Reglődi M.D., Ph.D., D.Sc.

Department of Anatomy

Medical School, University of Pécs

2020

CONTENTS

1. LIST OF ABBREVIATIONS

2-ME	2-mercaptoethanol
3-MA	3-methyladeine
4-PBA	4-phenylbutyrate
4T1	mouse mammary carcinoma
7-AAD	7-aminoactinomycin D
A549	human lung adenocarcinoma
AIF	apoptosis-inducing factor
AM	active mixture
ANOVA	analysis of variance
APAF1	apoptotic peptidase activating factor 1
ARHGEF25	Rho guanine nucleotide exchange factor 25
ATCC	American Type Culture Collection
ATF3	activating transcription factor 3
ATF4	activating transcription factor 4
ATF6	activating transcription factor 6
ATG	autophagy related
BAF	Bafilomycin A1
Bcl-2	B-cell lymphoma 2
BiP	binding immunoglobulin protein
BIRC2/BIRC3	baculoviral IAP repeat containing 2 and 3
BSA	bovine serum albumin
bZIP	basic leucine zipper protein
Caco-2	human colorectal adenocarcinoma
CAD	caspase-activated DNase
c-FLIP	cellular FLICE (FADD-like IL-1β-converting enzyme)-inhibitory protein
CHAC1	glutathione-specific gamma-glutamylcyclotransferase 1
CHLQ	chloroquine
CHOP	C/EBP homologous protein
CI	combination index
cIAP1/cIAP2	cellular inhibitor of apoptosis protein 1 and 2
CM	control mixture

CSA	cyclosporine A
CTRL	control
DDIT3	DNA damage inducible transcript 3
DFO	deferoxamine
DISC	death inducing signaling complex
DR4/DR5	death receptor 4 and 5
ECACC	European Collection of Authenticated Cell Cultures
EdU	5-ethynyl-2'-deoxyuridine
eIF2α	eukaryotic translation initiation factor 2 subunit alpha
ER	endoplasmic reticulum
ERAD	ER-associated degradation
ERSE	ER stress response element
FADD	Fas-associated death domain
FasR	Fas receptor
FBS	Fetal Bovine Serum
FCS	Fetal Calf Serum
FDA	Food and Drug Administration
FDRq	false discovery rate q-value
Fer-1	ferrostatin-1
GCN2	general control nonderepressible 2
GDF15	growth differentiation factor 15
GPX4	glutathione peroxidase 4
GRP78	78-kDa glucose regulated protein
GSEA	Gene Set Enrichment Analysis
GSG1	germ cell associated 1
GSH	glutathione
HDACs	histone deacetylases
hEGF	human Epidermal Growth Factor
HeLa	human cervix adenocarcinoma
HepG2	human hepatocellular carcinoma
HRE	primary human renal epithelial cells
HSPA5	heat shock protein family A, member 5
HT-29	human colorectal adenocarcinoma

IAP	inhibitor of apoptosis protein
IRE1α	inositol-requiring enzyme 1 alpha
ISR	integrated stress response
ISRIB	integrated stress response inhibitor
JDP2	Jun dimerization protein 2
LAT1	L-type amino acid transporter 1
LC3	microtubule-associated protein 1 light chain 3
LUBAC	linear ubiquitin chain assembly complex
MAPK	mitogen-activated protein kinase
MCF-7	human breast adenocarcinoma
MEK	mitogen-activated protein kinase kinase
MEM	Minimum Essential Medium
miRNA	microRNA
MLKL	mixed lineage kinase domain like pseudokinase
mTORC1	mammalian target of rapamycin complex 1
Nec-1	necrostatin-1
NES	normalized enrichment score
NFDM	non-fat dry milk
NF-κB	nuclear factor kappa-light-chain-enhancer of activated B cells
NM	new mixture
NSA	necrosulfonamide
PBS	phosphate buffered saline
PC-3	human prostate adenocarcinoma
PCDH7	protocadherin 7
PERK	protein kinase R (PKR)-like endoplasmic reticulum kinase
PET	Positron Emission Tomograpy
PI3KC3	class III phosphatidylinositol 3-kinase
PI3KC3-C1	class III phosphatidylinositol 3-kinase complex I
PKR	protein kinase R
PPP1R15A	protein phosphatase 1 regulatory subunit 15A
qRT-PCR	quantitative real time polymerase chain reaction
RIDD	regulated IRE1-dependent decay
RIPK1/RIPK3	receptor-interacting protein kinases 1 and 3

ROS	reactive oxygen species
RSL	RAS-selective lethal
SAL	salubrinal
SF3B2	splicing factor 3b subunit 2
siRNA	small interfering RNA
SMAC	second mitochondrial activator of caspases
TBS	Tris-buffered saline
TM	tunicamycin
TNF	tumor necrosis factor
TNFR1	tumor necrosis factor receptor 1
TNFRSF10A/TNFRSF10B	tumor necrosis factor receptor superfamily member 10A and 10B
TRADD	TNFR-associated death domain protein
TRAF2/TRAF5	TNFR-associated factor-2 and 5
TRAIL-R1/TRAIL-R2	TNF-related apoptosis-inducing ligand-receptor 1 and 2
TUBB	tubulin
TUNEL	terminal deoxynucleotidyl transferase-dUTP nick end labeling
ULK1/ULK2	unc-51-like kinase 1 and 2
UPR	unfolded protein response
UVRAG	ultraviolet irradiation resistance-associated gene protein
VPS34	vacuolar sorting protein 34
XBP1	X-box binding protein 1

2. SUMMARY

The main goal of this Ph.D. project was to identify the mechanism for apoptosis induction elicited by a mixture containing amino acids, monosaccharides, nucleobases, and other small molecules.

We demonstrated that a defined mixture of small molecules (active mixture [AM]) selectively induces endoplasmic reticulum stress and activates the unfolded protein response (UPR) signaling cascade in cancer cells, which leads to the activation of a pro-apoptotic transcription program.

We have revealed a novel miRNA mediated feedback mechanism of the transcriptional upregulation of certain UPR signaling components.

In addition, we have identified several new molecules found in the serum capable of enhancing the effect of the AM which have substantial cancer cell growth inhibitory effect when applied in a mixture.

3. INTRODUCTION

Through our work we have focused on small molecular weight compounds (amino acids, monosaccharides, nucleobases, etc.) which are present in the serum and many of which are differentially taken up by tumor and normal cells (Flodh and Ullberg 1968; Blomquist et al. 1969; Ong et al. 2010). In our earlier studies we have experimentally selected some molecules present in the serum whose mixture (AM) produced a selective *in vitro* and *in vivo* toxic effect on various tumor cell lines, but not on normal cells (Kulcsár 1995; Kulcsár 2000). The AM is composed of certain essential amino acids, vitamins, nucleobases and metabolic intermediates: L-arginine, L-histidine, L-methionine, L-phenylalanine, L-tryptophan, L-tyrosine, L-ascorbic acid, D-biotin, pyridoxine, (−)-riboflavin, adenine, 2-deoxy-D-ribose, hippuric acid, L-(−)-malic acid, D-(+)-mannose, and orotic acid. We have demonstrated that the AM selectively induces apoptosis of cancer cells *in vitro* (Kulcsár 1997; Kulcsár 2003). Furthermore, we have provided evidence that the treatment with AM has a significant tumor inhibitory effect *in vivo* (Kulcsár et al. 2013). In addition to our results Bonfili et al. reported that mixtures of essential amino acids also induce apoptosis in a cancer specific manner and showed that proteasome inhibition and induction of autophagy plays a role in this process (Bonfili et al. 2017). Our earlier mechanistic studies of the AM identified the mitochondrial pathway of apoptosis induction, which was accompanied by the upregulation of genes contributing to apoptosis

induction and cell cycle arrest (PMAIP1, BBC3, CDKN1A) (Kulcsár et al. 2013), however the signaling events leading to the initiation of apoptosis were not known.

4. LITERATURE OVERVIEW

4.1. Cancer metabolism

In 2000, Hanahan and Weinberg have described six essential features of most human cancers, the so-called hallmarks of cancer, acquired during tumor development and collectively dictate malignant growth. These are self-sufficiency in growth signals, insensitivity to anti-growth signals, evading apoptosis, limitless replicative potential, sustained angiogenesis, and tissue invasion and metastasis (Hanahan and Weinberg 2000). Later two other hallmarks of cancer were revealed, reprogramming of energy metabolism and evading immune destruction (Hanahan and Weinberg 2011).

Cancer cells reprogram their metabolism and energy production networks to support survival in inappropriate conditions, proliferation, invasion, metastasis, and resistance to cancer treatments (Phan et al. 2014). A well-known cancer-specific reprogrammed metabolic pathway is aerobic glycolysis, the so-called Warburg effect. Otto Warburg reported that cancer cells consume high amount of glucose and convert glucose into lactate, even in the presence of oxygen, and this is a striking metabolic difference between tumor and most normal tissues (Vander Heiden et al. 2009). Beside glucose, glutamine is the other most rapidly consumed nutrient by cancer cell lines, moreover, changes in metabolism of fatty acids, nucleotides, and several other amino acids, among others, have been revealed (Pavlova and Thompson 2016). L-type amino acid transporter 1 (LAT1) transports neutral amino acids such as leucine, isoleucine, valine, phenylalanine, tyrosine, tryptophan, methionine, histidine and was found highly expressed in several human cancer tissues. In addition, glutamine also has been reported to facilitate the uptake of a broad range of essential amino acids through LAT1 (Zhao et al. 2015). The accumulation of these substances by cancer cells has been exploited in Positron Emission Tomograpy (PET) imaging, for monitoring tumors (Zhu et al. 2011).

These cancer-associated changes in metabolism can also alter the levels of intracellular metabolites, that can influence the phenotypes of cancer. In addition, several oncogenic mutations lead to the accumulation of certain metabolites with oncogenic potentials (Sullivan et al. 2016). For example, high level of fumarate and succinate, caused by the loss of fumarate hydratase and succinate dehydrogenase, can positively affect tumorigenesis by competitive inhibition of the of α-ketoglutarate-dependent dioxygenases that have a role in epigenetic

regulation (Xiao et al. 2012). Changes in metabolite levels could have different consequences, some of them may inhibit cancer growth or others are required for tumorigenesis. These altered metabolic pathways in cancer have become a very attractive target for cancer therapeutics, and better understanding how altered metabolism affect tumorigenesis will help to identify novel therapeutic approaches (Sullivan et al. 2016).

4.2. Cell death

Cell death was initially divided into three types based on morphological characteristics: apoptosis (type I), autophagic cell death (type II) and necrosis (type III) (Yan et al. 2020). Apoptosis and autophagy are programmed cell death types, while necrosis is considered as unprogrammed. Apoptosis is characterized by series of typical morphological features, including shrinkage of the cell, chromatin condensation, nuclear fragmentation and apoptotic bodies. Autophagy is thought to be a protective pathway, however under certain circumstances, can induce cell death, manifesting with large intracellular vesicles. Necrosis is characterized by a gain in cell volume, swelling of organelles, and loss of membrane integrity (Green and Llambi 2015). In recent years, several novel cell death pathways have been identified and characterized, such as necroptosis, pyroptosis, ferroptosis, entotic cell death, netotic cell death, parthanatos, etc. (Galuzzi et al. 2018).

4.3. Apoptosis

Apoptosis is a programmed and energy-dependent cell death, crucial for normal cell turnover, proper development and functioning of the immune system, among others (Elmore 2007). It is characterized by various morphological changes and biochemical processes, including cell shrinkage, nuclear fragmentation, chromatin condensation, plasma membrane blebbing, finally cell fragmentation into apoptotic bodies which are phagocytosed without an inflammatory reaction (Kerr et al. 1972).

A wide variety of physiological or pathological stimuli can initiate apoptosis mediated by either the mitochondria-dependent (intrinsic) or the death receptor (extrinsic) pathways (Figure 1), both converge on the same execution pathway giving rise to the characteristics morphological and biochemical features of apoptosis (Elmore 2007).

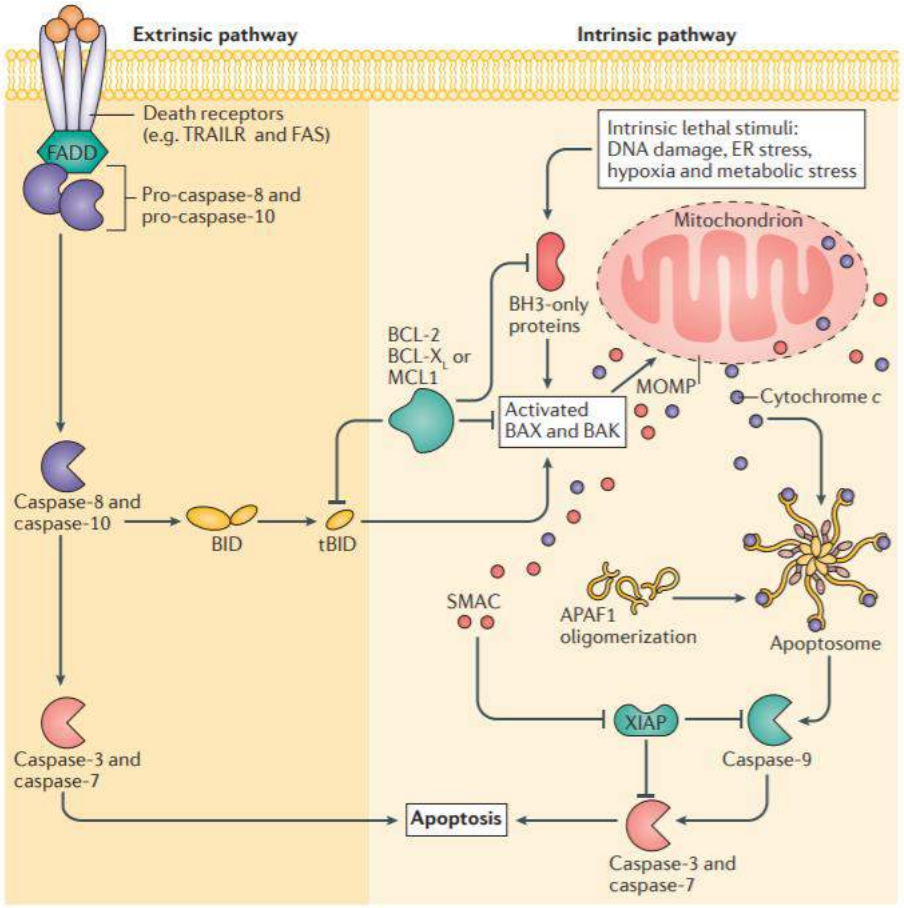

Figure 1. Extrinsic and intrinsic apoptotic signaling pathways (Ichim and Tait 2016).

4.3.1. Intrinsic apoptosis

The intrinsic pathway is activated by a plethora of stimuli, such as growth factor withdrawal, DNA damage, endoplasmic reticulum (ER) stress, reactive oxygen species (ROS) overload, replication stress, etc. (Figure 1) (Galuzzi et al. 2018). The functional consequence of all of these stimuli is the outer mitochondrial membrane permeabilization allowing the release of proapoptotic proteins such as cytochrome c and second mitochondrial activator of caspases (SMAC) into the cytoplasm (Orennius 2004; Galuzzi et al. 2019). The cytochrome c binds to apoptotic peptidase activating factor 1 (APAF1) and pro-caspase-9 to from a multisubunit protease activation complex called the apoptosome (Hill et al. 2003). This complex activates pro-caspase-9 to become caspase-9, which then cleaves and activates downstream effector caspases-3, -6 and -7 (Rowinsky 2005). Cytosolic SMAC promotes apoptosis by binding the inhibitor of apoptosis proteins (IAPs) and blocking their caspase inhibitory activity (Du et al. 2000). The mitochondria release other proapoptotic proteins, such as apoptosis-inducing factor (AIF), endonuclease G and caspase-activated DNase (CAD). AIF translocates to the nucleus and causes DNA fragmentation and chromatin condensation. Endonuclease G also translocates

to the nucleus leading to further fragmentation of the DNA (Arnoult et al. 2003). Finally, the caspase-activated DNase (CAD) is activated by caspase-3 which leads to oligonucleosomal DNA degradation and a more pronounced chromatin condensation (Elmore 2007).

The B-cell lymphoma 2 (Bcl-2) protein family tightly controls this intrinsic pathway by regulating the permeability of the outer mitochondrial membrane. These proteins can be classified as anti-apoptotic or pro-apoptotic, each containing one to four BCL-2 homology (BH) domains. The anti-apoptotic members of Bcl-2 family include Bcl-2, Bcl-w, Bcl-xL, Mcl-1 and A1/BFL-1 and possess four BH domains (Leibowitz and Yu 2010). The pro-apoptotic members can be further divided into multidomain effectors (BAX, BAK, BOK) and BH3-only proteins (BIM, BID, PUMA/BBC3, BAD, NOXA/PMAIP1, HRK, BMF, BIK and others) (Montero and Letai 2018). BAX, BAK and BOK possess three to four BH domains, and have the ability to form pores in the mitochondrial outer membrane promoting permeabilization and subsequent release of pro-apoptotic proteins including cytochorome c (Giam et al. 2008).
The BH3-only proteins can activate BAX/BAK thus inducing pore formation in the mitochondrial outer membrane. They bind and inhibit the pro-survival Bcl-2 proteins and/or directly interact and activate BAX/BAK proteins (Jeng et al. 2018).

4.3.2. Extrinsic apoptosis

The extrinsic pathway is triggered by perturbations of the extracellular microenvironment and mediated by the binding of ligands to the transmembrane death receptors (Figure 1) (Galuzzi et al. 2018). The death receptors belong to the tumor necrosis factor (TNF) receptor superfamily, such as Fas receptors (FasR), tumor necrosis factor receptor 1 (TNFR1), TNF-related apoptosis-inducing ligand-receptor 1 (TRAIL-R1, also known as death receptor 4 (DR4) or tumor necrosis factor receptor superfamily member 10A (TNFRSF10A)) and TRAIL-R2 (also known as DR5 or TNFRSF10B) (Elord and Sun 2008). These receptors are characterized by a cysteine-rich extracellular domain and a cytoplasmic domain called the death domain, which is essential for signal transduction (Elmore 2007). The ligand binding their cognate receptors: TNFα to TNFR1, Fas ligand (FasL) to FasR, TRAIL to TRAIL-R1 and TRAIL-R2, causes the recruitment of adaptor proteins such as the Fas-associated death domain (FADD). The death domains of these adaptor proteins recruit initiator procaspases (such as caspase-8 and caspase-10) forming together the death inducing signaling complex (DISC), which then activates downstream effector caspases (Rowinsky 2005). Activated caspase 8 and caspase 10 can cleave the BH3 only protein Bid which in turn translocates to the mitochondrial membrane

where it initiates the intrinsic pathway, establishing connection between the two apoptotic pathways (Walczak 2013).

The cellular FLICE (FADD-like IL-1β-converting enzyme)-inhibitory protein, called c-FLIP, can inhibit the death receptor mediated apoptosis by binding to FADD and/or caspase 8 or caspase 10 and DR5 (Safa 2012).

4.3.3. Apoptosis and cancer

A characteristic feature of human cancer is the ability to evade apoptosis. Alteration in apoptotic machinery contributes to both tumorigenesis and tumor resistance to therapies (Fulda 2010). There are variety of molecular mechanisms by which cancer cells try to escape apoptosis, including impaired death receptor signaling, disrupted balance of proapoptotic and anti-apoptotic proteins, reduced caspase function and impaired p53 function (Pistritto et al. 2016).
Several abnormalities in death receptor signaling can be found in human cancers. For instance, a decreased expression of Fas receptor has been described in treatment-resistant leukemia or neuroblastoma cells (Friesen et al. 1997; Fulda 1998). In addition, resistance to TRAIL-induced apoptosis has been reported in colon carcinoma because of the abnormal transport of TRAIL receptors to the cell surface (Jin et al. 2004). Absent or reduced expression of caspase-8 was revealed in different cancer including neuroblastoma, medulloblastoma, and small cell lung cancer (Pistritto et al. 2016).

Disruption of the tightly regulated balance of the anti- and pro-apoptotic members of Bcl-2 family can facilitate tumor development and resistance to therapy (Campbell and Tait 2018). Overexpression of anti-apoptotic Bcl-2 or Bcl-xL has been reported in various human cancers (Straten and Andersen 2010; Maji et al. 2018), and defective expression of pro-apoptotic proteins also occur in cancer (Yip and Reed 2008; Liu et al. 2016).
The p53 is one of the most studied tumor suppressor protein, and its coding gene is mutated in over 50% of human cancers (Muller and Vousden 2014; Liu et al. 2019). It acts as a transcription factor, activated in response to various cellular stresses such as DNA damage, and regulates the expression of genes involved in several biological processes, including apoptosis, cell cycle arrest and senescence (Liu et al. 2019). p53-mediated cell cycle arrest allows cells to repair DNA damage, while upon serious DNA damage, induces apoptosis mainly by the direct transcriptional activation of the pro-apoptotic BH3-only proteins PUMA and NOXA (Ozaki and Nakagawara 2011; Aubrey et al. 2018). Thus, p53 has a critical function in maintaining the

genomic integrity and prevents accumulation of genomic alterations that cause cancer (Toufektchan and Toledo 2018).

4.4. Autophagy

The autophagy literally means “self-eating”, it is a highly conserved, regulated and catabolic process (Yorimitsu and Klionsky 2005; Dikic and Elazar 2018). In this process, double-membrane vesicles, called autophagosomes, are formed to engulf misfolded or long-lived proteins, damaged intracellular organelles as well as invading microorganisms and delivers those cytoplasmic contents to lysosomes for degradation (Yang and Klionsky 2010). Under physiological conditions, autophagy occurs at basal levels, where it maintains cellular homeostasis via degradation and recycling of the resulting macromolecules. Autophagy is induced in response to cellular stress including energy or nutrient starvation and growth factor withdrawal. Under these conditions, autophagy provides metabolic building blocks to survive cellular deficiency. Thus, it is generally a cytoprotective response, however in certain circumstances, autophagy can lead to cell death and the molecular mechanisms and physiological roles of autophagy-dependent cell death are not well understood (Bialik et al. 2018; Denton and Kumar 2019).

Autophagy starts with the formation or nucleation of a double-membrane structure, called phagophore, which expands and starts to engulf the targeted intracellular components. As the phagophore closes around the sequestered components, the autophagosome is formed. The autophagosome will fuse with the lysosome, forming the so-called autolysosome, which leads to the degradation of engulfed contents by lysosomal acid proteases (Figure 2) (Glick 2010). The series of steps of autophagosome formation in mammalian cells are regulated by several protein complexes, including the unc-51-like kinase 1 or 2 (ULK1 or ULK2) complex; the class III phosphatidylinositol 3-kinase (PI3KC3) complex; autophagy related (ATG) protein complex - the ATG12–ATG5–ATG16L1 (ATG16 like 1) conjugation complex; and microtubule-associated protein 1 light chain 3 (LC3) conjugation with phosphatidylethanolamine to form LC3-II (Parzych and Klionsky 2014). The induction of autophagy is mediated by the ULK1/2 complex, which consists of the ULK1/2, ATG13, FIP200 (focal adhesion kinase family interacting protein of 200 kDa), and ATG101 (Zachari and Ganley 2017). Under nutrient rich environment, mammalian target of rapamycin complex 1 (mTORC1) inhibits ULK1/2 complex thereby preventing autophagy initiation (Jung et al. 2010).

Two types of mammalian PI3KC3 complex have been identified and are involved in distinct stages of autophagy. The complex I (PI3KC3-C1) contains PI3KC3 also known as vacuolar sorting protein 34 (VPS34), Beclin-1, P150 and ATG14L (ATG14-like), it works in the early phase of autophagy and is essential for autophagosome formation. The complex II (PI3KC3-C2) is differ in the fourth component of PI3KC3-C1, it contains ultraviolet irradiation resistance-associated gene protein (UVRAG) instead of ATG14L and is involved in the autophagolysosomal maturation and in other membrane trafficking processes (Ma et al. 2017; Vega-Rubín-de-Celis 2019). There are two conjugation systems participating in the elongation and expansion of phagophore. The first is the ATG12–ATG5–ATG16L1 conjugation complex, which associates with the phagophore membrane and dissociates from the completed autophagosome (Parzych and Klionsky 2014). The second conjugation step involves the conjugation of LC3-I with phosphatidylethanolamine to form LC3-II, that translocates from the cytosol to the autophagic membrane and is anchored on its surface (Parzych and Klionsky 2014; Ciechanover and Kwon 2015). Then, the newly formed autophagosome fuses with lysosomes to form autolysosomes.

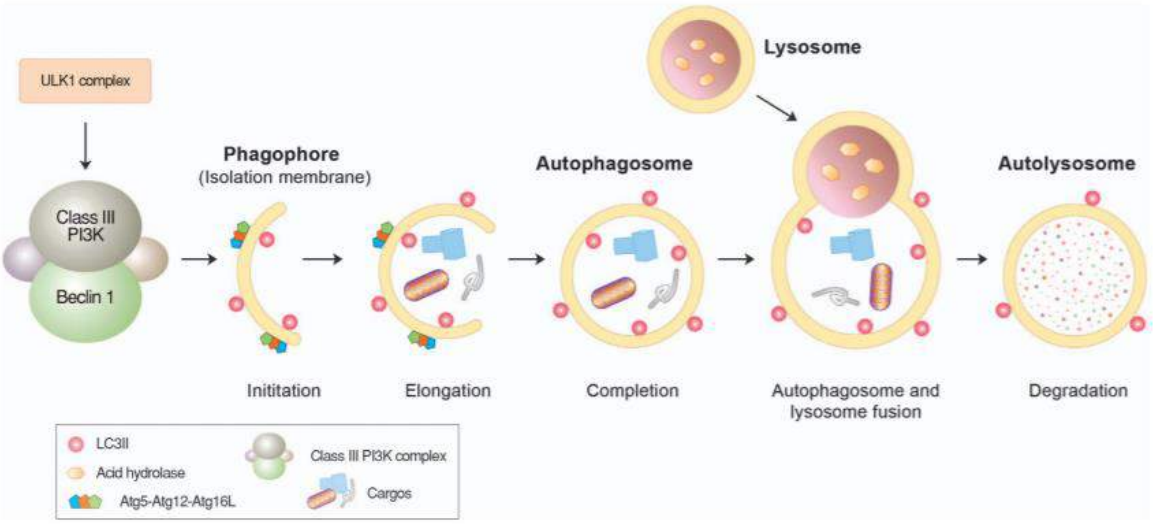

Figure 2. Steps of autolysosome formation (Ciechanover and Kwon 2015)

4.4.1. Autophagy and cancer

Autophagy has complex and paradoxical roles in carcinogenesis, tumor progression and cancer therapy. Autophagy can function as tumor suppressor but can also promote tumor cell survival (Liu and Ryan 2012). Monoallelic deletion of *BECN1* (encoded for Beclin-1) was found in around 50% of breast, ovarian and prostate cancers. Further studies with mice hemizygous for *BECN1* showed that they have an increased prevalence of lymphomas, liver and lung cancers. In addition, decreased level of Beclin-1 was revealed in various cancers, such as ovarian carcinomas, breast cancer and colon cancer (Vega-Rubín-de-Celis 2019). Tumor-associated deletions or mutations have been also reported in several other autophagy regulators. Mutations in *ATG5* and *ATG12* have been found in gastric and colorectal cancer (Kang et al. 2009). Under stress conditions, autophagy clears damaged proteins and organelles, autophagy deficiency causes oxidative stress, accumulation of DNA damage, which could subsequently promote cancer initiation and development. Whereas, autophagy can promote cancer survival and growth under extremely stressful conditions, such as hypoxia and nutrient deprivation. Autophagy is upregulated in several solid tumors, mainly in less-perfused areas. Cancer therapeutics can either upregulate or suppress autophagy, and the upregulation of autophagy can lead to tumor cell death or survival (Liu and Ryan 2012; Yun and Lee 2018). Altogether, the role of autophagy in cancer is likely to be context dependent (White 2012).

4.5. Necroptosis

Necroptosis is a regulated type of necrosis activated by death receptors (such as Fas, TNFR1), interferon receptors, toll-like receptors, and intracellular RNA- or DNA-sensing molecules, when caspase-8 dependent extrinsic apoptotic pathway is blocked/ in a caspase-independent fashion (Pasparakis and Vandenabeele 2015). Necroptosis has similar morphological features of necrosis, including plasma membrane rupture, cell swelling and lysis, which in turn provoke an inflammatory response. At a molecular level, necroptosis is regulated by receptor-interacting protein kinases 1 and 3 (RIPK1 and RIPK3) and mixed-lineage kinase domain–like protein (MLKL) (Choi et al. 2019). The best characterized necroptotic pathway is induced by the TNF-α (Figure 3).

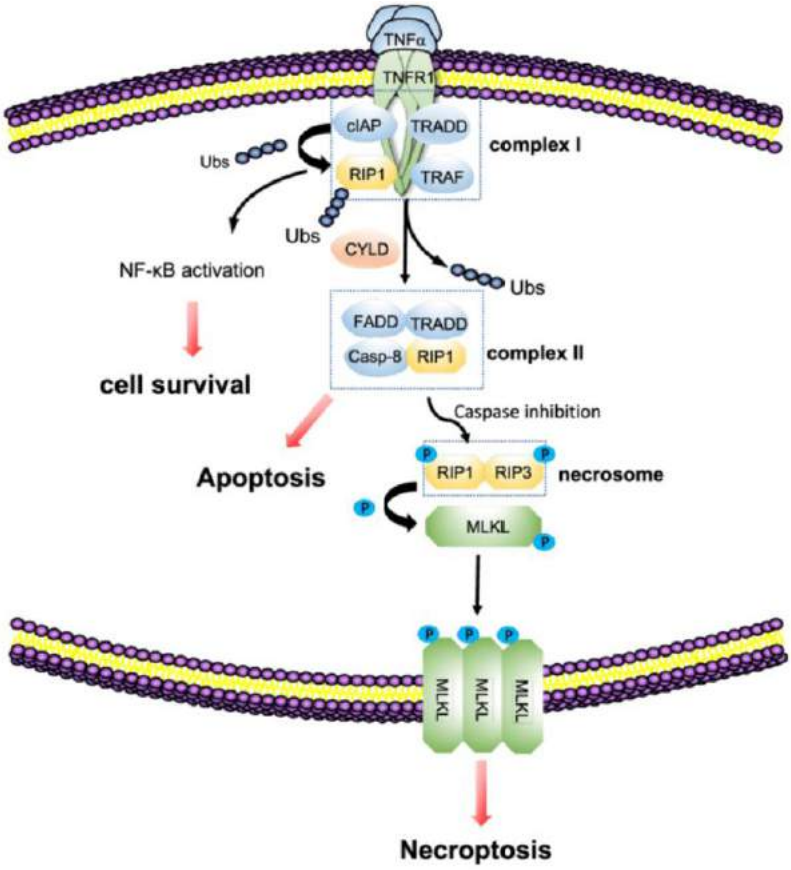

Figure 3. TNF-α induced necroptosis signaling pathway (Gong et al. 2019).

Binding of the TNF-α to TNFR1 leads to the formation of complex I at the cytosolic side of the TNFR1 containing TNFR-associated death domain protein (TRADD), FADD, TNFR-associated factor-2 and 5 (TRAF2/TRAF5), RIPK1, and cellular inhibitor of apoptosis protein 1 and 2 (cIAP1 and cIAP2, also known as baculoviral IAP repeat containing 2 and 3 (BIRC2 and BIRC3)) (Dhuriya and Sharma 2018). From this point, TNFR1 activation can have different cell fate outcomes. RIPK1 controls cell survival and can induce cell death through extrinsic apoptosis and necroptosis, depending on its post-translational modification status. Polyubiquitinated RIPK1 mediated by cIAP1/BIRC2, cIAP2/BIRC3, and linear ubiquitin chain assembly complex (LUBAC) promotes cell survival through nuclear factor kappa-light-chain-enhancer of activated B cells (NF-κB) and mitogen-activated protein kinase (MAPK) signaling pathways (Pasparakis and Vandenabeele 2015; Galluzzi et al. 2018). Deubiquitinated RIPK1 drives extrinsic apoptosis in the presence of caspase-8, however if caspase-8 is non-active, necroptosis is activated (Wegner et al. 2017). In case of necroptosis, RIPK1 and RIPK3 form the protein complex necrosome, in which RIPK1 associates with and phosphorylates RIPK3, which then phosphorylates MLKL. Phosphorylation of MLKL leads to the formation of MLKL

oligomers that translocate to the plasma membrane triggering permeabilization (Huang et al. 2017; Wegner et al. 2017). RIPK1 can be deubiquitinated by cylindromatosis (CYLD) or through inhibition of cIAP1/cIAP2 by SMAC mimetics treatment (Brenner et al. 2015). Chemical inhibitors such as necrostatin-1 (Nec-1) and necrosulfonamide (NSA) can block necroptotic cell death by inhibiting RIPK1 and MLKL, respectively (Degterev 2008; Liao 2014).

4.5.1. Necroptosis and cancer

Deregulation of necroptosis has been implicated in various pathological conditions, like neurodegeneration, cancer and infectious diseases (Fulda 2013; Dhuriya and Sharma 2018). Inducing necroptosis provides a new therapeutic approach in order to eliminate apoptosis-resistant cancer cells (Mezzatesta and Bornhauser 2019). Nevertheless, necroptosis has been reported as a double-edge sword in cancer, its both tumor growth reducing and promoting effects have been shown in different cancers. Necroptosis can trigger inflammatory responses that may protect against tumor progression, however inflammatory cells recruited by necroptosis may promote tumorigenesis and cancer metastasis (Gong et al. 2019).

The level of the key regulatory molecules is often downregulated in cancers, suggesting that cancer cell trying escape necroptotic cell death (Gong et al. 2019). RIPK3 expression is silenced in many cancer cell lines due to genomic methylation contributing to necroptosis resistance (Koo et al. 2015). Furthermore, reduced expression of RIPK3 has also been reported in different samples from cancer patients, such as breast cancer (Koo et al. 2015), colorectal cancer (Feng et al 2015), acute myeloid leukemia (Nugues et al. 2014) and melanoma (Geserick et al. 2015). Low RIPK3 expression was related to poor survival rates in breast and colorectal cancers (Feng et al. 2015; Koo et al. 2015). Similary, RIPK1 expression was found to be downregulated in head and neck squamous cell carcinoma and associated with disease progression (McCormick et al. 2016). Low levels of MLKL was correlated with poor prognosis for gastric (Ertao et al. 2016), ovarian (He et al. 2013) and colon cancers (Li et al. 2017). However, overexpression of the necroptotic factors has also been reported in some tumors. RIPK1 is commonly upregulated in glioblastoma and confers a poorer prognosis. In pancreatic ductal adenocarcinoma, expression of RIPK1, RIPK3 and MLKL was increased, promoting oncogenesis (Seifert et al. 2016).

The specific role of necroptosis in oncogenesis and cancer metastasis may vary depending on the tumor types and needs further investigations.

4.6. Ferroptosis

Ferroptosis is an iron-dependent programmed cell death process characterized by the accumulation of lipid reactive oxygen species (ROS). It has been associated with many diseases such as neurological diseases, cancer, ischemia-reperfusion injury, kidney injury, etc. (Li et al. 2020). The term was first proposed by Dixon in 2012, who described a unique form of non-apoptotic cell death induced by the oncogenic RAS-selective lethal (RSL) small molecules, named erastin and RSL3 (Dixon et al. 2012). It is morphologically, biochemically and genetically different from apoptosis, necrosis and autophagy, or other form of non-apoptotic cell deaths. Morphologically, the mitochondria become smaller with increased membrane density and reduced or absent mitochondrial crista, but the cell membrane remains intact (Dixon et al. 2012; Li et al. 2020).

The iron-dependent accumulation of lipid peroxidation products is considered the main cause of ferroptotic cell death. Hence, iron chelators (e.g. deferoxamine (DFO)) and lipophilic antioxidants (e.g. ferrostatin-1 (Fer-1), Trolox, vitamin E, coenzyme Q10) are potent inhibitors of ferroptosis (Dixon et al. 2014; Stockwell et al. 2017; Feng and Stockwell 2018).

It has been well documented that the cystine/glutamate antiporter (system Xc^- and the glutathione peroxidase 4 (GPX4) are crucial regulators of ferroptosis (Dixon et al. 2014; Yang et al. 2014). Additionally, changes in iron levels have important role in the development of ferroptosis. Free intracellular ferrous iron (Fe^{2+}) can produce lipid peroxides under the action of the Fenton reaction, however the exact role of iron in ferroptosis is still unclear (Yang and Stockwell 2016; Li et al. 2020).

The system Xc^- mediates the exchange of extracellular cystine and intracellular glutamate across the plasma membrane (Bridges et al. 2012). Cystine is reduced to the amino acid cysteine, which serves as a precursor of glutathione (GSH) synthesis. GPX4 converts toxic lipid hydroperoxides to non-toxic lipid alcohols, in the presence of GSH, a key cellular antioxidant and a cofactor of GPX4 (Yang and Stockwell 2016; Yu and Long 2016; Forcina and Dixon 2019). Glutamate, erastin or clinical drugs (e.g. sulfasalazine, sorafenib) were shown to target and inhibit system Xc^-, thereby prevents cystine import leading to GSH depletion and GPX4 inactivation, thus exposing the cells to excessive level of lipid peroxides. RSL3, and other ferroptosis-inducing compounds, referred to as DPI compounds, was reported to directly inhibit GPX4 without GSH depletion (Yang and Stockwell 2016; Feng and Stockwell 2018).

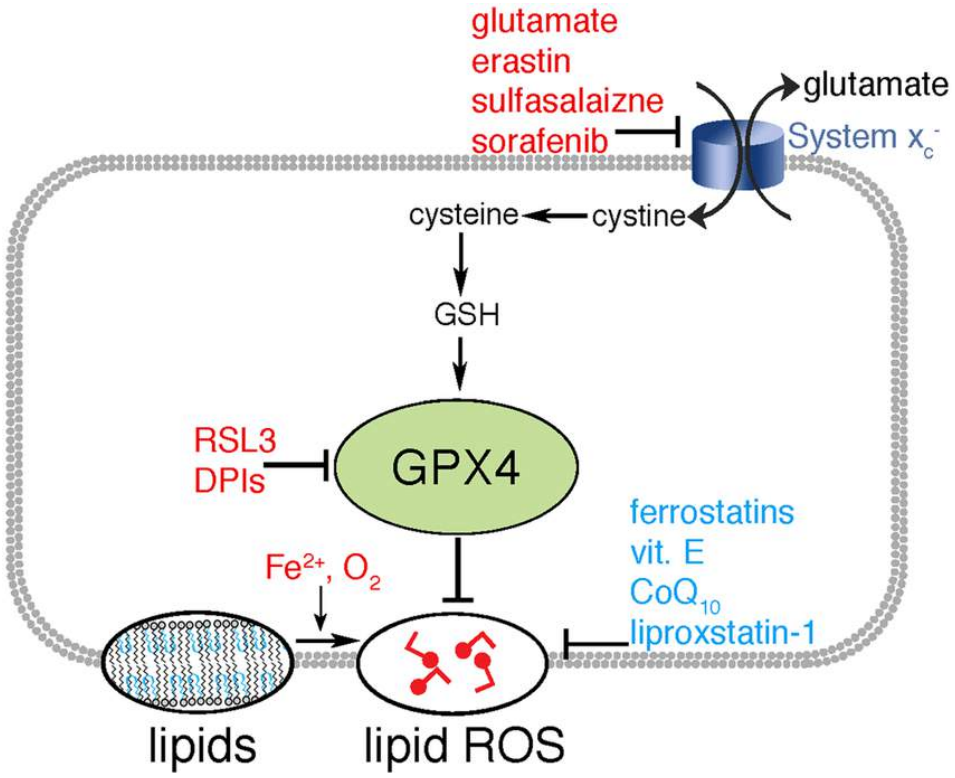

Figure 4. Schematic representation of ferroptosis pathway. Inducers (red) and inhibitors (blue) of ferroptosis (Agmon et al. 2018).

4.6.1. Ferroptosis and cancer

Ferroptosis was discovered in RAS-mutated tumor cells. Several types of cancers bearing RAS mutation are sensitive to ferroptosis induction. However, results have shown that ferroptosis can be induced in some cancer cell types without RAS mutation, thus mutant RAS seems to dispensable for ferroptosis (Xu et al. 2019). The role of ferroptosis in tumorigenesis is poorly understood. Some evidence suggests that it could have a role in tumor suppression in a p53 dependent manner. Acetylation-defective p53 mutants unable to induce apoptosis, cell-cycle arrest, or senescence were shown to promote ferroptosis preventing tumor formation in mice (Jiang et al. 2015). Nevertheless, other studies have shown that wild-type p53 expression may inhibits or delays the timing of ferroptosis in certain cancer cells (Xie et al. 2017; Tarangelo et al. 2018). Despite the roles of ferroptosis in tumor development need to be elucidated, there are several evidences reveal the importance of ferroptosis in cancer therapeutics. For example, erastin, an inducer of ferroptosis, effectively enhanced anticancer activity of cisplatin in cisplatin-resistant non-small cell lung cancer cells (Li et al. 2020). Furthermore, erastin increased the effect of two chemotherapeutic drugs (cytarabine and doxorubicin) in acute myeloid leukemia cells (Yu et al. 2015). In addition, Food and Drug

Administration (FDA) approved drugs (e.g. sorafenib, sulfasalazine and artesunate) have been shown to induce ferroptosis in various cancer cells, highlighting the significance of ferroptosis-based cancer treatment (Lu et al. 2018).

4.7. Endoplasmic reticulum stress and unfolded protein response

The endoplasmic reticulum (ER) is responsible for correct modification, folding and assembly of secretory and membrane-bound proteins prior to transport to the Golgi apparatus. The lumen of the ER is an oxidizing environment allowing formation of disulphide bonds and it contains the highest concentration of calcium within the cells, which are required for proper protein folding and protein chaperone functions (Gaut and Hendershot 1993).

Many disturbances, including alteration in redox state, depletion of ER calcium, perturbations in posttranslational modification or viral infections reduce the protein folding capacity of the ER, which results in the accumulation and aggregation of unfolded proteins leading to the so-called ER stress (Shen et al. 2004).

Under ER stress conditions, the cells activate a pro-survival response to reduce the accumulation of unfolded proteins termed the UPR. The UPR attenuates the translation of mRNAs to decrease the protein influx, induces the expression of genes that are involved in protein folding and degradation, and activates the process of ER-associated protein degradation (ERAD) to remove the unfolded proteins (Schröder and Kaufman 2005).

The UPR is primarily a pro-survival response, however if the ER dysfunction is severe or prolonged and the UPR fails to restore homeostasis, apoptotic cell death ensues. Apoptosis triggered by ER stress has been implicated in the pathogenesis of several human diseases, including diabetes, cancer, atherosclerosis, neurodegenerative and cardiovascular diseases (Xu et al. 2005; Hetz 2012). However, the molecular mechanisms regulating the switch from adaptive to pro-apoptotic responses are not fully understood.

4.7.1. UPR signaling pathways

In mammals, there are three main UPR signaling pathways initiated by ER transmembrane receptors: activating transcription factor-6 (ATF6), inositol-requiring transmembrane kinase/endoribonuclease 1 (IRE1), and double-stranded RNA-dependent protein kinase (PKR)-like eukaryotic initiation factor 2α (eIF2α) kinase (PERK) (Figure 5). In unstressed condition, the ER chaperone GRP78 (78-kDa glucose regulated protein), also referred to as BiP (Binding immunoglobulin protein) or HSPA5 (heat shock protein family A, member 5) binds to all three

ER stress receptors and keeps them in an inactive state. In response to the accumulation of unfolded proteins, GRP78 dissociates from the three receptors, leading to their activation and launching the UPR (Figure 5) (Szegezdi et al. 2006).

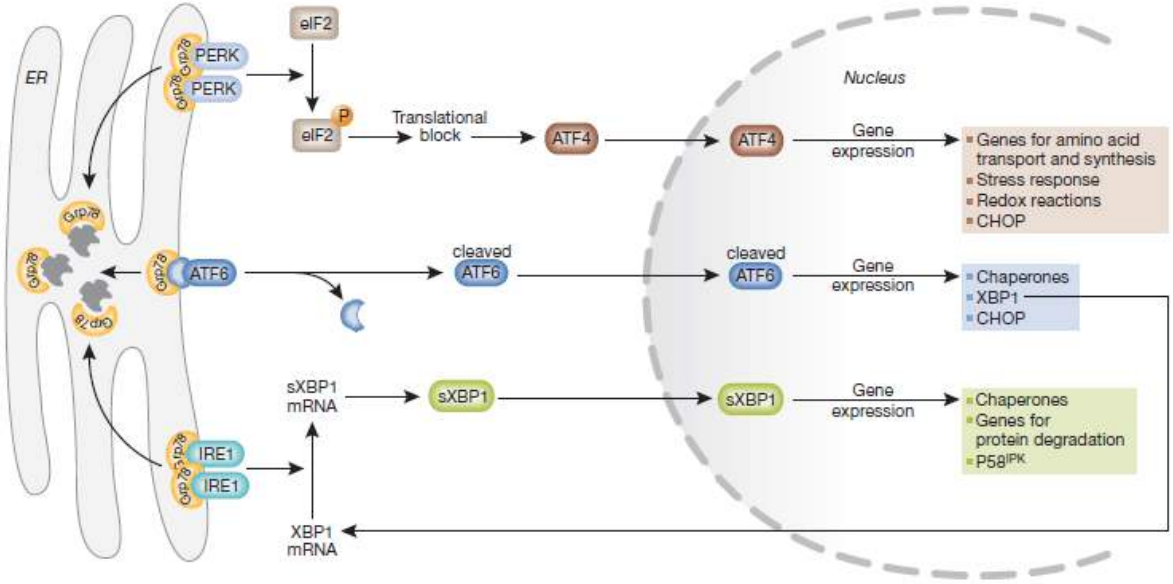

Figure 5. The unfolded protein response (Szegezdi et al. 2006).

4.7.2. The ATF6 pathway

ATF6 is a basic leucine zipper protein (bZIP)-containing transcription factor and a type II ER transmembrane protein, with its C-terminal domain present in the ER lumen and its N-terminal DNA-binding domain facing the cytosol (Haze et al. 1999). In mammals, two homologous proteins, ATF6α and ATF6β exist and they are ubiquitously expressed (Haze et al. 2001). In response to stress, BiP dissociates from ATF6, and in turn ATF6 translocates from the ER to the Golgi apparatus where it is cleaved by site-1 protease in the luminal domain and then by site-2 protease in the transmembrane domain. In turn, the cleaved bZIP containing domain translocates to the nucleus and induces genes with an ER stress response element (ERSE) in their promoter, such as ER chaperone proteins (e.g. GRP78, GRP94) and X-box-binding protein 1 (XBP1) (Chen et al. 2000; Schröder and Kaufmann 2005).

4.7.3. The IRE1 pathway

IRE1 is a type I transmembrane protein that has both serine-threonine protein kinase domain and an endoribonuclease domain. Two mammalian IRE1 protein homologues, IRE1α and IRE1β, were identified. IRE1α is ubiquitously expressed, whereas IRE1β is expressed in

epithelial cells of the gastrointestinal tract (Urano et al. 2000; Schröder and Kaufmann 2005). Dissociation of GRP78 triggers oligomerization and autophosphorylation of the kinase domain and leads to the activation of the RNase domain. Following activation, the endoribonuclease activity of IRE1 cleaves a 26-nucleotide intron from XBP1 mRNA to yield a stable, active bZIP-family transcription factor, spliced XBP1 (XBP1s) (Yoshida et al. 2001). sXBP1 upregulates transcription of different UPR target genes to restore homeostasis such as ER chaperones (GRP78, ERDj4, HEDJ, and PDI-P5), ERAD components (EDEM, $p58^{IPK}$) and secretory pathway genes (Lee et al. 2003; Shaffer et al. 2004).

Furthermore, the RNase activity of IRE1α mediates the selective degradation of mRNAs and microRNAs, in a process called as regulated IRE1α-dependent decay (RIDD). RIDD signaling has been associated with both pro-survival and pro-apoptotic roles depending on the duration and degree of the ER stress (Han et al. 2009; Hollien et al. 2009; Upton et al. 2012).

4.7.4. The PERK pathway

PERK (PKR-like ER kinase) is a serine-threonine protein kinase and dissociation of GRP78 from PERK upon ER stress, leads to its activation by dimerization and autophosphorylation. Activated PERK phosphorylates the eukaryotic initiation factor 2α (eIF2α) on serine 51, thereby causing general translational attenuation and reducing further protein load on the ER (Harding et al. 1999; Donelly et al. 2013). Inhibition of protein translation is important for cell survival because it serves to decrease the amount of nascent proteins arriving at the ER (Harding et al. 2000). However, certain set of mRNAs containing short open reading frames within the 5' untranslated region e.g. activating transcription factor 4 (*ATF4*), DNA damage-inducible transcript 3 (*DDIT3*), protein phosphatase 1 regulatory subunit 15A (*PPP1R15A*), can bypass the eIF2-dependent translational block, and are translationally induced (Young and Wek 2016).

ATF4 is a bZIP transcription factor family member which activates multiple genes that determine cell fate. ATF4 regulates the expression of ER chaperone proteins (GRP78 and GRP94), genes involved in amino acid biosynthesis, redox reactions, protein secretion, autophagy and apoptosis. One of the pro-death target gene of ATF4 is the transcription factor DDIT3, also known as C/EBP homologous protein (CHOP). The overexpression of DDIT3 has been reported to cause cell cycle arrest and/or cell death (McQuiston and Diehl 2017). ATF4 and DDIT3 were shown to interact and transcriptionally activate a number of additional UPR genes including activating transcription factor 3 (*ATF3*), *PPP1R15A*, and tribbles pseudokinase 3 (*TRIB3*) (Han et al. 2013). Additionally, ATF4 and ATF3 are able to induce glutathione-

specific gamma-glutamylcyclotransferase 1 (*CHAC1*), which has been demonstrated to be part of the UPR cascade and possess pro-apoptotic activity mediated by its capability to degrade glutathione (Mungrue et al. 2009; Crawford et al. 2015).

The phosphorylation of eIF2α serves as a point of convergence for ER stress independent signaling mechanisms mediated by EIF2AK4 (also known as GCN2), EIF2AK2 (also known as PKR) or EIF2AK1 (also known as HRI), which are activated by amino acid starvation, viral infection, or heme deprivation, respectively. Therefore, the phosphorylation of eIF2α and its downstream events of are also referred as the integrated stress response (ISR) (Pakos-Zebrucka et al. 2016).

4.7.5. ER stress and cancer

Proliferative cancer cells are exposed to variety of internal and environmental factors that perturb protein homeostasis, thus inducing ER stress. Extrinsic factors such as hypoxia, nutrient deprivation, and lactic acidosis, all of which pose difficulties for protein processing in the ER. In addition, intrinsic stresses shared by many cancer cells, including oncogene activation, alteration in chromosome number and increased glycolysis, lead to a higher demand for protein synthesis. Moreover, genomic instability and somatic mutations can perturb protein folding (Urra et al. 2016). All these factors associated with tumor progression result in the build up of misfolded proteins in the ER, which then causes the activation of the UPR. High-level activation of all arms of the UPR has been documented in several human hematopoietic and solid tumors, including leukemia, lymphoma, glioblastoma and carcinomas of the breast, colon, lung, prostate, pancreas and liver (Oakes 2020).

The ER chaperone protein GRP78/BiP is upregulated in different kinds of the tumor cells and associated with tumor survival, proliferation and metastasis (Casas 2017). Elevated expression of GRP78 alters responsiveness to anticancer drugs and is correlated with poor prognosis in multiple cancer (Siwecka et al. 2019).

The PERK-eIF2α-ATF4 pathway drives several steps of metastasis, including angiogenesis, migration, and colonization at secondary organ sites (Feng et al. 2017), and has been implicated in tumor chemoresistance (Shi et al. 2019). Increased PERK activation is also necessary for the metastatic spread of breast cancer cells that have undergone epithelial-to-mesenchymal transition (EMT) (Feng et al 2014), a process whereby adherent epithelial cells gain motile and invasive properties (Kalluri and Weinberg 2009).

The IRE1–XBP1 pathway has been linked to tumor progression and metastasis in a wide range of cancers, including colorectal carcinoma, breast cancer, hepatocellular carcinoma and oral squamous cell carcinoma (Li et al. 2015; Jin et al. 2016; Sun et al. 2018; Wu et al. 2018). Both up- or downregulation of IRE1 has been described to promote tumor growth depending on the tumor type, which refers to its dual nature in tumorigenesis (Bujisic et al. 2017; Logue et al. 2018). Moreover, IRE1-downstrean signals have opposite effects on progression of human brain tumor, glioblastoma multiform, where splicing of XBP1 induces pro-tumoral signals, while, on the other hand RIDD of mRNA exhibits anti-tumoral features (Lhomond et al 2018).

In addition, ATF6 was found to be elevated in pre-cancerous lesions of colorectal carcinoma (Hanaoka et al. 2018) and may have a role in hepatocellular carcinogenesis (Wu et al. 2014). ATF6 was also reported to contribute to radioresistance in glioblastoma (Dadey et al. 2016) and chemoresistance in osteosarcoma (Yarapureddy et al. 2019).

Based on the above mentioned role of ER stress in cancer progression, several anti-cancer strategies have been investigated that target the UPR pathways (Wang et al. 2018). The most commonly used ER stressors, tunicamycin (TM), which blocks N-glycosylation in the ER, and thapsigargin, which inhibits the endoplasmic reticulum Ca^{2+} ATPase, was shown to induce severe ER stress causing ER-stress mediated apoptosis in several cancer cells (Guha et al. 2017; Sehgal et al. 2017; Qi et al. 2018; Wu et al. 2019). In addition, disulfide bond disrupting agents selectively kill certain type of breast cancer cells *in vitro* and *in vivo* by activation all three branches of the UPR (Ferreira et al. 2017). Some drugs, such as GRP78 inhibitors promote cancer cell death by upregulating UPR, on the other hand IRE1 inhibitors and PERK inhibitors was reported to induce cancer cell death by inhibiting UPR (Wang et al. 2018).

Altogether, chronic and mild ER stress in cancer cells could be relieved by triggering UPR and helping them to survive under extreme conditions, however, severe and persistent ER stress is considered to be tumor suppressive (Wang et al. 2018).

5. AIMS OF THE STUDY

- Investigate the effect of AM in different cancer cell lines compared to HRE (primary human renal epithelial cells) normal cells at both transcriptional and translational level.
- Determine the extent to which ER stress contributes to the anticancer activity of the AM.
- Investigate the relative contribution of the individual components of AM to the activation of the ER stress.
- Knockdown of *ATF3* and growth differentiation factor 15 (*GDF15*) to examine whether they are essential for the cell growth inhibitory effect of the AM and investigate the role of mIR-3189-3p, intronic miRNA of GDF15, in the anticancer activity of AM and in the regulation of ATF3 and DDIT3 during ER stress.
- Reveal the contribution of apoptosis, autophagy, ferroptosis and necroptosis to the effect of AM.
- Study how the apoptosis mediators, BBC3 and PMAIP1 modulate the effect of AM.
- Identification of further compounds capable of enhancing the cancer growth inhibitory effect of the active mixture.

6. MATERIALS AND METHODS

6.1. Cell culture

Cell lines were obtained from the American Type Culture Collection (ATCC) through LGC Standards GMBH, Germany or from The European Collection of Authenticated Cell Cultures (ECACC) through Sigma-Aldrich. HeLa (human cervix adenocarcinoma), MCF-7 (human breast adenocarcinoma), PC-3 (human prostate adenocarcinoma), Caco-2 (human colorectal adenocarcinoma, male), A549 (human lung adenocarcinoma, male), HT-29 (human colorectal adenocarcinoma, female), HepG2 (human hepatocellular carcinoma) and 4T1 (mouse mammary carcinoma) cells were cultured in Minimum Essential Medium Eagle (MEM) (Sigma Aldrich) supplemented with 10% (v/v) Fetal Calf Serum (FCS), 100 U/ml penicillin and 0.1 mg/ml streptomycin. HRE cells were cultured in Renal Epithelial Cell Basal Medium supplemented with human Epidermal Growth Factor (hEGF), Hydrocortisone, Epinephrine, Insulin, Triiodothyronine, Transferrin, GA-1000, and 0.5% Fetal Bovine Serum (FBS) (Lonza). Cells were incubated at 37 °C in a humidified atmosphere at 5% CO_2.

6.2. Active mixture

The selection of the components of the AM has been described previously (Kulcsár 1995; Kulcsár 2000). Throughout the investigation of the mechanism of the AM effect we used a mixture of sixteen selected small molecules (AM16). The composition of AM16 was the following: 0.2 mM adenine, 0.5 mM L-tryptophan, 0.5 mM pyridoxine hydrochloride, 0.75 mM L-methionine, 0.5 mM biotin, 1 mM orotic acid monohydrate, 2.5 mM 2-deoxy-D-ribose, 2 mM L-tyrosine disodium salt hydrate, 2.5 mM L-histidine, 2.5 mM L-phenylalanine, 2.5 mM L-arginine, 5 mM L-(−)-malic acid, 5 mM sodium hippurate hydrate, 5 mM D-(+)-mannose, 0.0025 mM (−)-riboflavin, 0.15 mM L-ascorbic acid, and 8.95 mM sodium bicarbonate. In some experiments the components of AM16 were divided into subgroups (AM1, AM2, AM3, AM6 and AM10). The composition of AM1 was the following: 0.5 mM L-tryptophan, 0.75 mM L-methionine, 2 mM L-tyrosine disodium salt hydrate, 2.5 mM L-histidine, 2.5 mM L-phenylalanine, 2.5 mM L-arginine, and the pH was set to 7.4 with 1N hydrogen-chloride. The composition of AM2 was the following: 0.2 mM adenine, 1 mM orotic acid monohydrate, 2.5 mM 2-deoxy-D-ribose, 5 mM L-(−)-malic acid, 5 mM sodium hippurate hydrate, 5 mM D-(+)-mannose, and 10.8 mM sodium bicarbonate. The composition of AM3 was the following: 0.5 mM pyridoxine hydrochloride, 0.5 mM biotin, 0.0025 mM (−)-riboflavin, 0.15 mM L-ascorbic acid, and 0.65 mM sodium bicarbonate. The composition of AM6 was the following: 0.5 mM

pyridoxine hydrochloride, 0.5 mM biotin, 1 mM orotic acid monohydrate, 2.5 mM 2-deoxy-D-ribose, 0.0025 mM (−)-riboflavin, 0.15 mM L-ascorbic acid, and 1.65 mM sodium bicarbonate. The composition of AM10 was the following: 0.5 mM L-tryptophan, 0.75 mM L-methionine, 2 mM L-tyrosine disodium salt hydrate, 2.5 mM L-histidine, 2.5 mM L-phenylalanine, 2.5 mM L-arginine, 0.2 mM adenine, 5 mM L-(−)-malic acid, 5 mM sodium hippurate hydrate, 5 mM D-(+)-mannose, and 7.3 mM sodium bicarbonate.

The composition of the 100% AM during the selection process of the new compounds was the following: 4 mM L-methionine, 0.75 mM L-tryptophan, 0.08 mM L-tyrosine disodium salt, 5 mM L-phenylalanine, 5 mM L-arginine, 4 mM L-histidine, 5 mM N-benzoyl glycine, 2 mM D-biotin, 1 mM pyridoxine hydrochloride, 0.006 mM riboflavin-5-phosphate sodium salt, 0.3 mM L-ascorbic acid, 1 mM lipoic acid, 0.16 mM orotic acid, 1 mM adenine hydrochloride, 7.5 mM 2-deoxy-D-ribose, 5 mM D-mannose, 0.5 mM D-glucosamine hydrochloride, 7.5 mM malic acid, 5 mM oxaloacetic acid, 0.05 mM adenosine triphosphate disodium salt, and 23.46 mM sodium hydrogen carbonate. All chemicals were purchased from Sigma Aldrich.

6.3. Control mixture

The selection of the components of the CM has been described previously (Kulcsár 1995; Kulcsár 2000). The CM had the following composition: 0.2 mM hypoxanthine, 0.5 mM L-proline, 0.5 mM nicotinic acid, 0.75 mM glycine, 0.5 mM thiamine hydrochloride, 1 mM uracil, 2.5 mM D-(−)-ribose, 2 mM L-alanine, 2.5 mM L-serine, 2.5 mM L-valine, 2.5 mM L-asparagine, 5 mM sodium succinate dibasic hexahydrate, 5 mM betaine, 5 mM D-(+)-glucose, 0.0025 mM D-pantotenic acid hemicalcium salt, 0.15 mM folic acid. All chemicals were purchased from Sigma Aldrich.

6.4. New mixture

The composition of the 100% NM was the following: 2 mM D-phenylalanine, 1 mM D-tryptophan, 1 mM D-arginine, 0.5 mM 5-hydroxi-L-tryptophan, 0.05 mM melatonin, 5 mM mandelic acid, 2.5 mM 3,4-dihydroxymandelic acid, 0.8 mM p-coumaric acid, 0.8 mM trans-cinnamic acid, 1 mM indole-3-acetic acid, 1 mM phenylacetic acid, 0.1 mM 3,4-dihydroxyphenylacetic acid, 0.25 mM indole-3-pyruvic acid, 2.5 mM phenylpyruvic acid sodium salt, 1 mM 4-hydroxy-phenylpyruvic acid, 1 mM 3-phenyllactic acid, 2.5 mM D-glyceric acid calcium salt, 0.25 mM glyceraldehyde, 3 mM 3-methyl-2-oxobutyric acid sodium salt, 5 mM 4-guanidinobutyric acid, 2.5 mM 3-methyl-2-oxovaleric acid sodium salt, 3 mM 4-

methyl-2-oxovaleric acid sodium salt, 5 mM 3-hydroxy-3-methyl-glutaric acid, 1 mM gentisic acid sodium salt, 5 mM urocanic acid, 2.5 mM homovanillic acid, 2.5 mM xanthurenic acid, 5 mM levulinic acid calcium salt, 5 mM 4-hydroxy-benzoic acid, 5 mM pyrrole-2-carboxylic acid, 0.25 mM adenosine, 0.1 mM agmatine-sulphate, 0.5 mM cysteamine, 5 mM creatinin, 38.45 mM sodium-hydrogencarbonate. All chemicals were purchased from Sigma Aldrich.

6.5. Microarray analysis

HeLa cells were treated with AM16 for 3 hours, 6 hours and 24 hours in triplicates. Total RNA was isolated with RNeasy Plus mini kit (QIAGEN), RNA quality was assessed with agarose gel electrophoresis. Microarray hybridization and initial data processing were performed by Personmed Ltd. (Turku, Finland) as contract research. In brief, triplicate samples for each time point were converted into biotin-labeled cRNA and were hybridized to a Human HT-12 v.4 Expression BeadChip (Illumina) using standard protocols. Average probe intensities were computed with Genome Studio (Illumina) and analyzed with the following Bioconductor packages: affy, limma, gplots, beadarray, lattice, amap, simpleaffy, xtable, scatterplot3d, ade4 and made4. Data were quantile normalized and differentially expressed genes were identified with 2-sided t-test and fold change. Genes with >1.3 fold change and p value < 0.05 were considered differentially expressed.

6.6. Gene Set Enrichment Analysis

Gene set enrichment analysis (GSEA) was performed with the java GSEA Desktop Application version 2.2.3 (Subramanian et al. 2005; Mootha et al. 2003). The gene ontology biological process gene set collection (GO BP) version 5.2 (Liberzon et al. 2011) was used for the enrichment analysis. Upregulated pathways were defined by a normalized enrichment score (NES) > 3, downregulated pathways were identified by a NES < -3. Pathways with a false discovery rate (FDR) p value < 0.25 were considered significantly enriched.

6.7. Quantitative RT-PCR (qRT-PCR)

Total RNA was isolated with PureLink RNA Mini Kit (ThermoFisher Scientific) and was treated with DNase I (Sigma Aldrich). cDNA was prepared with High Capacity RNA-to-cDNA Kit (ThermoFisher Scientific). PCR primers used for real-time quantitative amplification of the human housekeeping genes *B2M*, *GAPDH*, *HPRT1*, *RPL32*, and *PPIA* were described previously (Zhang et al. 2005; Colell et al. 2007). PCR primers for human *APAF1*, *BAX*,

BCL2L1, *BIRC2*, *BIRC3*, *CASP3*, *CDKN1A*, *CDKN2A*, *IKBKG*, *NFKBIA*, *NFKB1* were also described previously (Kulcsár et al. 2013). Total XBP1, spliced XPB1, and unspliced XBP1 transcripts were quantified with primers described previously (Oslowski and Urano 2011). All other PCR primers were designed by Primer Express Software, primer sequences are listed in Supplementary data, Table S1. The expression levels of *BBC3*, *PMAIP1*, *RPL32* were measured with TaqMan gene expression assays. RPL32 was used for normalization. For miRNA analysis, small RNA fractions were isolated using the miRVana miRNA isolation kit (ThermoFisher Scientific). The expression of miR-3189-3p and U6 snRNA were measured using TaqMan microRNA assays (ThermoFisher Scientific) following the manufacturer's instructions. U6 snRNA was used for normalization. PCR reactions were run in triplicates using PowerUp SYBR Green Master Mix (ThermoFisher Scientific) or Taqman gene expression master mix II, no UNG (ThermoFisher Scientific) on an ABI StepOne Real Time PCR System. The stability of the expression level of the housekeeping genes was analyzed in preliminary experiments and RPL32 was chosen for normalization of target gene expression. Fold change values were calculated by dividing the normalized target gene expression measured in the treated samples by that of the untreated control samples (Schmittgen and Livak 2008).

6.8. Western blot

Cells were seeded onto 150 mm Petri dishes at a density of $1.6x10^6$ or onto 6-well plates at a density of $1.7x10^5$/well. Following the indicated treatments cells were lysed in ice cold 1X RIPA buffer (Abcam) containing Protease and Phosphatase Inhibitor Cocktail (Abcam). Protein concentrations were measured with the DC protein assay (Bio-Rad). 30-100 μg proteins were separated on SDS-polyacrylamide gels and transferred to nitrocellulose membranes. Membranes were blocked with 5% non-fat dry milk (NFDM) (Sigma Aldrich) or in the case of antibodies against phosphoproteins with 5% bovine serum albumin (BSA) (Sigma Aldrich) in Tris-buffered saline (150mM NaCl, 20mM Tris-base pH 7.6, 0.1% Tween 20) (TBS-T) for 1 hour at room temperature. Primary antibodies diluted in 5% NFDM/TBS-T or 5% BSA/ TBST-T were applied at 4°C overnight. HRP-conjugated anti-rabbit antibody diluted in 5% NFDM/TBS-T was applied for 1 hour at room temperature. Membranes were developed with LumiGLO chemiluminescent substrate (Cell Signaling Technology) and exposed to x-ray films. Densitometry analysis was performed with the Image Studio Lite software 5.2.5. Densities were normalized to the non-phosphorylated forms or β-tubulin for eIF2α, PERK, IRE1α or ATF6 and BiP, respectively.

6.9. Treatment with ER stress inhibitors

HeLa cells were pretreated with the 20 μM or 500 nM integrated stress response inhibitor (ISRIB) (Sigma Aldrich), 1 μM salubrinal (SAL) (Sigma Aldrich), or 1 mM 4-phenylbutyrate (4-PBA) (Sigma Aldrich) for 1 hour, followed by co-treatment with AM16. To investigate the effect of IRE1α inhibition, HeLa cells were treated with 10 μM GSK2850163 (Sigma Aldrich) or 10 μM STF-083010 (Sigma Aldrich) in combination with AM16 for 24 hours.

6.10. Reverse transfection

HeLa cells were reverse transfected in 96-well plates at a density of 2.5×10^3 cells per well or in 6-well plate at a density of 1.7×10^5 using DharmaFECT 1 (Dharmacon) according to the manufacturer's instructions. ON-TARGETplus Human GDF15 (9518) SMARTpool siRNA (Dharmacon, Cat#L-019875-00-0005), ON-TARGETplus Human ATF3 (467) SMARTpool siRNA (Dharmacon, Cat#L-008663-00-0005) and ON-TARGETplus Non-targeting Pool (Dharmacon, Cat#D-001810-10-05) siRNAs were used at a final concentration of 50 or 100 nM as indicated. The miRIDIAN microRNA hsa-miR-3189-3p Hairpin Inhibitor (Dharmcon, Cat#IH-301754-01-0005) and miRIDIAN microRNA Hairpin Inhibitor Negative Control (Dharmacon, Cat#IN-001005-01-05) miRNAs were transfected at a final concentration of 50 and 200 nM, respectively, as indicated. The miRIDIAN microRNA hsa-miR-3189-3p Mimic (Dhamacon, Cat#C-301754-00-0005) and miRIDIAN microRNA Mimic Negative Control (Dharmacon, Cat#CN-001000-01-05) miRNAs were transfected at a final concentration of 10 nM. The BBC3 and PMAIP1 silencer select pre-designed siRNAs (ThermoFisher Scientific, Cat#S25840, Cat#S10709) were used at a final concentration of 10 nM. At 24 hours post-transfection, the transfection medium was removed, and treatment was initiated. At 48 hours post-transfection, cells were either fixed and labeled for cell counting or were harvested and analyzed by qRT-PCR.

6.11. Cell counting and immunocytochemistry

HeLa cells were plated and transfected at 2.5×10^3 per well in 96-well black-walled, glass bottom plates (Corning, #CLS4580), then treated as indicated. The cells were fixed with 4 % paraformaldehyde in phosphate buffered saline (PBS) for 10 minutes, then were permeabilized with Triton X-100 for 10 minutes, followed by blocking with 5 % goat serum in PBS for 1 hour at room temperature. The antibody against ATF4 diluted in PBS containing 1 % BSA and 0.05 % Triton-X 100 was applied at 4 °C overnight. After washing three times with PBS for 5

minutes, the cells were incubated with Alexa Fluor 555 Anti-Rabbit IgG diluted as above, in the dark for 1 hour at room temperature. Cells were washed once with PBS for 5 minutes, and then the nuclei were counterstained with DAPI (Sigma Aldrich) (10 ug/ml in PBS) for 5 minutes. Cells were imaged using an automated, high-content screening station (Olympus IX83ZDC2 equipped with scan^R software platform, v2.5.0). In acquisition 25 fields per well and fluorescent channels were imaged using a 10x objective (UPLSAPO; Olympus, numeric aperture: 0.4; refraction: 1.0; correction: 1.0) and a highly sensitive digital CCD camera (C8484-05G02, Hamamatsu) to acquire abundant events for analysis. For the excitation and emission a multiband filter cube (M4DAFIC3C5, Chroma Technology GmbH) was used with a previously adjusted exposure time and other technical parameters. The collected images were analyzed using the Scan^R analysis module where nuclei were defined on the basis of DAPI staining with intensity gradient based event recognition and the nuclear intensity of ATF4 was also quantified. For experiments involving only cell counting, the fixation of the cells was directly followed by DAPI staining and imaging.

6.12. Live/dead staining, EdU and TUNEL labeling

HeLa cells were plated at 2.5×10^3 per well in 96-well plates and treated as indicated. For live/dead staining cytocalcein violet 450 and 7-Aminoactinomycin D (7-AAD) were used from the Apoptosis/Necrosis detection kit (blue, green, red) (Abcam) following the manufacturer's instructions. For EdU (5-ethynyl-2'-deoxyuridine, a nucleoside analog of thymidine) labeling EdU was added at a final concentration of 10 μM at treatment initiation. The incorporated EdU was detected with the Click-iT Plus EdU Alexa Fluor 555 imaging kit (ThermoFisher Scientific) following the manufacturer's instructions. TUNEL (terminal deoxynucleotidyl transferase-dUTP nick end labeling) was performed with the use of Click-iT TUNEL Alexa Fluor 594 imaging kit (ThermoFisher Scientific). For EdU and TUNEL nuclei were labeled with Hoechst 33342 (5 μg/ml). Image acquisition and analysis was performed as described for immunocytochemistry.

6.13. Determination of combination indexes

Cells were plated in 96-well plates and treated with three point, two-fold dilution series of the inhibitors, dilution series of AM16 alone (40–100%), or with the combination of the two higher concentration of inhibitors and 60 %, 80 %, 100 % AM16 for 24 hours. Cells were counted as described for cell counting and the combination indexes were calculated with the

Compusyn software (Chou and Talalay 1981; Chou and Talalay 1984; Chou 2006). The following inhibitors were tested (starting concentration of the dilution series in brackets): DFO (Abcam) (100 μM), Fer-1 (Sigma Aldrich) (20 μM), (±)-6-Hydroxy-2,5,7,8-tetramethylchromane-2-carboxylic acid (Trolox) (Sigma Aldrich) (300 μM), 2-mercaptoethanol (2-ME) (Sigma Aldrich) (20 μM), U0126 (Sigma Aldrich) (20 μM), Nec-1 (Abcam) (10 μM), NSA (Abcam) (5 μM), Z-VAD(OMe)-FMK (Abcam) (80 μM), E-64d (Aloxistatin) (Abcam) (50 μM), ALLN (Abcam) (500 nM), cyclosporine A (CSA) (Abcam) (10 μM), 3-methyladenine (3-MA) (Abcam) (4 mM), bafilomycin A1 (BAF) (Abcam) (1 μM), chloroquine diphosphate (CHLQ) (Abcam) (50 μM). Erastin (Sigma Aldrich) was used at 2.5–10 μM concentrations. Necroptosis was induced with 20 ng/ml recombinant human TNF alpha protein (Abcam) + 20 μM z-VAD-fmk + 500 nM BV6 (Smac mimetic) (Sigma Aldrich).

6.14. Statistical analysis

Statistical analysis was performed with IBM SPSS Statistics 22 using the statistical tests specified in the figure legends. Normal distribution of the data was evaluated with Shapiro-Wilk test. Homogeneity of variances was assessed with Levene-test. For normally distributed variables with equal variances p values were calculated with one-way analysis of variance (ANOVA) followed by Bonferroni post hoc test. For normally distributed variables with unequal variances p values were calculated with Welch test followed by Games-Howell test. P values less than 0.05 were considered statistically significant. For the quantification of nuclear intensity of ATF4 n represents the number of nuclei analyzed.

7. RESULTS

Throughout the investigation of the mechanism of the AM we used a mixture of sixteen selected small molecules (AM16). The composition of AM16 is described in the Materials and Methods section 5.2.

7.1 Gene expression analysis of AM16 treated cancer cells

Microarray analysis showed striking changes in gene expression in HeLa cells after 3 hours, 6 hours, and 24 hours treatment with AM16. GSEA of the upregulated transcripts revealed the enrichment of gene sets corresponding to RNA splicing and translational initiation at 3 hours, ER stress induced apoptosis and cell cycle regulation at 6 hours, and apoptosis and TGF-β signaling 24 hours **(Figure 6A)**. Among the gene sets enriched in all three time points "response to ER stress" had the highest NES **(Figure 6B)**.

In order to validate these results, we have analyzed one hundred genes with qRT-PCR. We also applied a control mixture (CM) which had the same osmolality as AM16 and contained ineffective small molecules with chemically or physiologically similar properties as components of AM16. HeLa and HRE normal cells were treated with AM16 or CM for 24 hours. We have found upregulation of genes contributing to the UPR (*CHAC1, TRIB3, ATF3, DDIT3, PPP1R15A, ATF4, XPB1*), to autophagy (*SESN2, ULK1*), and to apoptosis (*BIRC3, GADD45A, PMAIP1, BBC3*) only in HeLa cells treated with AM16 for 24 hours, but not in HeLa cells treated with CM or HRE treated with AM16 or CM **(Figure 6C)**.

Genes that showed specific and significant gene expression differences in AM16 treated HeLa cells were further analyzed in MCF-7, PC-3 and Caco-2 cells. We have found that *ATF3, DDIT3, PPP1R15A, PMAIP1* and *GDF15* were specifically upregulated in all of the four AM16 treated cell lines, while the upregulation of *CHAC1* could only be shown in AM16 treated HeLa and PC-3 cells **(Figure 6D)**.

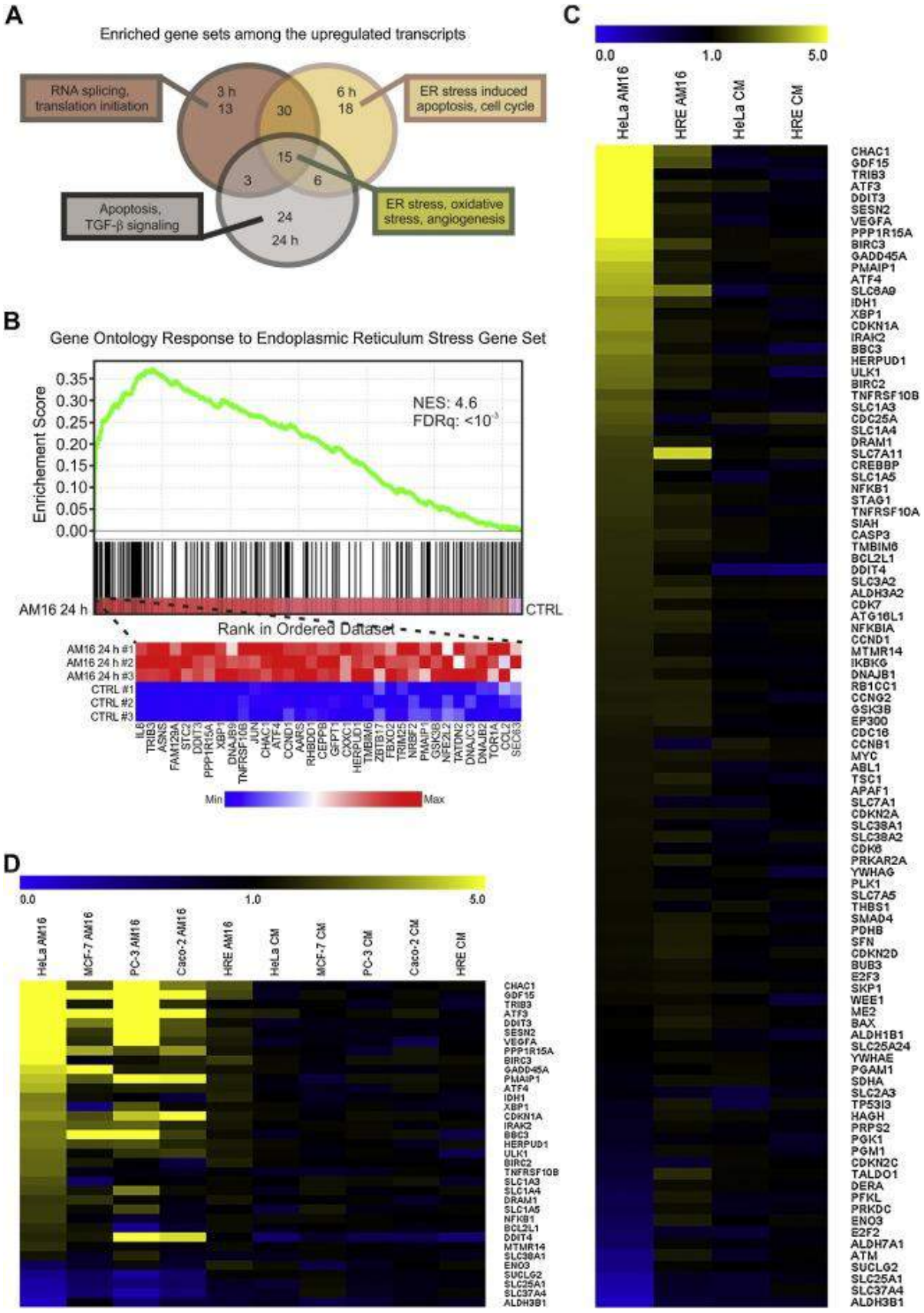

Figure 6. Gene expression profiling identifies the ER stress pathway in AM16 treated cancer cells. (A) Venn diagram indicating the number of enriched gene sets among the upregulated transcripts (normalized enrichment score ≥ 3 and false discovery rate q-value < 10-3) identified with gene set enrichment analysis (GSEA) after 3 h, 6 h, and 24 h treatments with

AM16 in HeLa cells. Texts in rectangles indicate predominant gene sets for each time point and in common. **(B)** Enrichment plot for the ER stress gene set after 24 h treatment with AM16 (top) and heatmap showing the expression of top ranking genes (fold-change ≥ 1.3 vs. control) in the gene set after 24 h treatment of HeLa cells with AM16 in three biological replicates (bottom). NES, normalized enrichment score. FDRq, false discovery rate q-value. **(C)** Heatmap of fold change values of gene expression determined by qRT-PCR in HeLa and HRE cells treated for 24 h with AM16 or CM. Values represent the average of three independent experiments. **(D)** Heatmap of fold change values of gene expression determined by qRT-PCR in HeLa, MCF-7, PC-3, Caco-2, and HRE cells treated for 24 h with AM16 or CM. Values represent the average of three independent experiments.

These results indicate that the AM16 specifically induces gene expression changes characteristic for ER stress in cancer cells.

7.2. Detection of proteins contributing to the ISR in AM16 treated cancer cells

The integrated stress response causes global attenuation of protein synthesis while allowing the preferential translation of certain upstream open reading frame containing mRNAs e.g. *ATF4*, *DDIT3* (Young and Wek 2016). Therefore, we examined the expression of ATF4, ATF3, DDIT3, CHAC1 and GDF15 proteins in AM16 or CM treated HeLa **(Figure 7A)**, PC-3 **(Figure 7B)**, Caco-2 **(Figure 7C)**, MCF-7 **(Figure 7D)**, and HRE **(Figure 7E)** cells by western blot.

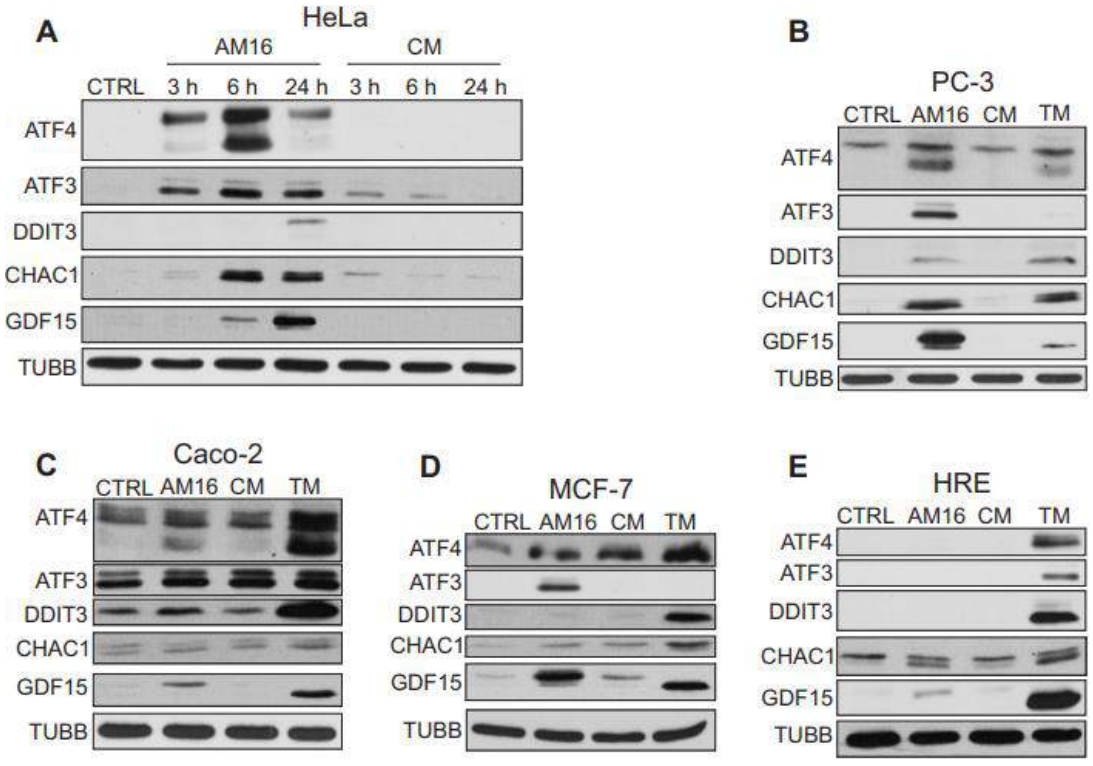

Figure 7. The AM16 induces proteins contributing to the integrated stress response. (A) Representative western-blots for ATF4, ATF3, DDIT3, CHAC1 and GDF15 in HeLa cells treated with AM16 or CM for the indicated periods of time. **(B-E)** Representative western-blots

for ATF4, ATF3, DDIT3, CHAC1 and GDF15 in PC-3 cells **(B)**, in Caco-2 cells **(C)**, in MCF-7 cells **(D)**, or in HRE cells **(E)** treated with AM16, CM, or TM (5 μM) for 24 hours. β-tubulin (TUBB) was used as loading control.

We observed a time-dependent induction of ATF4, ATF3, DDIT3, CHAC1, GDF15 in AM16 treated HeLa cells. We detected the accumulation of ATF4, ATF3 and GDF15 in PC-3, Caco-2 and MCF-7 cells treated with AM16 for 24 hours, but not in CM treated cells. The accumulation of DDIT3 could be demonstrated in AM16 treated PC-3 and Caco-2 cells, but not in MCF-7 cells, while CHAC1 was induced in AM16 treated PC-3, but not in Caco-2 and MCF-7 cells. ATF4, ATF3 and DDIT3 could not be detected in AM16 or CM treated HRE cells, while a slight induction of CHAC1 and GDF15 could be observed upon treatment with AM16.

Furthermore, we examined the sub-cellular localization of ATF4 with immunocytochemistry, and we found that ATF4 is accumulated in the nuclei of HeLa cells after 24 hours treatment with AM16 **(Figure 8A,B)**.

These results confirm the activation of the ISR pathway and revealed the activation and nuclear accumulation of ATF4 upon treatment with AM16.

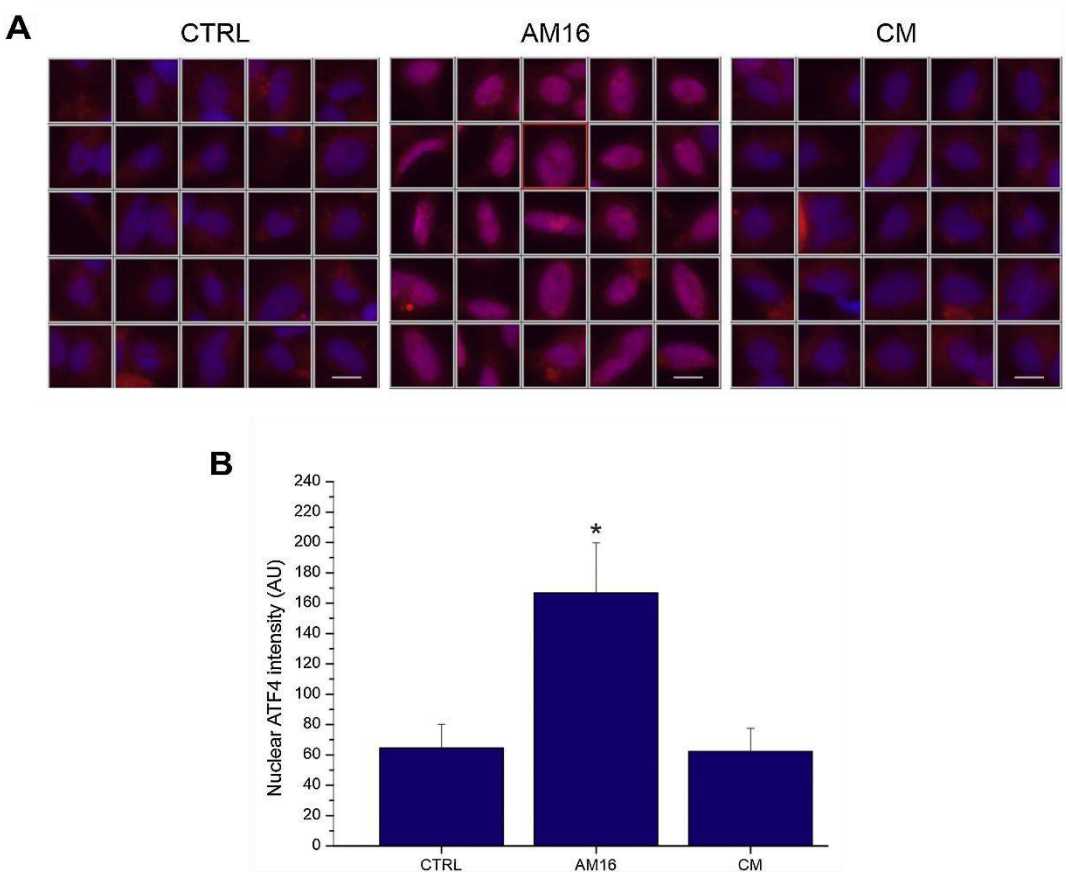

Figure 8. Sub-cellular localization of ATF4 with immunocytochemistry. (A) Immunofluorescence pictures of HeLa cells treated with AM16 or CM for 24 h. Nuclei were labeled with DAPI (blue) and ATF4 was detected with antibody (red). Representative image galleries of 25 nuclei per condition from three independent experiments are shown. Scale bars:

15 µm. **(B)** Quantification of nuclear ATF4 fluorescence intensity. Fluorescence intensity is presented in arbitrary units (AU) and represents mean ± SD of three independent experiments. *p < 0.001 vs. CTRL (Welch test followed by Games-Howell test). n(CTRL) = 4187, n(AM16) = 2202, n(CM) = 4417.

Next we investigated the phosphorylation of eIF2α, the core event in the ISR pathway, which mediates the global translational shutdown and the simultaneous preferential translation of certain mRNAs. We found a time dependent phosphorylation of eIF2α in AM16 treated HeLa cells **(Figure 9A)**.

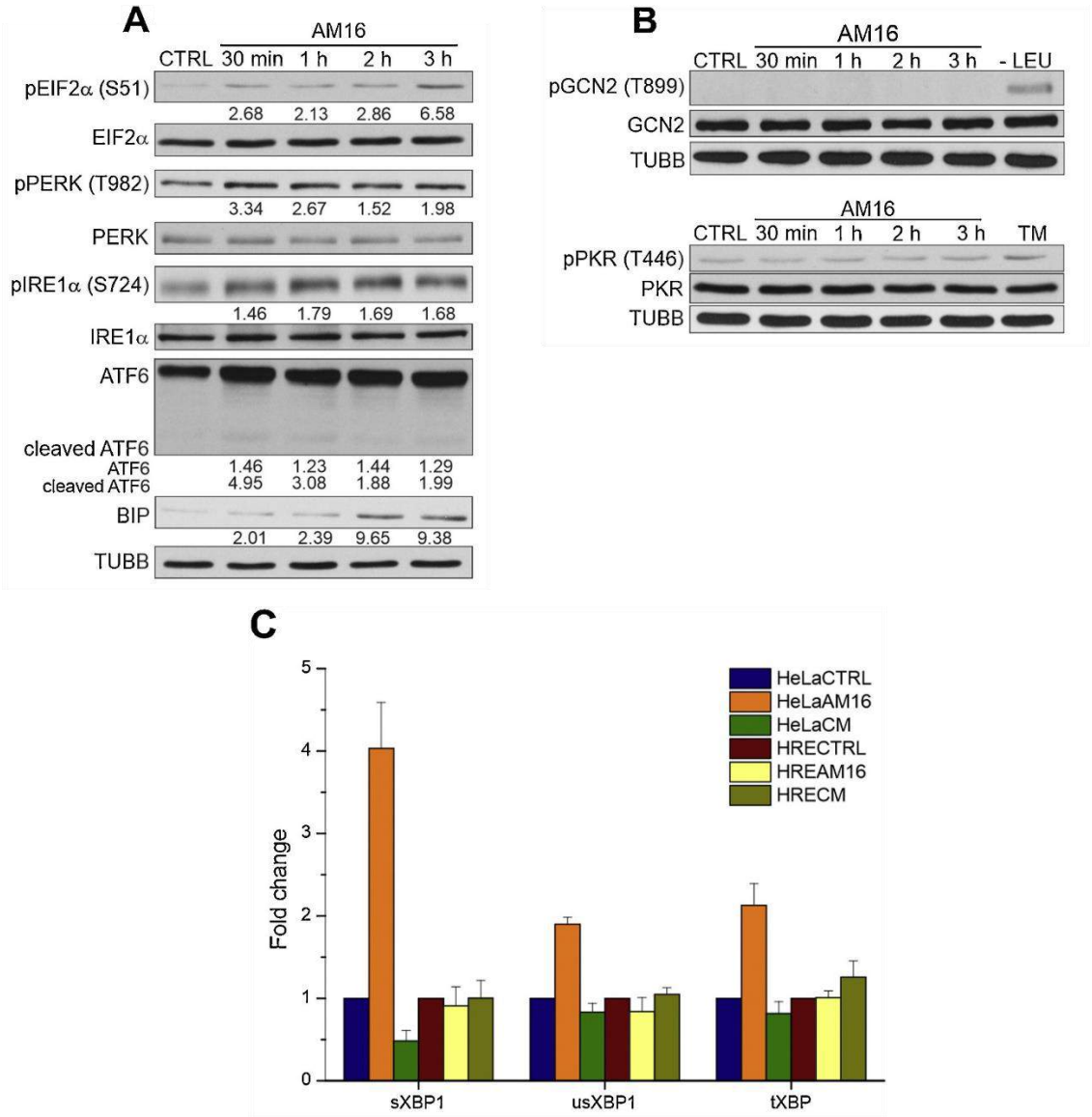

Figure 9. The AM16 induced stress response is mediated by ER stress sensors. (A) Representative western-blots of phosphorylated eIF2α (S51), eIF2α, phosphorylated PERK (T982), PERK, phosphorylated IRE1α (S724), IRE1α, ATF6 and BiP in HeLa cells treated with AM16 for the indicated periods of time. TUBB was used as loading control. Numbers below the bands indicate relative densities compared to the untreated control. **(B)** Representative

western-blots of phosphorylated GCN2 (T899), GCN2, phosphorylated PKR (T466) and PKR in HeLa cells treated with AM16 for the indicated periods of time. TUBB was used as loading control. Leucine starvation for 30 min (- LEU) or 3 h of TM treatment (5 μM) was applied as positive control for phosphorylated GCN2 or phosphorylated PKR, respectively. **(C)** XBP1 mRNA splicing was detected with qRT-PCR analysis in HeLa and HRE cells treated for 24 h with AM16 or CM. Bars represent the fold change compared to CTRL. Normalized expression values and significance values are provided in Table S2.

Next we investigated the phosphorylation of the ER stress responsive eIF2α kinase PERK and the phosphorylation two ER stress independent kinases, GCN2 and PKR in HeLa cells. We found a time dependent phosphorylation of PERK **(Figure 9A)**, however GCN2 and PKR were not phosphorylated upon treatment with AM16 **(Figure 9B)**. Since PERK was activated upon treatment, we also investigated two further ER stress sensors IRE1α and ATF6, and the accumulation of BiP, a chaperone playing a crucial role in ER stress. The treatment with AM16 induced a time dependent phosphorylation of IRE1α, and a time dependent increase in the amount of ATF6 and BiP in HeLa cells **(Figure 9A)**. The activation of ATF6 was confirmed by the detection of the cleaved fragment of ATF6, the 50kDa transcription factor domain **(Figure 9A)**, whereas the activation of IRE1α was demonstrated with the elevated splicing of *XBP1* mRNA upon treatment with AM16 **(Figure 9C)**.

All together these results show that the phosphorylation of eIF2α induced upon treatment with AM16 is caused by the activation of PERK and not by other ER stress independent kinases, and that AM16 activates all three branches of the UPR.

7.3. Effects of ER stress inhibitors in AM16 treated cells

Several ER stress inhibitors were applied to determine the extent to which ER stress contributes to the anticancer activity of the AM16. We investigated the effect of the ISR inhibitor ISRIB - a molecule which renders cells resistant to the effect of eIF2α phosphorylation (Sidrauski et al. 2015) -, salubrinal (SAL) - an inhibitor of eIF2α dephosphorylation and ER stress induced apoptosis (Boyce et al. 2005) -, and 4-phenylbutyrate (4-PBA) – a chemical chaperone able to reduce the amount of misfolded proteins in the ER (Kubota et al. 2006) -, on the AM16 treated cells. We have found that ISRIB completely blocked the AM16 triggered induction of ATF4, while as expected had no effect on the AM16 induced eIF2α phosphorylation **(Figure 10A)**.

ISRIB completely inhibited the upregulation of *ATF4*, *CHAC1*, *DDIT3* and *GDF15* mRNA level induced by 6 hours AM16 treatment, however the induction of *ATF3* was only reduced **(Figure 10B)**. The effect on cell growth inhibition was investigated with direct counting of cells

instead of metabolic assays to avoid any possible interference caused by treatment with AM16. ISRIB was able to significantly attenuate, but not completely block the cell growth inhibitory effect of the AM16, however SAL or 4-PBA had no effect **(Figure 10C)**.

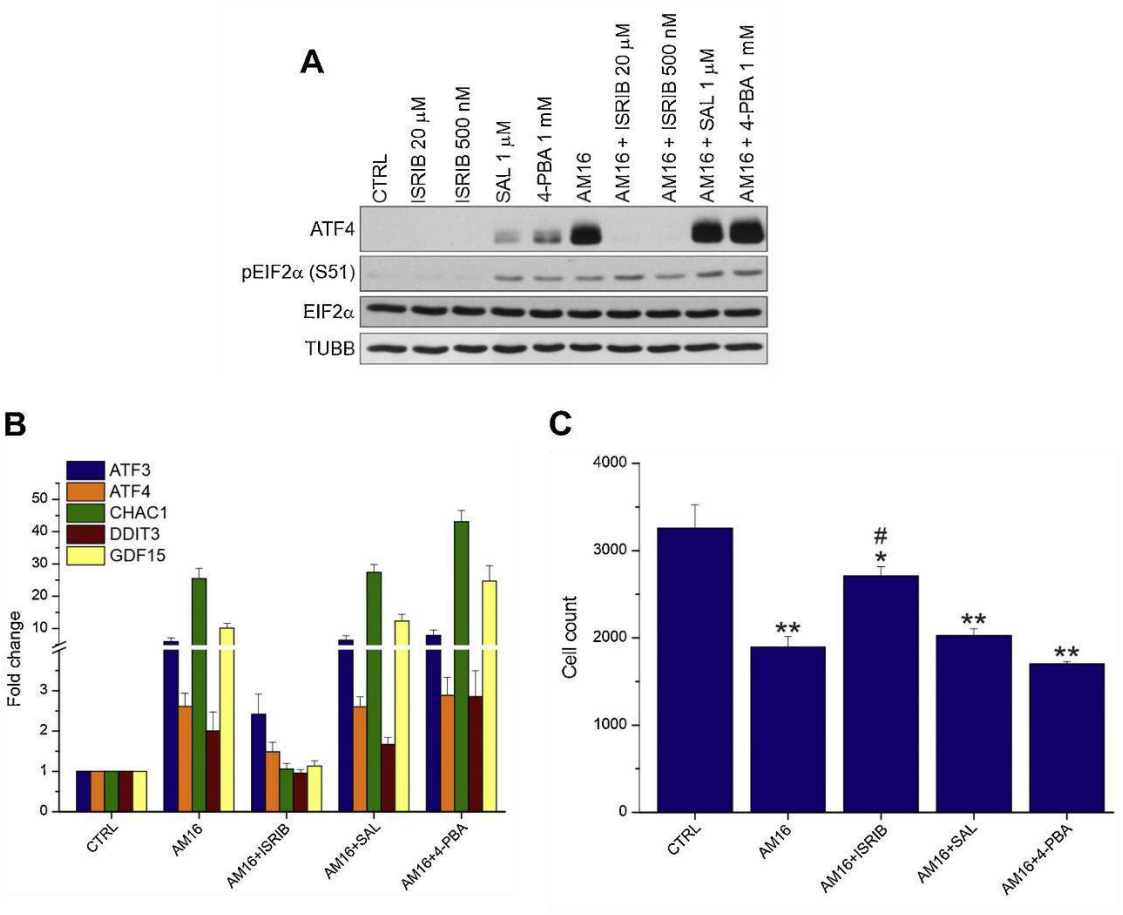

Figure 10. ISRIB is able to attenuate the cell growth inhibitory effect of AM16. (A) HeLa cells were pretreated with the indicated concentrations of ISRIB, SAL, or 4-PBA for 1 h, followed by co-treatment with AM16 for 2 h. ATF4, phosphorylated eIF2α (S51), and eIF2α were analyzed by western-blot. TUBB was used as loading control. **(B)** HeLa cells were pretreated with 500 nM ISRIB, 1 µM SAL, or 1 mM 4-PBA for 1 h, followed by co-treatment with AM16 for 6 h. mRNA levels were detected with qRT-PCR. Bars represent the fold change compared to CTRL. Normalized expression values and significance values are provided in Table S2. **(C)** HeLa cells were pretreated as in panel (B), followed by co-treatment with AM16 for 24 h. Bars represent the cell counts per well (average ± standard deviation of three independent experiments). *p < 0.05, **p < 0.001 vs. CTRL; #p < 0.001 vs. AM16 (ANOVA, Bonferroni test).

Furthermore, we also tested two additional IRE1α inhibitors GSK2850163 and STF-083010, but these inhibitors also failed to block the AM16 induced cell growth inhibition **(Figure 11B)**, despite the significant inhibition of the AM16 induced XBP1 splicing **(Figure 11A)**.

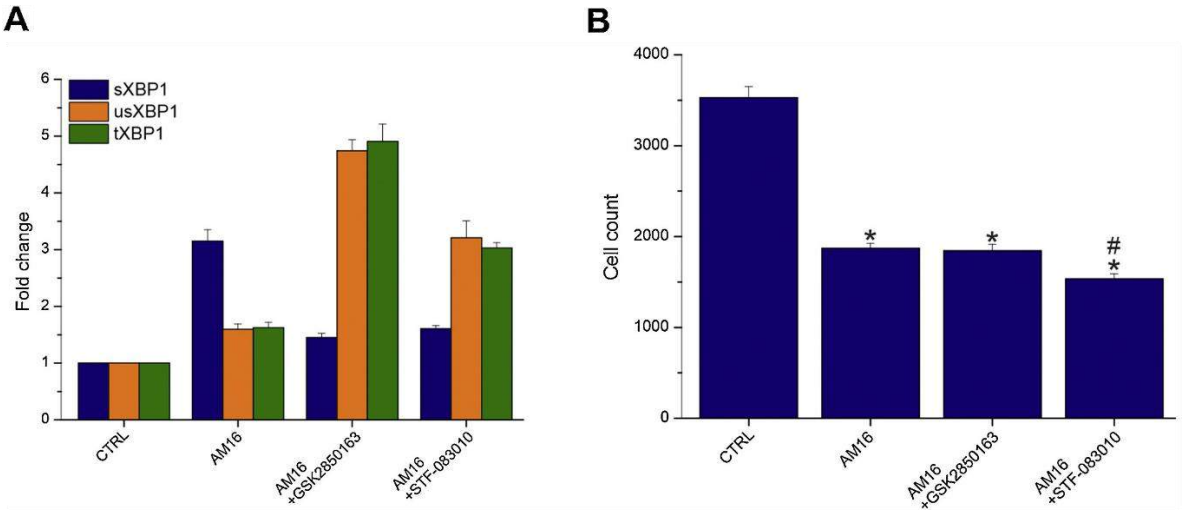

Figure 11. IRE1α inhibitors failed to block AM16 induced growth inhibition. (A) HeLa cells were treated with 10 μM GSK2850163 or 10 μM STF-083010 in combination with AM16 for 24 h. XBP1 mRNA splicing was detected with qRT-PCR analysis. Bars represent the fold change compared to CTRL. Normalized expression values and significance values are provided in Table S2. **(B)** HeLa cells were treated as in panel (A). Bars represent the cell counts per well (average ± standard deviation of two independent experiments). *$p < 0.001$ vs. CTRL, #$p < 0.001$ vs. AM16 (ANOVA, Bonferroni test).

Taken together these results show that the UPR plays a significant role in the AM16 cell growth inhibitory effect, and suggest that eIF2α phosphorylation is the major arm of the UPR activated by AM16.

7.4. Relative contribution of the individual components of AM16 to the ER stress induction

To determine whether all of the sixteen small molecules of the AM16 are required to the induction of ER stress, first we formed three groups from the compounds of the AM16 and tested the effect of them alone or in combination. AM1 contained the amino acid components, AM2 contained adenine, L-(-)-malic acid, 2-deoxy-D-ribose, orotic acid, D-(+)-mannose and hippuric acid, AM3 contained the vitamin components (pyridoxine, D-biotin, (-)-riboflavin, and L-ascorbic acid), and AM16 contained all of the sixteen components (AM1 + AM2 + AM3). We have found that the combination of AM1 and AM2 was able to significantly reduce the cell number **(Figure 12A)**, induced the expression of *ATF3*, *ATF4*, *CHAC1*, *DDIT3*, *GDF15* transcripts **(Figure 12B)**, and increased the nuclear accumulation of ATF4 **(Figure 12C,D)**, while the other combinations or the per se application of AM1, AM2, AM3 had no effect. Important to note, that the growth inhibitory effect and ATF4 induction of AM16 was still significantly higher than the effect of AM1+AM2, while the level of ER stress related gene induction elicited by AM16 was similar to that of AM1 + AM2 **(Figure 12B).** These results

demonstrate that the amino acid components (AM1) together with the heterogeneous group of other small molecules (AM2) are sufficient to induce ER stress, while the vitamin components (AM3) are only able to enhance this effect, but are not sufficient to initiate it.

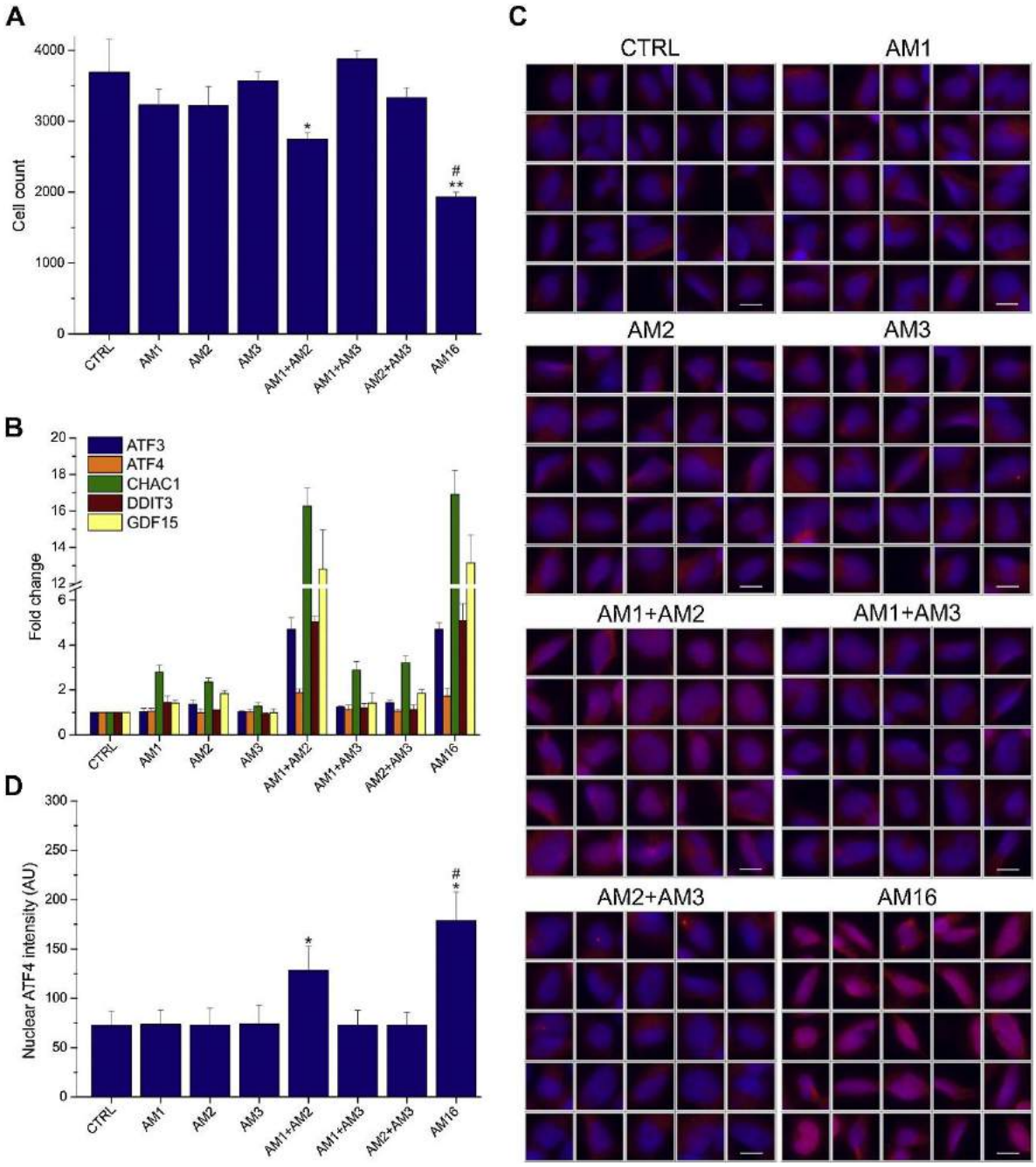

Figure 12. Components of AM16 differentially contribute to the ER stress induction. (A) HeLa cells were treated with AM1, AM2, AM3 or the indicated combinations of them for 24 h. AM16 represents a mixture containing all of the sixteen components (AM1 + AM2 + AM3). Cell number was determined with DAPI staining followed by counting the nuclei using an automated microscope. Bars represent the cell counts per well (average ± standard deviation of three independent experiments). *$p < 0.05$, **$p < 0.001$ vs. CTRL; #$p < 0.001$ vs. AM1 + AM2 (ANOVA, Bonferroni test). **(B)** HeLa cells were treated as in panel **(A)**. *ATF3*, *ATF4*, *CHAC1*, *DDIT3*, *GDF15* mRNA levels were detected with qRT-PCR. Bars represent the fold change compared to CTRL. Normalized expression values and significance values are provided in

Table S2. **(C)** Immunofluorescence pictures of HeLa cells treated as in panel (A). Nuclei were labelled with DAPI (blue) and ATF4 was detected with antibody (red). Representative image galleries of 25 nuclei per condition from three independent experiments are shown. Scale bars: 15 μm. **(D)** Quantification of nuclear ATF4 fluorescence intensity of the same representative experiment as shown in panel (C). Fluorescence intensity is presented in arbitrary units (AU) and represents mean ± SD of three independent experiments. *$p < 0.001$ vs. CTRL; #$p < 0.001$ vs. AM1 + AM2 (Welch test followed by Games-Howell test). n (CTRL) = 4968, n(AM1) = 4787, n(AM2) = 4869, n(AM3) = 4721, n(AM1 + AM2) = 3183, n(AM1 + AM3) = 4819, n(AM2 + AM3) = 4774, n(AM16) = 2649.

Next we combined randomly paired components of AM2 with AM1 **(Figure 13A)**, or vice versa randomly paired components of AM1 with AM2 **(Figure 13B)** and measured the expression of *ATF3*, *ATF4*, *CHAC1*, *DDIT3*, *GDF15*. On the basis of our results we identified 10 (adenine (Ade), L- (-)-malic acid (Mal), D-(+)-mannose (Man) and hippuric acid (Hip) with AM1 (amino acids)) compounds out of the sixteen, those which were able to activate the ER stress genes to levels comparable with AM1+AM2 **(Figure 13A)**. The amino acid components equally contribute to the induction of ER stress genes **(Figure 13B)** and all six of them are necessary to reach the gene expression levels caused by AM1 + AM2, while 2-deoxy-D-ribose (Deo) and orotic acid (O) are not necessary to the ER stress induction **(Figure 13A)**.

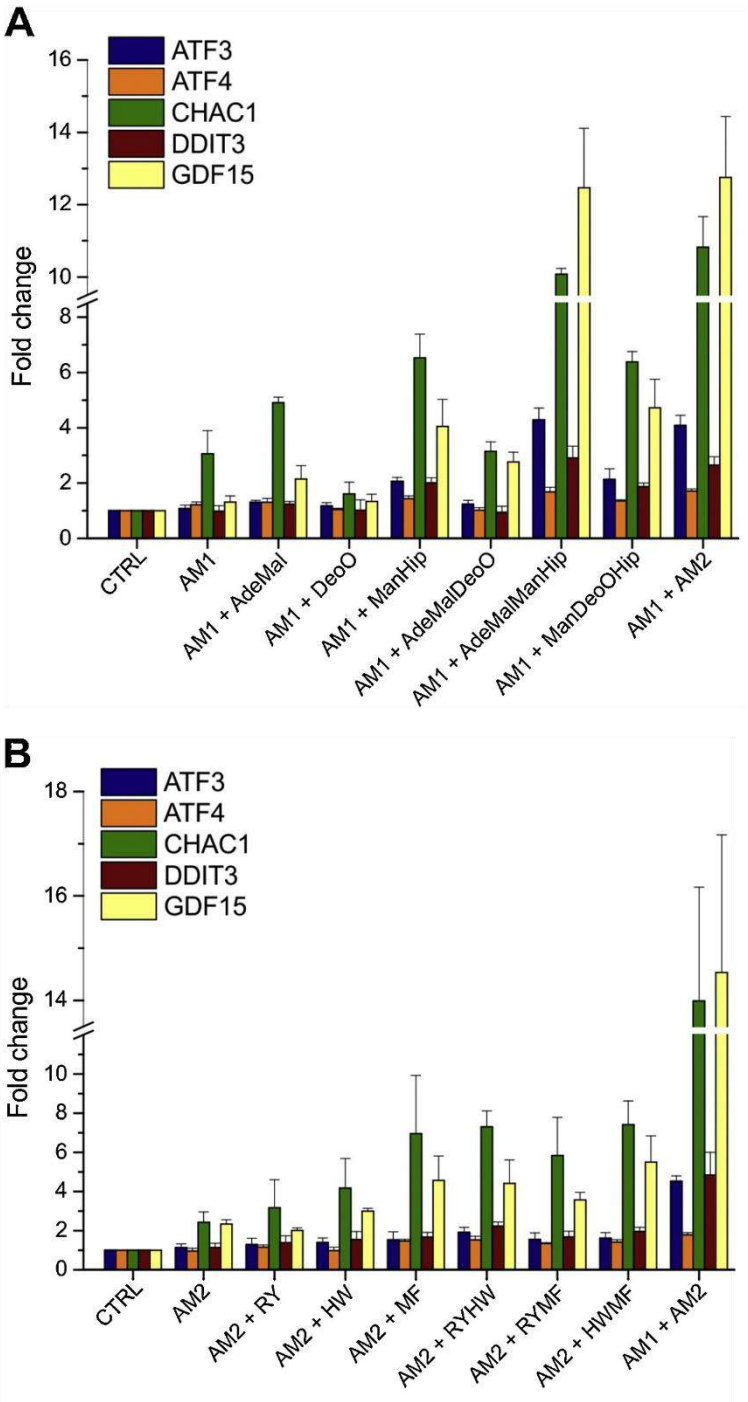

Figure 13. Ten out of the sixteen AM16 components are sufficient to induce ER stress. (A) HeLa cells were treated with AM1, AM1 + AM2, or AM1 and the indicated combinations of adenine (Ade), L-(-)-malic acid (Mal), 2-deoxy-D-ribose (Deo), orotic acid (O), D-(+)-mannose (Man) and hippuric acid (Hip) for 24 h. ATF3, ATF4, CHAC1, DDIT3, GDF15 mRNA levels were detected with qRT-PCR. Bars represent the fold change compared to CTRL. Normalized expression values and significance values are provided in Table S2. **(B)** HeLa cells were treated with AM2, AM1 + AM2, or AM2 and the indicated combinations of L-arginine (R), L-tyrosine (Y), L-histidine (H), L-tryptophan (W), L-methionine (M), L-phenylalanine (F) for 24 h. ATF3, ATF4, CHAC1, DDIT3, GDF15 mRNA levels were detected with qRT-PCR. Bars represent the fold change compared to CTRL. Normalized expression values and significance values are provided in Table S2.

The effect of this ten component mixture (AM10) was further analyzed, together with the six component mixture (AM6) containing compounds not necessary for ER stress gene induction (vitamins, Deo, O). We have found that AM10 induced the expression of ER stress genes to levels comparable with AM16, while AM6 had no effect **(Figure 14A)**. ISRIB completely inhibited the increase of *ATF4*, *CHAC1*, *DDIT3* transcripts after 24 hours AM10 or AM16 treatment, but was not able to completely block the induction of *ATF3* and *GDF15* **(Figure 14A)**. The cell growth inhibitory effect of AM10 was also attenuated but not completely blocked by ISRIB **(Figure 14B)**.

The AM10 induced changes in gene expression and the cell growth inhibitory effect could also be demonstrated in PC-3 **(Figure 15A,D)**, MCF-7 **(Figure 15B,E)** and Caco-2 cells **(Figure 15C,F)**.

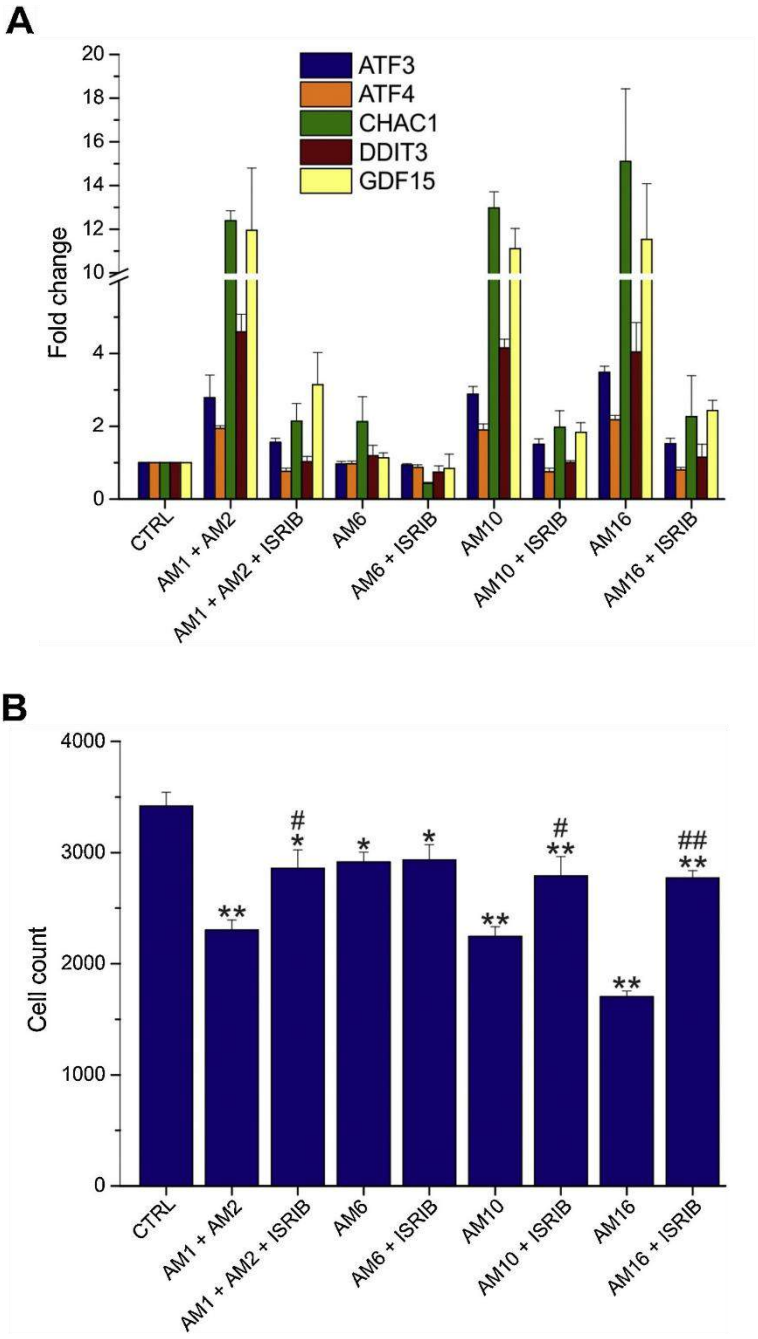

Figure 14. AM10 induces ER stress relelated gene expression and cell growth inhibition to levels comparable with AM16. (A) HeLa cells were pretreated with vehicle or 500 nM ISRIB for 1 h, followed by co-treatment with AM1 + AM2, AM6, AM10 or AM16 for 24 h. *ATF3*, *ATF4*, *CHAC1*, *DDIT3*, *GDF15* mRNA levels were detected with qRT-PCR. Bars represent the fold change compared to CTRL. Normalized expression values and significance values are provided in Table S2. **(B)** HeLa cells were treated as in panel (A). Bars represent the cell counts per well (average ± standard deviation of three independent experiments). *$p < 0.05$, **$p < 0.001$ vs. CTRL; #$p < 0.05$, ##$p < 0.001$ vs. the corresponding vehicle treated sample (ANOVA, Bonferroni test).

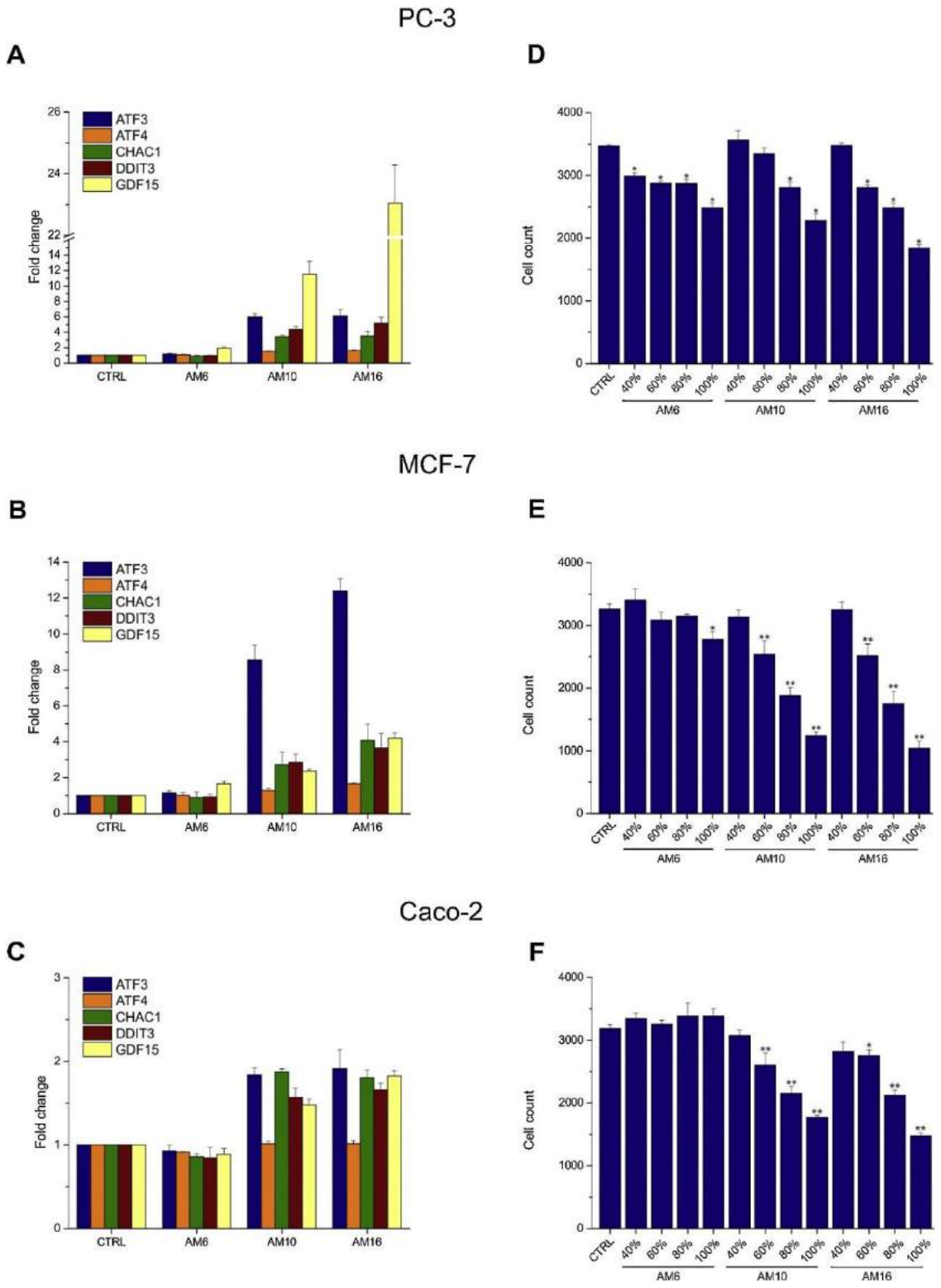

Figure 15. Ten out of the sixteen AM16 components are sufficient to induce ER stress in PC-3, MCF-7, and Caco-2. (A-C) PC-3 (A), MCF-7 (B), Caco-2 (C) cells were treated with AM6, AM10, or AM16 for 24 h. *ATF3*, *ATF4*, *CHAC1*, *DDIT3*, *GDF15* mRNA levels were detected with qRT-PCR. Bars represent the fold change compared to CTRL. Normalized expression values and significance values are provided in Table S2. **(D-F)** PC-3 (D), MCF-7 (E), Caco-2 (F) cells were treated as in panel (A-C). Bars represent the cell counts per well (average ± standard deviation of three independent experiments). *$p < 0.05$, **$p < 0.001$ vs. CTRL (ANOVA, Bonferroni test).

Taken together, the components of AM10 are sufficient to induce ER stress, while the other six components are able to enhance the cell growth inhibitory effect.

7.5. Role of ATF3, GDF15 and mIR-3189-3p on the effect of AM16

Since *ATF3* and *GDF15* expression could not be completely blocked by ISRIB upon AM16 treatment, the effect of the knockdown of these proteins alone, or in combination with ISRIB was analyzed on AM16 induced cell growth inhibition. We found that the knockdown of *ATF3* and *GDF15* **(Figure 16A,B)** had no effect on cell number decrease caused by 24 hours treatment with AM16, even in the presence of ISRIB **(Figure 16C)**.

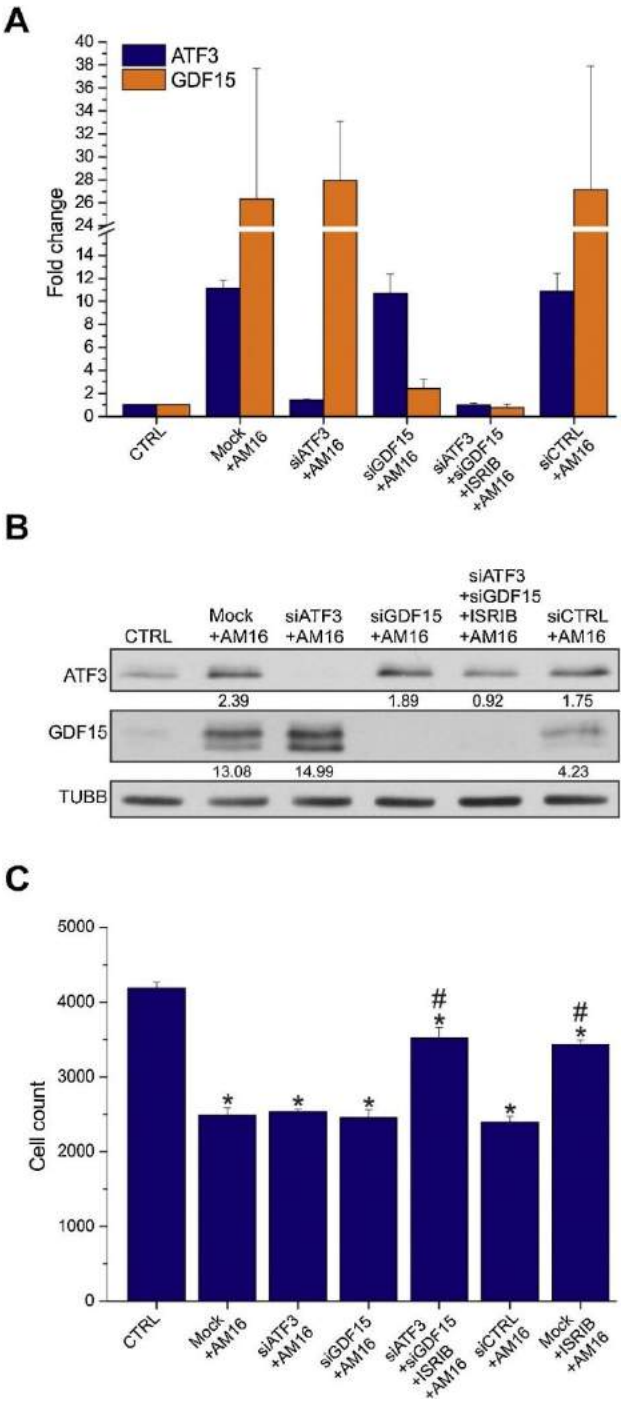

Figure 16. Knockdown of ATF3 and GDF15 does not attenuate the effect of AM. (A) HeLa cells were transfected with 50 nM siRNA against *ATF3* (siATF3), 50 nM siRNA against *GDF15* (siGDF15), with the combination of 50 nM siATF3 and 50 nM siGDF15, 100 nM siRNA control (siCTRL), or were mock transfected (Mock). 24 h after transfection cells were treated with vehicle or 500 nM ISRIB for 1 h, followed by co-treatment with AM16 for 24 h. *ATF3* and *GDF15* mRNA levels were detected with qRT-PCR. Bars represent the fold change compared to CTRL. Normalized expression values and significance values are provided in Table S2. **(B)** Representative western-blot for ATF3 and GDF15 in Hela cells transfected and treated as in panel (A). TUBB was used as loading control. **(C)** HeLa cells were transfected and treated as in panel (A). Bars represent the cell counts per well (average ± standard deviation of three independent experiments). *p < 0.001 vs. CTRL; #p < 0.001 vs. Mock (ANOVA, Bonferroni test).

Next, we focused on an intronic miRNA of *GDF15*, the mIR-3189-3p, which is co-expressed with *GDF15* and was demonstrated to have pro-apoptotic activity (Jones et al 2015). We measured the induction of mIR-3189-3p upon treatment with AM16, and we found a 3-fold increase in the expression of mIR-3189-3p after 24 hours treatment with AM16 in HeLa cells, CM had no effect. Tunicamycin, a known inducer of ER stress, also produced a 4-fold increase in mIR-3189-3p level **(Figure 17A)**. To test whether mIR-3189-3p has a role in the cell growth inhibition caused by AM16, we applied a miRNA inhibitor. To verify the functionality of the mIR-3189-3p inhibitor we have tested the ability of the inhibitor to block the effect of mIR-3189-3p mimic on the transcript levels of two verified mIR-3189-3p targets, Rho guanine nucleotide exchange factor 25 (ARHGEF25) and splicing factor 3b subunit 2 (SF3B2) (Jeansonne et al. 2015). As expected, the mIR-3189-3p mimic significantly reduced the transcript levels of ARHGEF25 and SF3B2, which was completely blocked by the mIR-3189-3p inhibitor, but not by a negative control miRNA inhibitor **(Figure 17B)**. However, despite the efficient knockdown of miR-3189-3p, we could not prevent the decrease the cell growth inhibitory effect of AM16 **(Figure 17C)**. Interestingly, the combination of mIR-3189-3p inhibitor with siGDF15 at high concentrations (200 nM and 100 nM, respectively) also failed to reduce the cell growth inhibitory effect of the AM16 **(Figure 17C)**.

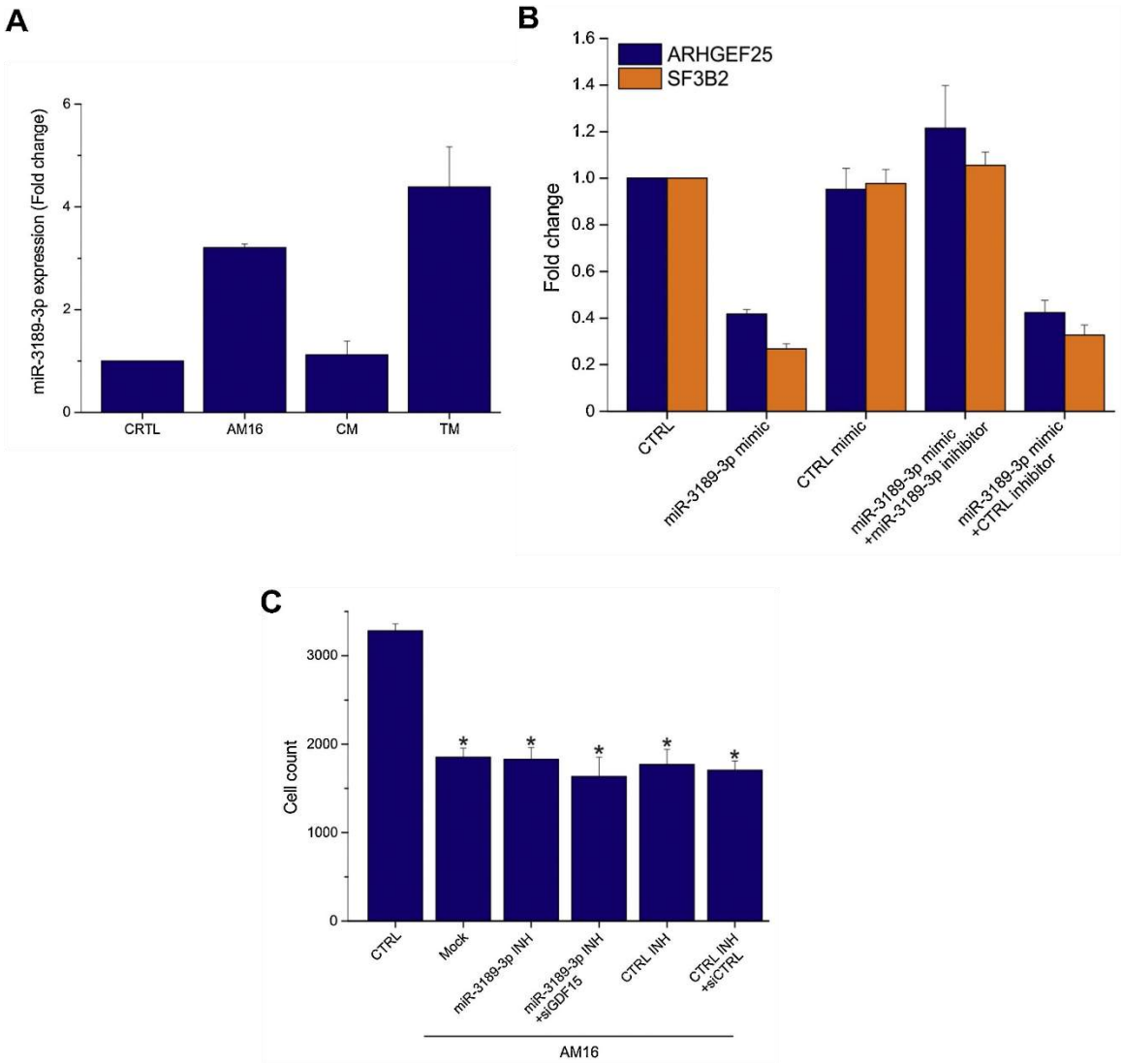

Figure 17. Knockdown of mIR-3189-3p failed to inhibit the cell growth inhibitory effect of AM16. (A) HeLa cells were treated for 24 h with AM16, CM or TM (5 μM). mIR-3189-3p level was detected with qRT-PCR. Bars represent the fold change compared to CTRL. Normalized expression values and significance values are provided in Table S2. **(B)** HeLa cells were transfected with 10 nM miR-3189-3p mimic, 10 nM negative control miRNA mimic (CTRL mimic), with the combination of 10 nM miR-3189-3p mimic and 50 nM miR-3189-3p inhibitor (miR-3189-3p mimic + miR-3189-3p INH), or with the combination of 10 nM miR-3189-3p mimic and 50 nM negative control miRNA inhibitor (miR-3189-3p mimic + CTRL INH) for 24 h. ARHGEF25 and SF3B2 mRNA levels were detected with qRT-PCR after an additional 24 h. Bars represent the fold change compared to CTRL. Normalized expression values and significance values are provided in Table S2. **(C)** HeLa cells were transfected with 50 nM miR-3189-3p inhibitor (miR-3189-3p INH), with the combination of 200 nM miR-3189-3p inhibitor and 100 nM siRNA against GDF15 (miR-3189-3p INH + siGDF15), 50 nM negative control miRNA inhibitor (CTRL INH), or with the combination of 200 nM negative control miRNA inhibitor and 100 nM siRNA control (miR-3189-3p INH + siCTRL), 24 h after transfection cells were treated with AM16 for 24 h. Bars represent the cell counts per well (average ± standard deviation of three independent experiments). *$p < 0.001$ vs. CTRL (ANOVA, Bonferroni test).

The role of mIR-3189-3p was further investigated, and we found that mIR-3189-3p mimic was able to significantly increase the levels of *ATF3*, *DDIT3*, and *GDF15* transcripts, which was completely blocked by miR-3189-3p inhibitor, but not by negative control miRNA inhibitor **(Figure 18A)**. The increase in CHAC1 transcript level proved to be non-specific as a negative control miRNA mimic also produced a significant increase **(Figure 18A)**. At the protein level the increased expression of ATF3 and GDF15 could be verified, while CHAC1, DDIT3 and ATF4 were not specifically induced by mIR-3189-3p transfection **(Figure 18B)**.

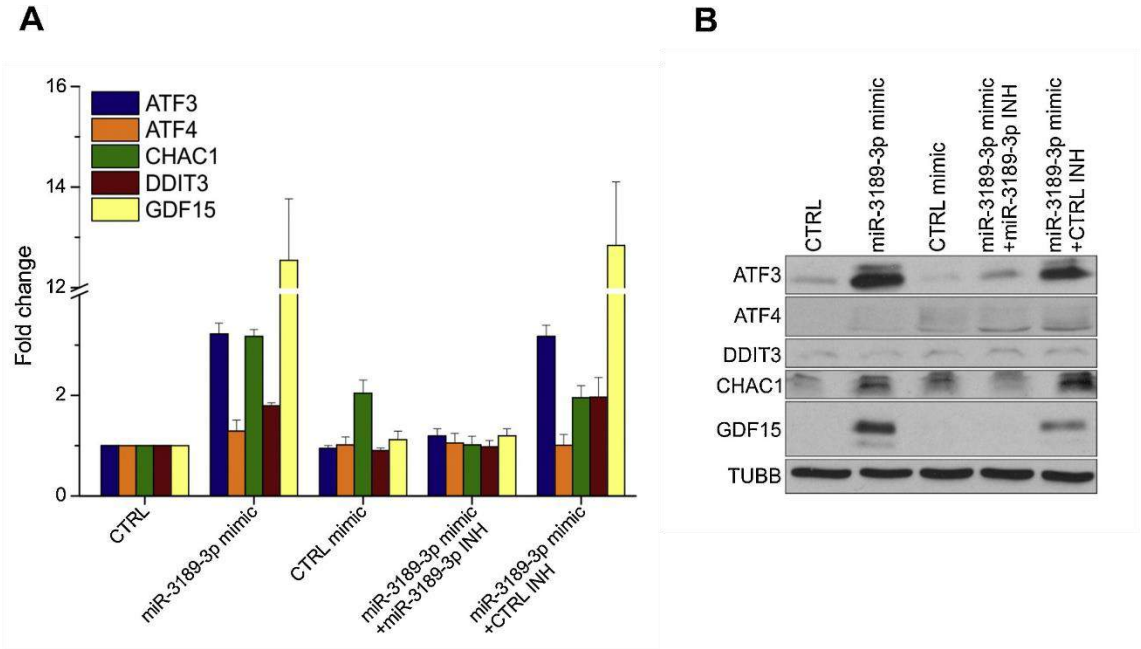

Figure 18. mIR-3189-3p enhances the expression of ER stress genes. (A) HeLa cells were transfected with 10 nM miR-3189-3p mimic, 10 nM negative control miRNA mimic (CTRL mimic), with the combination of 10 nM miR-3189-3p mimic and 50 nM miR-3189-3p inhibitor (miR-3189-3p mimic + miR-3189-3p INH), or with the combination of 10 nM miR-3189-3p mimic and 50 nM negative control miRNA inhibitor (miR-3189-3p mimic + CTRL INH) for 24 h. *ATF3*, *ATF4*, *CHAC1*, *DDIT3*, *GDF15* mRNA levels were detected with qRT-PCR after an additional 24 h. Bars represent the fold change compared to CTRL. Normalized expression values and significance values are provided in Table S2. **(B)** Representative western-blots for ATF3, ATF4, DDIT3, CHAC1 and GDF15 in Hela cells transfected as in panel (A). TUBB was used as loading control.

The transcription factor Jun dimerization protein 2 (JDP2) suppresses the transcription of *ATF3* and *DDIT3* (Chérasse et al. 2008; Weidenfeld-Baranboim et al. 2009), and multiple histone deacetylase family (HDACs) members are associated with JDP2 at the promoters of *ATF3* and *DDIT3* (Chérasse et al. 2008; Darlyuk-Saadon et al. 2012). Hence we measured the mRNA levels of *HDAC1-6*, *JDP2* and two additional JDP2 targets germ cell associated 1 (*GSG1*) and protocadherin 7 (*PCDH7*) (Weidenfeld-Baranboim et al. 2009) after transfection with mIR-3189-3p mimic. As a result, it was observed that the levels of *HDAC1*, *HDAC3*, *JDP2*

transcripts were decreased, which was completely blocked by mIR-3189-3p inhibitor, and the levels of *GSG1*, *PCDH7* transcripts were significantly increased **(Figure 19)**. The upregulation of *GSG1* and *PCDH7* further verifies the downregulation of *JDP2*.

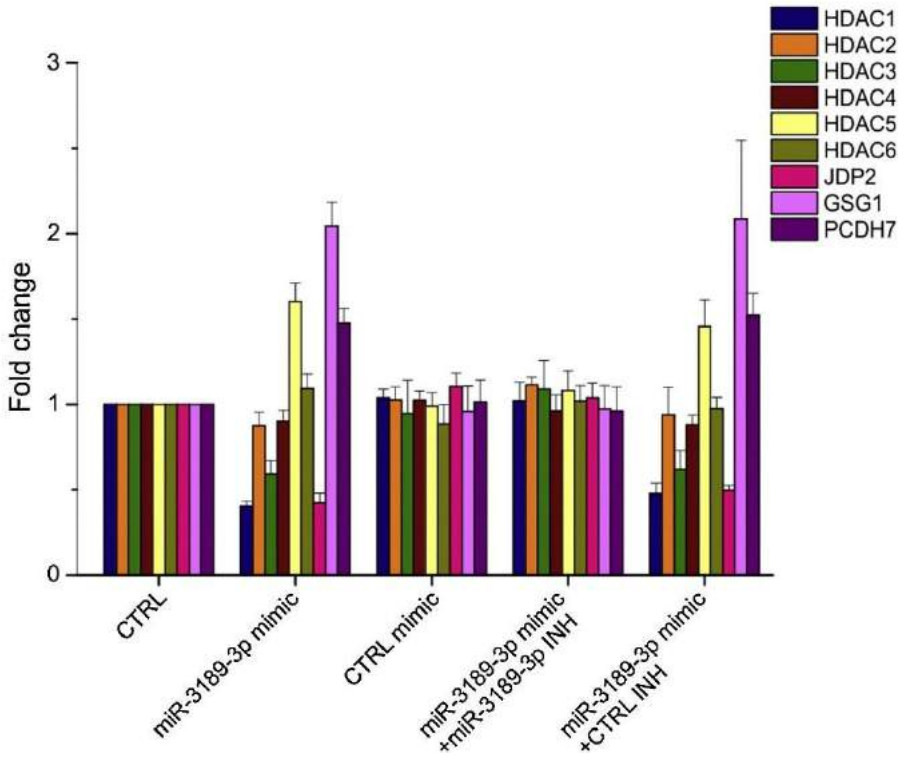

Figure 19. Expression of HDAC1-6, JDP2, GSG1, and PCDH7 after miR-3189-3p transfection. HeLa cells were transfected with 10 nM miR-3189-3p mimic, 10 nM negative control miRNA mimic (CTRL mimic), with the combination of 10 nM miR-3189-3p mimic and 50 nM miR-3189-3p inhibitor (miR-3189-3p mimic + miR-3189-3p INH), or with the combination of 10 nM miR-3189-3p mimic and 50 nM negative control miRNA inhibitor (miR-3189-3p mimic + CTRL INH) for 24 hours. *HDAC1-6*, *JDP2*, *GSG1*, and *PCDH7* mRNA levels were detected with qRT-PCR after an additional 24 hours. Bars represent the fold change compared to CTRL. Normalized expression values and significance values are provided in Table S2.

Taken together these results indicate that ATF3 and GDF15 are not essential for the cell growth inhibitory effect of the AM16, whereas the mIR-3189-3p, upregulated by treatment with AM16, is probably able to increase the expression of *ATF3* and *DDIT3* through the downregulation of *JDP2*, *HDAC1* and *HDAC3*.

7.6. Investigation of cell fate outcomes- cell cycle arrest and cell death- caused by AM16 treatment in cancer cells

Since we were not able to completely inhibit the effect of AM16, we further investigated whether the effect of AM16 is mainly due to cytotoxic, growth arresting or apoptosis inducing activity. The number of necrotic/late apoptotic cells was increased in HeLa cells upon treatment with AM16 as demonstrated with cytocalcein/7-AAD staining **(Figure 20A,B)**. In addition, treatment of HeLa cells with AM16 caused cell growth arrest measured with EdU incorporation **(Figure 20C-E)** and significantly increased the number of apoptotic cells measured with TUNEL assay **(Figure 20F,G)**.

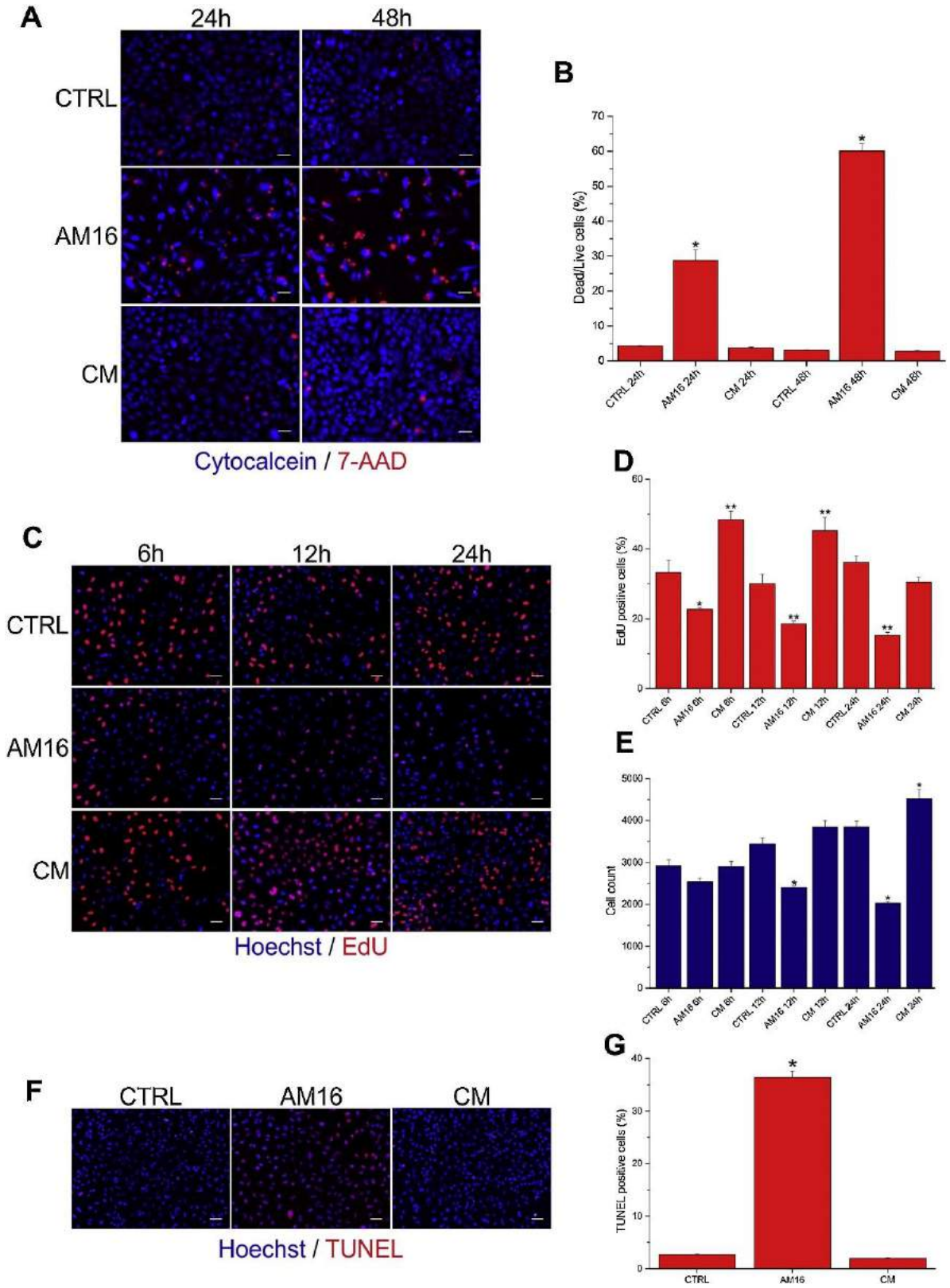

Figure 20. The AM16 has cytotoxic, anti-proliferative and apoptosis inducing effect. (A) Immunofluorescence pictures of HeLa cells treated with AM16 or CM for 24 h and 48 h. Live cells were labeled with cytocalcein violet 450 (blue), and dead cells were detected with 7-AAD (red). **(B)** Quantification of the percentage of dead cells treated as in panel (A). Bars represent the average ± standard deviation of three independent experiments. *p < 0.05 vs. the corresponding control sample (Welch test followed by Games-Howell test). **(C)** EdU labelling

(red) of HeLa cells treated with AM16 or CM for the indicated periods of time. Nuclei were labelled with Hoechst 33342 (blue). **(D)** Quantification of the percentage of EdU positive HeLa cells treated as in panel (C). Bars represent the average ± standard deviation of three independent experiments. *p < 0.05, **p < 0.001 vs. the corresponding CTRL (ANOVA, Bonferroni test). **(E)** Quantification of the number of HeLa cells treated as in panel (C). Bars represent the cell counts per well (average ± standard deviation of three independent experiments). *p < 0.001 vs. the corresponding CTRL (ANOVA, Bonferroni test). **(F)** TUNEL labelling (red) of HeLa cells treated with AM16 or CM for 24 h. Nuclei were labelled with Hoechst 33342 (blue). **(G)** Quantification of the percentage of TUNEL positive HeLa cells treated as in panel (F). Bars represent the average ± standard deviation of three independent experiments. *p < 0.001 vs. CTRL (ANOVA, Bonferroni test). Scale bars: 60 μm.

Next we investigated the contribution of apoptosis, autophagy, ferroptosis and necroptosis to the effect of AM16 using different inhibitors of these cell death pathways. AM16 and the inhibitors were applied in dilution series. AM16 was used alone or in combination with the inhibitors, and we measured the combination index (CI) using cell counting. The CI is the quantitative measure of interaction between the effect of inhibitors and AM16 (CI > 1.1 indicates antagonism, CI < 0.9 indicates synergism) (Chou and Talalay 1981; Chou and Talalay 1984; Chou 2006).

We showed that the treatment with AM16 causes a dose dependent decrease in the number of HeLa, MCF-7, PC-3, Caco-2, HT-29 and A549 cells **(Figure 21A)**. Then we selected the optimal cell line for investigating the role of ferroptosis. Erastin, a known inducer of ferroptosis, was tested on HeLa, MCF-7, PC-3, Caco-2, HT-29 and A549 cells, in combination with the inhibitors of ferroptosis: the iron chelator DFO and the lipid peroxidation inhibitor Fer-1. Effect of erastin could be only inhibited in A549 cells **(Figure 21B)**, indicating that mutant RAS present only in A549 cells, while Hela, MCF-7, PC-3, Caco-2, and HT-29 cells have wild-type RAS. Thus we have chosen the HeLa and A549 cell lines to test the modulatory effect of ferroptosis inhibitors: DFO, Fer-1, the lipophilic antioxidant trolox, the system Xc^- bypassing agent 2-ME (Dixon et al. 2012) and the mitogen-activated protein kinase kinase (MEK) inhibitor/antioxidant U0126 (Stockwell et al. 2017) on the effect of AM16. We demonstrated a dose dependent decrease in cell number of HeLa and A549 cells upon treatment with AM16, however the inhibitors of ferroptosis could not prevent the effect of AM16 in HeLa and A549 cells **(Figure 21C)**.

To determine whether AM16 treatment causes necroptosis we tested the RIPK1 inhibitor Nec-1 and the MLKL inhibitor NSA on HT-29 cells because HeLa, PC-3, MCF-7 and Caco-2 cells are missing components of the necroptosis signaling cascade and not responding to the TNF-α + z-VAD-fmk + Smac mimetic (T + Z + S) necroptosis inducing stimulus (Sosna et al.

2014; Su et al. 2016). The inhibitors of necroptosis failed to prevent the dose dependent cell number decrease of AM16 in HT-29 cells, while effectively blocked the necroptosis induced by (T + Z + S) **(Figure 21D)**.

Next we examined the effect of inhibitors of caspase, cathepsin or calpain proteases (z-VAD-fmk, E64d, ALLN), cyclophilin D (CSA), and autophagy/lysosomal function (BAF, 3-MA, and CHLQ) in HeLa, A549, and HT-29 cells. We have found that z-VAD-fmk partially antagonized the effect of AM16 in A549 and HT-29 (CI: 1.14-1.42), but not in HeLa cells, whereas E64d, ALLN, CSA partially antagonized the effect of AM16 in all three cell lines (CI: 1.2-1.67) **(Figure 21E)**. We have also tested the combination of z-VAD-fmk, E64d, ALLN and CSA (Z + E + A + C), which also caused a partial and consistent antagonism, however it failed to completely block the effect of AM16. Moreover, Z + E + A + C significantly reduced the cell number when applied alone, therefore it was not investigated further. The autophagy inhibitors BAF and 3-MA enhanced the effect of the AM16 in all three cell lines (CI: 0.32-0.86).

These results show that ferroptosis and necroptosis are not participated in AM16 induced cell death, while apoptosis has an important role in the effect of AM16.

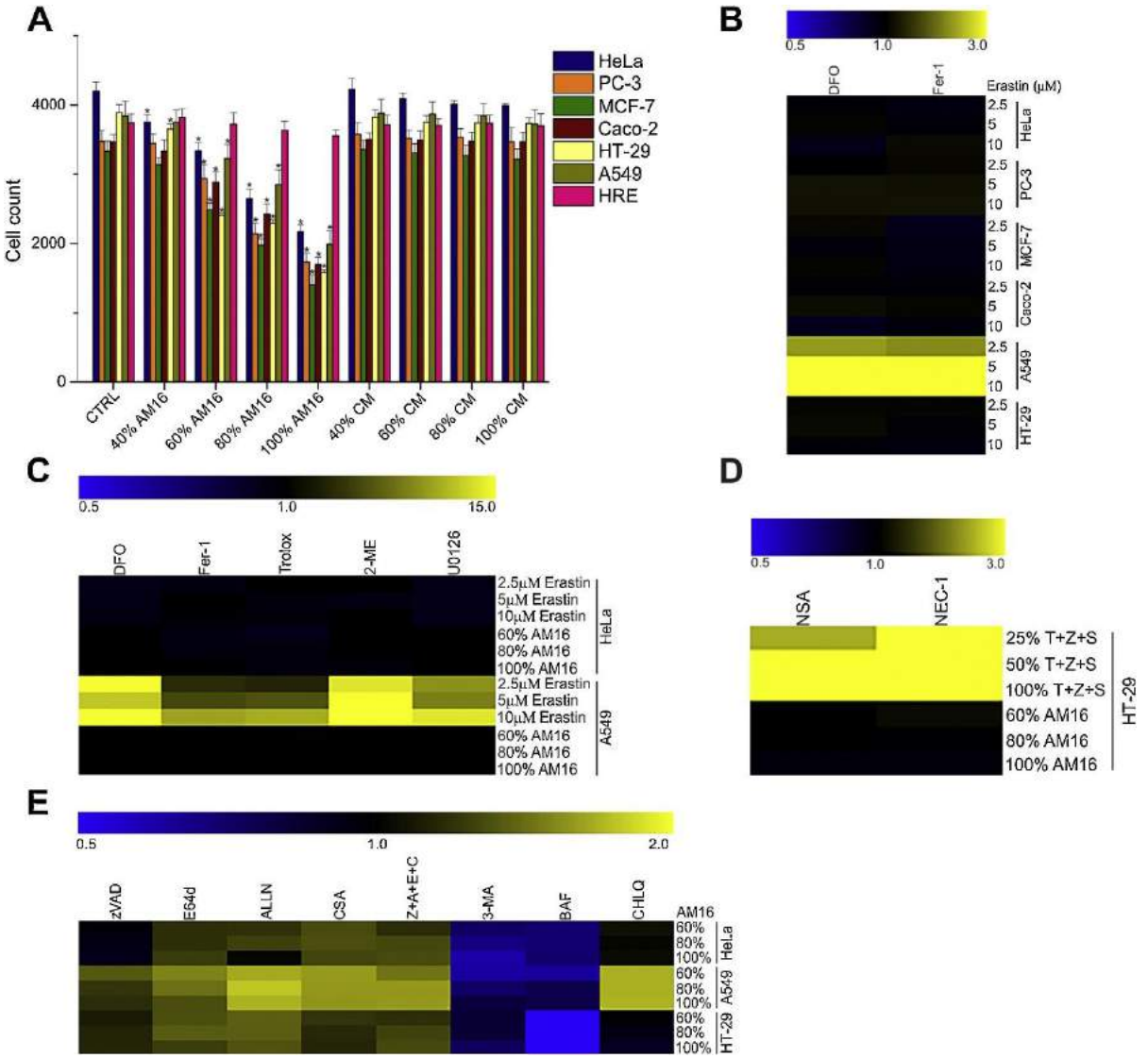

Figure 21. Inhibitors of apoptosis, but not autophagy, ferroptosis and necroptosis attenuate the effect of the AM16. (A) HeLa, PC-3, MCF-7, Caco-2, HT-29, A549 and HRE cells were treated with dilution series of AM16 or CM for 24 h. The dilution of the mixtures is expressed in percentage. Bars represent the cell counts per well (average ± standard deviation of two independent experiments). *p < 0.001 vs. the corresponding CTRL (ANOVA, Bonferroni test). **(B)** Heatmap of combination index (CI) values for HeLa, PC-3, MCF-7, Caco-2, HT-29, A549 cells treated with the indicated concentrations of erastin in combination with 100 μM DFO or 20 μM Fer-1 for 24 h. Values represent the average of two independent experiments. **(C)** Heatmap of CI values for HeLa, A549 cells were treated with the indicated concentrations of erastin or AM16 in combination with 100 μM DFO, 20 μM Fer-1, 300 μM trolox, 20 μM 2-ME or 20 μM U0126 for 24 h. Values represent the average of two independent experiments. **(D)** Heatmap of CI values for HT-29 cells treated with the indicated concentrations of TNF-α + z-VAD-fmk + smac mimetic (T+Z+S) or AM16 in combination with 5 μM NSA or 10 μM Nec-1 for 24 h. 100 % T+Z+S contains 20 ng/ml TNF-α, 20 μM z-VAD-fmk and 0.5 μM BV6 smac mimetic. Values represent the average of two independent experiments. **(E)** Heatmap of CI values for HeLa, A549 and HT-29 cells treated with the indicated concentrations of AM16 in combination with 80 μM z-VAD-fmk, 50 μM E64d, 0.5 μM ALLN, 10 μM CSA, 40 μM z-VAD-fmk + 25 μM E64d + 0.25 μM ALLN + 50 μM CSA (Z+E+A+C), 4 mM 3-methyladenine (3-MA), 1 μM BAF or 50 μM CHLQ for 24 h. Values represent the average of two independent experiments.

7.7. Role of BBC3 and PMAIP1 on the effect of AM16

Next we wanted to investigate whether the induction of ER stress is responsible for the anti-proliferative and apoptosis inducing effect of the AM16. HeLa cells were treated with AM16 in the presence of ISRIB and determined the number of dead, EdU positive and TUNEL positive cells after 24 hours. ISRIB significantly but not totally inhibited the AM16 induced increase in the number of dead and TUNEL positive cells, while it completely restored the AM16 suppressed cell proliferation **(Figure 22A,B)**.

Since we were not able to inhibit totally the effect of AM16, we searched for additional mediators of AM16 induced apoptosis. We found that the transcript levels of the apoptotic mediators, *BBC3* and *PMAIP1* were elevated upon treatment with AM16 in HeLa, MCF-7, PC-3 and Caco-2 cells. In addition, we tested how the knockdown of these mediators could influence the effect of AM16. The efficacy of knockdown was verified by qRT-PCR **(Figure 22C)**. The results show that both the single-knockdown of *BBC3* or *PMAIP1*, and double-knockdown, and the combination of knockdown and ISRIB significantly inhibited the effect of the AM16 **(Figure 22D)**. Interestingly, the combination of double knockdown and ISRIB completely inhibited the effect of AM16.

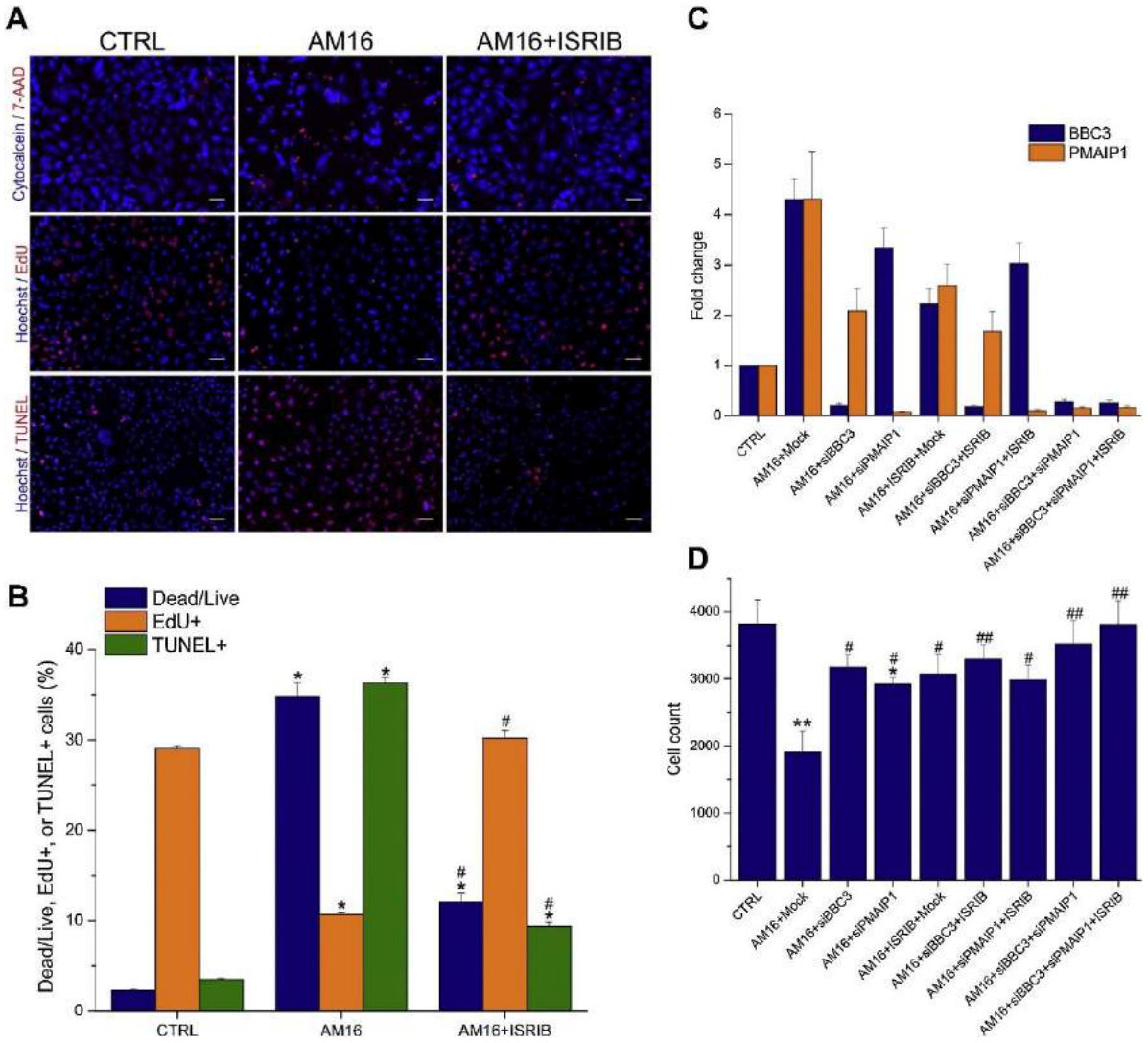

Figure 22. Combination of ER stress inhibition with knockdown of BBC3 and PMAIP1 completely abrogates the effect of the AM16. (A) Immunofluorescence pictures of HeLa cells treated with AM16 or AM16 + 500 nM ISRIB for 24 h. Upper row: live cells were labeled with cytocalcein violet 450 (blue), dead cells were detected with 7-AAD (red). Middle row: EdU labelling (red), Hoechst 33342 (blue). Lower row: TUNEL labelling (red), Hoechst 33342 (blue). Scale bars: 60 μm. **(B)** Quantification of the percentage of dead, EdU positive and TUNEL positive cells treated as in panel (A). Bars represent the average ± standard deviation of three independent experiments. *p < 0.001 vs. CTRL, #p < 0.001 vs. AM16 (ANOVA, Bonferroni test). **(C)** HeLa cells were transfected with 10 nM siRNA against BBC3 (siBBC3), 10 nM siRNA against PMAIP1 (siPMAIP1), with the combination of 10 nM siBBC3 and 10 nM siPMAIP1, or were mock transfected (Mock). 24 h after transfection cells were treated with vehicle or 500 nM ISRIB for 1 h, followed by co-treatment with AM16 for 24 h. *BBC3* and *PMAIP1* mRNA levels were detected with qRT-PCR. Bars represent the fold change compared to CTRL. Normalized expression values and significance values are provided in Table S2. **(D)** HeLa cells were transfected and treated as in panel (C). Bars represent the cell counts per well (average ± standard deviation of three independent experiments). *p < 0.05 vs. CTRL, **p < 0.001 vs. CTRL, #p < 0.05 vs. AM16, ##p < 0.001 vs. AM16 (ANOVA, Bonferroni test).

7.8. Identification of additional compounds capable to enhance the cell growth inhibitory effect of AM

Our next aim was to investigate additional molecules found in the serum to test whether other compounds are able to enhance the effect of the previously identified components of the AM. We examined 130 new compounds in a per se non-toxic concentration in combination with AM. We identified 34 new compounds which are able to enhance the effect of AM, though the extent of enhancement differed between the compounds **(Figure 23)**. The newly identified compounds are the following: D-phenylalanine, D-tryptophan, D-arginine, 5-hydroxi-L-tryptophan, melatonin, mandelic acid, 3,4-dihydroxymandelic acid, p-coumaric acid, trans-cinnamic acid, indole-3- acetic acid, phenylacetic acid, 3,4-dihydroxyphenylacetic acid, indole-3-pyruvic acid, phenylpyruvic acid, 4-hydroxy-phenylpyruvic acid, 3-phenyllactic acid, D-glyceric acid, glyceraldehyde, 3-methyl-2-oxobutyric acid, 4-guanidinobutyric acid, 3-methyl-2-oxovaleric acid, 4-methyl-2-oxovaleric acid, 3-hydroxy-3-methyl-glutaric acid, gentisic acid, urocanic acid, homovanillic acid, xanthurenic acid, levulinic acid, 4-hydroxy-benzoic acid, pyrrole-2-carboxylic acid, adenosine, agmatine, cysteamine, creatinine.

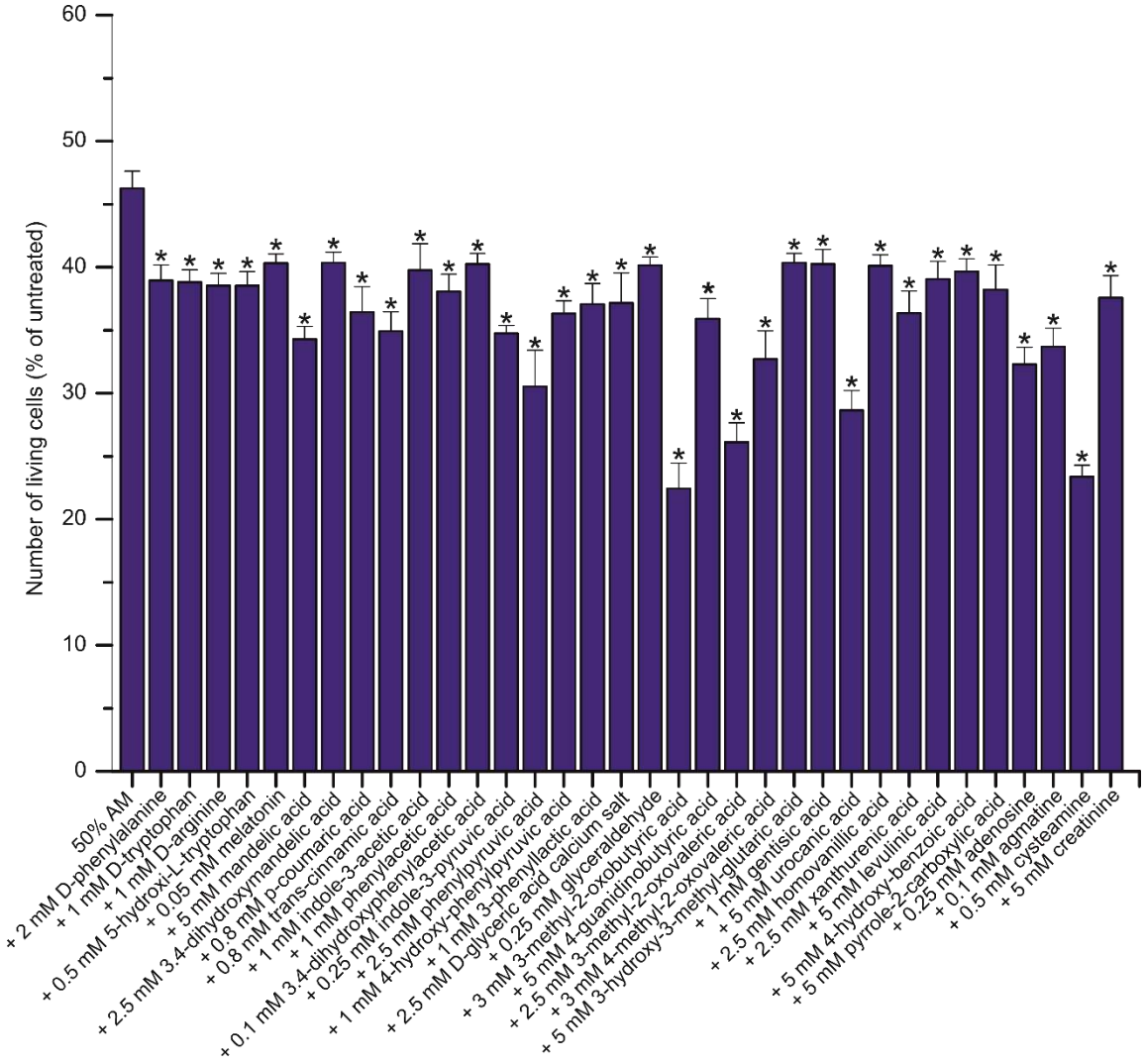

Figure 23. The newly identified 34 compounds enhance the cell growth inhibitory effect of AM. HeLa cells were treated with 50% AM alone or with the individual combination of 34 compounds and 50% AM for 48 h. The newly examined compounds were applied in per se nontoxic concentrations. Results are expressed as percentage of untreated control cells. The bars represent the average ± standard deviation of three independent experiments. *$p < 0.001$ versus 50% AM (ANOVA, Bonferroni test).

7.9. Effect of the new mixture on cancer cells

Next we examined the effect of the mixture containing the newly identified 34 compounds, called the new mixture (NM), compared to AM on HELA **(Figure 24A)**, PC-3 **(Figure 24B)**, MCF-7 **(Figure 24C)**, Caco-2 **(Figure 24D)**, HepG-2 **(Figure 24E)**, 4T1 **(Figure 24F)** cancer cells and on HRE **(Figure 24G)** normal cells. For the optimal detection of differences in efficacy, we used dilution series of the different mixtures (10%, 15%, 20%, 25%, and 30%). We have found that NM caused a significantly greater cell growth inhibition in different cancer cells than AM ($p<0.001$ vs. corresponding dilution of AM). We also tested the combination of AM and NM. The combined treatment (AM+NM) produced a more efficient cell growth

inhibition compared to AM or NM alone ($p<0.001$ vs. corresponding dilution of NM and vs. corresponding dilution of AM), furthermore the 30% AM+NM killed all the cells after 48 hours. The proliferation of HRE cells was not decreased by any of the mixtures **(Figure 24G)**.

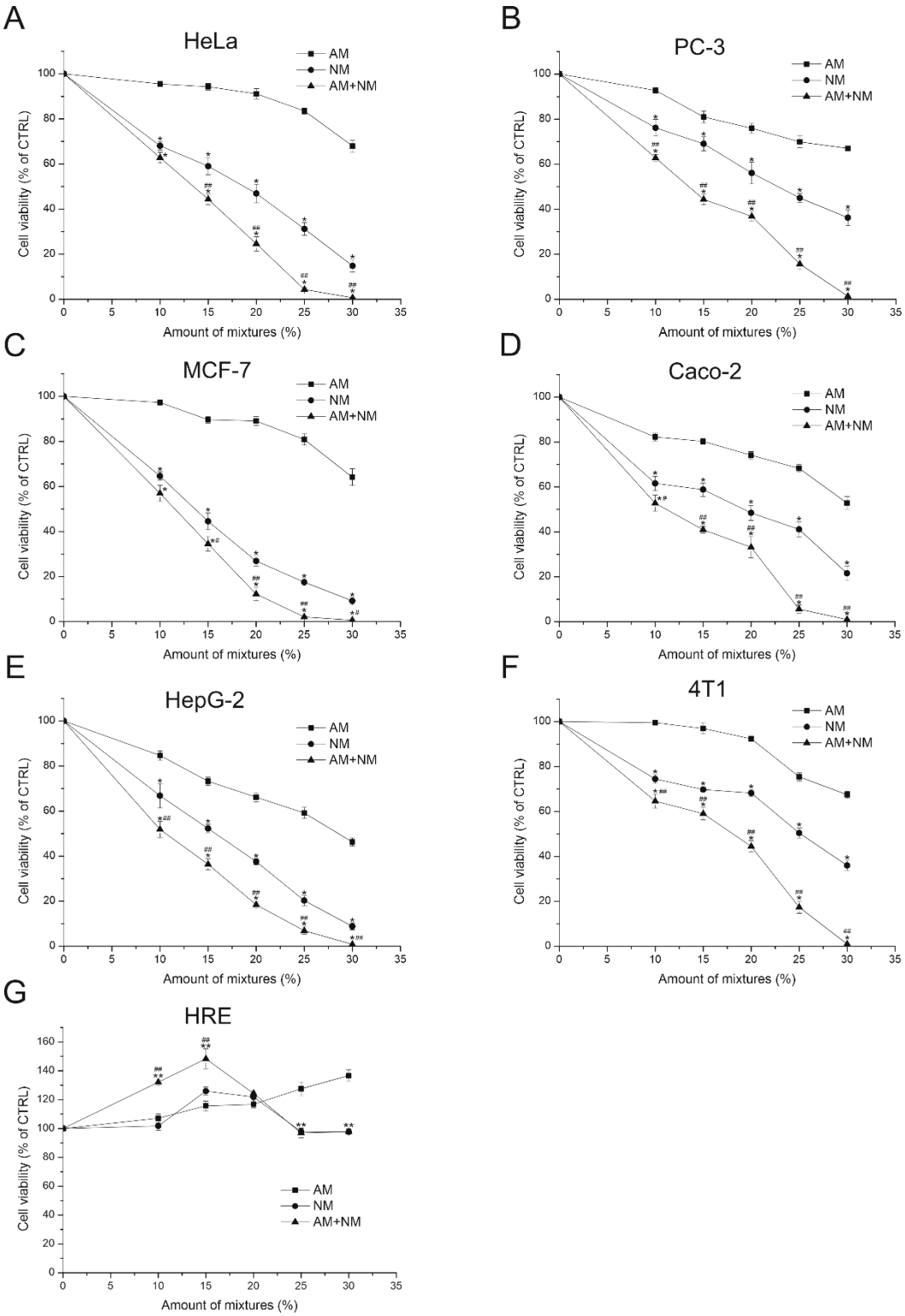

Figure 24. Comparison of the effect of NM and AM on the growth of cancer and normal cells. HeLa **(A)**, PC-3 **(B)**, MCF-7 **(C)**, Caco-2 **(D)**, HepG-2 **(E)**, 4T1 **(F)**, and HRE **(G)** cells were treated with the dilution series of AM, NM, or AM+NM for 48 h. The dilution of the

mixtures is expressed in percentage (10%, 15%, 20%, 25%, and 30%). The values represent the average ± standard deviation of three independent experiments. **$p < 0.001$; *$p < 0.05$ versus the corresponding dilution of AM; ##$p < 0.001$; #$p < 0.05$ versus the corresponding dilution of NM (ANOVA, Bonferroni test).

To further investigate the effect of NM, we measured the expression of certain pro- and anti-apoptotic genes, as well as genes regulating the cell cycle by qRT-PCR. HeLa cells were treated with 30% AM, 20% NM or the combination of 30% AM and 20% NM **(Figure 25)**. The combined treatment with 30% AM and 20% NM significantly induced the expression of the pro-apoptotic BH3-only protein encoding *BIM*, *BBC3*, *PMAIP1*, and the anti-apoptotic member of BCL-2 family encoding *BCL-2* compared to the untreated control. The expression levels of the pro-apoptotic death receptor genes, *DR4* (*TNFRSF10A*) and *DR5* (*TNFRSF10B*) were also increased, together with the anti-apoptotic protein encoding *BIRC2* and *BIRC3* transcript levels. The level of cell cycle inhibitor, *CDKN1A* was also substantially induced. 20% NM mixture applied alone also induced changes in the expression of pro- and anti-apoptotic genes but to a lesser extent than AM+NM. Treatment with 30% AM had a slight or no effect on the expression of genes investigated compared to the control.

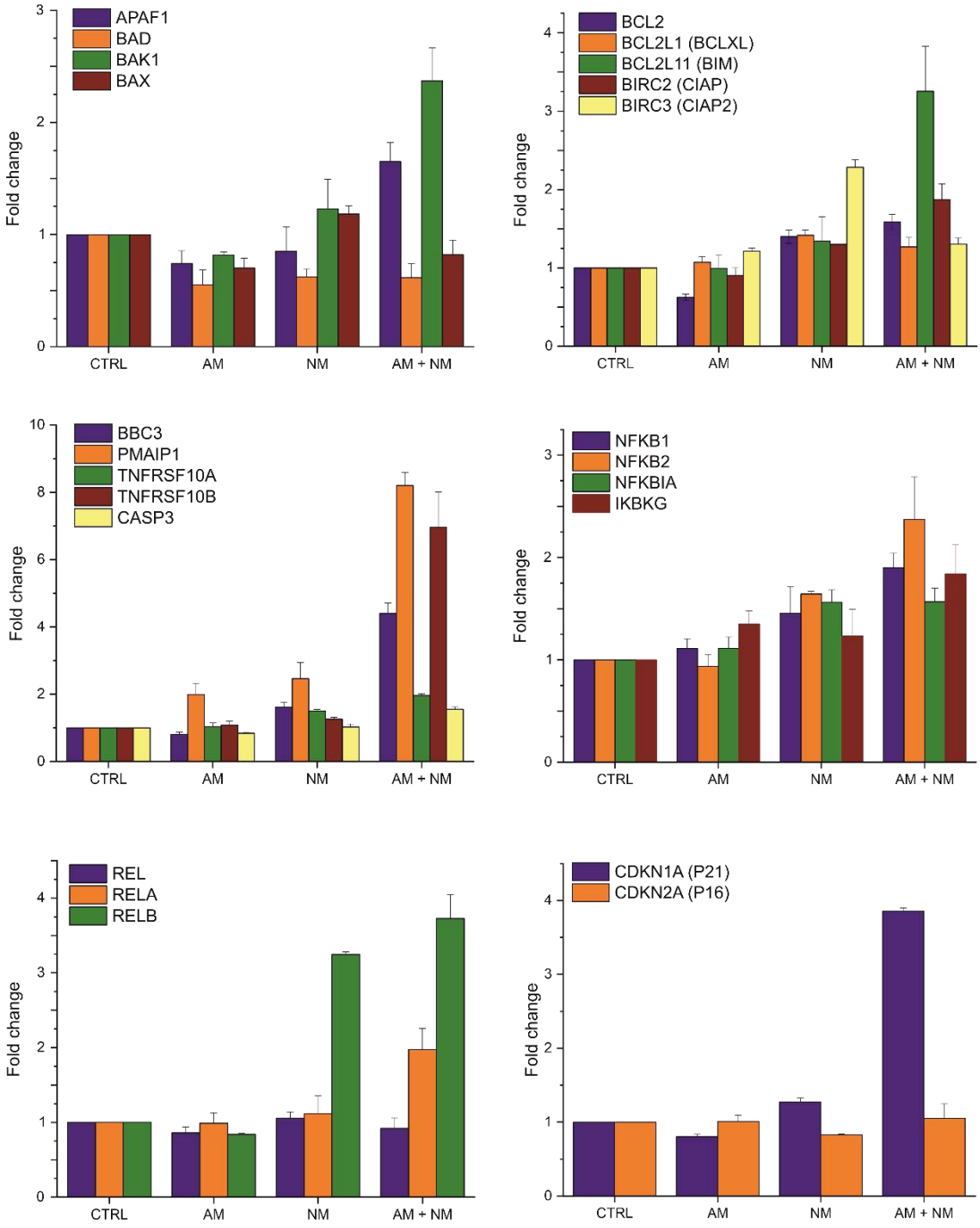

Figure 25. NM and the combination of AM and NM influence the expression of genes involved in apoptosis and cell cycle regulation. HeLa cells were treated with 20% AM, 30% NM, or the combination of 20% AM and 30% NM for 24 h. mRNA levels were detected with qRT-PCR. Bars represent the fold change compared to CTRL. Normalized expression values and significance values are provided in Table S2.

All together these results show that the mixture of new substances has a specific inhibitory effect on cancer cells greater than the AM, and the combination of AM and NM induces gene expression changes related to apoptosis and cell cycle arrest.

8. COLLECTION OF THE RESULTS GENERATED BY THIS STUDY

Investigation of the effect of AM16 in different cancer cell lines compared to HRE normal cells at both transcriptional and translational level revealed, that AM16 specifically induces gene expression changes characteristic for ER stress in cancer cells and upregulates UPR-induced proteins.

Results show that the UPR plays a significant role in the AM16 cell growth inhibitory effect and suggest that the PERK pathway is the major arm of the UPR activated by AM16.

Investigation of the relative contribution of the individual components of AM16 to the activation of the ER stress showed, that the amino acid components (L-arginine, L-tyrosine, L-histidine, L-tryptophan, L-methionine, and L-phenylalanine) if applied in conjunction with adenine, L-(-)-malic acid, D-(+)-mannose and hippuric acid are necessary and sufficient to induce ER stress.

Knockdown experiments of *ATF3* and *GDF15* revealed that they are not essential for the cell growth inhibitory effect of the AM16.

An intronic miRNA of *GDF15*, the mIR-3189-3p, upregulated by treatment with AM16, is probably able to increase the expression of *ATF3* and *DDIT3* through the downregulation of *JDP2*, *HDAC1* and *HDAC3*, which could be a novel miRNA mediated feedback mechanism of the transcriptional upregulation of certain UPR signaling components. However, mIR-3189-3p induction did not influenced the cell number reducing effect of AM16.

Results show the cell proliferation inhibition and the induction of apoptosis are the two main mechanisms involved in the effect of AM16, while ferroptosis and necroptosis are not participated in AM16 induced cell death.

The transcript levels of the apoptotic mediators, *BBC3* and *PMAIP1* were elevated upon treatment with AM16 in cancer cells, and the knockdown experiments showed that these mediators can influence the effect of AM16, moreover the combination of double knockdown of *BBC3* and *PMAIP1* and ISRIB completely inhibited the effect of AM16.

34 new compounds were identified which were able to significantly enhance the effect of the AM on different cancer cells when applied in a per se non-toxic concentration. These

compounds are mainly L-amino-acid metabolites, phenolic acids, D-amino acids and keto acids.

The mixture of new substances has a specific inhibitory effect on cancer cells greater than the AM and caused no toxic effect on HRE normal cells.

Investigation of the effect of the combination of AM and NM in cancer cells at transcriptional level showed the induction of apoptosis and cell cycle arrest.

9. DISCUSSION

In this work, we demonstrated that a defined mixture of amino acids, vitamins and other small molecules found in the serum (AM) selectively induce endoplasmic reticulum stress and activates the unfolded protein response in cancer cells. The treatment with AM first induces the expression of ER stress related genes (*ATF3, ATF4, DDIT3, XBP1*), followed by the upregulation of genes playing role in apoptosis and cell cycle regulation (*BBC3, PMAIP1, TNFRSF10B, CDKN1A*). These results, together with the temporally sustained induction of ATF4, ATF3, and DDIT3 proteins, point toward that AM induces ER stress mediated induction of apoptosis **(Figure 26)**.

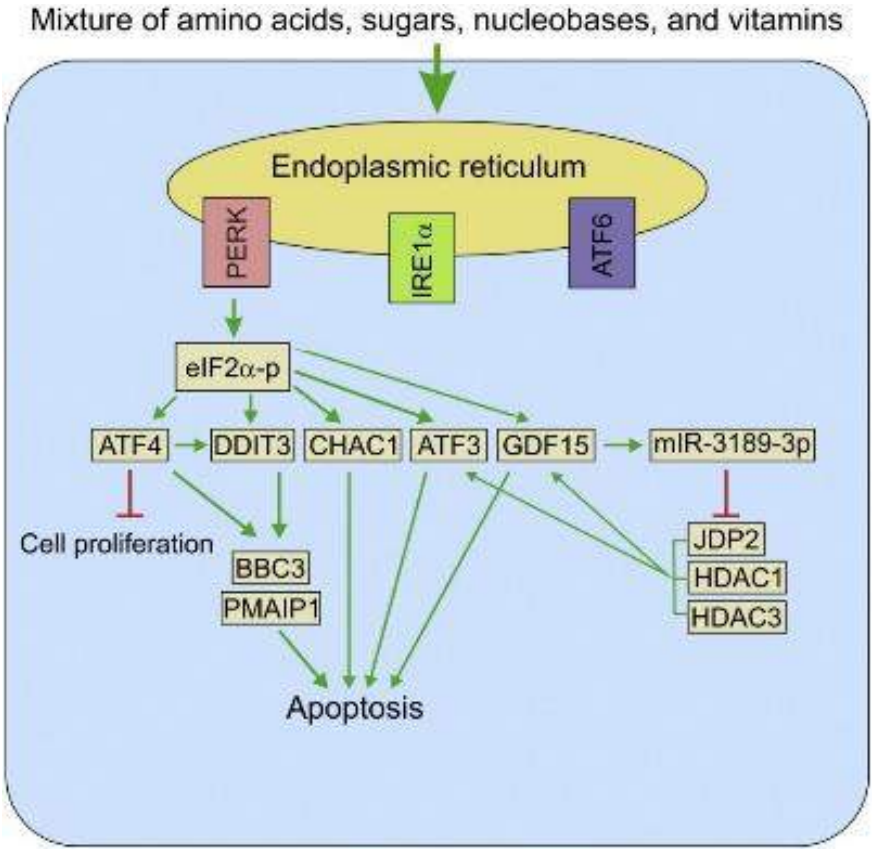

Figure 26. Schematic representation of the possible signaling pathways induced by AM16 in cancer cells.

Further analysis revealed that AM activates all three arms of the UPR signaling pathway (PERK, ATF6, IRE1α), however the results of our inhibition experiments suggest that the activation of PERK and the consequential eIF2α phosphorylation, accompanied by the preferential translation of the upstream open reading frame containing mRNA of *ATF4* (Young and Wek 2016) are the dominant ER stress contributors in the effect of AM.

ATF4 is considered to be the master transcription factor in UPR which can form heterodimers with various basic leucine zipper transcription factors, including its own target DDIT3 (Pakos-Zebrucka et al. 2016). The induction of ATF4 precedes the appearance of DDIT3 indicates, together with the finding that when the accumulation of ATF4 is blocked by ISRIB the increase in *DDIT3* transcript is diminished, that AM elicited induction of DDIT3 is mediated by ATF4. These findings are in agreement with the established role of ATF4 in the transcriptional activation of *DDIT3* (Averous et al. 2004; Clarke et al. 2014). The heterodimer formed by ATF4 and DDIT3 transcriptionally activates a number of additional UPR genes including *ATF3*, *PPP1R15A*, and *TRIB3* (Han et al. 2013). This is in agreement with our results which also show the induction of these genes upon treatment with AM.

ATF4 together with ATF3 is able to induce *CHAC1*, a gamma-glutamylcyclotransferase family member, which has been demonstrated to be part of the UPR cascade and possess pro-apoptotic activity mediated by its capability to degrade glutathione (Mungrue et al. 2009; Crawford et al. 2015). In agreement with this, our results demonstrate that AM induces CHAC1 in an ATF4 dependent manner, and raise the possibility that CHAC1 plays an important role in the apoptosis inducing effect of AM.

GDF15 is a member of the TGF-β superfamily with a diverse and controversial role in cancer development and progression. Depending on the experimental models used, the signaling context, or the histological type and stage of cancers both anti-tumorigenic and pro-tumorigenic functions of GDF15 have been reported (Wang et al. 2013). Our results demonstrate that treatment with AM induces GDF15 in all cancer cell lines tested.

The *GDF15* locus contains an intronic miRNA (mIR-3189), the 3p product of which (mIR-3189-3p) has been shown to transcriptionally co-regulated with *GDF15* and demonstrated to have potent *in vitro* pro-apoptotic and *in vivo* anti-tumorigenic activity in colon cancer cells (Jones et al. 2015). In addition, the tumor growth inhibitory effect of mIR-3189-3p on glioblastoma xenografts and the downregulation of mIR-3189-3p in glioblastoma clinical samples have been also reported (Jeansonne et al. 2015). Our finding that both AM and the known ER stress inducer tunicamycin increase the amount of mIR-3189-3p points toward the possible role of this miRNA in the UPR and the consequential induction of apoptosis. In fact, we have found that mIR-3189-3p specifically increased the amounts of *ATF3, DDIT3,* and *GDF15* transcripts. The transcription factor JDP2 has been shown to repress *ATF3* and *DDIT3* transcription (Chérasse et al. 2008; Weidenfeld-Baranboim et al. 2009), and various members of the histone deacetylase family (HDACs) were demonstrated to be associated with JDP2 at the promoters of *ATF3* and *DDIT3* (Chérasse et al. 2008; Darlyuk-Saadon et al. 2012). Our

results demonstrate a specific downregulation of *JDP2*, *HDAC1* and *HDAC3* transcripts by mIR-3189-3p, indicating that these mRNAs are targets of mIR-3189-3p. The downregulation of JDP2 was further confirmed by the increase in the transcript levels of *GSG1* and *PCDH7*, which are known targets of the repressor JDP2 (Weidenfeld-Baranboim et al. 2009). The downregulation of *HDAC1* and *HDAC3* transcripts by mIR-3189-3p is in agreement with a previous report (Jones et al. 2015). Based on the data above, we speculate that mIR-3189-3p enhances the expression of *ATF3* and *DDIT3* most probably through the downregulation of *JDP2*, *HDAC1* and *HDAC3* thereby lifting the repression form the promoters of *ATF3* and *DDIT3*. The increased amount of ATF3 and DDIT3 in turn could potentially stimulate the transcription of *GDF15* or stabilize the *GDF15* transcript, thus providing the basis for the mIR-3189-3p feedback loop **(Figure 26)**.

However, the fact that the individual inhibition of *ATF3*, *GDF15*, or mIR-3189-3p induction did not influenced the cell number reducing effect of AM indicate that these components are not essential for the anti-cancer activity of AM.

The relative contribution of individual AM components to the activation of the UPR revealed that the amino acid components (L-arginine, L-tyrosine, L-histidine, L-tryptophan, L-methionine, and L-phenylalanine) if applied in conjunction with adenine, L-(-)-malic acid, D-(+)-mannose and hippuric acid are necessary and sufficient to induce ER stress. To the best of our knowledge there are no reports implicating these substances in the activation of the UPR except L-arginine and D-(+)-mannose (Kubisch et al. 2006; Gao et al. 2011; Xu and DT 2015).

Our investigation revealed that the cell proliferation inhibition and the induction of apoptosis are the two main mechanisms involved in the effect of AM. In addition, our result link AM induced ER stress to the inhibition of the cell proliferation and to the BBC3 and PMAIP1 mediated induction of apoptosis, which is in agreement with the role of ER stress in cell fate control **(Figure 26)**.

In addition, we have identified 34 new compounds which were able to significantly enhance the effect of the AM on different cancer cells when applied in a per se non-toxic concentration. These compounds are mainly L-amino-acid metabolites, phenolic acids, D-amino acids and keto acids. Treatment with any given mixtures, new mixture alone or in combination with AM, caused no toxic effect on HRE normal cells. These results revealed that the mixture of selected substances has a specific inhibitory effect on cancer cells. The upregulation of *BBC3*, *PMAIP1* and *CDKN1* transcripts upon treatment with the combination of AM and NM points toward the induction of apoptosis and cell cycle arrest, which is also in agreement with our results.

10. REFERENCES

Agmon E, Solon J, Bassereau P and Stockwell BR (2018) Modeling the effects of lipid peroxidation during ferroptosis on membrane properties. Sci Rep 8(1), 5155.

Arnoult D, Gaume B, Karbowski M, Sharpe JC, Cecconi F and Youle RJ (2003) Mitochondrial release of AIF and EndoG requires caspase activation downstream of Bax/Bak-mediated permeabilization. EMBO J 22(17), 4385-4399.

Aubrey BJ, Kelly GL, Janic A, Herold MJ and Strasser A (2018) How does p53 induce apoptosis and how does this relate to p53-mediated tumour suppression? Cell Death Differ 25(1), 104-113.

Averous J, Bruhat A, Jousse C, Carraro V, Thiel G and Fafournoux P (2004) Induction of CHOP expression by amino acid limitation requires both ATF4 expression and ATF2 phosphorylation. J Biol Chem 279 (7), 5288-5297.

Bialik S, Dasari SK and Kimchi A (2018) Autophagy-dependent cell death - where, how and why a cell eats itself to death. J Cell Sci 131(18), jcs215152.

Blomquist L, Flodh H and Ullberg S (1969) Uptake of 125I-labelled 4-iodophenylalanine in tumours of mice. Br J Cancer 23, 150-152.

Bonfili L, Cecarini V, Cuccioloni M, Angeletti M, Flati V, Corsetti G, Pasini E, Dioguardi FS and Eleuteri AM (2017) Essential amino acid mixtures drive cancer cells to apoptosis through proteasome inhibition and autophagy activation. FEBS J 284(11), 1726-1737.

Boyce M, Bryant KF, Jousse C, et al. (2005) A selective inhibitor of eIF2alpha dephosphorylation protects cells from ER stress. Science 307(5711), 935-939.

Brenner D, Blaser H and Mak TW (2015) Regulation of tumour necrosis factor signalling: live or let die. Nat Rev Immunol 15(6), 362-374.

Bridges RJ, Natale NR and Patel SA (2012) System xc^- cystine/glutamate antiporter: an update on molecular pharmacology and roles within the CNS. Br J Pharmacol 165(1), 20-34.

Bujisic B, De Gassart A, Tallant R, Demaria O, Zaffalon L, Chelbi S, Gilliet M, Bertoni F and Martinon F (2017) Impairment of both IRE1 expression and XBP1 activation is a hallmark of GCB DLBCL and contributes to tumor growth. Blood 129(17), 2420-2428.

Campbell KJ and Tait SWG (2018) Targeting BCL-2 regulated apoptosis in cancer. Open Biol 8(5), 180002.

Casas C (2017) GRP78 at the Centre of the Stage in Cancer and Neuroprotection. Front Neurosci 11, 177.

Chen X, Shen J and Prywes R (2002) The Luminal Domain of ATF6 Senses Endoplasmic Reticulum (ER) Stress and Causes Translocation of ATF6 from the ER to the Golgi. J Biol Chem 277(15), 13045-13052.

Chérasse Y, Chaveroux C, Jousse C, Maurin AC, Carraro V, Parry L, Fafournoux P and Bruhat A (2008) Role of the repressor JDP2 in the amino acid-regulated transcription of CHOP. FEBS Lett 582, 1537-1541.

Choi ME, Price DR, Ryter SW and Choi AMK (2019) Necroptosis: a crucial pathogenic mediator of human disease. JCI Insight 4(15), e128834.

Chou TC (2006) Theoretical basis, experimental design, and computerized simulation of synergism and antagonism in drug combination studies. Pharmacol Rev 58(3), 621–681.

Chou TC and Talalay P (1981) Generalized equations for the analysis of inhibitions of Michaelis-Menten and higher-order kinetic systems with two or more mutually exclusive and nonexclusive inhibitors. Eur J Biochem 115(1), 207–216.

Chou TC and Talalay P (1984) Quantitative analysis of dose−effect relationships: the combined effects of multiple drugs or enzyme inhibitors. Adv Enzyme Regul 22, 27-55.

Ciechanover A and Kwon YT (2015) Degradation of misfolded proteins in neurodegenerative diseases: therapeutic targets and strategies. Exp Mol Med 47(3), e147.

Clarke HJ, Chambers JE, Liniker E and Marciniak SJ (2014) Endoplasmic reticulum stress in malignancy. Cancer Cell 25(5), 563-573.

Colell A, Ricci JE, Tait S, Milasta S, Maurer U, Bouchier-Hayes L, Fitzgerald P, Guio-Carrion A, Waterhouse NJ and Li CW (2007) GAPDH and autophagy preserve survival after apoptotic cytochrome c release in the absence of caspase activation. Cell 129(5), 983-997.

Crawford RR, Prescott ET, Sylvester CF, Higdon AN, Shan J, Kilberg MS and Mungrue IN (2015) Human CHAC1 Protein Degrades Glutathione, and mRNA Induction Is Regulated by the Transcription Factors ATF4 and ATF3 and a Bipartite ATF/CRE Regulatory Element. J Biol Chem 290(25), 15878-15891.

Dadey DY, Kapoor V, Khudanyan A, Urano F, Kim AH, Thotala D and Hallahan DE (2016) The ATF6 pathway of the ER stress response contributes to enhanced viability in glioblastoma. Oncotarget 7(2), 2080-2092.

Darlyuk-Saadon I, Weidenfeld-Baranboim K, Yokoyama KK, Hai T and Aronheim A (2012) The bZIP repressor proteins, c-Jun dimerization protein 2 and activating transcription factor 3, recruit multiple HDAC members to the ATF3 promoter. Biochim Biophys Acta 1819(11-12), 1142-1153.

Degterev A, Hitomi J, Germscheid M, et al. (2008) Identification of RIP1 kinase as a specific cellular target of necrostatins. Nat Chem Biol 4(5), 313-321.

Denton D and Kumar S (2019) Autophagy-dependent cell death. Cell Death Differ 26, 605–616.

Dhuriya YK and Sharma D (2018) Necroptosis: a regulated inflammatory mode of cell death. J Neuroinflammation 15(1), 199.

Dikic I and Elazar Z (2018) Mechanism and medical implications of mammalian autophagy. Nat Rev Mol Cell Biol 19(6), 349-364.

Dixon SJ, Lemberg KM, Lamprecht MR, et al. (2012) Ferroptosis: an iron-dependent form of nonapoptotic cell death. Cell 149(5), 1060-1072.

Dixon SJ, Patel DN, Welsch M, et al. (2014) Pharmacological inhibition of cystine-glutamate exchange induces endoplasmic reticulum stress and ferroptosis. Elife 3, e02523.

Donnelly N, Gorman AM, Gupta S and Samali A (2013) The eIF2α kinases: their structures and functions. Cell Mol Life Sci 70(19), 3493-3511.

Du C, Fang M, Li Y, Li L and Wang X (2000) Smac, a mitochondrial protein that promotes cytochrome c-dependent caspase activation by eliminating IAP inhibition. Cell 102(1), 33-42.

Elmore S (2007) Apoptosis: a review of programmed cell death. Toxicol Pathol 35(4), 495-516.

Elrod HA and Sun SY (2008) Modulation of death receptors by cancer therapeutic agents. Cancer Biol Ther 7(2), 163-173.

Ertao Z, Jianhui C, Kang W, Zhijun Y, Hui W, Chuangqi C, Changjiang Q, Sile C, Yulong H and Shirong C (2016) Prognostic value of mixed lineage kinase domain-like protein expression in the survival of patients with gastric caner. Tumour Biol 37(10), 13679-13685.

Feng H and Stockwell BR (2018) Unsolved mysteries: How does lipid peroxidation cause ferroptosis? PLoS Biol 16(5), e2006203.

Feng X, Song Q, Yu A, Tang H, Peng Z and Wang X (2015) Receptor-interacting protein kinase 3 is a predictor of survival and plays a tumor suppressive role in colorectal cancer. Neoplasma 62(4), 592-601.

Feng YX, Jin DX, Sokol ES, Reinhardt F, Miller DH and Gupta PB (2017) Cancer-specific PERK signaling drives invasion and metastasis through CREB3L1. Nat Commun 8(1), 1079.

Feng YX, Sokol ES, Del Vecchio CA, et al. (2014) Epithelial-to-mesenchymal transition activates PERK-eIF2α and sensitizes cells to endoplasmic reticulum stress. Cancer Discov 4(6), 702-715.

Ferreira RB, Wang M, Law ME, et al. (2017) Disulfide bond disrupting agents activate the unfolded protein response in EGFR- and HER2-positive breast tumor cells. Oncotarget 8(17), 28971-28989.

Flodh H and Ullberg S (1968) Accumulation of labelled vitamin B12 in some transplanted tumours. Int J Cancer 3(5), 694-699.

Forcina GC and Dixon SJ (2019) GPX4 at the Crossroads of Lipid Homeostasis and Ferroptosis. Proteomics 19(18), e1800311.

Friesen C, Fulda S and Debatin K (1997) Deficient activation of the CD95 (APO-1/Fas) system in drug-resistant cells. Leukemia 82(11), 1833–1841.

Fulda S (2010) Evasion of apoptosis as a cellular stress response in cancer. Int J Cell Biol 2010, 370835.

Fulda S (2013) The mechanism of necroptosis in normal and cancer cells. Cancer Biol Ther 14(11), 999-1004.

Fulda S, Los M, Friesen C and Debatin KM (1998) Chemosensitivity of solid tumor cells in vitro is related to activation of the CD95 system. Int J Cancer 76(1), 105-114.

Galluzzi L, Vitale I, Aaronson SA, et al. (2018) Molecular mechanisms of cell death: recommendations of the Nomenclature Committee on Cell Death. Cell Death Differ 25(3), 486-541.

Gao N, Shang J, Huynh D, et al. (2011) Mannose-6-phosphate regulates destruction of lipid-linked oligosaccharides. Mol Biol Cell 22(17), 2994-3009.

Gaut JR and Hendershot LM (1993) The modification and assembly of proteins in the endoplasmic reticulum. Curr Opin Cell Biol 5(4), 589-595.

Geserick P, Wang J, Schilling R, Horn S, Harris PA, Bertin J, Gough PJ, Feoktistova M and Leverkus M (2015) Absence of RIPK3 predicts necroptosis resistance in malignant melanoma. Cell Death Dis 6, e1884.

Giam M, Huang D and Bouillet P (2008) BH3-only proteins and their roles in programmed cell death. Oncogene 27, S128–S136.

Glick D, Barth S and Macleod KF (2010) Autophagy: cellular and molecular mechanisms. J Pathol 221(1), 3-12.

Gong Y, Fan Z, Luo G, et al. (2019) The role of necroptosis in cancer biology and therapy. Mol Cancer 18(1), 100.

Green DR and Llambi F (2015) Cell Death Signaling. Cold Spring Harb Perspect Biol 7(12), a006080.

Guha P, Kaptan E, Gade P, Kalvakolanu DV and Ahmed H (2017) Tunicamycin induced endoplasmic reticulum stress promotes apoptosis of prostate cancer cells by activating mTORC1. Oncotarget 8(40), 68191-68207.

Han D, Lerner AG, Vande Walle L, Upton JP, Xu W, Hagen A, Backes BJ, Oakes SA and Papa FR (2009) IRE1α kinase activation modes control alternate endoribonuclease outputs to determine divergent cell fates. Cell 138(3), 562-575.

Han J, Back SH, Hur J, et al. (2013) ER-stress-induced transcriptional regulation increases protein synthesis leading to cell death. Nat Cell Biol 15(5), 481-490.

Hanahan D and Weinberg RA (2000) The hallmarks of cancer. Cell 100(1), 57-70.

Hanahan D and Weinberg RA (2011) Hallmarks of cancer: the next generation. Cell 144(5), 646-674.

Hanaoka M, Ishikawa T, Ishiguro M, Tokura M, Yamauchi S, Kikuchi A, Uetake H, Yasuno M and Kawano T (2018) Expression of ATF6 as a marker of pre-cancerous atypical change in ulcerative colitis-associated colorectal cancer: a potential role in the management of dysplasia. J Gastroenterol 53(5), 631-641.

Harding HP, Zhang Y and Ron D (1999) Protein translation and folding are coupled by an endoplasmic-reticulum-resident kinase. Nature 397(6716), 271-274.

Harding HP, Zhang Y, Bertolotti A, Zeng H and Ron D (2000) Perk is essential for translational regulation and cell survival during the unfolded protein response. Mol Cell 5(5), 897-904.

Haze K, Okada T, Yoshida H, Yanagi H, Yura T, Negishi M and Mori K (2001) Identification of the G13 (cAMP-response-element-binding protein-related protein) gene product related to activating transcription factor 6 as a transcriptional activator of the mammalian unfolded protein response. Biochem J 355(Pt 1), 19-28

Haze K, Yoshida H, Yanagi H, Yura T and Mori K (1999) Mammalian Transcription Factor ATF6 Is Synthesized as a Transmembrane Protein and Activated by Proteolysis in Response to Endoplasmic Reticulum Stress. Mol Biol Cell 10(11), 3787-3799.

He L, Peng K, Liu Y, Xiong J and Zhu FF (2013) Low expression of mixed lineage kinase domain-like protein is associated with poor prognosis in ovarian cancer patients. Onco Targets Ther 6, 1539-1543.

Hetz C (2012) The unfolded protein response: controlling cell fate decisions under ER stress and beyond. Nat Rev Mol Cell Biol 13(2), 89-102.

Hill MM, Adrain C and Martin SJ (2003) Portrait of a killer: the mitochondrial apoptosome emerges from the shadows. Mol Interv 3(1), 19-26.

Hollien J, Lin JH, Li H, Stevens N, Walter P and Weissman JS (2009) Regulated Ire1-dependent decay of messenger RNAs in mammalian cells. J Cell Biol 186(3), 323-331.

Huang D, Zheng X, Wang ZA, et al. (2017) The MLKL Channel in Necroptosis Is an Octamer Formed by Tetramers in a Dyadic Process. Mol Cell Biol 37(5), e00497-16.

Ichim G and Tait SW (2016) A fate worse than death: apoptosis as an oncogenic process. Nat Rev Cancer 16(8), 539-548.

Jeansonne D, DeLuca M, Marrero L, Lassak A, Pacifici M, Wyczechowska D, Wilk A, Reiss K and Peruzzi F (2015) Anti-tumoral effects of miR-3189-3p in glioblastoma. J Biol Chem 290(13), 8067-8080.

Jeng PS, Inoue-Yamauchi A, Hsieh JJ and Cheng EH (2018) BH3-Dependent and Independent Activation of BAX and BAK in Mitochondrial Apoptosis. Curr Opin Physiol 3, 71-81.

Jiang L, Kon N, Li T, Wang SJ, Su T, Hibshoosh H, Baer R and Gu W (2015) Ferroptosis as a p53-mediated activity during tumour suppression. Nature 520(7545), 57-62.

Jin C, Jin Z, Chen NZ, Lu M, Liu CB, Hu WL and Zheng CG (2016) Activation of IRE1α-XBP1 pathway induces cell proliferation and invasion in colorectal carcinoma. Biochem Biophys Res Commun 470(1), 75-81.

Jin Z, McDonald ER 3rd, Dicker DT and El-Deiry WS (2004) Deficient tumor necrosis factor-related apoptosis-inducing ligand (TRAIL) death receptor transport to the cell surface in human colon cancer cells selected for resistance to TRAIL-induced apoptosis. J Biol Chem 279(34), 35829-35839.

Jones MF, Li XL, Subramanian M, et al. (2015) Growth differentiation factor-15 encodes a novel microRNA 3189 that functions as a potent regulator of cell death. Cell Death Differ 22(10), 1641-1653.

Jung CH, Ro SH, Cao J, Otto NM and Kim DH (2010) mTOR regulation of autophagy. FEBS Lett 584(7), 1287-1295.

Kalluri R and Weinberg RA (2009) The basics of epithelial-mesenchymal transition. J Clin Invest 119(6), 1420-1428.

Kang MR, Kim MS, Oh JE, Kim YR, Song SY, Kim SS, Ahn CH, Yoo NJ and Lee SH (2009) Frameshift mutations of autophagy-related genes ATG2B, ATG5, ATG9B and ATG12 in gastric and colorectal cancers with microsatellite instability. J Pathol 217(5), 702-706.

Kerr JF, Wyllie AH and Currie AR (1972) Apoptosis: a basic biological phenomenon with wide-ranging implications in tissue kinetics. Br J Cancer 26(4), 239-257.

Koo GB, Morgan MJ, Lee DG, et al. (2015) Methylation-dependent loss of RIP3 expression in cancer represses programmed necrosis in response to chemotherapeutics. Cell Res 25(6), 707-725.

Kubisch CH, Sans MD, Arumugam T, Ernst SA, Williams JA and Logsdon CD (2006) Early activation of endoplasmic reticulum stress is associated with arginine-induced acute pancreatitis. Am J Physiol Gastrointest Liver Physiol 291(2), G238-G245.

Kubota K, Niinuma Y, Kaneko M, Okuma Y, Sugai M, Omura T, Uesugi M, Uehara T, Hosoi T and Nomura Y (2006). Suppressive effects of 4-phenylbutyrate on the aggregation of Pael receptors and endoplasmic reticulum stress. J Neurochem 97(5), 1259-1268.

Kulcsár G (1995) Inhibition of the growth of a murine and various human tumor cell lines in culture and in mice by mixture of certain substances of the circulatory system. Cancer Biother 10(2), 157-176.

Kulcsár G (1997) Apoptosis of tumor cells induced by substances of the circulatory system. Cancer Biother Radiopharm 12(1), 19–26.

Kulcsár G (2000) Synergistic potentiating effect of D(+)-mannose, orotic, and hippuric acid sodium salt on selective toxicity of a mixture of 13 substances of the circulatory system in culture for various tumor cell lines. Cancer Detect Prev 24(5), 485-495.

Kulcsár G (2003) Experimental evidence for the existence of the passive antitumor defense system formed by the synergistic action of certain small substances of the circulatory system. Cancer Biother Radiopharm 18(6), 949-963.

Kulcsár G, Gaál D, Kulcsár PI, Schulcz Á and Czömpöly T (2013) A mixture of amino acids and other small molecules present in the serum suppresses the growth of murine and human tumors in vivo. Int J Cancer 132(5), 1213-1221.

Lee AH, Iwakoshi NN and Glimcher LH (2003) XBP-1 regulates a subset of endoplasmic reticulum resident chaperone genes in the unfolded protein response Mol Cell Biol 23(21), 7448-7459.

Leibowitz B and Yu J (2010) Mitochondrial signaling in cell death via the Bcl-2 family. Cancer Biol Ther 9(6), 417-422.

Lhomond S, Avril T, Dejeans N, et al. (2018) Dual IRE1 RNase functions dictate glioblastoma development. EMBO Mol Med 10(3), e7929.

Li H, Chen X, Gao Y, Wu J, Zeng F and Song F (2015) XBP1 induces snail expression to promote epithelial- to-mesenchymal transition and invasion of breast cancer cells. Cell Signal 27(1), 82-89.

Li J, Cao F, Yin H, Huang ZJ, Lin ZT, Mao N, Sun B and Wang G (2020) Ferroptosis: past, present and future. Cell Death Dis 11, 88.

Li X, Guo J, Ding AP, Qi WW, Zhang PH, Lv J, Qi WS and Sun ZQ (2017) Association of Mixed Lineage Kinase Domain-Like Protein Expression With Prognosis in Patients With Colon Cancer. Technol Cancer Res Treat 16(4), 428-434.

Li Y, Guo Y, Tang J, Jiang J and Chen Z (2014) New insights into the roles of CHOP-induced apoptosis in ER stress. Acta Biochim Biophys Sin (Shanghai). 46(8), 629-640.

Li Y, Yan H, Xu X, Liu H, Wu C and Zhao L (2020) Erastin/sorafenib induces cisplatin-resistant non-small cell lung cancer cell ferroptosis through inhibition of the Nrf2/xCT pathway. Oncol Lett 19(1):323-333.

Liao D, Sun L, Liu W, He S, Wang X and Lei X (2014) Necrosulfonamide inhibits necroptosis by selectively targeting the mixed lineage kinase domain-like protein. Med Chem Comm 5(3), 333.

Liberzon A, Subramanian A, Pinchback R, Thorvaldsdóttir H, Tamayo P and Mesirov JP (2011) Molecular signatures database (MSigDB) 3.0. Bioinformatics 27(12), 1739–1740.

Liu EY and Ryan KM (2012) Autophagy and cancer--issues we need to digest. J Cell Sci 125(Pt 10), 2349-2358.

Liu J, Zhang C, Hu W and Feng (2019) Tumor suppressor p53 and metabolism. J Mol Cell Biol 11(4), 284-292.

Liu Z, Ding Y, Ye N, Wild C, Chen H and Zhou J (2016) Direct Activation of Bax Protein for Cancer Therapy. Med Res Rev 36(2), 313-341.

Logue SE, McGrath EP, Cleary P, et al. (2018) Inhibition of IRE1 RNase activity modulates the tumor cell secretome and enhances response to chemotherapy. Nat Commun 9(1), 3267.

Lu B, Chen XB, Ying MD, He QJ, Cao J and Yang B (2018) The Role of Ferroptosis in Cancer Development and Treatment Response. Front Pharmacol 8, 992.

Ma M, Liu JJ, Li Y, et al. (2017) Cryo-EM structure and biochemical analysis reveal the basis of the functional difference between human PI3KC3-C1 and -C2. Cell Res 27(8), 989-1001.

Maji S, Panda S, Samal SK, Shriwas O, Rath R, Pellecchia M, Emdad L, Das SK, Fisher PB and Dash R (2018) Bcl-2 Antiapoptotic Family Proteins and Chemoresistance in Cancer. Adv Cancer Res 137, 37-75.

McCormick KD, Ghosh A, Trivedi S, Wang L, Coyne CB, Ferris RL and Sarkar SN (2016) Innate immune signaling through differential RIPK1 expression promote tumor progression in head and neck squamous cell carcinoma. Carcinogenesis 37(5), 522-529.

McQuiston A and Diehl JA (2017) Recent insights into PERK-dependent signaling from the stressed endoplasmic reticulum. F1000Res 6, 1897.

Mezzatesta C and Bornhauser BC (2019) Exploiting Necroptosis for Therapy of Acute Lymphoblastic Leukemia. Front Cell Dev Biol 7, 40.

Montero J and Letai A (2018) Why do BCL-2 inhibitors work and where should we use them in the clinic? Cell Death Differ 25, 56–64.

Mootha VK, Lindgren CM, Eriksson KF, Subramanian A, Sihag S, Lehar J, Puigserver P, Carlsson E, Ridderstråle M and Laurila E (2003) PGC-1alpha-responsive genes involved in oxidative phosphorylation are coordinately downregulated in human diabetes. Nat Genet 34(3), 267-273.

Moquin DM, McQuade T and Chan FK (2013) CYLD deubiquitinates RIP1 in the TNFα-induced necrosome to facilitate kinase activation and programmed necrosis. PLoS One 8(10), e76841.

Muller PA and Vousden KH (2014) Mutant p53 in cancer: new functions and therapeutic opportunities. Cancer Cell 25(3), 304-317.

Mungrue IN, Pagnon J, Kohannim O, Gargalovic PS and Lusis AJ (2009) CHAC1/MGC4504 is a novel proapoptotic component of the unfolded protein response, downstream of the ATF4-ATF3-CHOP cascade. J Immunol 182(1), 466-476.

Nugues AL, El Bouazzati H, Hétuin D, Berthon C, Loyens A, Bertrand E, Jouy N, Idziorek T and Quesnel B (2014) RIP3 is downregulated in human myeloid leukemia cells and modulates apoptosis and caspase-mediated p65/RelA cleavage. Cell Death Dis 5(8), e1384.

Oakes SA (2020) Endoplasmic Reticulum Stress Signaling in Cancer Cells. Am J Pathol S0002-9440(20)30088-2.

Ong ES, Zou L, Li S, Cheah PY, Eu KW and Ong CN (2010) Metabolic profiling in colorectal cancer reveals signature metabolic shifts during tumorigenesis. Mol Cell Proteomics doi: 10.1074/mcp.M900551-MCP200.

Orrenius S (2004) Mitochondrial regulation of apoptotic cell death. Toxicol Lett 149(1-3), 19-23.

Oslowski CM and Urano F (2011) Measuring ER stress and the unfolded protein response using mammalian tissue culture system. Methods Enzymol 490, 71-92.

Ozaki T and Nakagawara A (2011) Role of p53 in Cell Death and Human Cancers. Cancers (Basel) 3(1), 994-1013.

Pakos-Zebrucka K, Koryga I, Mnich K, Ljujic M, Samali A and Gorman AM (2016) The integrated stress response. EMBO Rep 17(10), 1374-1395.

Parzych KR and Klionsky DJ (2014) An overview of autophagy: morphology, mechanism, and regulation. Antioxid Redox Signal 20(3), 460-473.

Pasparakis M and Vandenabeele P (2015) Necroptosis and its role in inflammation. Nature 517(7534), 311-320.

Pavlova NN and Thompson CB (2016) The Emerging Hallmarks of Cancer Metabolism. Cell Metab 23(1), 27-47.

Phan LM, Yeung SC and Lee MH (2014) Cancer metabolic reprogramming: importance, main features, and potentials for precise targeted anti-cancer therapies. Cancer Biol Med 11(1), 1-19.

Pistritto G, Trisciuoglio D, Ceci C, Garufi A and D'Orazi G (2016) Apoptosis as anticancer mechanism: function and dysfunction of its modulators and targeted therapeutic strategies. Aging (Albany NY) 8(4), 603-619.

Qi W, Zeng S, Liu M, Yang S, Tan X and Yu B (2018) Tunicamycin induces apoptosis in non-small cell lung cancer cells through C/EBP homologous protein activation-mediated endoplasmic reticulum stress. Int J Clin Exp Med 11(5), 5310-5322.

Rowinsky EK (2005) Targeted induction of apoptosis in cancer management: the emerging role of tumor necrosis factor-related apoptosis-inducing ligand receptor activating agents. J Clin Oncol 23(36), 9394-9407.

Safa AR (2012) c-FLIP, a master anti-apoptotic regulator. Exp Oncol 34(3), 176-184.

Schmittgen TD and Livak KJ (2008) Analyzing real-time PCR data by the comparative C(T) method. Nat Protoc 3(6), 1101-1108.

Schröder M and Kaufman RJ (2005) ER stress and the unfolded protein response. Mutat Res 569(1-2), 29-63.

Schröder M and Kaufman RJ (2005) The mammalian unfolded protein response. Annu Rev Biochem 74, 739-789.

Sehgal P, Szalai P, Olesen C, Praetorius HA, Nissen P, Christensen SB, Engedal N and Møller JV (2017) Inhibition of the sarco/endoplasmic reticulum (ER) Ca2+-ATPase by thapsigargin analogs induces cell death via ER Ca2+ depletion and the unfolded protein response. J Biol Chem 292(48), 19656-19673.

Seifert L, Werba G, Tiwari S, et al. (2016) The necrosome promotes pancreatic oncogenesis via CXCL1 and Mincle-induced immune suppression. Nature 532(7598), 245-249.

Shaffer AL, Shapiro-Shelef M, Iwakoshi NN, et al. (2004) XBP1, downstream of blimp-1, expands the secretory apparatus and other organelles, and increases protein synthesis in plasma cell differentiation. Immunity 21(1), 81-93.

Shen X, Zhang K and Kaufman RJ (2004) The unfolded protein response—a stress signaling pathway of the endoplasmic reticulum. J Chem Neuroanat 28(1-2), 79-92.

Shi Z, Yu X, Yuan M, Lv W, Feng T, Bai R and Zhong H (2019) Activation of the PERK-ATF4 pathway promotes chemo-resistance in colon cancer cells. Sci Rep 9, 3210.

Sidrauski C, Tsai JC, Kampmann M, et al. (2015) Pharmacological dimerization and activation of the exchange factor eIF2B antagonizes the integrated stress response. Elife 4, e07314.

Siwecka N, Rozpędek W, Pytel D, Wawrzynkiewicz A, Dziki A, Dziki L, Diehl JA and Majsterek I (2019) Dual role of Endoplasmic Reticulum Stress-Mediated Unfolded Protein Response Signaling Pathway in Carcinogenesis. Int J Mol Sci 20(18), 4354.

Sosna J, Voigt S, Mathieu S, et al. (2014) TNF-induced necroptosis and PARP-1-mediated necrosis represent distinct routes to programmed necrotic cell death. Cell Mol Life Sci 71(2), 331-348.

Stockwell BR, Friedmann Angeli JP, Bayir H, et al. (2017) Ferroptosis: A Regulated Cell Death Nexus Linking Metabolism, Redox Biology, and Disease. Cell 171(2), 273–285.

Straten Pt and Andersen MH (2010) The anti-apoptotic members of the Bcl-2 family are attractive tumor-associated antigens. Oncotarget 1(4), 239-245.

Su Z, Yang Z, Xie L, DeWitt JP and Chen Y (2016) Cancer therapy in the necroptosis era. Cell Death Differ 23(5), 748-56.

Subramanian A, Tamayo P, Mootha VK, et al. (2005) Gene set enrichment analysis: a knowledge-based approach for interpreting genome-wide expression profiles. Proc Natl Acad Sci USA 102(43), 15545-15550.

Sullivan LB, Gui DY and Vander Heiden MG (2016) Altered metabolite levels in cancer: Implications for tumour biology and cancer therapy. Nat Rev Cancer 16(11), 680.

Sun Y, Jiang F, Pan Y, Chen X, Chen J, Wang Y, Zheng X and Zhang J (2018) XBP1 promotes tumor invasion and is associated with poor prognosis in oral squamous cell carcinoma. Oncol Rep 40(2), 988-998.

Szegezdi E, Logue SE, Gorman AM and Samali A (2006) Mediators of endoplasmic reticulum stress-induced apoptosis EMBO Rep 7(9), 880-885.

Tarangelo A, Magtanong L, Bieging-Rolett KT, Li Y, Ye J, Attardi LD and Dixon SJ (2018) p53 Suppresses Metabolic Stress-Induced Ferroptosis in Cancer Cells. Cell Rep 22(3), 569-575.

Upton JP, Wang L, Han D, et al. (2012) IRE1α cleaves select microRNAs during ER stress to derepress translation of proapoptotic caspase-2. Science 338(6108), 818-822.

Urano F, Bertolotti A and Ron D (2000) IRE1 and efferent signaling from the endoplasmic reticulum. J Cell Sci 113 Pt 21, 3697-3702.

Urra H, Dufey E, Avril T, Chevet E and Hetz C (2016) Endoplasmic Reticulum Stress and the Hallmarks of Cancer. Trends Cancer 2(5), 252-262.

Vander Heiden MG, Cantley LC and Thompson CB (2009) Understanding the Warburg effect: the metabolic requirements of cell proliferation. Science 324(5930), 1029-1033.

Vega-Rubín-de-Celis S (2019) The Role of Beclin 1-Dependent Autophagy in Cancer. Biology (Basel) 9(1), 4.

Walczak H (2013) Death receptor-ligand systems in cancer, cell death, and inflammation. Cold Spring Harb Perspect Biol 5(5), a008698.

Wang M, Law ME, Castellano RK and Law BK (2018) The unfolded protein response as a target for anticancer therapeutics. Crit Rev Oncol Hematol 127, 66-79.

Wang X, Baek SJ and Eling TE (2013). The diverse roles of nonsteroidal anti-inflammatory drug activated gene (NAG-1/GDF15) in cancer. Biochem Pharmacol 85(5), 597-606.

Wegner KW, Saleh D and Degterev A (2017) Complex Pathologic Roles of RIPK1 and RIPK3: Moving Beyond Necroptosis. Trends Pharmacol Sci 38(3), 202-225.

Weidenfeld-Baranboim K, Hasin T, Darlyuk I, Heinrich R, Elhanani O, Pan J, Yokoyama KK and Aronheim A (2009) The ubiquitously expressed bZIP inhibitor, JDP2, suppresses the transcription of its homologue immediate early gene counterpart, ATF3. Nucleic Acids Res 37(7), 2194-2203.

White E (2012) Deconvoluting the context-dependent role for autophagy in cancer. Nat Rev Cancer 12(6), 401-410.

Wu L, Huang X, Kuang Y, Xing Z, Deng X and Luo Z (2019) Thapsigargin induces apoptosis in adrenocortical carcinoma by activating endoplasmic reticulum stress and the JNK signaling pathway: an in vitro and in vivo study. Drug Des Devel Ther 13, 2787-2798.

Wu S, Du R, Gao C, Kang J, Wen J and Sun T (2018) The role of XBP1s in the metastasis and prognosis of hepatocellular carcinoma. Biochem Biophys Res Commun 500(3), 530-537.

Wu X, Xin Z, Zhang W, et al. (2014) A missense polymorphism in ATF6 gene is associated with susceptibility to hepatocellular carcinoma probably by altering ATF6 level. Int J Cancer 135(1), 61-68.

Xiao M, Yang H, Xu W, et al. (2012) Inhibition of α-KG-dependent histone and DNA demethylases by fumarate and succinate that are accumulated in mutations of FH and SDH tumor suppressors. Genes Dev 26(12), 1326-1338.

Xie Y, Zhu S, Song X, et al. (2017) The Tumor Suppressor p53 Limits Ferroptosis by Blocking DPP4 Activity. Cell Rep 20(7), 1692-1704.

Xu C and Ng DT (2015) O-mannosylation: The other glycan player of ER quality control. Semin Cell Dev Biol 41, 129-134.

Xu C, Bailly-Maitre B and Reed JC (2005). Endoplasmic reticulum stress:cell life and death decisions. J Clin Invest 115(10), 2656-2664.

Xu T, Ding W, Ji X, Ao X, Liu Y, Yu W and Wang J (2019) Molecular mechanisms of ferroptosis and its role in cancer therapy. J Cell Mol Med 23(8), 4900-4912.

Yan G, Elbadawi M and Efferth T (2020) Multiple cell death modalities and their key features (Review). World Acad Sci J 2, 39-48.

Yang WS and Stockwell BR (2016) Ferroptosis: Death by Lipid Peroxidation. Trends Cell Biol 26(3), 165-176.

Yang WS, SriRamaratnam R, Welsch ME, et al. (2014) Regulation of ferroptotic cancer cell death by GPX4. Cell 156(1-2), 317-331.

Yang Z and Klionsky DJ (2010) Eaten alive: a history of macroautophagy. Nat Cell Biol 12(9), 814-822.

Yarapureddy S, Abril J, Foote J, et al. (2019) ATF6α Activation Enhances Survival against Chemotherapy and Serves as a Prognostic Indicator in Osteosarcoma. Neoplasia 21(6), 516-532.

Yip KW and Reed JC (2008) Bcl-2 family proteins and cancer. Oncogene 27(50), 6398-6406.

Yorimitsu T and Klionsky DJ. Autophagy: molecular machinery for self-eating. Cell Death Differ 12 Suppl 2(Suppl 2), 1542-1552.

Yoshida H, Matsui T, Yamamoto A, Okada T and Mori K (2001) XBP1 mRNA is induced by ATF6 and spliced by IRE1 in response to ER stress to produce a highly active transcription factor. Cell 107(7), 881-891.

Young SK and Wek RC (2016) Upstream Open Reading Frames Differentially Regulate Gene-specific Translation in the Integrated Stress Response. J Biol Chem 291(33), 16927-16935.

Yu X and Long Y (2016) Crosstalk between cystine and glutathione is critical for the regulation of amino acid signaling pathways and ferroptosis. Sci Rep 6, 30033.

Yu Y, Xie Y, Cao L, Yang L, Yang M, Lotze MT, Zeh HJ, Kang R and Tang D (2015) The ferroptosis inducer erastin enhances sensitivity of acute myeloid leukemia cells to chemotherapeutic agents. Mol Cell Oncol 2(4), e1054549.

Yun CW and Lee SH (2018) The Roles of Autophagy in Cancer. Int J Mol Sci 19(11), 3466.

Zachari M and Ganley IG (2017) The mammalian ULK1 complex and autophagy initiation. Essays Biochem 61(6), 585-596.

Zhang X, Ding L and Sandford AJ (2005) Selection of reference genes for gene expression studies in human neutrophils by real-time PCR. BMC Mol Biol 6, 4.

Zhao Y, Wang L and Pan J (2015) The role of L-type amino acid transporter 1 in human tumors. Intractable Rare Dis Res 4(4), 165-169.

Zhu A, Lee D and Shim H (2011) Metabolic positron emission tomography imaging in cancer detection and therapy response. Semin Oncol 38(1), 55-69.

11. LIST OF PUBLICATIONS

List of publications related to this thesis:

Scheffer D, Kulcsár G, Czömpöly T. Identification of Further Components of an Anticancer Defense System Composed of Small Molecules Present in the Serum. Cancer Biother Radiopharm. 2019 Apr; 34(3):160-170. Impact factor: 1.894

Scheffer D, Kulcsár G, Nagyéri G, Kiss-Merki M, Rékási Z, Maloy M, Czömpöly T. Active mixture of serum-circulating small molecules selectively inhibits proliferation and triggers apoptosis in cancer cells via induction of ER stress. Cell Signal. 2020 Jan; 65:109426. Impact factor: 3.388

Posters related to this thesis:

Dalma Scheffer, Tamás Czömpöly, Gyula Kulcsár. Effects of a mixture of amino acids and other small molecules on gene expression profile in human cervical cancer cells (HeLa). 45. Membrane Transport Congress, Sümeg, Hungary, 2015.

Dalma Scheffer, Tamás Czömpöly, Gyula Kulcsár. A mixture of amino acids and other small molecules induces endoplasmic reticulum stress in different cancer cell lines. 46. Membrane Transport Congress, Sümeg, Hungary, 2016.

Other posters:

Viktor Sándor, **Dalma Scheffer**, Ágnes Dörnyei, Anikó Kilár, Béla Kocsis, Ferenc Kilár. Electrophoretic and mass spectrometric analysis of the lipid A part of bacterial lipopolysaccharides. 8th International Interdisciplinary Meeting on Bioanalysis. Brno, Czech Republic, 2011.

Árpád Czéh, Tamás Czömpöly, Gyula Kulcsár, Erika Lantos, György Nagyéri, Viktória Németh, **Dalma Scheffer**, Marianna Merki, György Lustyik. A novel approach for in vitro characterization of anticancer effects of experimentally selected mixtures of amino acids and other small molecules. CYTO Congress, Glasgow, Scotland, 2015.

12. ACKNOWLEDGMENT

I would like to thank first and foremost my supervisor Dr. Tamás Czömpöly, for his support, mentoring and guidance during my PhD work.

I give my special thanks to Dr. Gyula Kulcsár for the possibility to work on this topic, professional help and encouraging words over the years.

I would also like to thank Dr. Zoltán Rékási for the support and useful advices through the years.

I am very grateful for Anikó Heitmanné Lendvai for her technical support during my experiments.

I would like to express my gratitude to Dr. György Nagyéri for his help with image acquisition using an automated, high-content screening system.

13. SUPPLEMENTARY DATA

Table S1. Primers used for quantitative RT-PCR amplification of selected genes		
Gene Symbol	**Forward Primer (5'-3')**	**Reverse Primer (5'-3')**
ABL1	GGT CTA TGA ACT CAT GCG AGC AT	GTT TCA AAG GCT TGG TGG ATT T
ALDH1B1	TGG TCA TGC AGG GTT GGA A	GCC ACC TTC ATA ACC ACA GTG TT
ALDH3A2	CAG GAG CGC GAG AAG GAT AT	TTC CTG ACT GTA CAC ATT GAA TTC AC
ALDH3B1	CAT GGG AAA CAG TGC AGT GAC T	GGT GCC GTG TCT GTC CTC TT
ALDH7A1	CGA CCT ATT GCC CTG CTA ACA	CCA TGC TTC TCT TGC TTT CTT TAC A
APAF1	TGC GCT GCT CTG CCT TCT	CAT GGG TAG CAG CTC CTT CTT C
ARHGEF25	CGG TGT CTG AAA GAT CCT GAT TG	CCG GCG CTC GTG TTT G
ATF3	CGC CTT TCA TCT GGA TTC TAC AA	CCC ACC CGA GGT ACA GAC ACT
ATF4	TTA AGC ACA TTC CTC GAT TCC A	CCT CGC TGC TCA GGA AGC T
ATG16L1	GCT TTC TCT CGT CCT TCC AAA G	GAG TTC ACC GGG CAA ATG AA
ATM	CCG ACG GGC CGA ATG T	AGC CGC AGA GCA CGG TAT
B2M	ACT GAA TTC ACC CCC ACT GA	CCT CCA TGA TGC TGC TTA CA
BAD	GCT GTG CCT TGA CTA CGT AAC ATC	TGC TCA CTC GGC TCA AAC TCT
BAK1	CAC GGC AGA GAA TGC CTA TGA	CCC AAT TGA TGC CAC TCT CA
BAX	GGT TGT CGC CCT TTT CTA CTT TG	CAG TTC CGG CAC CTT GGT
BCL2	CCG CAT CAG GAA GGC TAG AG	CTG GGA CAC AGG CAG GTT CT
BCL2L1	GAT TGC CTT TGT TTT GAT GTT TGT	GGA AAG GGA ACC CAG GTT AGT G
BCL2L11	GCC GCC ACT ACC ACC ACTT	AAC CGA ATA CCG CGA TGA TG
BIRC2	AGT AAC TGG GAA CCA AAG GAT GAT	CAT GTG TCT GCA TGC TCA GAT TT
BIRC3	TGGTTTCCAAGGTGTGAGTACT TG	GGG CTG TCT GAT GTG GAT AGC
BUB3	ACC TCC CAG TTC CTG CTT GTC	TTG GCC GGC ACA TCG TA
CASP3	CAG TGG AGG CCG ACT TCT TG	ATG AAC CAG GAG CCA TCC TTT

CCNB1	GCT GCT GCC TGG TGA AGA G	TTT CAG CAT TAA TTT TCG AGT TCC T
CCND1	GTC TGT GCA TTT CTG GTT GCA	GCT GGA AAC ATG CCG GTT A
CCNG2	AGC ACT TGG CAG GTC ATG AAG	TCA GCC CTT TTT CTC GAG GTT
CDC16	TGA AAG GTT CTT CAG CCA AGC T	CGC CGA CCT CAT GCA TAA C
CDC25A	TCT TGC TGG CTA CGC CTC TT	CAG AAC TGC ATT GTG GCA CAG T
CDK6	TGA ACC AAA ATG CCA CAT ACA CT	TTC GGC CTT TCG CAT AGG
CDK7	CAC ACA GGC ACT GAA AAT GAA GTA T	GTC TTG GCA GCT GAC ATC CA
CDKN1A	GCG GCA GAC CAG CAT GA	ATT AGG GCT TCC TCT TGG AGA AG
CDKN2A	GCC TTT TCA CTG TGT TGG AGT TT	CGC AAG AAA TGC CCA CAT G
CDKN2C	GAT TAA CCA TCC CAG TCC TTC TGT	TCC CCT TTC CTT TGC TCC TAA
CDKN2D	GCT TTC TGG CAG CTG AAT CTG	CTG CAG TGC CAG CTC CAA
CHAC1	GTC TCC AAG AGC CTC GAT CCT	CCT TGG CAG GTG GAA TTC C
CREBBP	AAC TTT GTG ATG TTT CGG GAA GA	CGC CGG AGT CAA TTC CTA TC
DDIT3	AGA ACC AGG AAA CGG AAA CAG A	TCT CCT TCA TGC GCT GCT TT
DDIT4	CAC TCT GAG TTC ATC AGC AAA CG	ACG AGA AGC GGT CCC AAA G
DERA	GGC ACC GAG CTC GAC CTT A	TTC CGC ACG CCT CAG AA
DNAJB1	CGG CTG TAC CAA GAA GAT GAA AA	TTC GTT TCG AAT GCT CTT TCC
DRAM1	TTT GAA ATT CTG CCA CCT TGT TT	ATG GGC AAT TAG CAG CAA GAG
E2F2	GCC TAT GTG ACT TAC CAG GAT ATC C	CCT TGA CGG CAA TCA CTG TCT
E2F3	GTC AGC TGC AAA TCC TAC CAG TT	GGA CCG GAG ATA CTA CGC CAT A
ENO3	GAC CCC TTT GAC CAG GAT GA	CCC CAC AAT CTG GAT GTT CAC
EP300	TTG AAT GTA CAG AGT GCG GAA GA	AAC AGC CAT CAC AGA CGA ATC C
GADD45A	GGA TGC CCT GGA GGA AGT G	TCG TAC ACC CCG ACA GTG ATC
GAPDH	CAA TGA CCC CTT CAT TGA CC	TGG ACT CCA CGA CGT ACT CA
GDF15	AAC CAG AGC TGG GAA GAT TCG	GCA CTT CTG GCG TGA GTA TCC

GSG1	TGA CCA GCT ACC ACC AGT ATC ATA A	CCG CAG CTC GGA GTA GAA GT
GSK3B	CAC CGG AGG CAA TTG CA	GGT CCC GTA ATT CAT CAA AAA ATG
HAGH	CCC CCG GAC ACA AGA GTC TAC	CCA CGT GGC GTG CAA AC
HDAC1	ACG GGA GGC GAG CAA GAT	CAT CCC CGT CGT AGT AGT AAC AGA
HDAC2	ACT ATC GCC CCC ACG TTT C	GCG GAT TCT ATG AGG CTT CAT G
HDAC3	CCC GAC GTG GGC AAC TT	ACC AGG CTA TGG GTC AAT GC
HDAC4	ATG AAT GCA GAT TGC GAA GGT	ACG GGA GCG GTT CTG TTA GA
HDAC5	GCA GCT GGT CAT GCA ACA AC	TCC TTA ACC TGG ATG CAA TCC T
HDAC6	GGA CCC TCC AGT TCT AAG TTG GT	TGT GGT CAT CCG CTC AGC TA
HERPUD1	CCT GGA TGG GAA AAC ATC TCA	GGT GTG TAA CCG GAG AAA CCA
HPRT1	GGA CAG GAC TGA ACG TCT TGC	CTT GAG CAC ACA GAG GGC TAC A
IDH1	ACT ACC GCA TGT ACC AGA AAG GA	TCT GGT CCA GGC AAA AAT GG
IKBKG	CTG TCC CAA GTG CCA GTA TCA G	CCG GCC CTA CTC AAT GCA
IRAK2	CCC CAG CAG ATT CCA TTA CCT	TGC TAT GGC ATT GCA GAA CTG
JDP2	CCT GTA TCG CTC AGT AAA CAT TGC	GGC CTT GCA CCC ATT CC
ME2	CCT GCT GCC AGA TGT GTA TGA A	CCT GGA GCA CAG AAA GTA TTT ATC AG
MTMR14	TGA GCA AGT TGC AAG ACC TCA T	ACA GGA TTA CTG GGC AGA CAA AC
MYC	CGT CTC CAC ACA TCA GCA CAA	TCT TGG CAG CAG GAT AGT CCT T
NFKB1	GGC TAC ACC GAA GCA ATT GAA	CAG CGA GTG GGC CTG AGA
NFKB2	ACG AGG GAC CAG CCA AGA T	TGC TTG CCC ACC AGA CTG T
NFKBIA	GCT GAA GAA GGA GCG GCT ACT	TCG TAC TCC TCG TCT TTC ATG GA
PCDH7	TGG CGA CAG ACG CAG ACA	ATC GGG ATC GAT GGC AAA
PDHB	AGG TTA TAA ACT CAG CTG CCA AGA C	CAT TGG GCC CCC TGA AG
PFKL	AGG AGC TCT GCA TCG TCA TGT	GGC GGC ATT TAC AGC AGT GT
PGAM1	GGA GTG CTT CCT GGT GTG TGT	CAG GAC CAA GAG GCA TTT CAC

PGK1	GCA GTC GGC TCC CTC GTT	CGA CCC GCT TCC CTT TAA C
PGM1	GGA CCT GCG GGC TTA GAT C	AAT ACC CAC GCA GCA GCA A
PLK1	GGA TCA CAC CAA GCT CAT CTT G	CCC GCT TCT CGT CGA TGT
PPIA	GTC GAC GGC GAG CCC TTG G	TCT TTG GGA CCT TGT CTG CAA
PPP1R15A	TCC CAG TTG TTG ATC TTA TGC AA	AAG TGC CGT GGC GAC AAG
PRKAR2A	CTG CTG ACA GCT GCA CAC ATT	GGG TCC TGA GCA GGG TCT TT
PRKDC	CCA GCT CTC ACG CTC TGA TAT G	CAA ACG CAT GCC CAA AGT C
PRPS2	ACA ACC TGA TGG AAC TCC TCA TC	CGG GAT CAC GGC AGT TAC TC
REL	GCC CAT CTC AAG TGG ATT GTC	GCC ACT GAT GAC CAG CTT GAA
RELA	GCC GGG ATG GCT TCT ATG A	TGG ATT CCC AGG TTC TGG AA
RELB	GAC CCC CAT GGC ATC GA	CGT GGT TGG GCA GGA AGT
RB1CC1	GGA TTG GTC ATC TGG GTT CTA AA	GGA AGG TTT GAG TCT GCA TTT GA
RPL32	TGT CCT GAA TGT GGT CAC CTG A	CTG CAG TCT CCT TGC ACA CCT
SDHA	TGG GAA AAT CAG CAA GCT CTA TG	GGT CCG TGT TCC AGA CCA TT
SESN2	AAT ACC ATC GCC ATG CAC AGT	ATG CCA AAG ACG CAG TGG AT
SF3B2	AGG AGC TTC AGG CCA AGT TG	CCT CGC GAT TAC CCT GGA T
SFN	CAA AGA CAG CAC CCT CAT CAT G	CTC TTC CCC GGC GTT GT
SIAH	CGA TGG TCA CCA GCA GTT CTT	CAA GTC GGT AAG CAA AAT TTT CAG
SKP1	AGT GGC TTC GTC TTC GGT TTT	GCA TGG TGT TCG GTG TTA AGG
SLC1A3	GAG AAC AAT GGC GTG GAC AA	GGG CAG TCC CAT CCA TGT TA
SLC1A4	TGC GCA ACT CAA CAA CGT AGA	CAC GCC TGC TGC TCC AA
SLC1A5	CCC GCC TTG GCA AGT ACA	GCG GGT GAA GAG GAA GTA GAT G
SLC25A1	ACA GCC ACT GTC CTG AAG CA	GTT GCG CAG GGA GGT CAT
SLC25A24	GGC ATT GCT GGT GCT GTC T	CGT GAA CCT GCA TCA TGA TTT T
SLC2A3	TTC CTG AGG ACG TGG AGA AAA	TCA GCC AAC AAA ACC TTC AAA A

SLC37A4	CAT GTA CCT CTT CCG GGT AAC AG	ACC AAA TAC AGC TCC CAA TAC CA
SLC38A1	CTT TTT CGC CAT GTT TGT TAT GTA CT	GAC AGC CAG CCG CAC TGT
SLC38A2	GGA GCC CAG CGC TAC TAG CT	TTG AAG TCG CTG TTG GAA CTG T
SLC3A2	TGA AAC TGG AGC CTC ACG AA	GAA GGG TAG TGG GTC CAT GTC A
SLC6A9	GCT TCC TAC AAC AAG TTC CAC AAT AA	CAT AGA CGC TGG TGG CAC AGT
SLC7A1	TGG CCC GTG AGA ATG CA	TAG AGG TAA GCT GAG CCC GTC TT
SLC7A11	GCC CAG ATA TGC ATC GTC CTT	ATG ACG AAG CCA ATC CCT GTA
SLC7A5	GAA GGG TGA TGT GTC CAA TCT AGA	GCT GTA TAA TGC CAG CAC AAT GTT
SMAD4	TTC TGG CCT TAC TCC TGT ACA GAT ATT	AAA TCC CTG AAA ACA CTA GCA ATT ACT
STAG1	GCC CAT GTC AGT GGC ATT AA	AAC TCT ATG CCA TCC TTG TGA AGT G
SUCLG2	TGA AGG AAC CAA CGT CCA AGA	TCC AGG TCA ATG GCT GAA GTA A
SXBP1	CTG AGT CCG AAT CAG GTG CAG	ATC CAT GGG GAG ATG TTC TGG
TALDO1	GCG GGT GTG ACC CTC ATC T	TGT CGG TGT TTG CCA CAT G
THBS1	CAT GCC ACG GCC AAC AA	GGC CCA GGT AGT TGC ACT TG
TMBIM6	GCT TCA CCC TCA GTG CAC TCT	CTG ACA TCA AGA TAC CTC CCA GAA
TNFRSF10A	CAA TGC TCA CAA CGA GAT TCT GA	CGG CTC CTG GCT TTC CAT
TNFRSF10B	TTT GCA GTT GCA CAT TGG ATC T	GGC GCG GCT GTA CTT TCA
TP53I3	CGG CTC CTT TCT CTT CTC TTA GC	GCA TCC CGC CCA TCT TG
TRIB3	TGG GAG TAC AGC AGT GAG CAA	CTA TGG TCA TGG AAA AGT GTT GTC A
TSC1	TGC AGA ACG GTT TTT GGA TCT	GAA CAC ACT GCG AGG TAA ATG AGA
TXBP1	TGG CCG GGT CTG CTG AGT CCG	ATC CAT GGG GAG ATG TTC TGG
ULK1	AAA GCG AAT TTT GTG TGA TTT CC	CCC AAC AAT TCC AAA GGT TTA TTT
USXBP1	CAG CAC TCA GAC TAC GTG CA	ATC CAT GGG GAG ATG TTC TGG
VEGFA	GGA GGC GCA GCG GTT AG	AAC CCG GAT CAA TGA ATA TCA AA

WEE1	GCT TGC CCT CAC AGT GGT ATG	TGT CTG ATT TCA TGC CAT TGA TC
XBP1	GTG AAG GAA GAA CCT GTA GAA GAT GA	TTT GGG CAG TGG CTG GAT
YWHAE	AAA AGC ATG GTG CTG GTA ACA GT	CCT GCT TCA GTG GGA GAG TAA AG
YWHAG	GCT AGC TGT GCT GGT ATT GGA A	TCC ACT TGC ATG AAT CTA CAG AAC A

Table S2. Normalized gene expression levels for Figure 9C, 10B, 11A, 12B, 13A, 13B, 14A, 15A, 15B, 15C, 16A, 17A, 17B, 18A, 19, 22C

Figure 9C

Treatment	Gene	Average $2^{-\Delta C_T}$	SD	Significance
Hela CTRL	SXBP1	0,0115	0,0019	
	UXBP1	0,4575	0,0917	
	TXBP	1,2448	0,2263	
Hela AM16	SXBP1	0,0458	0,0053	*
	UXBP1	0,8621	0,1388	#
	TXBP	2,6307	0,4780	#
Hela CM	SXBP1	0,0054	0,0012	
	UXBP1	0,3748	0,0402	
	TXBP	0,9942	0,1353	
HRE CTRL	SXBP1	0,0222	0,0038	
	UXBP1	0,4161	0,0202	
	TXBP	1,1562	0,1265	
HRE AM16	SXBP1	0,0196	0,0034	
	UXBP1	0,3484	0,0679	
	TXBP	1,1754	0,2154	
HRE CM	SXBP1	0,0222	0,0058	
	UXBP1	0,4364	0,0418	
	TXBP	1,4363	0,1052	

Data represent the average ± standard deviation of two independent experiments.
*p≤0.001, #p<0.05 vs. HeLa CTRL, HeLa CM, HRE CTRL, HRE AM16, HRE CM (Welch test followed by Games-Howell test)

Figure 10B				
Treatment	Gene	Average $2^{-\Delta C_T}$	SD	Significance
CTRL	ATF3	0,0899	0,0166	
	ATF4	2,8027	0,1348	
	CHAC1	0,0313	0,0028	
	DDIT3	0,0641	0,0018	
	GDF15	0,0254	0,0035	
AM16	ATF3	0,5157	0,0224	**
	ATF4	7,2879	0,8058	**
	CHAC1	0,7896	0,0393	**
	DDIT3	0,1277	0,0268	*
	GDF15	0,2548	0,0190	**
AM16+ISRIB	ATF3	0,2111	0,0138	**, ##
	ATF4	4,1573	0,7000	*, ##
	CHAC1	0,0328	0,0016	##
	DDIT3	0,0613	0,0039	#
	GDF15	0,0285	0,0035	##
AM16+SAL	ATF3	0,5547	0,0334	**
	ATF4	7,2575	0,4921	**
	CHAC1	0,8506	0,0338	**
	DDIT3	0,1066	0,0115	*
	GDF15	0,3074	0,0218	**, #
AM16+4-PBA	ATF3	0,6905	0,0957	**, #
	ATF4	8,0933	1,3512	*
	CHAC1	1,3496	0,1974	**, #
	DDIT3	0,1820	0,0377	*
	GDF15	0,6170	0,0622	**, ##
Data represent the average ± standard deviation of two independent experiments. *p< 0.05, **p<0.001 vs. CTRL; #p<0.05, ##p <0.001 vs. AM16 (Welch test followed by Games-Howell test)				

Figure 11A				
Treatment	Gene	Average $2^{-\Delta C_T}$	SD	Significance
CTRL	SXBP1	0,0030	0,0001	
	UXBP1	0,5232	0,0412	
	TXBP	0,8520	0,0931	
AM16	SXBP1	0,0093	0,0007	*
	UXBP1	0,8331	0,0272	*
	TXBP	1,3774	0,0933	*
AM16 + GSK2850163	SXBP1	0,0043	0,0002	*, #
	UXBP1	2,4786	0,1798	*, #
	TXBP	4,1794	0,5299	*, #
AM16 + STF-083010	SXBP1	0,0047	0,0003	*, #
	UXBP1	1,6674	0,0521	*, #
	TXBP	2,5783	0,2704	*, #
Data represent the average ± standard deviation of two independent experiments. *p<0.001 vs. CTRL; #p <0.001 vs. AM16 (Welch test followed by Games-Howell test)				

Figure 12B				
Treatment	Gene	Average $2^{-\Delta C_T}$	SD	Significance
CTRL	ATF3	0,0660	0,0029	
	ATF4	3,6261	0,3793	
	CHAC1	0,0270	0,0016	
	DDIT3	0,0760	0,0077	
	GDF15	0,1253	0,0116	
AM1	ATF3	0,0682	0,0085	
	ATF4	3,7753	0,1211	
	CHAC1	0,0749	0,0055	**
	DDIT3	0,1082	0,0100	*
	GDF15	0,1780	0,0263	*
AM2	ATF3	0,0900	0,0079	*
	ATF4	3,5363	0,2750	
	CHAC1	0,0632	0,0020	**
	DDIT3	0,0832	0,0082	
	GDF15	0,2283	0,0190	**
AM3	ATF3	0,0676	0,0039	
	ATF4	3,6748	0,1820	
	CHAC1	0,0344	0,0045	
	DDIT3	0,0705	0,0093	
	GDF15	0,1229	0,0145	
AM1+AM2	ATF3	0,3096	0,0268	**
	ATF4	6,7851	0,3399	**
	CHAC1	0,4374	0,0021	**
	DDIT3	0,3812	0,0306	**
	GDF15	1,5851	0,1209	**
AM1+AM3	ATF3	0,0816	0,0033	**
	ATF4	3,9961	0,2947	
	CHAC1	0,0776	0,0078	**
	DDIT3	0,0890	0,0075	
	GDF15	0,1742	0,0443	
AM2+AM3	ATF3	0,0951	0,0058	**
	ATF4	3,8010	0,2712	
	CHAC1	0,0866	0,0086	**
	DDIT3	0,0841	0,0083	
	GDF15	0,2301	0,0163	**
AM16	ATF3	0,3104	0,0199	**
	ATF4	6,1475	0,6027	**
	CHAC1	0,4542	0,0142	**
	DDIT3	0,3824	0,0246	**
	GDF15	1,6326	0,0455	**

Data represent the average ± standard deviation of two independent experiments. *p< 0.05, **p<0.001 vs. CTRL (Welch test followed by Games-Howell test)

Figure 13A				
Treatment	Gene	Average $2^{-\Delta C_T}$	SD	Significance
CTRL	ATF3	0,0802	0,0062	
	ATF4	4,0476	0,3282	
	CHAC1	0,0428	0,0032	
	DDIT3	0,1116	0,0135	
	GDF15	0,1172	0,0118	
AM1	ATF3	0,0863	0,0068	##
	ATF4	4,9088	0,2601	*, ##
	CHAC1	0,1300	0,0264	##
	DDIT3	0,1058	0,0261	##
	GDF15	0,1545	0,0146	*, ##
AM1 + AdeMal	ATF3	0,1046	0,0077	*, ##
	ATF4	5,2784	0,2753	**, ##
	CHAC1	0,2118	0,0163	**, ##
	DDIT3	0,1329	0,0170	##
	GDF15	0,2513	0,0337	*, ##
AM1 + DeoO	ATF3	0,0938	0,0140	##
	ATF4	4,2216	0,2510	##
	CHAC1	0,0694	0,0185	##
	DDIT3	0,1082	0,0322	##
	GDF15	0,1570	0,0143	##
AM1 + ManHip	ATF3	0,1642	0,0125	**, ##
	ATF4	5,8582	0,5648	*
	CHAC1	0,2801	0,0245	**, ##
	DDIT3	0,2178	0,0305	*, #
	GDF15	0,4727	0,0664	**, ##
AM1 + AdeMalDeoO	ATF3	0,0978	0,0050	*, ##
	ATF4	4,1573	0,1532	##
	CHAC1	0,1356	0,0177	*, ##
	DDIT3	0,1005	0,0206	##
	GDF15	0,3256	0,0140	**, ##
AM1 + AdeMalManHip	ATF3	0,3412	0,0132	**
	ATF4	6,7891	0,2406	**
	CHAC1	0,4357	0,0415	**
	DDIT3	0,3105	0,0247	**
	GDF15	1,4700	0,0395	**
AM1 + ManDeoOHip	ATF3	0,1687	0,0175	**, ##
	ATF4	5,5382	0,6196	*, #
	CHAC1	0,2769	0,0371	**, ##
	DDIT3	0,2013	0,0192	**, #
	GDF15	0,5522	0,0614	**, ##
AM1 + AM2	ATF3	0,3272	0,0198	**
	ATF4	6,8511	0,2657	**
	CHAC1	0,4566	0,0180	**
	DDIT3	0,3025	0,0273	**
	GDF15	1,4521	0,0567	**

Data represent the average ± standard deviation of two independent experiments. *p< 0.05, **p<0.001 vs. CTRL; CTRL; #p < 0.05, ##p <0.001 vs. AM1+AM2 (Welch test followed by Games-Howell test)

Figure 13B				
Treatment	Gene	Average $2^{-\Delta C_T}$	SD	Significance
CTRL	ATF3	0,0740	0,0062	
	ATF4	3,9986	0,3570	
	CHAC1	0,0348	0,0086	
	DDIT3	0,0857	0,0106	
	GDF15	0,1206	0,0205	
AM2	ATF3	0,0860	0,0188	##
	ATF4	3,9126	0,3830	##
	CHAC1	0,0736	0,0169	*, ##
	DDIT3	0,0999	0,0182	##
	GDF15	0,2844	0,0442	*, ##
AM2 + RY	ATF3	0,0954	0,0214	##
	ATF4	4,7022	0,2138	*, ##
	CHAC1	0,0915	0,0306	##
	DDIT3	0,1197	0,0231	##
	GDF15	0,2463	0,0402	*, ##
AM2 + HW	ATF3	0,1041	0,0175	##
	ATF4	4,0286	0,4161	##
	CHAC1	0,1218	0,0240	*, ##
	DDIT3	0,1325	0,0256	##
	GDF15	0,3696	0,0733	*, ##
AM2 + MF	ATF3	0,1137	0,0255	##
	ATF4	5,9943	0,2541	**, #
	CHAC1	0,1993	0,0444	*, ##
	DDIT3	0,1452	0,0170	*, ##
	GDF15	0,5386	0,0503	**, ##
AM2 + RYHW	ATF3	0,1423	0,0158	*, ##
	ATF4	6,2000	0,3431	**
	CHAC1	0,2219	0,0292	**, ##
	DDIT3	0,1945	0,0200	**, ##
	GDF15	0,5197	0,0474	**, ##
AM2 + RYMF	ATF3	0,1155	0,0172	*, ##
	ATF4	5,4932	0,4820	*, #
	CHAC1	0,1702	0,0268	**, ##
	DDIT3	0,1466	0,0208	*, ##
	GDF15	0,4308	0,0377	**, ##
AM2 + HWMF	ATF3	0,1206	0,0194	*, ##
	ATF4	5,7872	0,2579	**, #
	CHAC1	0,2235	0,0252	**, ##
	DDIT3	0,1709	0,0275	*, ##
	GDF15	0,6516	0,0443	##
AM1 + AM2	ATF3	0,3290	0,0288	**
	ATF4	6,9010	0,2843	**
	CHAC1	0,5236	0,0487	**
	DDIT3	0,3950	0,0384	**
	GDF15	1,6781	0,1241	**
Data represent the average ± standard deviation of two independent experiments. *p< 0.05, **p<0.001 vs. CTRL; CTRL; #p < 0.05, ##p <0.001 vs. AM1+AM2 (Welch test followed by Games-Howell test)				

Figure 14A				
Treatment	Gene	Average $2^{-\Delta CT}$	SD	Significance
CTRL	ATF3	0,1189	0,0136	
	ATF4	3,3385	0,1841	
	CHAC1	0,0393	0,0105	
	DDIT3	0,0782	0,0088	
	GDF15	0,1410	0,0215	
AM1 + AM2	ATF3	0,3311	0,0511	*
	ATF4	6,5642	0,1619	**
	CHAC1	0,4496	0,0589	**
	DDIT3	0,3502	0,0256	**
	GDF15	1,6356	0,1442	**
AM1 + AM2 + ISRIB	ATF3	0,1876	0,0203	*, #
	ATF4	2,5986	0,2901	*, ##
	CHAC1	0,0759	0,0072	**, ##
	DDIT3	0,0786	0,0116	##
	GDF15	0,4271	0,0558	**, ##
AM6	ATF3	0,1161	0,0058	
	ATF4	3,2886	0,2731	
	CHAC1	0,0755	0,0204	
	DDIT3	0,0904	0,0166	
	GDF15	0,1583	0,0100	
AM6 + ISRIB	ATF3	0,1128	0,0137	
	ATF4	2,9578	0,2690	
	CHAC1	0,0154	0,0014	**, #
	DDIT3	0,0562	0,0071	#
	GDF15	0,1128	0,0375	
AM10	ATF3	0,3483	0,0444	**
	ATF4	6,4369	0,5300	**
	CHAC1	0,4692	0,0487	**
	DDIT3	0,3191	0,0425	**
	GDF15	1,5503	0,1189	**
AM10 + ISRIB	ATF3	0,1825	0,0303	*, #
	ATF4	2,5424	0,3442	*, ##
	CHAC1	0,0709	0,0175	##
	DDIT3	0,0770	0,0111	##
	GDF15	0,2635	0,0773	##
AM16	ATF3	0,4204	0,0510	**
	ATF4	7,3639	0,3413	**
	CHAC1	0,5351	0,0426	**
	DDIT3	0,3054	0,0303	**
	GDF15	1,5810	0,1093	**
AM16 + ISRIB	ATF3	0,1769	0,0188	*, ##
	ATF4	2,6224	0,3007	*, ##
	CHAC1	0,0833	0,0164	*, ##
	DDIT3	0,0899	0,0230	##
	GDF15	0,3410	0,0501	*, ##

Data represent the average ± standard deviation of two independent experiments. *p< 0.05, **p<0.001 vs. CTRL; ##p <0.001 vs. the corresponding vehicle treated sample (Welch test followed by Games-Howell test)

Figure 15A				
Treatment	Gene	Average $2^{-\Delta C_T}$	SD	Significance
PC3 CTRL	ATF3	0,0408	0,0030	
	ATF4	2,3436	0,1236	
	CHAC1	0,1041	0,0144	
	DDIT3	0,2130	0,0068	
	GDF15	0,0744	0,0035	
PC3 AM6	ATF3	0,0477	0,0023	
	ATF4	2,5159	0,2358	
	CHAC1	0,0923	0,0052	
	DDIT3	0,2068	0,0161	
	GDF15	0,1481	0,0112	*
PC3 AM10	ATF3	0,2433	0,0174	*
	ATF4	3,5917	0,1333	*
	CHAC1	0,3541	0,0308	*
	DDIT3	0,9403	0,0510	*
	GDF15	0,8538	0,0865	*
PC3 AM16	ATF3	0,2493	0,0366	*
	ATF4	3,8525	0,0957	**
	CHAC1	0,3590	0,0163	**
	DDIT3	1,1037	0,1667	*
	GDF15	1,7142	0,0797	*
Data represent the average ± standard deviation of three independent experiments. *p< 0.05, **p<0.001 vs. CTRL (ANOVA, Bonferroni test)				

Figure 15B				
Treatment	Gene	Average $2^{-\Delta C_T}$	SD	Significance
MCF-7 CTRL	ATF3	0,0587	0,0042	
	ATF4	7,1624	0,4928	
	CHAC1	0,0998	0,0273	
	DDIT3	0,2819	0,0672	
	GDF15	2,8516	0,2087	
MCF-7 AM6	ATF3	0,0676	0,0041	
	ATF4	7,2414	0,6214	
	CHAC1	0,0829	0,0037	
	DDIT3	0,2514	0,0115	
	GDF15	4,7340	0,1581	*
MCF-7 AM10	ATF3	0,4994	0,0174	*
	ATF4	9,2147	0,2071	*
	CHAC1	0,2590	0,0126	*
	DDIT3	0,7854	0,0970	*
	GDF15	6,7522	0,7865	*
MCF-7 AM16	ATF3	0,7263	0,0238	*
	ATF4	11,9140	0,6361	*
	CHAC1	0,3897	0,0356	*
	DDIT3	0,9968	0,0464	*
	GDF15	11,9075	0,0927	**
Data represent the average ± standard deviation of three independent experiments. *p< 0.05, **p<0.001 vs. CTRL (ANOVA, Bonferroni test)				

Figure 15C				
Treatment	Gene	Average $2^{-\Delta C_T}$	SD	Significance
Caco-2 CTRL	ATF3	0,1297	0,0174	
	ATF4	7,6645	0,1720	
	CHAC1	0,0819	0,0024	
	DDIT3	0,3357	0,0226	
	GDF15	0,3045	0,0134	
Caco-2 AM6	ATF3	0,1196	0,0076	
	ATF4	7,0201	0,1089	
	CHAC1	0,0705	0,0018	*
	DDIT3	0,2826	0,0206	
	GDF15	0,2702	0,0111	
Caco-2 AM10	ATF3	0,2381	0,0223	*
	ATF4	7,7643	0,2796	
	CHAC1	0,1538	0,0073	*
	DDIT3	0,5279	0,0319	*
	GDF15	0,4505	0,0317	*
Caco-2 AM16	ATF3	0,2457	0,0102	*
	ATF4	7,7712	0,1525	
	CHAC1	0,1481	0,0086	*
	DDIT3	0,5558	0,0114	*
	GDF15	0,5567	0,0313	*
Data represent the average ± standard deviation of three independent experiments. *p< 0.05, **p<0.001 vs. CTRL (ANOVA, Bonferroni test)				

Figure 16A				
Treatment	Gene	Average $2^{-\Delta C_T}$	SD	Significance
CTRL	ATF3	0,0652	0,0057	
	GDF15	0,1473	0,0485	
Mock	ATF3	0,7222	0,0429	**
	GDF15	3,4323	0,4151	**
siATF3	ATF3	0,0902	0,0095	#
	GDF15	3,9230	0,6748	**
siGDF15	ATF3	0,6891	0,0552	**
	GDF15	0,3317	0,0659	*, #
siATF3+siGDF15+ISRIB	ATF3	0,0638	0,0047	#
	GDF15	0,0988	0,0159	#
siCTRL	ATF3	0,7056	0,1079	**
	GDF15	3,5717	0,4217	**
Data represent the average ± standard devation of two independent experiments. *p< 0.05, **p<0.001 vs. CTRL; #p <0.001 vs. Mock (Welch test followed by Games-Howell test)				

Figure 17A				
Treatment	Gene	Average $2^{-\Delta C_T}$	SD	Significance
CRTL	miR-3189-3p	0,000029	0,000002	
AM16	miR-3189-3p	0,000093	0,000006	*
CM	miR-3189-3p	0,000032	0,000006	
TM	miR-3189-3p	0,000127	0,000017	*
Data represent the average ± standard deviation of two independent experiments. *p<0.001 vs. CTRL (Welch test followed by Games-Howell test)				

Figure 17B				
Treatment	Gene	Average $2^{-\Delta C_T}$	SD	Significance
CTRL	ARHGEF25	0,0094	0,0008	
	SF3B2	1,6033	0,1186	
miR-3189-3p mimic	ARHGEF25	0,0039	0,0004	*
	SF3B2	0,4289	0,0415	*
CTRL mimic	ARHGEF25	0,0089	0,0011	
	SF3B2	1,5625	0,0977	
miR-3189-3p mimic +miR-3189-3p INH	ARHGEF25	0,0115	0,0025	
	SF3B2	1,6905	0,1191	
miR-3189-3p mimic +CTRL INH	ARHGEF25	0,0039	0,0003	*
	SF3B2	0,5203	0,0515	*
Data represent the average ± standard deviation of two independent experiments. *p<0.001 vs. CTRL (Welch test followed by Games-Howell test)				

Figure 18A				
Treatment	Gene	Average $2^{-\Delta C_T}$	SD	Significance
CTRL	ATF3	0,0842	0,0037	
	ATF4	2,0816	0,3263	
	CHAC1	0,0206	0,0007	
	DDIT3	0,1300	0,0109	
	GDF15	0,1299	0,0141	
miR-3189-3p mimic	ATF3	0,2707	0,0111	**
	ATF4	2,6313	0,0953	*
	CHAC1	0,0652	0,0025	**
	DDIT3	0,2328	0,0179	**
	GDF15	1,6182	0,1122	**
CTRL mimic	ATF3	0,0798	0,0026	
	ATF4	2,0689	0,0898	
	CHAC1	0,0420	0,0046	**
	DDIT3	0,1168	0,0103	
	GDF15	0,1439	0,0097	
miR-3189-3p mimic +miR-3189-3p INH	ATF3	0,1003	0,0128	
	ATF4	2,1462	0,1924	
	CHAC1	0,0210	0,0040	
	DDIT3	0,1266	0,0142	
	GDF15	0,1538	0,0107	
miR-3189-3p mimic +CTRL INH	ATF3	0,2667	0,0169	**
	ATF4	2,0447	0,1595	
	CHAC1	0,0401	0,0040	**
	DDIT3	0,2520	0,0311	*
	GDF15	1,6555	0,1141	**
Data represent the average ± standard deviation of two independent experiments. *p< 0.05, **p<0.001 vs. CTRL (Welch test followed by Games-Howell test)				

Figure 19				
Treatment	Gene	Average $2^{-\Delta C_T}$	SD	Significance
CTRL	HDAC1	1,3318	0,0621	
	HDAC2	0,5398	0,0371	
	HDAC3	0,5604	0,0489	
	HDAC4	0,0193	0,0015	
	HDAC5	0,0261	0,0018	
	HDAC6	0,1698	0,0078	
	JPD2	0,0043	0,0002	
	GSG1	0,0010	0,0001	
	PCDH7	0,3026	0,0226	
miR-3189-3p mimic	HDAC1	0,5360	0,0320	**
	HDAC2	0,4723	0,0481	
	HDAC3	0,3300	0,0320	**
	HDAC4	0,0174	0,0022	
	HDAC5	0,0418	0,0042	*
	HDAC6	0,1855	0,0134	
	JPD2	0,0018	0,0002	**
	GSG1	0,0021	0,0002	**
	PCDH7	0,4453	0,0289	**
CTRL mimic	HDAC1	1,3776	0,0359	
	HDAC2	0,5516	0,0232	
	HDAC3	0,5233	0,0736	
	HDAC4	0,0198	0,0017	
	HDAC5	0,0257	0,0011	
	HDAC6	0,1503	0,0199	
	JPD2	0,0047	0,0004	
	GSG1	0,0010	0,0001	
	PCDH7	0,3048	0,0241	
miR-3189-3p mimic +miR-3189-3p INH	HDAC1	1,3553	0,0987	
	HDAC2	0,6002	0,0250	
	HDAC3	0,6034	0,0461	
	HDAC4	0,0185	0,0013	
	HDAC5	0,0280	0,0015	
	HDAC6	0,1730	0,0163	
	JPD2	0,0044	0,0005	
	GSG1	0,0010	0,0000	
	PCDH7	0,2880	0,0234	
miR-3189-3p mimic +CTRL INH	HDAC1	0,6315	0,0602	**
	HDAC2	0,5014	0,0559	
	HDAC3	0,3431	0,0401	**
	HDAC4	0,0170	0,0006	
	HDAC5	0,0378	0,0030	**
	HDAC6	0,1653	0,0072	
	JPD2	0,0021	0,0002	**
	GSG1	0,0021	0,0002	**
	PCDH7	0,4586	0,0176	**
Data represent the average ± standard deviation of two independent experiments. *p< 0.05, **p<0.001 vs. CTRL (Welch test followed by Games-Howell test)				

Figure 22C				
Treatment	Gene	Average $2^{-\Delta C_T}$	SD	Significance
CTRL	BBC3	0,042015926	0,004535675	
	PMAIP1	0,154087469	0,025390682	
AM16	BBC3	0,17958325	0,015494582	**
	PMAIP1	0,646076448	0,070870777	**, ##
AM16 + ISRIB	BBC3	0,092357534	0,008108926	**, ##
	PMAIP1	0,389952488	0,032370203	**, ##
siBBC3 + AM16	BBC3	0,008516223	0,001600375	**, ##
	PMAIP1	0,317287905	0,062993656	**, ##
siBBC3 + AM16 + ISRIB	BBC3	0,00738297	0,000830297	**, ##
	PMAIP1	0,253144023	0,049243982	*, ##
siPMAIP1 + AM16	BBC3	0,140387857	0,019570806	**, #
	PMAIP1	0,011218556	0,001333588	**, ##
siPMAIP1 + AM16 + ISRIB	BBC3	0,126799263	0,019091827	**, ##
	PMAIP1	0,01355831	0,002659293	**, ##
siBBC3 + siPMAIP1 + AM16	BBC3	0,01133261	0,001530102	**, ##
	PMAIP1	0,022965276	0,002794189	**, ##
siBBC3 + siPMAIP1 + AM16 + ISRIB	BBC3	0,010597567	0,002581539	**, ##
	PMAIP1	0,024459408	0,003103871	**, ##
Data represent the average ± standard deviation of three independent experiments. **p<0.001, *p<0.05 vs. CTRL; ##p<0.001, #p<0.05 vs. AM16 (Welch test followed by Games-Howell test)				

Figure 25	CTRL			AM			NM			AM+NM		
Gene	Average $2^{-\Delta CT}$	SD	Sig.	Average $2^{-\Delta CT}$	SD	Sig.	Average $2^{-\Delta CT}$	SD	Sig.	Average $2^{-\Delta CT}$	SD	Sig.
APAF1	0,148596	0,009825399		0,109365736	0,009376405		0,125404047	0,02650329		0,245146938	0,029256715	*
BAD	0,013207083	0,002900333		0,007063526	0,000935671	*	0,008132867	0,001420377	*	0,007908643	0,000637306	*
BAK1	0,06819675	0,012788163		0,055674881	0,010537525		0,083543105	0,022346897		0,159252482	0,011492547	**
BAX	0,689311716	0,175138516		0,475923773	0,091457765		0,805865086	0,157345953		0,551754206	0,083342808	
BCL2	0,022849716	0,00252466		0,014269043	0,000871635		0,032104505	0,005336101		0,036343734	0,00555871	*
BCL2L1	0,228386447	0,024678176		0,244064207	0,017689859		0,324880415	0,048962388		0,290258739	0,042833802	
BCL2L11	0,115423405	0,008197175		0,114167225	0,013841343		0,15657934	0,043463187		0,373314936	0,047717036	**
CIAP	0,125146208	0,025863337		0,111968465	0,018166998		0,162877296	0,034406075		0,231404968	0,030727273	*
CIAP2	0,063490046	0,002431256		0,077176631	0,005113898		0,145131763	0,007971725	**	0,082761691	0,002006974	*
BBC3	0,027062029	0,003293733		0,021775006	0,002663746		0,043567347	0,003693156		0,119027246	0,016961367	**
PMAIP1	0,141560463	0,016759356		0,282747169	0,063239108		0,349861136	0,0787034	*	1,156749814	0,084764064	**
TNFRSF10A	0,133619719	0,01112933		0,138716673	0,024774334		0,19970013	0,009674387	*	0,262631548	0,025775937	**
TNFRSF10B	0,012463071	0,00245159		0,013358057	0,001268024		0,015628179	0,00238333		0,085009744	0,002858165	**
CASP3	0,1302557	0,036058692		0,110021643	0,032653876		0,133515641	0,034093142		0,20075635	0,046698929	
NFKB1	0,37310719	0,019431016		0,414292821	0,039099617		0,540241082	0,076794166	*	0,708774186	0,060540804	**
NFKB2	0,005666243	0,000936307		0,005244451	0,000198246		0,009322989	0,001611623	*	0,013211909	0,001203743	**
NFKBIA	0,208136344	0,028688096		0,232486169	0,046960984		0,324361412	0,040750925		0,326046908	0,04984537	
IKBKG	0,189741162	0,042647562		0,256649404	0,060575205		0,226587623	0,004421087		0,341035474	0,025880142	*
REL	0,142158373	0,037809616		0,120657861	0,025661231		0,14787802	0,029663217		0,12842977	0,027326622	
RELA	0,818072055	0,222826813		0,78601183	0,118306409		0,878891671	0,092448624		1,583424539	0,333495986	*
RELB	0,083124876	0,00422101		0,069912913	0,004616271		0,269598058	0,010821476	*	0,309125791	0,02124332	**
CDKN1A	0,801967038	0,020170736		0,642052449	0,012025469		1,017999845	0,056078916	*	3,092940978	0,096417449	**
CDKN2A	3,170992397	0,547564643		3,215411462	0,685457149		2,623926416	0,461453793		3,278615751	0,319721278	
Data represent the average ± standard deviation of three independent experiments. **p<0.001, *p<0.05 vs. CTRL (ANOVA, Bonferroni test)												

CANCER BIOTHERAPY AND RADIOPHARMACEUTICALS
Volume 00, Number 00, 2019

DOI: 10.1089/cbr.2018.2673

Identification of Further Components of an Anticancer Defense System Composed of Small Molecules Present in the Serum

Dalma Scheffer, Gyula Kulcsár, and Tamás Czömpöly

Abstract

Background: Earlier we assumed that small molecules selectively accumulated in cancer cells might have a role in a defense system capable of killing cancer cells. We reported earlier that an experimentally selected mixture of substances present in the serum (''active mixture,'' AM) shows a selective toxic effect *in vitro* and *in vivo* on various cancer cells. In this study we investigated additional compounds found in the serum to further expand our knowledge of this defense system.
Materials and Methods: The cell proliferation was detected by WST-1 assay. The mRNA level of the examined genes was measured by quantitative real-time polymerase chain reaction.
Results: We identified 34 additional compounds (L-amino acid metabolites, phenolic acids, D-amino acids, keto acids, etc.), which when applied in a *per se* nontoxic concentration are able to enhance the effect of AM. The combination of the mixture of these newly identified substances (new mixture, NM) with AM produced a significantly higher cancer cell growth inhibitory effect than NM or AM applied alone on HeLa, MCF-7, PC-3, Caco-2, HepG2, and 4T1 cancer cell lines, and more efficiently induced the expression of certain proapoptotic genes in HeLa cells. Any given combinations of the individual compounds of AM and NM always produced an increased effect compared with AM alone.
Conclusions: The newly identified compounds significantly enhance the anticancer effect of AM. The components of AM and NM together may form part of a defense system capable of killing cancer cells and are worthy of further investigation.

Keywords: antitumor defense, apoptosis, cancer, cancer targeting, small molecules

Introduction

The antitumor defense system of higher order species uses mechanisms sensing and repairing DNA damage, processes regulating the cell cycle, molecules playing a role in the regulation of apoptosis, and the antitumor effect of the immune system.[1] During our earlier work on the basis of epidemiological and experimental data we assumed that beside the immunological and nonimmunological surveillance an additional defense mechanism might provide protection against tumor development.

Through our research we have focused on small molecular weight compounds (amino acids, monosaccharides, nucleobases, etc.) that are present in the circulatory system and are differentially taken up by tumor and normal cells.[2] It has been shown that in addition to glucose many molecules (amino acids, vitamins) are accumulated in cancer cells.[3–6] The elevated uptake of these substances by cancer cells is utilized in positron emission tomography,[7] and based on the accumulation of amino acids or vitamins potential targeting strategies have been described.[8,9] According to our hypothesis, some of the accumulated substances beside their role in metabolism might participate in a defense system capable of killing cancer cells.

We have experimentally identified small molecular weight compounds present in the serum whose mixture (''active mixture,'' [AM]) showed a selective toxic effect *in vitro* and *in vivo* on different cancer cell lines.[10,11] We have analyzed mainly different L-amino acids, sugars and derivatives, vitamins, citric acid cycle intermediates, nucleobases and nucleosides, and selected those compounds that were able to significantly enhance each other cancer cell killing effect and

Cancer Research and Drug Development Center, Culevit Ltd., Pécs, Hungary.

Address correspondence to: Tamás Czömpöly; Cancer Research and Drug Development Center, Culevit Ltd., Finn u. 1/1; Pécs 7630, Hungary
E-mail: **czompoly@culevit.hu**

were nontoxic at the applied concentration when applied alone. The mixture of those selected substances were called the ''AM.''[10,11] We have demonstrated that AM selectively induces apoptosis of cancer cells *in vitro*.[12,13] Furthermore, we have provided evidence that the treatment with AM has a significant tumor inhibitory effect *in vivo*.[14] In addition, we have described that AM upregulated the expression of proapoptotic genes and induced apoptosis through the mitochondrial pathway.[14]

The aim of this study was to find additional compounds present in the serum that can enhance the effect of AM. We analyzed another 130 molecules that were not included in the previous studies and from these we identified 34 additional substances (D-amino acids, L-amino acid metabolites, phenolic acids, keto acids, etc.) that can increase the cancer cell killing effect of AM when applied individually in a *per se* nontoxic concentration.

Furthermore, we demonstrate that the mixture of the newly identified substances (''new mixture,'' [NM]) applied in combination with AM has a significantly greater cell growth inhibitory effect on different cancer cells, and more efficiently activates genes involved in apoptosis than either NM or AM applied alone. In addition, we provide evidence that various combinations of the compounds of NM and AM always produce an enhanced antitumor activity compared with the effect of AM.

Materials and Methods

Cell culture

HeLa (human cervix adenocarcinoma), 4T1 (mouse mammary carcinoma) cell lines were obtained from the American Type Culture Collection through LGC Standards GmbH, Germany. MCF-7 (human breast adenocarcinoma), PC-3 (human prostate adenocarcinoma), Caco-2 (human colorectal adenocarcinoma, male), and HepG-2 (human hepatocellular carcinoma, male) cell lines were obtained from The European Collection of Authenticated Cell Cultures through Sigma-Aldrich. Cells were expanded and early passage stocks were stored under liquid nitrogen. All stocks were tested for mycoplasma with the Mycoplasma Detection Kit both before cryopreservation and after thawing. Cancer cells were cultured in minimal essential medium (Sigma-Aldrich, Budapest, Hungary) supplemented with 10% (v/v) fetal calf serum, 100 U/mL penicillin, and 0.1 mg/mL streptomycin. Human renal epithelial (HRE cells pooled from donors with different sex) cells were obtained from Lonza and cultured in renal epithelial cell basal medium (Lonza, Szeged, Hungary) supplemented with human epidermal growth factor, hydrocortisone, epinephrine, insulin, triiodothyronine, transferrin, GA-1000, and 0.5% fetal bovine serum. Cells were incubated at 37°C in a humidified atmosphere at 5% CO_2.

Active mixture

The selection of the components of AM has been described previously.[10,11] The composition of 100% AM is as follows: 4 mM L-methionine, 0.75 mM L-tryptophan, 0.08 mM L-tyrosine disodium salt, 5 mM L-phenylalanine, 5 mM L-arginine, 4 mM L-histidine, 5 mM *N*-benzoyl glycine, 2 mM D-biotin, 1 mM pyridoxine hydrochloride, 0.006 mM riboflavin-5-phosphate sodium salt, 0.3 mM L-ascorbic acid, 1 mM lipoic acid, 0.16 mM orotic acid, 1 mM adenine hydrochloride, 7.5 mM 2-deoxy-D-ribose, 5 mM D-mannose, 0.5 mM D-glucosamine hydrochloride, 7.5 mM malic acid, 5 mM oxaloacetic acid, 0.05 mM adenosine triphosphate disodium salt, and 23.46 mM sodium hydrogen carbonate. In some experiments, 15 compounds from AM were randomly selected and divided into three subgroups (AM5.1, AM5.2, and AM5.3). The composition of the 100% AM5.1 is as follows: 1 mM adenine hydrochloride, 0.75 mM L-tryptophan, 1 mM pyridoxine hydrochloride, 7.5 mM malic acid, 4 mM L-histidine, and 15 mM sodium hydrogen carbonate. The composition of the 100% AM5.2 is as follows: 5 mM L-phenylalanine, 5 mM L-arginine, 4 mM L-methionine, 1 mM lipoic acid, 0.5 mM D-glucosamine hydrochloride, and 1 mM sodium hydrogen carbonate. The composition of the 100% AM5.3 is as follows: 2 mM D-biotin, 7.5 mM 2-deoxy-D-ribose, 5 mM *N*-benzoyl glycine, 0.006 mM riboflavin-5-phosphate sodium salt, 0.3 mM L-ascorbic acid, and 2.3 mM sodium hydrogen carbonate. All chemicals were purchased from Sigma-Aldrich.

New mixture

The composition of the 100% NM, identified in this article, is as follows: 2 mM D-phenylalanine, 1 mM D-tryptophan, 1 mM D-arginine, 0.5 mM 5-hydroxy-L-tryptophan, 0.05 mM melatonin, 5 mM mandelic acid, 2.5 mM 3,4-dihydroxymandelic acid, 0.8 mM *p*-coumaric acid, 0.8 mM *trans*-cinnamic acid, 1 mM indole-3-acetic acid, 1 mM phenylacetic acid, 0.1 mM 3,4-dihydroxyphenylacetic acid, 0.25 mM indole-3-pyruvic acid, 2.5 mM phenylpyruvic acid sodium salt, 1 mM 4-hydroxyphenylpyruvic acid, 1 mM 3-phenyllactic acid, 2.5 mM D-glyceric acid calcium salt, 0.25 mM glyceraldehyde, 3 mM 3-methyl-2-oxobutyric acid sodium salt, 5 mM 4-guanidinobutyric acid, 2.5 mM 3-methyl-2-oxovaleric acid sodium salt, 3 mM 4-methyl-2-oxovaleric acid sodium salt, 5 mM 3-hydroxy-3-methyl-glutaric acid, 1 mM gentisic acid sodium salt, 5 mM urocanic acid, 2.5 mM homovanillic acid, 2.5 mM xanthurenic acid, 5 mM levulinic acid calcium salt, 5 mM 4-hydroxybenzoic acid, 5 mM pyrrole-2-carboxylic acid, 0.25 mM adenosine, 0.1 mM agmatine sulfate, 0.5 mM cysteamine, 5 mM creatinine, and 38.45 mM sodium hydrogen carbonate. In some experiments, 15 compounds of the 34 were randomly selected and divided into three subgroups (NM5.1, NM5.2, and NM5.3). The composition of the 100% NM5.1 is as follows: 2 mM D-phenylalanine, 1 mM D-tryptophan, 5 mM mandelic acid, 0.1 mM agmatine sulfate, 0.25 mM indole-3-pyruvic acid, 5.25 mM sodium hydrogen carbonate. The composition of the 100% NM5.2 is as follows: 0.8 mM *p*-coumaric acid, 0.8 mM *trans*-cinnamic acid, 3 mM 3-methyl-2-oxobutyric acid sodium salt, 3 mM 4-methyl-2-oxovaleric acid sodium salt, 1 mM indole-3-acetic acid, 2.6 mM sodium hydrogen carbonate. The composition of the 100% NM5.3 is as follows: 2.5 mM 3-methyl-2-oxovaleric acid sodium salt, 0.1 mM 3,4-dihydroxyphenylacetic acid, 1 mM gentisic acid sodium salt, 5 mM urocanic acid, 1 mM D-arginine, 5.1 mM sodium hydrogen carbonate. All chemicals were purchased from Sigma-Aldrich.

WST-1 assay

The cells were seeded at a density of 4×10^3 cells/well on 96-well plates, and then the cells were treated with the test

compounds for 48 h in triplicates. 5-fluorouracil (5-FU) (Sigma-Aldrich) was used as a positive control of the inhibition of cell proliferation in the concentration range of 5–60 μM. The number of viable cells was measured with WST-1 cell proliferation reagent[15] according to the manufacturer's instructions (Roche, Budapest, Hungary). At the end of the treatment, cells were washed with phosphate-buffered saline, and then 90 μL phenol-red free RPMI medium (Sigma-Aldrich) and 10 μL WST-1 reagent were added to the cells. The cells were incubated for 30 min at 37°C, and then the optical density of each well was measured at 450 nm using an EL800 microplate reader. The results were expressed as the percentage of the untreated control. Experiments were repeated three times. The half maximal inhibitory concentration (IC50) was determined by fitting the dose–response curve using the OriginPro 8.6 software.

Quantitative real-time polymerase chain reaction

Total RNA was isolated with PureLink RNA Mini Kit (Thermo Fisher Scientific, Budapest, Hungary) and was treated with DNase I (Sigma-Aldrich). cDNA was prepared with High-Capacity RNA-to-cDNA Kit (Thermo Fisher Scientific). Polymerase chain reaction (PCR) primers used for real-time quantitative amplification of the human housekeeping genes B2M, GAPDH, HPRT1, RPL32, and PPIA were described previously.[16,17] PCR primers for human APAF1, BAD, BAK1, BAX, BCL2, BCL2L1, BCL2L11, BIRC2, BIRC3, CASP3, CDKN1A, CDKN2A, IKBKG, NFKBIA, NFKB1, NFKB2, REL, RELA, and RELB were also described previously.[14] All other PCR primers were designed by Primer Express Software, primer sequences are listed in Supplementary Table S1 (Supplementary Data are available online at www.liebertpub.com/cbr). The expression levels of BBC3, PMAIP1, RPL32 were measured with TaqMan gene expression assays (BBC3:Hs00248075_mL, PMAIP1: Hs00560402_mL, RPL32: Hs00851655_gL from Thermo Fisher Scientific). RPL32 was used for normalization. PCR reactions were run in triplicates using PowerUp SYBR Green Master Mix (Thermo Fisher Scientific) or TaqMan gene expression master mix II, no uracil n-glycosylase (Thermo Fisher Scientific) on an ABI StepOne Real-Time PCR System (Applied Biosystems, Budapest, Hungary). The relative quantity values were calculated by dividing the normalized target gene expression measured in the treated samples by that of the untreated control samples.[18]

Statistical analysis

Statistical analysis was performed with IBM SPSS Statistics 22. Normal distribution of the data was examined by Shapiro–Wilk test, homogeneity of variances was assessed with Levene test, and then one-way analysis of variance followed by Bonferroni *post hoc* test was performed. Values of $p < 0.05$ were considered statistically significant.

Data availability

The datasets generated during this study are available in the Open Science Framework repository, https://osf.io/vsb4c/; DOI 10.17605/OSF.IO/VSB4C.

Results

Identification of molecules capable to enhance the cell growth inhibitory effect of AM

To find additional compounds capable to increase the effect of AM we investigated an additional 130 compounds present in the serum. To be able to detect the potentiating effect of various compounds found in the serum, AM was used in a concentration that killed ~50%–60% of cancer cells. HeLa cells were treated with 50% AM alone or in combination with the newly examined 130 individual compounds. The newly examined compounds were applied in *per se* nontoxic concentrations determined in preliminary experiments. The cells were treated for 48 h, and then the cell proliferation was measured by WST-1 assay. After 48 h of treatment, we selected those compounds for further evaluation that were able to significantly enhance the effect of AM. Of the 130 examined compounds 34 was able to significantly potentiate ($p < 0.001$) the cancer cell killing effect of AM (Fig. 1). Treatment with 50% AM reduced the number of living cells to 46.25% ± 1.36% of the untreated control. Each of the newly identified 34 compounds significantly enhanced this effect, although the extent of the enhancement was different among the compounds: the number of living cells was reduced to 22.41%–40.36% of the untreated control. The 34 newly identified compounds are the following: D-phenylalanine, D-tryptophan, D-arginine, 5-hydroxy-L-tryptophan, melatonin, mandelic acid, 3,4-dihydroxymandelic acid, *p*-coumaric acid, *trans*-cinnamic acid, indole-3-acetic acid, phenylacetic acid, 3,4-dihydroxyphenylacetic acid, indole-3-pyruvic acid, phenylpyruvic acid, 4-hydroxyphenylpyruvic acid, 3-phenyllactic acid, D-glyceric acid, glyceraldehyde, 3-methyl-2-oxobutyric acid, 4-guanidinobutyric acid, 3-methyl-2-oxovaleric acid, 4-methyl-2-oxovaleric acid, 3-hydroxy-3-methyl-glutaric acid, gentisic acid, urocanic acid, homovanillic acid, xanthurenic acid, levulinic acid, 4-hydroxybenzoic acid, pyrrole-2-carboxylic acid, adenosine, agmatine, cysteamine, and creatinine.

Comparison of the effect of NM and AM on cancer cells

Next we investigated the effect of the mixture comprising the newly identified 34 compounds, called NM, compared with AM on HeLa (Fig. 2A), PC-3 (Fig. 2B), MCF-7 (Fig. 2C), Caco-2 (Fig. 2D), HepG-2 (Fig. 2E), 4T1 (Fig. 2F) cancer cells and on HRE normal cells (Fig. 2G). For the optimal detection of differences in efficacy, we used dilution series of the different mixtures (10%, 15%, 20%, 25%, and 30%). Figure 2 shows that NM has a significantly greater cell growth inhibitory effect compared with the treatment with AM ($p < 0.001$ vs. corresponding dilution of AM) on the different cancer cells. The combination of AM and NM was also tested. We found that the combined treatment (AM+NM) was able to more efficiently inhibit the cancer cell growth compared with AM or NM ($p < 0.001$ vs. corresponding dilution of NM and vs. corresponding dilution of AM), and the 30% AM+NM killed all the cells after 48 h of incubation. These results demonstrate that AM, NM, and the combined mixture reduced the number of cancer cells in a dose-dependent manner, but showed differences in their potency. However, the proliferation of HRE cells (Fig. 2G) was not decreased by any of the mixtures, rather they slightly increased the cell number. As a positive control of the inhibition of cell

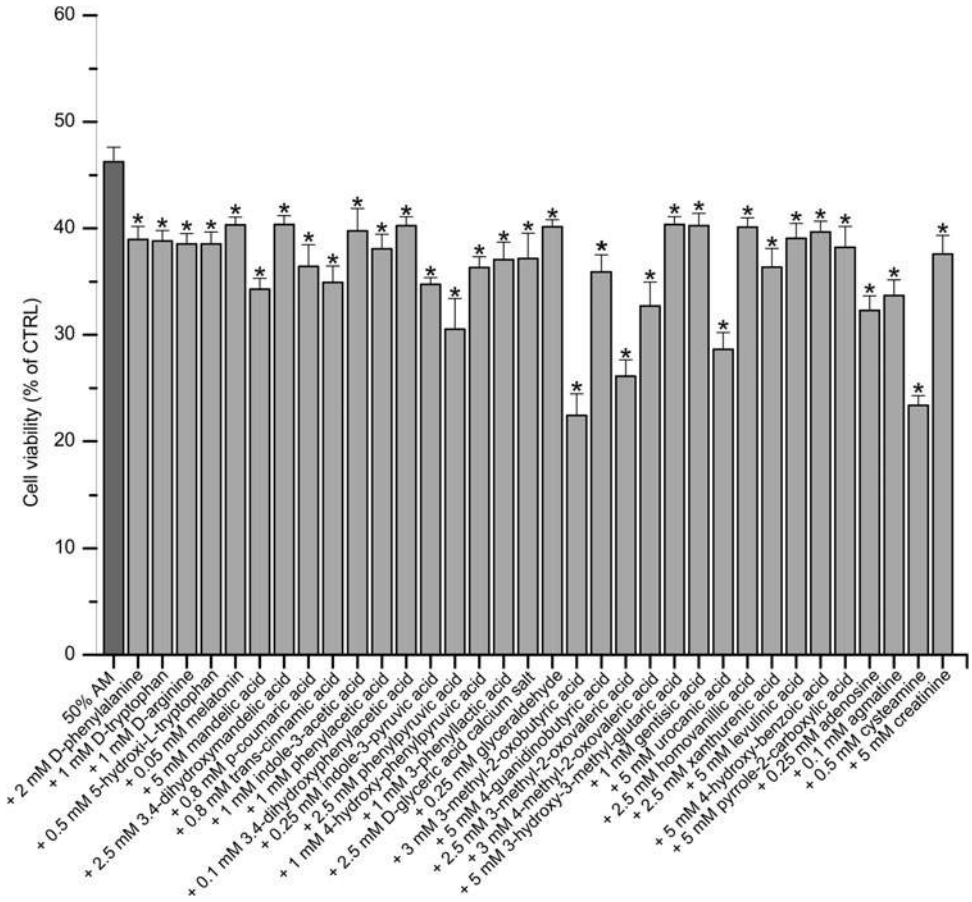

FIG. 1. The newly identified 34 compounds enhance the cell growth inhibitory effect of AM. HeLa cells were treated with 50% AM alone or with the individual combination of 34 compounds and 50% AM for 48 h. The newly examined compounds were applied in *per se* nontoxic concentrations. Results are expressed as percentage of untreated control cells. The *bars* represent the average ± standard deviation of three independent experiments. $*p < 0.001$ versus 50% AM (ANOVA, Bonferroni test). AM, active mixture; ANOVA, analysis of variance.

proliferation we used 5-FU in the concentration range of 5–60 μM. Figure 2H shows that 60 μM of 5-FU produced approximately the same degree of inhibition as 15% AM+NM (5-FU: 38.44%–48.2% of the untreated control vs. 15% AM+NM: 34.49%–44.37% of the untreated control) on the tested human cancer cell lines (HeLa, PC-3, MCF-7, Caco-2, and HepG-2), whereas the murine 4T1 cell line was more sensitive to 5-FU (20 μM killed all the cells), and 20% of AM+NM was required to produce approximately the same inhibition as we have seen on the human cell lines (44.44% of the untreated control).

AM and NM influence the expression of genes involved in apoptosis

Next we measured the expression of certain pro- and antiapoptotic genes, as well as genes regulating the cell cycle by quantitative PCR after the treatment of HeLa cells with 30% AM, 20% NM, or the combination of 30% AM and 20% NM (Fig. 3). Treatment with 30% AM had a slight or no effect on the expression of genes investigated compared with the control. Combined treatment with 30% AM and 20% NM significantly increased the expression of the proapoptotic BH3-only protein encoding *BIM* (3.23-fold, $p < 0.001$), *PUMA* (4.40-fold, $p < 0.001$), *NOXA* (8.17-fold, $p < 0.001$), and the antiapoptotic member of BCL-2 family encoding *BCL-2* (1.59-fold, $p < 0.05$) compared with the untreated control. The expression level of the proapoptotic death receptor genes, *DR4* (*TNFRSF10A*) (1.97-fold, $p < 0.001$) and *DR5* (*TNFRSF10B*) (6.82-fold, $p < 0.001$) were increased, together with the antiapoptotic protein encoding *cIAP* (1.85-fold, $p < 0.05$) and *cIAP2* (1.30-fold, $p < 0.05$) transcript levels. Among the nuclear factor κB (NF-kB) signaling-related genes the expression level of *NFKB1* (1.90-fold, $p < 0.001$), *NFKB2* (2.33-fold, $p < 0.001$), *IKBKG* (1.80-fold, $p < 0.05$), *RELA* (1.94-fold, $p < 0.05$), and *RELB* (3.72-fold, $p < 0.001$) were increased. The level of *CDKN1A* was increased to 4.82-fold ($p < 0.001$). Twenty percent NM mixture applied alone also induced changes in the expression of pro- and antiapoptotic genes but to a lesser extent than AM+NM, levels of *NOXA* (2.47-fold, $p < 0.05$), *cIAP2* (2.29-fold, $p < 0.001$), *TNFRSF10A* (1.49-fold, $p < 0.05$), *NFKB2* (1.65-fold, $p < 0.05$), and *RELB* (3.24-fold, $p < 0.001$) were increased.

FIG. 2. Comparison of the effect of NM and AM on the growth of cancer and normal cells. HeLa **(A)**, PC-3 **(B)**, MCF-7 **(C)**, Caco-2 **(D)**, HepG-2 **(E)**, 4T1 **(F),** and HRE **(G)** cells were treated with the dilution series of AM, NM, or AM+NM for 48 h. The dilution of the mixtures is expressed in percentage (10%, 15%, 20%, 25%, and 30%). 5-Fluorouracil was used as a positive control of the inhibition of cell proliferation in the concentration range of 5–60 μM **(H)**. The values represent the average ± standard deviation of three independent experiments. $**p < 0.001$; $*p < 0.05$ versus the corresponding dilution of AM; $\#\#p < 0.001$; $\#p < 0.05$ versus the corresponding dilution of NM (ANOVA, Bonferroni test). NM, new mixture; HRE, human renal epithelial cells.

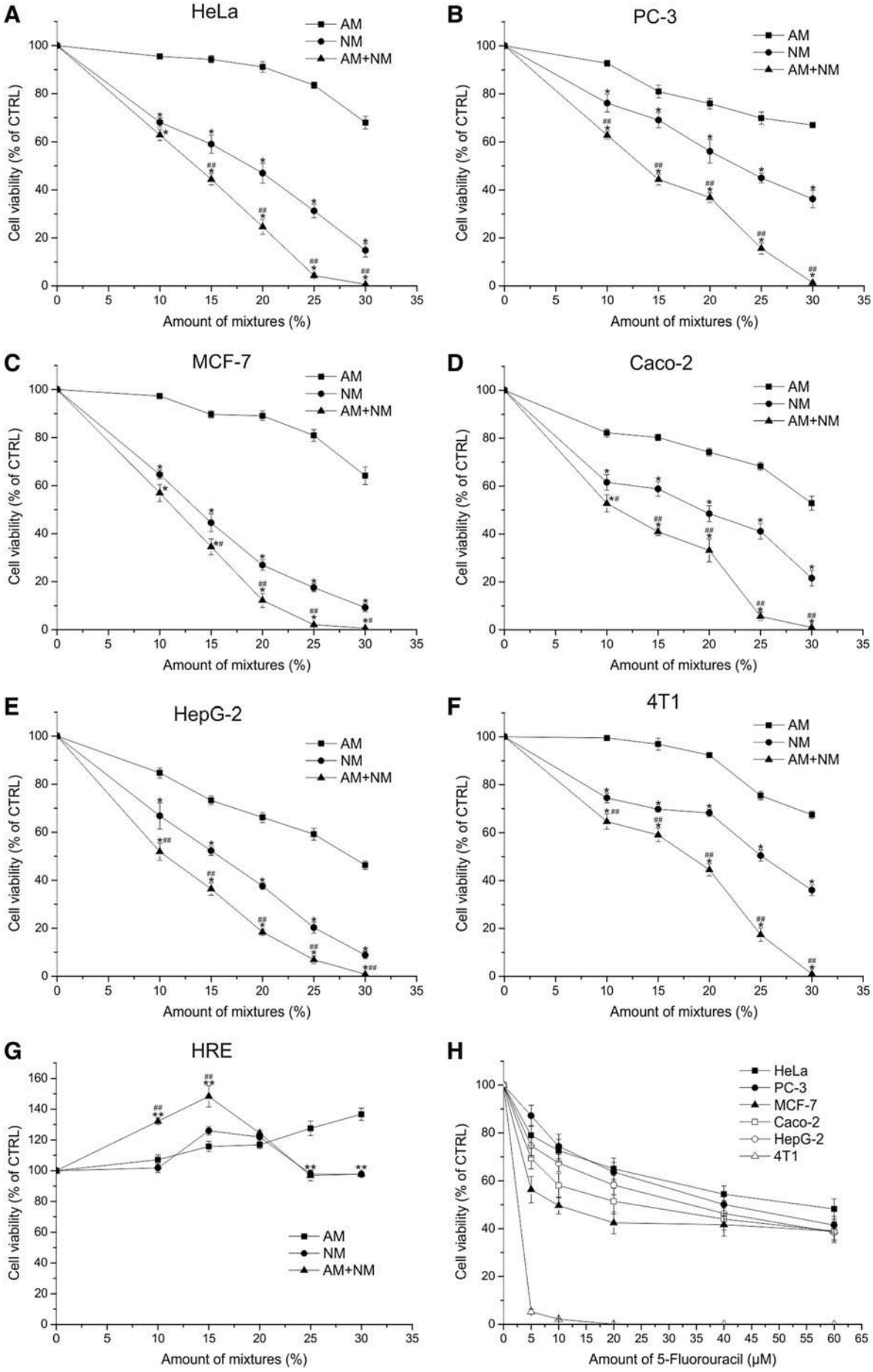
A
HeLa
AM
NM
AM+NM
Cell viability (% of CTRL)
Amount of mixtures (%)
B
PC-3
C
MCF-7
D
Caco-2
E
HepG-2
F
4T1
G
HRE
H
HeLa
PC-3
MCF-7
Caco-2
HepG-2
4T1
Amount of 5-Fluorouracil (μM)

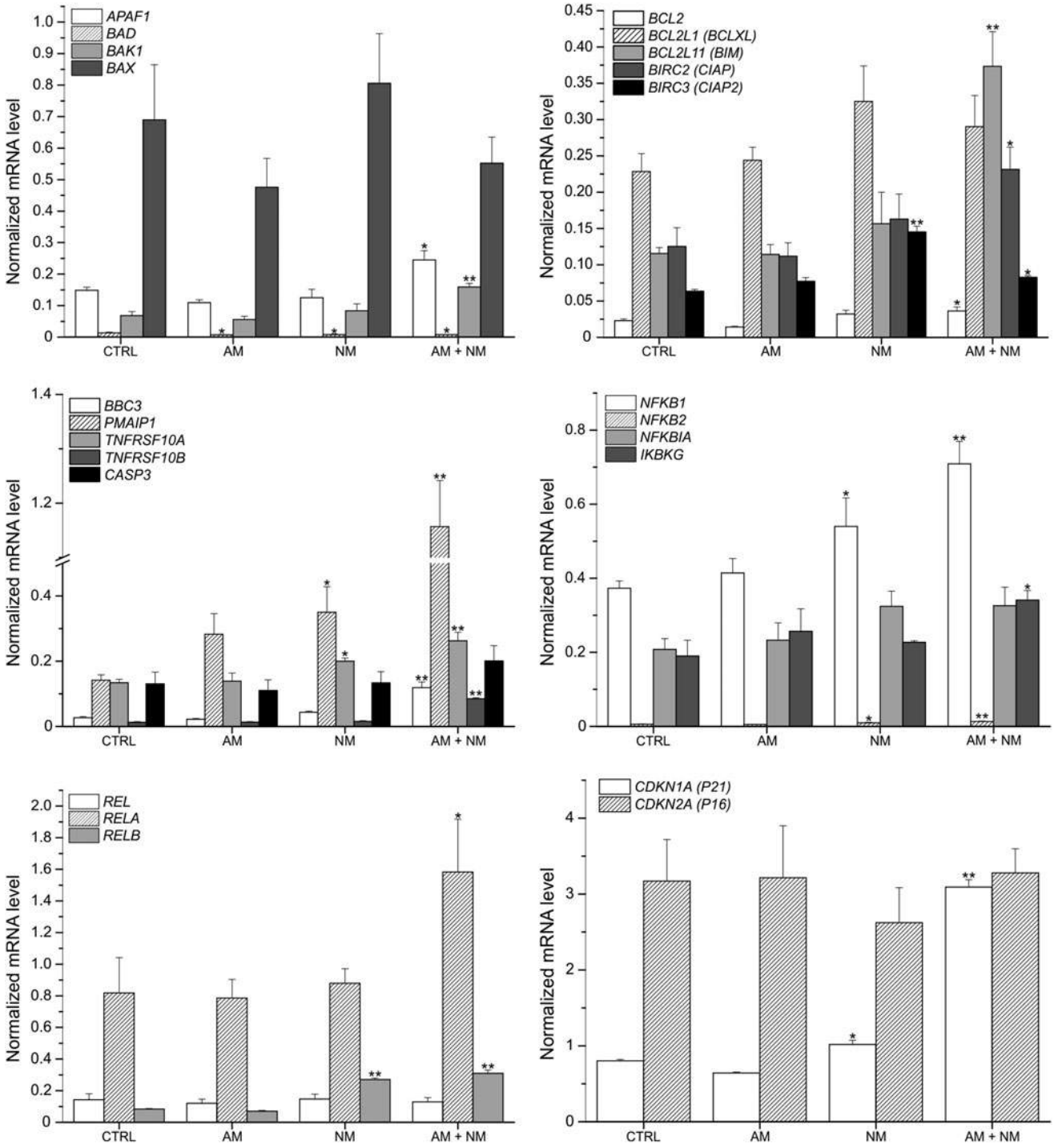

FIG. 3. NM and the combination of AM and NM influence the expression of genes involved in apoptosis and cell cycle regulation. HeLa cells were treated with 20% AM, 30% NM, or the combination of 20% AM and 30% NM for 24 h. mRNA levels were detected with quantitative real-time polymerase chain reaction. The *bars* represent the average ± standard deviation of three independent experiments. $^{**}p < 0.001$; $^{*}p < 0.05$ versus control (ANOVA, Bonferroni test). CTRL, untreated control.

Comparison of the tumor cell killing effect of various mixtures of the newly identified substances with mixtures of compounds identified earlier

To further investigate the potentiating effect of the newly identified 34 compounds on the compounds identified earlier, we compared 15 component mixtures comprising 5 compounds selected from NM (NM5.1, NM5.2, NM5.3) and 10 compounds selected from AM (AM5.1+AM5.2, AM5.2+AM5.3, AM5.1+AM5.3) with a 15 component mixture comprising compounds solely from AM (AM5.1+AM5.2+AM5.3) (Fig. 4).

For the optimal detection of differences in efficacy, we used dilution series of the different mixtures (20%, 40%, 60%, 80%, 100%). Treatment with 60% AM5.1+AM5.2+AM5.3

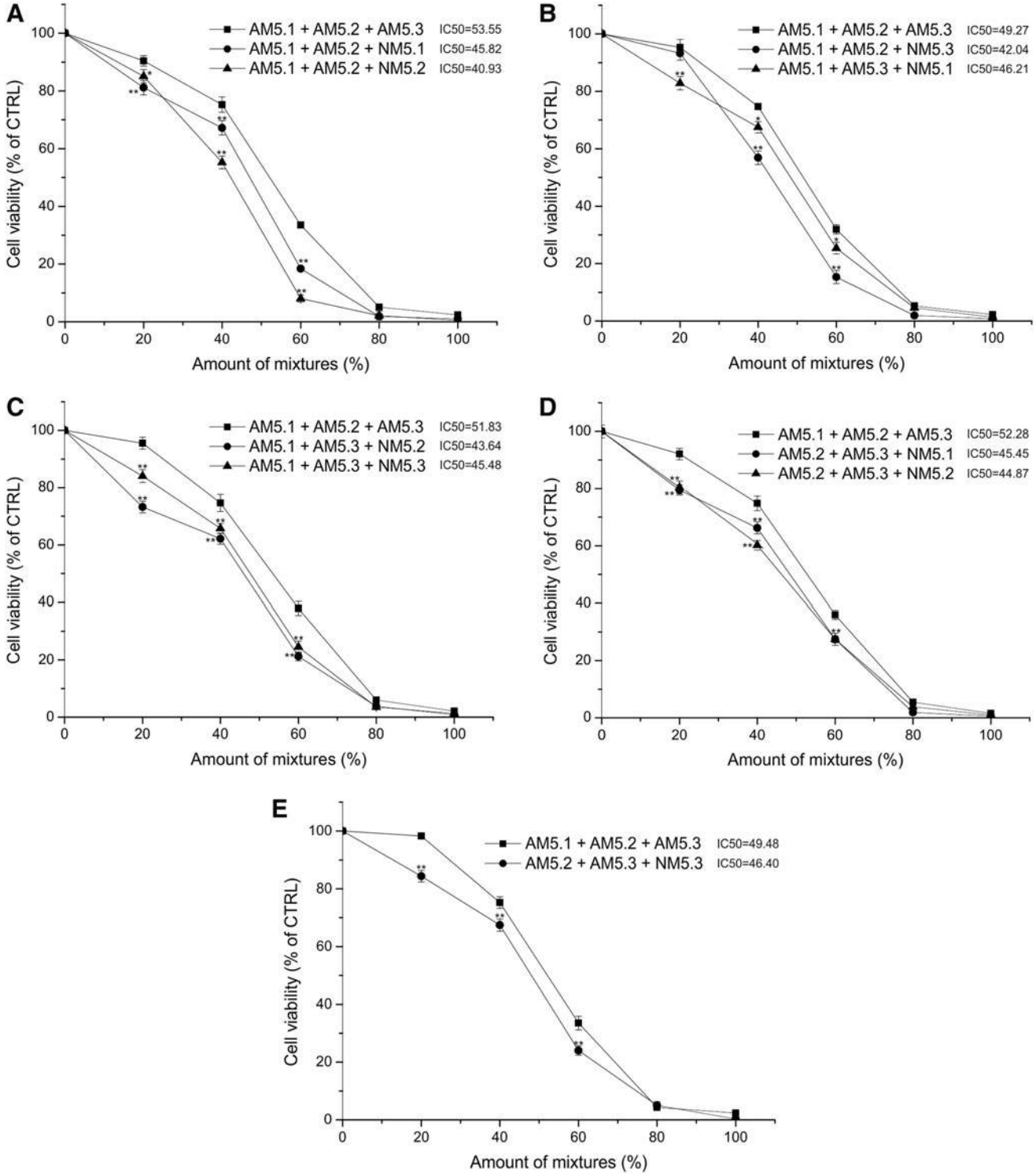

FIG. 4. Fifteen component mixtures that comprise 10 earlier identified compounds and 5 newly identified compounds have higher cell growth inhibitory effect on HeLa cells than mixtures containing exclusively components of AM. The cells were treated with the dilution series of the indicated combinations of AM5.1, AM5.2, AM5.3, NM5.1, NM5.2, and NM5.3 for 48 h. **(A–E)** The dilution of the mixtures is expressed in percentage (20%, 40%, 60%, 80%, and 100%). The values represent the average ± standard deviation of three independent experiments. $^{**}p < 0.001$; $^{*}p < 0.05$ versus the corresponding dilution of AM5.1+AM5.2+AM5.3 (ANOVA, Bonferroni test). The IC50 is defined as the concentration causing 50% growth inhibition compared with the untreated control. IC50, half maximal inhibitory concentration.

reduced the number of living cells to 31.93% ± 1.59%–37.91% ± 2.43% of the untreated control. When AM5.1 or AM5.2 or AM5.3 was replaced by a 60% mixture containing 5 compounds selected from the newly identified 34 compounds, the tumor cell killing effect was significantly enhanced, the number of living cells was reduced to 8.06% ± 1.26% ($p < 0.001$)–27.45% ± 2.09% ($p < 0.001$) of the untreated control. IC50 values of the 15 component mixtures comprising compounds solely from AM were between 49.27% and 53.55%. IC50 values of the mixtures containing 5 compounds from NM and 10 compounds from AM were between 40.93% and 46.40%.

Next, we evaluated the effectiveness of 15 component mixtures that contain 10 compounds from NM (NM5.1+NM5.2, NM5.2+NM5.3, NM5.1+NM5.3) and 5 compounds from AM (AM5.1, AM5.2, AM5.3) compared with the mixture of AM5.1+AM5.2+AM5.3 (Fig. 5). Treatment with 60% AM5.1+AM5.2+AM5.3 reduced the number of living cells to 33.49% ± 2.14%–36.39% ± 1.98% of the untreated control. When either two of AM5.1, AM5.2, or AM5.3 mixtures was replaced by two 60% mixtures comprising five compounds selected from NM (NM5.1+NM5.2, NM5.2+NM5.3, NM5.1+NM5.3), the cell growth inhibitory effect was even more pronounced. The number of living cells was reduced to 3.82% ± 0.85%–25.45% ± 2.72% to the untreated control. IC50 values of the 15 component mixtures comprising compounds solely from AM were between 50.21% and 52.29%. IC50 values of the mixtures containing 10 compounds from NM and 5 compounds from AM were between 27.69% and 42.70%.

These results show that combinations of the newly identified compounds with the earlier identified compounds always produced an enhanced cancer cell killing effect compared with the single application of mixtures comprised solely of compounds identified earlier (AM).

Discussion

Previously we demonstrated that a mixture of experimentally selected substances (amino acids, vitamins, nucleobases, etc.) found in the serum called AM induced apoptosis of cancer cells both *in vitro* and *in vivo* and had a significant tumor inhibitory effect *in vivo*.[12,14] On the basis of our assumption that some of the accumulated substances might be part of an antitumor defense system,[13] in this study we tested another 130 compounds found in the serum and we identified 34 additional substances that are capable to kill cancer cells and synergistically enhance each other's and the earlier identified compound's effect. We applied the tested compounds in a *per se* nontoxic concentration; thus, it can be stated that the 34 newly identified compounds potentiated in a synergistic manner the tumor cell killing effect of AM on HeLa cells.

To further investigate the synergistic effect of the newly identified substances, we performed additional cell viability assays with randomly selected compounds of NM and/or AM. We have tested other combinations as well, which always produced the same results (data not given). These results raise the possibility that any given combination of the newly identified compounds with the earlier identified compounds would produce an enhanced tumor cell killing effect compared with the single application of any given combination of the earlier identified compounds.

The components of NM are mainly L-amino acid metabolites, phenolic acids (benzoic acid derivatives, cinnamic acid derivatives), D-amino acids, and keto acids. Some of these newly identified compounds have been reported to have anticancer activities. The antiproliferative properties of phenolic acids have been widely studied. *Trans*-cinnamic acid has growth inhibitory effect on leukemia,[19] melanoma,[20] colon adenocarcinoma,[21,22] lung adenocarcinoma and pancreatic carcinoma cell lines,[21] *p*-coumaric acid (hydroxycinnamic acid) inhibits the proliferation of colon cancer cells,[23] and 3,4-dihydroxyphenylacetic acid has antiproliferative effect on prostate and colon cancer cell lines.[24]

Besides, there are reports that demonstrate that agmatine, metabolite of L-arginine, inhibits the proliferation of human intestinal and prostate cancer cell lines, human and rat hepatoma cell lines.[25,26] Furthermore, cysteamine, the degradation product of coenzyme A, inhibits pancreatic cancer cell migration and invasion *in vitro*.[27]

To further evaluate the anticancer activity of the newly identified substances, the effect of the mixture of the new substances (NMs) was investigated on various cancer cells. We applied the different substances in a *per se* nontoxic concentration and showed that NM and the combined mixture of AM and NM have a significant growth-inhibiting effect on HeLa human cervix adenocarcinoma, MCF-7 human breast adenocarcinoma, PC-3 human prostate adenocarcinoma, Caco-2 human colorectal adenocarcinoma, HepG-2 human hepatocellular carcinoma, and 4T1 mouse mammary carcinoma compared with the mixture of AM. Treatment with any given mixtures caused no toxic effect on HRE normal cells. This is in agreement with our hypothesis that the mixture of substances we have selected has a specific inhibitory effect on cancer cells. Our findings that NM has anticancer activity on a broad spectrum of cancer cells with different histological origin in our view indicates that the inhibitory effect of NM could represent a general defense mechanism.

Furthermore, treatment with the combination of AM and NM elicited induction of *PUMA*, *NOXA*, *BIM*, and *CDKN1A* in HeLa cells, which points toward the induction of apoptosis through the mitochondrial pathway and probably leading to cell cycle arrest, is also in agreement with our previous result.[14] The expression level of two death receptors, *DR4* and *DR5*, were also upregulated. As death receptors are important components of the extrinsic apoptotic pathway,[28] increased expression of *DR4* and *DR5* raises the possibility that this pathway also contributes to the cell growth inhibition caused by AM+NM. In this study, the treatment with AM was not able to activate the examined genes. This is most likely because of the fact that we applied a lower dose of AM compared with our previous reports to notice the synergistic effect of NM. However, treatment solely with NM could induce changes in gene expression but could not reach the same level as produced by the combined treatment.

Given the multicomponent nature of AM and NM, the anticancer activity of them is probably mediated by the interplay of several different mechanisms. In our earlier mechanistic studies of AM, which in part is composed of essential amino acids, we described the mitochondrial pathway of apoptosis induction and the upregulation of genes contributing to apoptosis induction and cell cycle

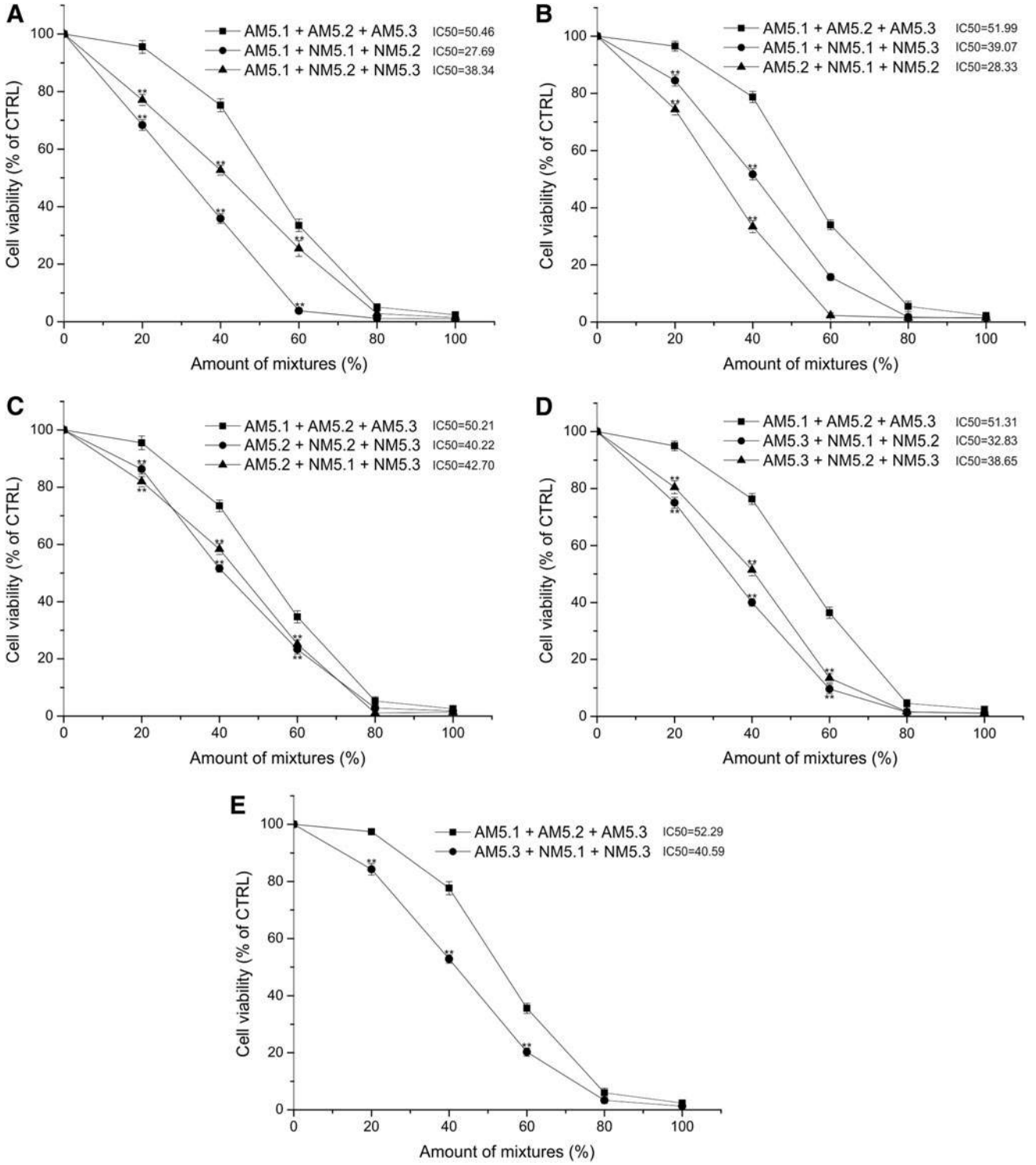

FIG. 5. Fifteen component mixtures that comprise 5 earlier identified compounds and 10 newly identified compounds have higher cell growth inhibitory effect on HeLa cells than mixtures containing exclusively components of AM. The cells were treated with the dilution series of the indicated combinations of AM5.1, AM5.2, AM5.3, NM5.1, NM5.2, and NM5.3 for 48 h. **(A–E)** The dilution of the mixtures is expressed in percentage (20%, 40%, 60%, 80%, and 100%). The values represent the average ± standard deviation of three independent experiments. $^{**}p < 0.001$ versus the corresponding dilution of AM5.1+AM5.2+AM5.3 (ANOVA, Bonferroni test). The IC50 is defined as the concentration causing 50% growth inhibition compared with the untreated control.

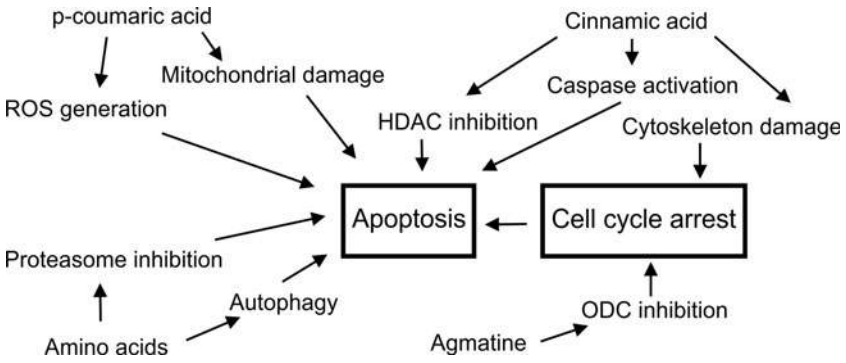

FIG. 6. Possible mechanisms contributing to the anticancer effect of AM+NM.

arrest (*PMAIP1*, *BBC3*, *CDKN1A*).[14] In addition to our results it has been reported by Bonfili et al. that mixtures of essential amino acids inhibit proteasomal activity, induce autophagy, and apoptosis in a cancer-specific manner.[29] Of the components of NM, cinnamic acid has been reported to induce cytoskeletal damage and caspase activation in melanoma cells.[20] In addition, it has been shown to inhibit histone deacetylases and increase the expression of certain proapoptotic genes in colon cancer and pancreatic cancer cells.[21] *p*-coumaric acid is known to increase the production of reactive oxygen species and induce apoptosis through the mitochondrial pathway in colon cancer cells.[23] Agmatine has been shown to interfere with the polyamine metabolism by inhibition of ornithine decarboxylase in colon cancer cells.[25] There are no data about the possible mechanisms involved in the anticancer activity of every one of the components of AM or NM, and we would like to stress out that this study focused on the experimental selection of new substances (components of NM) and not on identifying all possible mechanisms involved. The various mechanisms that might contribute to the anticancer activity of AM+NM mixture are summarized in Figure 6; however, we would like to emphasize that there might be additional signaling pathways that could be activated because of the multicomponent nature of these mixtures.

Cancer cells have altered metabolism to support their growth and survival.[30] The increased consumption of glucose accompanied by increased aerobic glycolysis is one example of that. Aerobic glycolysis and other cancer-associated changes in metabolism can alter the intracellular metabolite levels.[3,31] Many oncogenic mutations lead to the accumulation of certain metabolites with oncogenic potential.[31] For example, high level of fumarate and succinate, caused by the loss of fumarate hydratase and succinate dehydrogenase, can positively affect tumorigenesis by competitive inhibition of the of α-ketoglutarate-dependent dioxygenases that have a role in epigenetic regulation.[32] The elevated glycolytic flux can increase the level of glycolytic intermediates, such as methylglyoxal (MG) produced by the spontaneous decomposition of glyceraldehyde-3-phosphate and dihydroxyacetone phosphate.[33] MG may have oncogenic roles[31]; however, there are emerging evidences that excess level of MG can inhibit various cancer cells.[34,35] Thus, changes in metabolite levels could have different consequences, some of them may inhibit cancer growth or others are required for tumorigenesis.[31]

Thus, our overloading strategy of defined substances that may alter the metabolite level in a way that is deleterious for cancer cells might be a potential therapeutic approach.

Conclusions

We demonstrated that the newly identified compounds are able to significantly enhance the antitumor effect of AM. The combined mixture of AM and NM inhibits the growth of various cancer cells *in vitro* more effectively than the individual mixtures *per se*, without any toxic effect on normal cells.

The high number of compounds and the fact that they enhance each other's effect provide the opportunity to design mixtures that might be more effective against specific types of cancer.

Authors' Contributions

Conceptualization, G.K., D.S., and T.C.; Methodology, G.K., D.S., and T.C.; Formal analysis, G.K., D.S. and T.C.; Investigation, G.K., D.S., and T.C.; Writing–Original Draft, D.S., G.K., and T.C.; Supervision, G.K. and T.C.; Funding Acquisition, G.K. and T.C. The corresponding author declares that all coauthors have reviewed and approved the article.

Acknowledgments

This work has been supported in part by a Ministry for National Economy, Hungary grant GINOP-2.1.1.-15-2015-00046.

Disclosure Statement

G.K. owns a 15% share in Culevit Ltd.

References

1. Klein G, Klein E. Surveillance against tumors-is it mainly immunological? Immunol Lett 2005;100:29.
2. Kulcsár G. Theoretical and literary evidence for the existence of the passive antitumor defense system. Cancer Biother Radiopharm 1997;12:281.
3. Vander Heiden MG, Cantley LC, Thompson CB. Understanding the Warburg effect: The metabolic requirements of cell proliferation. Science 2009;324:1029.
4. Flodh H, Ullberg S. Accumulation of labelled vitamin B12 in some transplanted tumours. Int J Cancer 1968;3:694.

5. Blomquist L, Flodh H, Ullberg S. Uptake of 125I-labelled 4-iodophenylalanine in tumours of mice. Br J Cancer 1969; 23:150.
6. Ong ES, Zou L, Li S, et al. Metabolic profiling in colorectal cancer reveals signature metabolic shifts during tumorigenesis. Mol Cell Proteomics 2010; DOI: 10.1074/mcp.M900551-MCP200
7. Qi Y, Liu X, Li J, et al. Fluorine-18 labeled amino acids for tumor PET/CT imaging. Oncotarget 2017;8:60581.
8. Giese C, Lepthien S, Metzner L, et al. Intracellular uptake and inhibitory activity of aromatic fluorinated amino acids in human breast cancer cells. Chem Med Chem 2008;3:1449.
9. Waibel R, Treichler H, Schaefer NG, et al. New derivatives of vitamin B12 show preferential targeting of tumors. Cancer Res 2008;68:2904.
10. Kulcsár G. Inhibition of the growth of a murine and various human tumor cell lines in culture and in mice by mixture of certain substances of the circulatory system. Cancer Biother 1995;10:157.
11. Kulcsár G. Synergistic potentiating effect of D(+)-mannose, orotic, and hippuric acid sodium salt on selective toxicity of a mixture of 13 substances of the circulatory system in culture for various tumor cell lines. Cancer Detect Prev 2000;24:485.
12. Kulcsár G. Apoptosis of tumor cells induced by substances of the circulatory system. Cancer Biother Radiopharm 1997;12:19.
13. Kulcsár G. Experimental evidence for the existence of the passive antitumor defense system formed by the synergistic action of certain small substances of the circulatory system. Cancer Biother Radiopharm 2003;18:949.
14. Kulcsár G, Gaál D, Kulcsár PI, et al. A mixture of amino acids and other small molecules present in the serum suppresses the growth of murine and human tumors in vivo. Int J Cancer 2013;132:1213.
15. Berridge MV, Herst PM, Tan AS. Tetrazolium dyes as tools in cell biology: New insights into their cellular reduction. Biotechnol Annu Rev 2005;11:127.
16. Colell A, Ricci JE, Tait S, et al. GAPDH and autophagy preserve survival after apoptotic cytochrome c release in the absence of caspase activation. Cell 2007;129:983.
17. Zhang X, Ding L, Sandford AJ. Selection of reference genes for gene expression studies in human neutrophils by real-time PCR. BMC Mol Biol 2005;6:4.
18. Schmittgen TD, Livak KJ. Analyzing real-time PCR data by the comparative C(T) method. Nat Protoc 2008;3:1101.
19. Zhang J, Xiao A, Wang T, et al. Effect and mechanism of action of cinnamic acid on the proliferation and apoptosis of leukaemia cells. Biomed Res 2014;25:405.
20. Niero EL, Machado-Santelli GM. Cinnamic acid induces apoptotic cell death and cytoskeleton disruption in human melanoma cells. J Exp Clin Cancer Res 2013;32:31.
21. Zhu B, Shang B, Li Y, et al. Inhibition of histone deacetylases by trans-cinnamic acid and its antitumor effect against colon cancer xenografts in athymic mice. Mol Med Rep 2016;13:4159.
22. Ekmekcioglu C, Feyertag J, Marktl W. Cinnamic acid inhibits proliferation and modulates brush border membrane enzyme activities in Caco-2 cells. Cancer Lett 1998;128:137.
23. Jaganathan SK, Supriyanto E, Mandal M. Events associated with apoptotic effect of p-Coumaric acid in HCT-15 colon cancer cells. World J Gastroenterol 2013;19:7726.
24. Gao K, Xu A, Krul C, et al. Of the major phenolic acids formed during human microbial fermentation of tea, citrus, and soy flavonoid supplements, only 3,4-dihydroxyphenylacetic acid has antiproliferative activity. J Nutr 2006;136:52.
25. Molderings GJ, Kribben B, Heinen A, et al. Intestinal tumor and agmatine (decarboxylated arginine): Low content in colon carcinoma tissue specimens and inhibitory effect on tumor cell proliferation in vitro. Cancer 2004;101:858.
26. Mayeur C, Veuillet G, Michaud M, et al. Effects of agmatine accumulation in human colon carcinoma cells on polyamine metabolism, DNA synthesis and the cell cycle. Biochim Biophys Acta 2005;1745:111.
27. Fujisawa T, Rubin B, Suzuki A, et al. Cysteamine suppresses invasion, metastasis and prolongs survival by inhibiting matrix metalloproteinases in a mouse model of human pancreatic cancer. PLoS One 2012;7:e34437.
28. Elmore S. Apoptosis: A review of programmed cell death. Toxicol Pathol 2007;35:495.
29. Bonfili L, Cecarini V, Cuccioloni M, et al. Essential amino acid mixtures drive cancer cells to apoptosis through proteasome inhibition and autophagy activation. FEBS J 2017; 284:1726.
30. Pavlova NN, Thompson CB. The emerging hallmarks of cancer metabolism. Cell Metab 2016;23:27.
31. Sullivan LB, Gui DY, Vander Heiden MG. Altered metabolite levels in cancer: Implications for tumour biology and cancer therapy. Nat Rev Cancer 2016;16:680.
32. Xiao M, Yang H, Xu W, et al. Inhibition of α-KG-dependent histone and DNA demethylases by fumarate and succinate that are accumulated in mutations of FH and SDH tumor suppressors. Genes Dev 2012;26:1326.
33. Bellahcène A, Nokin MJ, Castronovo V, et al. Methylglyoxal-derived stress: An emerging biological factor involved in the onset and progression of cancer. Semin Cancer Biol 2018; 49:64.
34. Guo Y, Zhang Y, Yang X, et al. Effects of methylglyoxal and glyoxalase I inhibition on breast cancer cells proliferation, invasion, and apoptosis through modulation of MAPKs, MMP9, and Bcl-2. Cancer Biol Ther 2016;17:169.
35. Antognelli C, Mezzasoma L, Fettucciari K, et al. A novel mechanism of methylglyoxal cytotoxicity in prostate cancer cells. Int J Biochem Cell Biol 2013;45:836.

Cellular Signalling 65 (2020) 109426

Contents lists available at ScienceDirect

Cellular Signalling

journal homepage: www.elsevier.com/locate/cellsig

Active mixture of serum-circulating small molecules selectively inhibits proliferation and triggers apoptosis in cancer cells via induction of ER stress

Dalma Scheffer[a,1], Gyula Kulcsár[a], György Nagyéri[b], Marianna Kiss-Merki[b], Zoltán Rékási[c], Magnus Maloy[c], Tamás Czömpöly[a,*,1]

[a] Cancer Research and Drug Development Center, Culevit Ltd., Pécs, Finn u. 1/1., 7630, Hungary
[b] Soft Flow Hungary Ltd., Pécs, Ürögi fasor 2/A, 7628, Hungary
[c] Department of Anatomy, Medical School, University of Pécs, Pécs, Szigeti u. 12., 7624, Hungary

ARTICLE INFO

Keywords:
Cancer
ER stress
Unfolded protein response
Apoptosis
Amino acids

ABSTRACT

Genetic and epigenetic regulation as well as immune surveillance are known defense mechanisms to protect organisms from developing cancer. Based on experimental evidence, we proposed that small metabolically active molecules accumulating in cancer cells may play a role in an alternative antitumor surveillance system. Previously, we reported that treatment with a mixture of experimentally selected small molecules, usually found in the serum (defined 'active mixture', AM), selectively induces apoptosis in cancer cells and significantly inhibits tumor formation in vivo. In this study, we show that the AM elicits gene expression changes characteristic of endoplasmic reticulum (ER) stress in HeLa, MCF-7, PC-3 and Caco-2 cancer cells, but not in primary human renal epithelial cells. The activation of the ER stress pathway was confirmed by the upregulation of ATF3, ATF4, CHAC1, DDIT3 and GDF15 proteins. Mechanistically, our investigation revealed that eIF2α, PERK and IRE1α are phosphorylated upon treatment with the AM, linking the induction of ER stress to the antiproliferative and proapoptotic effects of the AM previously demonstrated. Inhibition of ER stress in combination with BBC3 and PMAIP1 knockdown completely abrogated the effect of the AM. Moreover, we also demonstrated that the AM induces mIR-3189-3p, which in turn enhances the expression of *ATF3* and *DDIT3*, thus representing a possible new feedback mechanism in the regulation of *ATF3* and *DDIT3* during ER stress. Our results highlight small molecules as attractive anticancer agents and warrant further evaluation of the AM in cancer therapy, either alone or in combination with other ER stress inducing agents.

1. Introduction

All complex organisms apply various mechanisms to reduce the probability of cancer development. On the basis of epidemiological and experimental evidences we have hypothesized that in addition to the apparatus of intracellular, genetic, epigenetic and immune surveillance an additional defense mechanism might operate to prevent the development of tumors [1]. We have focused on small substances (amino

Abbreviations: 7-AAD, 7-aminoactinomycin D; Ade, adenine; AM, active mixture; ARHGEF25, Rho guanine nucleotide exchange factor 25; ATF3, activating transcription factor 3; ATF4, activating transcription factor 4; ATF6, activating transcription factor 6; BAF, bafilomycin A1, BiP binding immunoglobulin protein; CHAC1, ChaC glutathione specific gamma-glutamylcyclotransferase 1; CHLQ, chloroquine; CI, combination index; CM, control mixture; CSA, cyclosporine A; DDIT3, DNA damage inducible transcript 3; Deo, 2-deoxy-D-ribose; DFO, deferoxamine; EdU, 5-ethynyl-2'-deoxyuridine; eIF2α, eukaryotic translation initiation factor 2 subunit alpha; ER, endoplasmic reticulum; ERAD, ER-associated degradation; Fer-1, ferrostatin-1; GCN2, general control nonderepressible 2; GDF15, growth differentiation factor 15; GSEA, Gene Set Enrichment Analysis; GSG1, germ cell associated 1; HDACs, histone deacetylases; Hip, hippuric acid; IRE1α, inositol-requiring enzyme 1 alpha; ISR, integrated stress response; ISRIB, integrated stress response inhibitor; JDP2, Jun dimerization protein 2; 3-MA, 3-methyladenine; Mal, L-(-)-malic acid; Man, D-(+)-mannose; 2-ME, 2-mercaptoethanol; MEK, mitogen-activated protein kinase kinase; miRNA, microRNA; MLKL, mixed lineage kinase domain like pseudokinase; Nec-1, necrostatin-1; NES, normalized enrichment score; NSA, necrosulfonamide; O, orotic acid; PCDH7, protocadherin 7; PERK, protein kinase R (PKR)-like endoplasmic reticulum kinase; 4-PBA, 4-phenylbutyrate; PKR, protein kinase R; qRT-PCR, quantitative real time polymerase chain reaction; RIDD, regulated IRE1-dependent decay; RIPK1, Receptor-interacting serine/threonine-protein kinase 1; SF3B2, splicing factor 3b subunit 2; siRNA, small interfering RNA; TM, tunicamycin; TUNEL, terminal deoxynucleotidyl transferase-dUTP nick end labeling; UPR, unfolded protein response; XBP1, X-box binding protein 1

* Corresponding author. Present address: Soft Flow Hungary Ltd., Pécs, Ürögi fasor 2/A, 7628, Hungary.
E-mail address: tczompoly@foss.dk (T. Czömpöly).
[1] Present address: Soft Flow Hungary Ltd., Pécs, Ürögi fasor 2/A, 7628, Hungary.

https://doi.org/10.1016/j.cellsig.2019.109426
Received 14 August 2019; Accepted 19 September 2019
Available online 07 November 2019

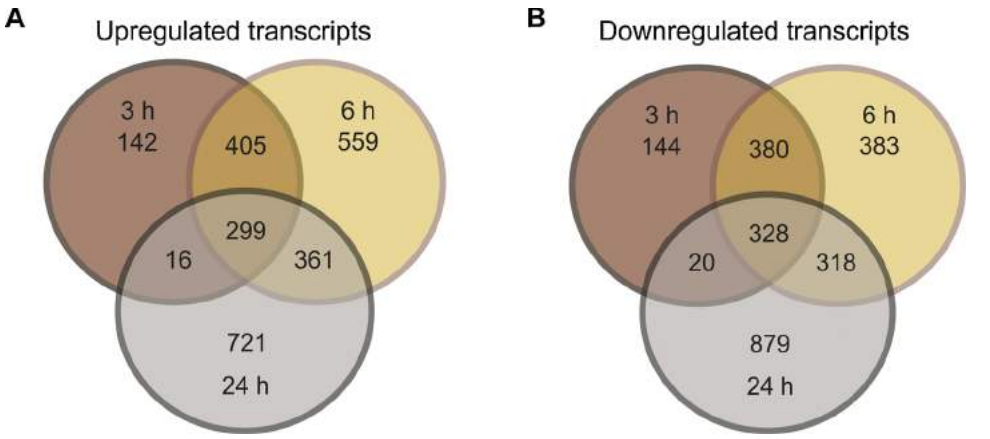

Fig. 1. The AM16 induces large scale gene expression changes in HeLa cells. (**A**) Venn diagram indicating the number of upregulated genes (fold-change vs. control ≥ 1.3) after 3 h, 6 h, and 24 h treatments with AM16. (**B**) Venn diagram indicating the number of downregulated genes (fold-change vs. control ≥ -1.3) after 3 h, 6 h, and 24 h treatments with AM16.

acids, monosaccharides, nucleobases, etc.) which are present in the serum and many of which are differentially taken up by tumor and normal cells [2–4]. The accumulation of glucose and certain amino acids in cancer cells is utilized in positron emission tomography [5], and amino acid or vitamin accumulation based targeting strategies has been reported [6,7]. During the last two decades it became evident that the regulation of cellular metabolism and cell proliferation, apoptosis, autophagy, ER stress, or other cell fate determining signaling cascades are closely interconnected [8,9]. We assumed that in addition to their established roles in metabolism, some of the accumulated substances might participate in a defense system capable of killing emerging cancer cells. In our earlier studies we have experimentally selected some molecules present in the serum whose mixture ("active mixture", AM) produced a selective in vitro and in vivo toxic effect on various tumor cell lines, but not on normal cells [10,11]. The AM is composed of certain essential amino acids, vitamins, nucleobases and metabolic intermediates: L-arginine, L-histidine, L-methionine, L-phenylalanine, L-tryptophan, L-tyrosine, L-ascorbic acid, D-biotin, pyridoxine (−)-riboflavin, adenine, 2-deoxy-D-ribose, hippuric acid, L-(−)-malic acid, D-(+)-mannose, and orotic acid. We have demonstrated earlier that the AM selectively induces apoptosis of cancer cells [12,13]. In addition, we have shown that the combination of the AM with various cytostatic agents or irradiation produces an increased in vitro cytotoxic effect [14]. Previously we have also provided evidence that the AM has a significant tumor inhibitory effect in both murine and human xenograft tumor models and increases the in vivo antitumor activity of cytostatic agents [15]. In addition to our results Bonfili et al. reported that mixtures of essential amino acids also induce apoptosis in a cancer specific manner, and showed that proteasome inhibition and induction of autophagy plays a role in this process [16]. Our earlier mechanistic studies of the AM identified the mitochondrial pathway of apoptosis induction, which was accompanied by the upregulation of genes contributing to apoptosis induction and cell cycle arrest (*PMAIP1*, *BBC3*, *CDKN1A*) [15], however the signaling events leading to the initiation of apoptosis were not known.

Accumulation of unfolded proteins in the ER due to various environmental stresses (ER stress) initiates a signaling cascade known as the unfolded protein response (UPR) [17]. The UPR could be initiated by three ER resident signal transducers EIF2AK3 (also known as PERK), ERN1 (also known as IRE1α) and ATF6 [17]. Upon activation of the UPR PERK phosphorylates the translation initiation factor EIF2S1 (also known as eIF2α), causing the global attenuation of translation accompanied by the preferential translation of certain upstream open reading frame containing mRNAs e.g. *ATF4*, *DDIT3,* and *PPP1R15A* [18,19]. The phosphorylation of eIF2α serves as a point of convergence for ER stress independent signaling mechanisms mediated by EIF2AK4 (also known as GCN2), EIF2AK2 (also known as PKR) or EIF2AK1 (also known as HRI), which are activated by amino acid starvation, viral infection, or heme deprivation, respectively. Therefore, the phosphorylation of eIF2α and the events downstream of it are also referred as the integrated stress response (ISR) [20]. IRE1α through its endoribonuclease activity splices the *XBP1* transcript to yield a stable and active form of XBP1 (spliced XBP1), which in turn controls the transcription of genes playing a role in protein folding, secretion or ER-associated degradation (ERAD) [21]. In addition, through regulated IRE1-dependent decay (RIDD) it specifically cleaves a number of RNAs controlling cellular metabolism or apoptosis [22]. Activation of ATF6 results in the release of its cytoplasmic domain, which induces the expression of HSPA5 (BiP), a chaperone known to maintain the ER stress sensors in an inactive state, and genes contributing to ERAD [23]. The translational arrest together with the UPR elicited transcriptional changes are adaptive responses to resolve cellular stress, however long-term and high level activation of the UPR signaling promotes cell death instead of restoring ER homeostasis [18,24,25], through the activation of various branches of the apoptotic signaling cascade [26] and the concomitant induction of another adaptive response, autophagy [27].

Here we describe that a defined mixture of small molecules (AM) selectively activates the UPR signaling cascade in cancer cells, which leads to the activation of a pro-apoptotic transcription program, thus providing a mechanism for the AM elicited apoptosis induction.

2. Results

2.1. Gene expression profiling identifies the ER stress pathway in AM16 treated cancer cells

Except otherwise indicated we have used a mixture of sixteen previously selected small molecules ("active mixture", AM16: L-arginine, L-tyrosine, L-histidine, L-tryptophan, L-methionine, L-phenylalanine, adenine, L-(-)-malic acid, 2-deoxy-D-ribose, orotic acid, D-(+)-mannose, hippuric acid, pyridoxine, D-biotin, (-)-riboflavin, and L-ascorbic acid) throughout this study [10,11].

To investigate the transcriptional changes induced by treatment with AM16 we performed microarray analysis in which HeLa cells were treated with AM16 for 3 h, 6 h, and 24 h. Treatment with AM16 caused striking changes in gene expression (Fig. 1 and Table S1). Gene set enrichment analysis (GSEA) of the upregulated transcripts revealed a sequence of events starting with the enrichment of gene sets corresponding to RNA splicing and translation initiation at 3 h, followed by the induction of genes responsible for ER stress induced apoptosis and cell cycle regulation at 6 h, and closed by the upregulation of genes participating in apoptosis and TGF-β signaling at 24 h (Fig. 2A and Table S2). Among the gene sets enriched in all three time points "response to ER stress" had the highest normalized enrichment score (NES), and was accompanied with gene sets of several related pathways (Fig. 2B and Table S2).

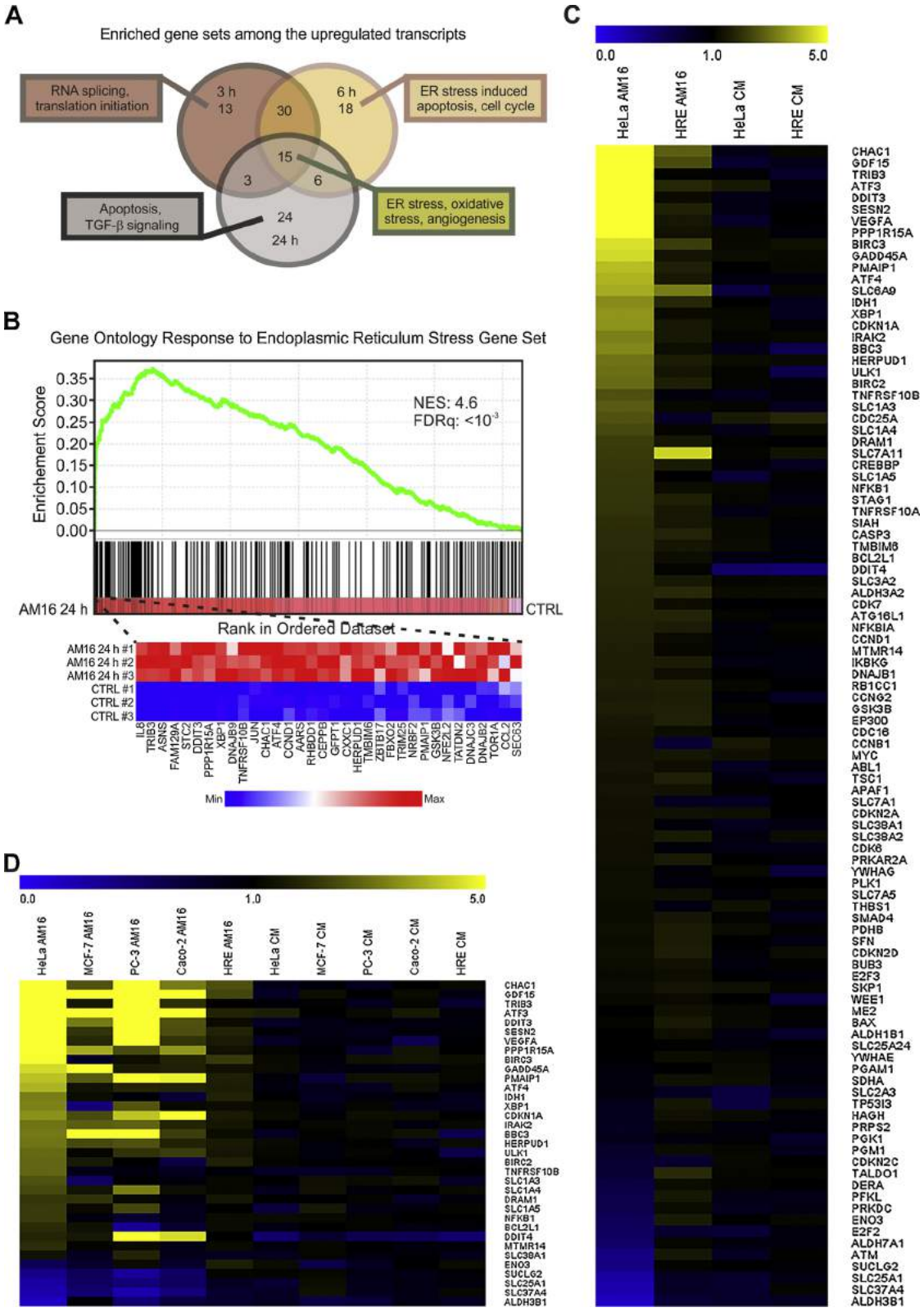

Fig. 2. Gene expression profiling identifies the ER stress pathway in AM16 treated cancer cells. (**A**) Venn diagram indicating the number of enriched gene sets among the upregulated transcripts (normalized enrichment score ≥ 3 and false discovery rate q-value < 10-3) identified with gene set enrichment analysis (GSEA) after 3 h, 6 h, and 24 h treatments with AM16 in HeLa cells. Texts in rectangles indicate predominant gene sets for each time point and in common. (**B**) Enrichment plot for the ER stress gene set after 24 h treatment with AM16 (top) and heatmap showing the expression of top ranking genes (fold-change ≥ 1.3 vs. control) in the gene set after 24 h treatment of HeLa cells with AM16 in three biological replicates (bottom). NES, normalized enrichment score. FDRq, false discovery rate q-value. (**C**) Heatmap of fold change values of gene expression determined by qRT-PCR in HeLa and HRE cells treated for 24 h with AM16 or CM. Values represent the average of three independent experiments. (**D**) Heatmap of fold change values of gene expression determined by qRT-PCR in HeLa, MCF-7, PC-3, Caco-2, and HRE cells treated for 24 h with AM16 or CM. Values represent the average of three independent experiments.

In order to validate these results we have chosen one hundred genes for qRT-PCR analysis. To test the specificity of our findings a control mixture (CM) which had the same osmolality as the AM16 and contained ineffective small molecules with chemically or physiologically similar properties as components of the AM16 was also applied. We have found substantial upregulation of genes contributing to the UPR (*CHAC1*, *GDF15*, *TRIB3*, *ATF3*, *DDIT3*, *PPP1R15A, ATF4*, *XPB1*), to autophagy (*SESN2*, *ULK1*, *DRAM161*), and to apoptosis (*BIRC3, GADD45A*, *PMAIP1*, *BBC3*) in HeLa cells treated with AM16 for 24 h, but not in HeLa cells treated with CM or in primary human renal epithelial cells (HRE, used as normal cell control) treated with AM16 or CM (Fig. 2C and Table S3). Genes showing a significantly different expression in AM16 treated HeLa cells compared to CM treated HeLa, AM16 treated HRE and CM treated HRE cells were further validated in MCF-7, PC-3 and Caco-2 cells. We have found that *ATF3*, *DDIT3, PPP1R15A*, *PMAIP1* and *GDF15* was specifically upregulated in all of the four AM16 treated cell lines, while the upregulation of *CHAC1* could only be shown in AM16 treated HeLa and PC-3 cells (Fig. 2D and Table S4). Taken together these results demonstrate that the AM16 specifically induces gene expression changes characteristic for ER stress in cancer cells.

2.2. The AM16 induces proteins contributing to the ISR

Since the ISR is characterized by a global attenuation of translation accompanied by the preferential translation of certain upstream open reading frame containing mRNAs e.g. *ATF4*, *DDIT3* [18,19], we investigated the abundance of ATF4, ATF3, DDIT3, CHAC1 and GDF15 proteins in AM16 or CM treated HeLa, PC-3, Caco-2, MCF-7 and HRE cells by western blot. We have found a time dependent induction of ATF4, ATF3, DDIT3, CHAC1 and GDF15 in AM16 treated HeLa cells, but not in CM treated HeLa cells (Fig. 3A, full blots are shown in Fig. S1). We observed the induction of ATF4, ATF3 and GDF15 in PC-3, Caco-2 and MCF-7 cells treated with AM16 for 24 h, but not in CM treated cells (Fig. 3B-D, full blots are shown in Figs. S2-4). The accumulation of DDIT3 could be demonstrated in AM16 treated PC-3 and Caco-2 cells, but not in MCF-7 cells, while CHAC1 was induced in AM16 treated PC-3, but not in Caco-2 and MCF-7 cells (Fig. 3B-D). ATF4, ATF3 and DDIT3 could not be detected in AM16 or CM treated HRE cells, while a slight induction of CHAC1 and GDF15 could be observed upon treatment with AM16 (Fig. 3E, full blots are shown in Fig. S5), which is consistent with the small and non-significant increase of the *CHAC1* and *GDF15* transcript levels in AM16 treated HRE cells (Table S4). To further investigate the significance of ATF4 induction we analyzed the subcellular localization of ATF4 with immunocytochemistry. We have found that the induced ATF4 accumulates in the nuclei of HeLa cells treated with AM16 for 24 h (Fig. 3F,G). Collectively these results confirm the activation of the ISR pathway, and demonstrate the induction and nuclear accumulation of ATF4 upon treatment with AM16.

2.3. The AM16 induced stress response is mediated by ER stress sensors

Next we investigated the phosphorylation status of the translation initiation factor eIF2α which mediates the global translational shutdown and the simultaneous preferential translation during the course of ISR, together with the phosphorylation status of the ER stress responsive eIF2α kinase PERK. We have found a time dependent phosphorylation of eIF2α and PERK in AM16 treated HeLa cells (Fig. 4A, full blots are shown in Fig. S6). In addition we also investigated two further ER stress sensors IRE1α and ATF6, and the accumulation of BiP a chaperone known to play a crucial role in ER stress. We have found that treatment with AM16 induces a time dependent phosphorylation of IRE1α, and a time dependent increase in the amount of ATF6 and BIP in HeLa cells (Fig. 4A). The activation of ATF6 was evidenced by the appearance of the 50 kDA cleavage fragment corresponding to the transcription factor domain (Fig. 4A). The activation of IRE1α was confirmed by the increased splicing of *XBP1* mRNA upon treatment with AM16 (Fig. 4B). Since eIF2α could be phosphorylated by other ER stress independent kinases, we also investigated the phosphorylation status of GCN2 and PKR. We have found that GCN2 and PKR were not phosphorylated upon treatment with AM16 (Fig. 4C, full blots are shown in Fig. S7). Taken together these results demonstrate that AM16 activates all three branches of the UPR, and that the activation of PERK and not other ER stress independent kinases leads to the phosphorylation of eIF2α.

2.4. Inhibition of the ISR attenuates the effect of AM16

To determine the extent to which ER stress contributes to the anticancer activity of the AM16, we investigated the effect of the ISR inhibitor ISRIB, a molecule which protects cells form the consequences of eIF2α phosphorylation through the stabilization of eIF2B dimers [28], on the AM16 induced decrease in cell number. The effect on AM16 induced changes in gene and protein expression was also examined. In addition the effect of salubrinal, an inhibitor of eIF2α dephosphorylation and ER stress induced apoptosis [29], and 4-phenylbutyrate (4-PBA), a chemical chaperone reported to suppress ER stress by reducing the amount of misfolded proteins in the ER [30], was also investigated. We have found that ISRIB completely blocked the AM16 triggered induction of ATF4, while as expected had no effect on the AM16 induced eIF2α phosphorylation (Fig. 4D, full blots are shown in Fig. S8). ISRIB also completely blocked the 6 h AM16 treatment elicited increase in *ATF4*, *CHAC1*, *DDIT3* and *GDF15* transcript levels, while the induction of *ATF3* was reduced but not completely abolished (Fig. 4E). Salubrinal and 4-PBA had no effect on the AM16 elicited changes mentioned above. The effect on cell growth inhibition was investigated with direct counting of cells instead of metabolic assays to avoid any possible interference caused by treatment with AM16. As shown in Fig. 4F, ISRIB significantly attenuated the cell growth inhibitory effect of the AM16, while salubrinal or 4-PBA had no effect. However, it is important to note that ISRIB was not able to completely block the cell growth inhibitory effect of AM16. Since IRE1α is activated upon treatment with AM16 (Fig. 4A), we tested whether the inhibition of IRE1α attenuates the effect of the AM16 with the use of IRE1α inhibitors GSK2850163 and STF-083010. Despite the significant inhibition of the AM16 induced XBP1 splicing (Fig. 4G), these inhibitors failed to inhibit the cell number reducing effect of the AM16 (Fig. 4H).These results indicate that the UPR plays an important role in the AM16 induced cell growth inhibitory effect, and suggest that eIF2α phosphorylation is the dominant branch of the UPR activated by AM16.

2.5. Components of AM16 differentially contribute to the ER stress induction

Since the AM16 is a mixture of sixteen small molecules, we wanted to investigate the extent to which the individual components contribute to the induction of ER stress. To this end, we have formed three groups from the compounds of AM16 and tested the effect of them alone or in combination on cell number, ER stress related gene expression, and ATF4 induction. AM1 contained the amino acid components (L-arginine, L-tyrosine, L-histidine, L-tryptophan, L-methionine, and L-phenylalanine), AM2 contained adenine, L-(-)-malic acid, 2-deoxy-D-ribose, orotic acid, D-(+)-mannose and hippuric acid, AM3 contained the vitamin components (pyridoxine, D-biotin, (-)-riboflavin, and L-ascorbic acid), and AM16 contained all of the sixteen components (AM1 + AM2 + AM3). We have found that the combination of AM1 and AM2 (AM1 + AM2) was able to significantly inhibit the cell growth (Fig. 5A), induced the expression of *ATF3, ATF4, CHAC1, DDIT3, GDF15* (Fig. 5B), and increased the nuclear accumulation of ATF4 (Fig. 5C,D), while other combinations or the per se application of AM1, AM2 or AM3 had no effect. Importantly, the highest degree of cell growth

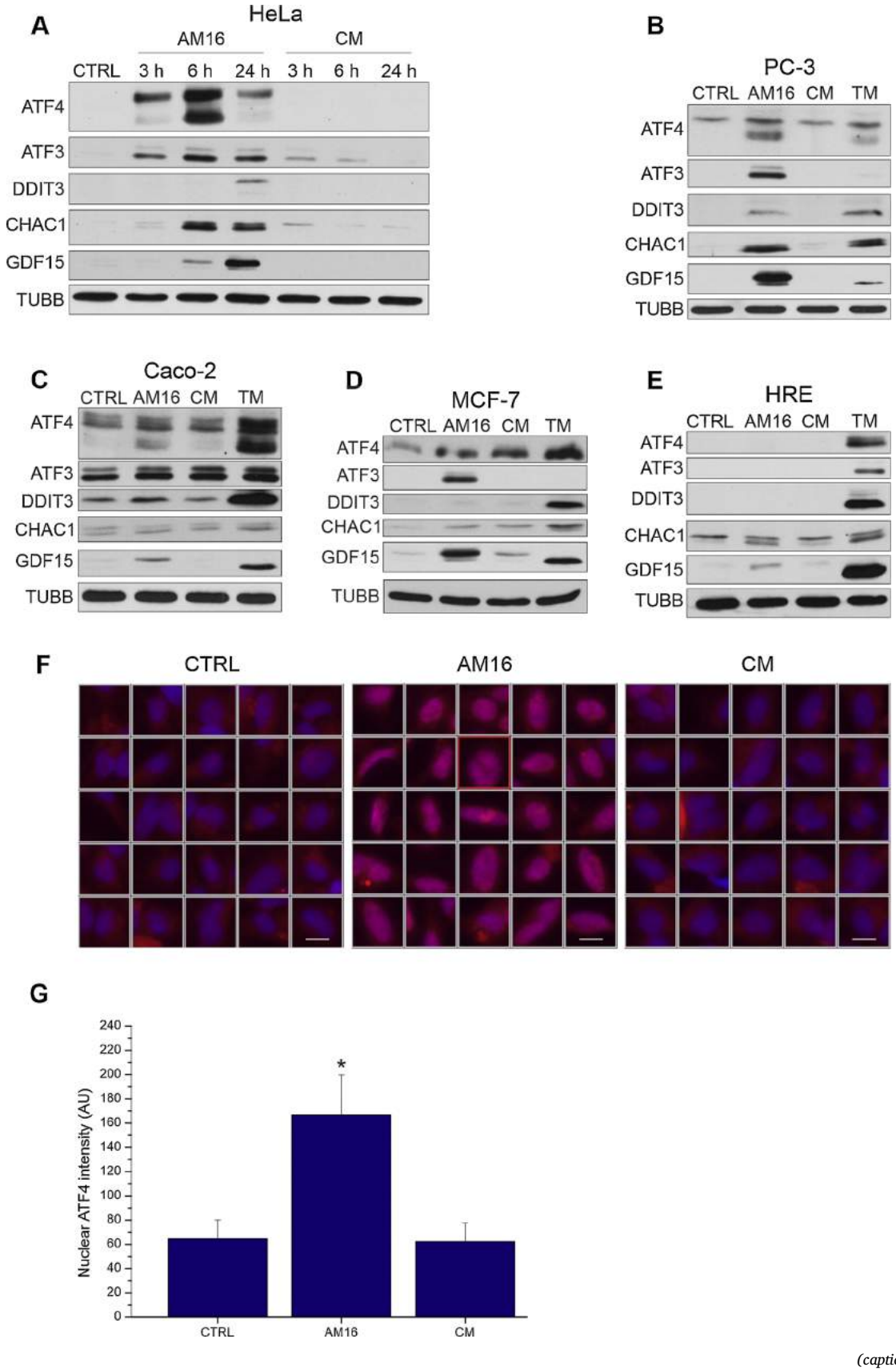

(caption on next page)

Fig. 3. The AM16 induces proteins contributing to the integrated stress response. (**A**) Representative western-blots for ATF4, ATF3, DDIT3, CHAC1 and GDF15 in HeLa cells treated with AM16 or CM for the indicated periods of time. β-tubulin (TUBB) was used as loading control. Full blots are shown in Fig. S1. (**B-E**) Representative western-blots for ATF4, ATF3, DDIT3, CHAC1 and GDF15 in PC-3 cells (**B**), in Caco-2 cells (**C**), in MCF-7 cells (**D**), or in HRE cells (**E**) treated with AM16, CM, or tunicamycin (5 μM) for 24 h. β-tubulin (TUBB) was used as loading control. Full blots are shown in Figs. S2-5. (**F**) Immunofluorescence pictures of HeLa cells treated with AM16 or CM for 24 h. Nuclei were labeled with DAPI (blue) and ATF4 was detected with antibody (red). Representative image galleries of 25 nuclei per condition from three independent experiments are shown. Scale bars: 15 μm. (**G**) Quantification of nuclear ATF4 fluorescence intensity. Fluorescence intensity is presented in arbitrary units (AU) and represents mean ± SD of three independent experiments. *$p < 0.001$ vs. CTRL (Welch test followed by Games-Howell test). n(CTRL) = 4187, n(AM16) = 2202, n(CM) = 4417.

inhibition and ATF4 induction was produced by AM16, which were significantly higher than those caused by AM1 + AM2, while the level of ER stress related gene induction elicited by AM16 was similar to that of AM1 + AM2 (Fig. 5B). These results demonstrate that the amino acid components (AM1) together with the heterogeneous group of other small molecules (AM2) are sufficient to induce ER stress, while the vitamin components (AM3) are only able to enhance this effect, but are not sufficient to initiate it.

2.6. Ten out of the sixteen AM16 components are sufficient to induce ER stress

To further narrow the circle of ER stress inducing components of the AM16, we continued our investigations with constituents of AM1 and AM2. We have combined randomly paired components of AM2 with AM1 (Fig. 6A), or vice versa randomly paired components of AM1 with AM2 (Fig. 6B) and measured the effect on *ATF3, ATF4, CHAC1, DDIT3,* and *GDF15* expression. The combinations of paired components (i.e. four component mixtures) were also tested in combination with AM1 or AM2. Our results indicate that the combination of adenine (Ade), L-(-)-malic acid (Mal), D-(+)-mannose (Man) and hippuric acid (Hip) with AM1 (amino acids) induces the expression of ER stress genes to levels comparable with AM1 + AM2 (Fig. 6A), while 2-deoxy-D-ribose (Deo) and orotic acid (O) are not necessary to the ER stress induction. As shown in Fig. 6B the amino acid components equally contribute to the induction of ER stress genes and all six of them are necessary to reach the gene expression levels caused by AM1 + AM2.

On the basis of the above results we have split the sixteen component AM16 to a ten component mixture (AM10) which contained compounds sufficient to ER stress gene induction (amino acids, Ade, Mal, Man, Hip), and to a six component mixture (AM6) which contained compounds not necessary for ER stress gene induction (vitamins, Deo, O). As shown in Fig. 6C, AM10 induced the expression of ER stress genes to levels comparable with AM16, while AM6 had no effect. ISRIB completely blocked the 24 h AM10 or AM16 treatment elicited increase in *ATF4*, *CHAC1* and *DDIT3* transcript levels, while the induction of *ATF3* and *GDF15* were significantly attenuated but not completely blocked. Treatment with AM10 caused a significant cell growth inhibitory effect, which was also attenuated but not completely blocked by ISRIB (Fig. 6D). The AM10 induced changes in gene expression and the cell growth inhibitory effect could also be demonstrated in PC-3 (Fig. 7A,D), MCF-7 (Fig. 7B,E), and Caco-2 cells (Fig. 7C,F). Taken together these results indicate that the amino acid components together with Ade, Mal, Man and Hip are sufficient to induce ER stress, however the other six components are able to enhance the cell growth inhibitory effect.

2.7. Knockdown of ATF3 and GDF15 does not attenuate the effect of AM16

The finding that the AM16 induced increase in *ATF3* and *GDF15* transcript levels could not be completely blocked by ISRIB (Fig. 6C) raised the possibility that the residual induction of these proteins in the presence of ISRIB could be responsible for the uncomplete block of AM16 caused cell growth inhibition. Therefore we investigated the effect of the knockdown of these proteins alone, or in combination with ISRIB on AM16 induced cell growth inhibition. Despite the efficient knockdown of ATF3 or GDF15, or both in the presence of ISRIB (Fig. 8A,B, full blots are shown in Fig. 9S), we could not completely prevent the decrease in cell number caused by 24 h treatment with AM16 (Fig. 8C). The only effect was the partial attenuation of the AM16 caused cell growth inhibitory effect by ISRIB. These experiments were also performed with AM10 and produced the same results. The above results indicate that ATF3 and GDF15 are not essential for the cell growth inhibitory effect of the AM16.

2.8. The AM16 induced mIR-3189-3p enhances the expression of ER stress genes

The *GDF15* locus contains an intronic miRNA (mIR-3189), the 3p product of which (mIR-3189-3p) has been shown to transcriptionally co-regulated with *GDF15* and was demonstrated to have potent pro-apoptotic activity [31]. Hence we investigated the induction of mIR-3189-3p upon treatment with AM16, and found that treatment with AM16 for 24 h produced a 3-fold increase in mIR-3189-3p level, while CM had no effect. Tunicamycin, a known inducer of ER stress, also caused a 4-fold increase in mIR-3189-3p level (Fig. 9A). Next, we tested whether knockdown of mIR-3189-3p with miRNA inhibitor has an effect on the cell growth inhibition caused by the AM16. To verify the functionality of the mIR-3189-3p inhibitor we have tested the ability of the inhibitor to block the effect of mIR-3189-3p mimic on the transcript levels of two verified mIR-3189-3p targets, *ARHGEF25* and *SF3B2* [32]. As expected, the mIR-3189-3p mimic significantly reduced the transcript levels of *ARHGEF25* and *SF3B2*, which was completely blocked by the mIR-3189-3p inhibitor, but not by a negative control miRNA inhibitor (Fig. 9B). However, the mIR-3189-3p inhibitor applied at 50 nM concentration was not able to reduce the cell growth inhibitory effect of the 24 h AM16 treatment (Fig. 9C). We have also tested other inhibitor concentrations (10 nM and 200 nM), which produced the same results. Interestingly, the combination of mIR-3189-3p inhibitor with siGDF15 at high concentrations (200 nM and 100 nM, respectively) also failed to reduce the cell growth inhibitory effect of the AM16 (Fig. 9C). These experiments were also performed with AM10 and produced the same results.

Next, we investigated whether mIR-3189-3p influences the transcript levels of genes participating in the AM16 induced ER stress (*ATF3*, *ATF4*, *CHAC1*, *DDIT3* and *GDF15)*. Interestingly, the mIR-3189-3p mimic significantly increased the levels of *ATF3, DDIT3,* and *GDF15* transcripts, which was completely blocked by mIR-3189-3p inhibitor, but not by a negative control miRNA inhibitor (Fig. 9D). The increase in *CHAC1* transcript level proved to be non-specific as a negative control miRNA mimic also produced a significant increase (Fig. 9D). At the protein level the increased expression of ATF3 and GDF15 could be verified, while CHAC1, DDIT3 and ATF4 were not specifically induced by mIR-3189-3p transfection (Fig. 9E).

Both *ATF3* and *DDIT3* have been shown to be transcriptionally repressed by the transcription factor JDP2 [33,34], and various members of the histone deacetylase family (HDACs) were demonstrated to be associated with JDP2 at the promoters of *ATF3* and *DDIT3* [34,35]. Thus we measured the transcript levels of *HDAC1-6* and *JDP2* following transfection with mIR-3189-3p mimic. Furthermore the transcript levels of two additional JDP2 targets *GSG1* and *PCDH7* [33] were also analyzed. As shown in Fig. 9**F**, the mIR-3189-3p mimic significantly

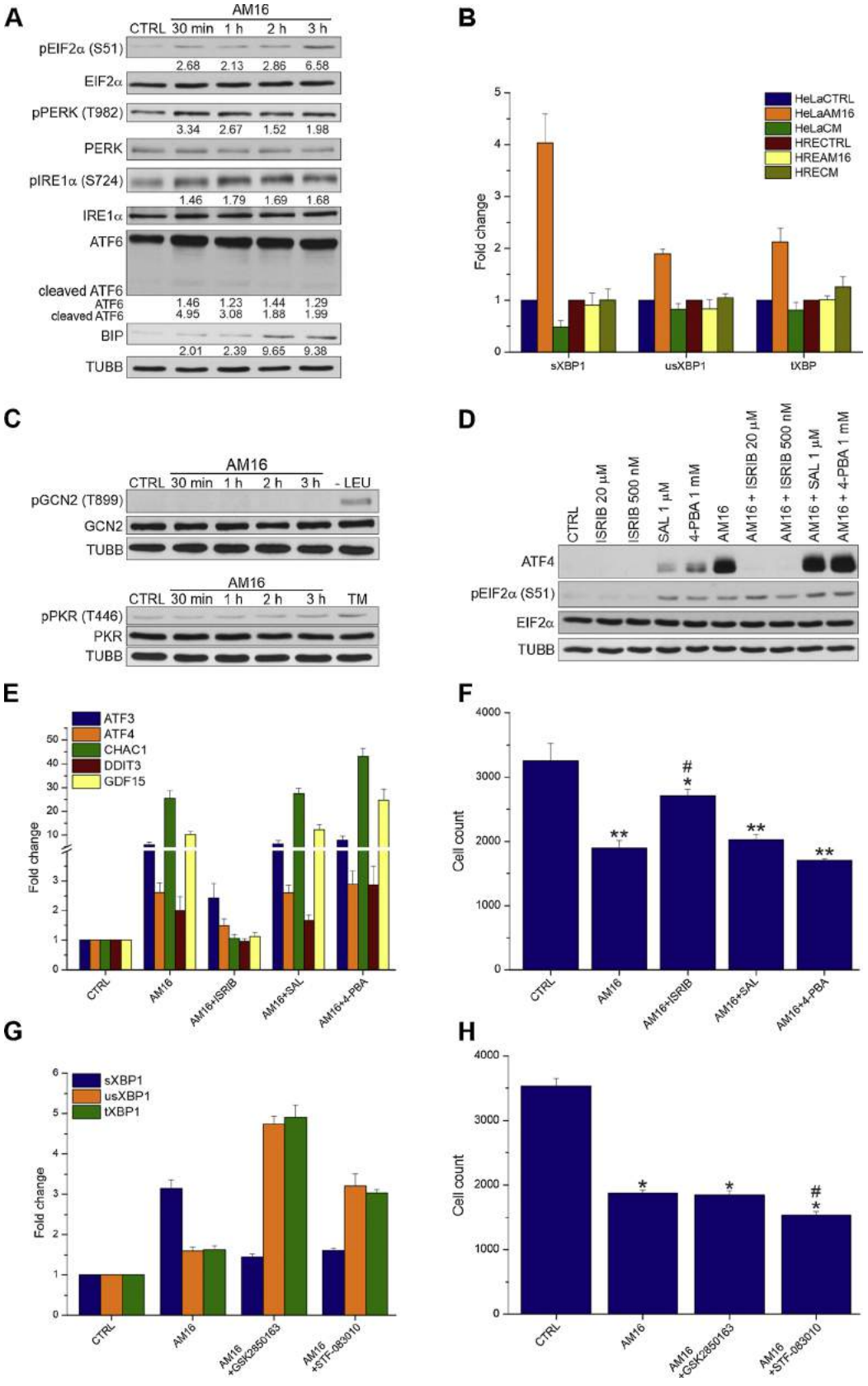

Fig. 4. The AM16 induced stress response is mediated by ER stress sensors. (**A**) Representative western-blots of phosphorylated eIF2α (S51), eIF2α, phosphorylated PERK (T982), PERK, phosphorylated IRE1α (S724), IRE1α, ATF6 and BIP in HeLa cells treated with AM16 for the indicated periods of time. β-tubulin (TUBB) was used as loading control. Numbers below the bands indicate relative densities compared to the untreated control. Full blots are shown in Fig. S6. (**B**) XBP1 mRNA splicing was detected with qRT-PCR analysis in HeLa and HRE cells treated for 24 h with AM16 or CM. Bars represent the fold change compared to CTRL. Normalized expression values and significance values are provided in Table S5. (**C**) Representative western-blots of phosphorylated GCN2 (T899), GCN2, phosphorylated PKR (T466) and PKR in HeLa cells treated with AM16 for the indicated periods of time. β-tubulin (TUBB) was used as loading control. Leucine starvation for 30 min (- LEU) or 3 h of tunicamycin treatment (5 μM) was applied as positive control for phosphorylated GCN2 or phosphorylated PKR, respectively. Full blots are shown in Fig. S7. (**D**) HeLa cells were pretreated with the indicated concentrations of ISRIB, salubrinal, or 4-phenylbutyrate (4-PBA) for 1 h, followed by co-treatment with AM16 for 2 h. ATF4, phosphorylated eIF2α (S51), and eIF2α were analyzed by western-blot. β-tubulin (TUBB) was used as loading control. Full blots are shown in Fig. S7. (**E**) HeLa cells were pretreated with 500 nM ISRIB, 1 μM salubrinal, or 1 mM 4-phenylbutyrate (4-PBA) for 1 h, followed by co-treatment with AM16 for 6 h. mRNA levels were detected with qRT-PCR. Bars represent the average ± standard deviation of two independent experiments. *p < 0.05, **p < 0.001 vs. CTRL; #p < 0.05, ##p < 0.001 vs. AM16 (Welch test followed by Games-Howell test). (**F**) HeLa cells were pretreated as in panel (E), followed by co-treatment with AM16 for 24 h. Bars represent the cell counts per well (average ± standard deviation of three independent experiments). *p < 0.05, **p < 0.001 vs. CTRL; #p < 0.001 vs. AM16 (ANOVA, Bonferroni test). (**G**) HeLa cells were treated with 10 μM GSK2850163 or 10 μM STF-083010 in combination with AM16 for 24 h. XBP1 mRNA splicing was detected with qRT-PCR analysis. Bars represent the fold change compared to CTRL. Normalized expression values and significance values are provided in Table S5. **(H)** HeLa cells were treated as in panel (G). Bars represent the cell counts per well (average ± standard deviation of two independent experiments). *p < 0.001 vs. CTRL, #p < 0.001 vs. AM16 (ANOVA, Bonferroni test).

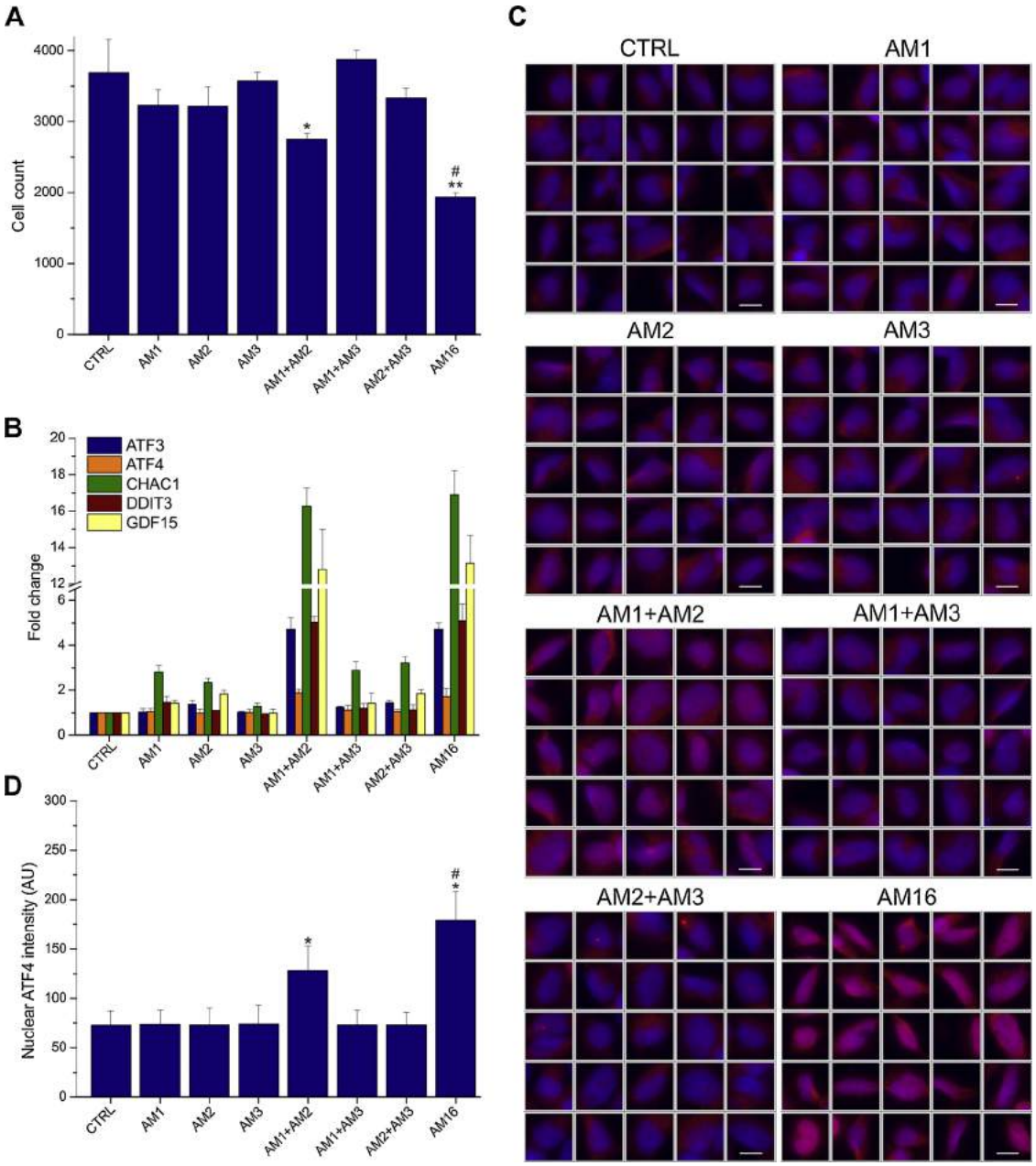

Fig. 5. Components of AM16 differentially contribute to the ER stress induction. (**A**) HeLa cells were treated with AM1, AM2, AM3 or the indicated combinations of them for 24 h. AM16 represents a mixture containing all of the sixteen components (AM1 + AM2 + AM3). Cell number was determined with DAPI staining followed by counting the nuclei using an automated microscope. Bars represent the cell counts per well (average ± standard deviation of three independent experiments). *p < 0.05, **p < 0.001 vs. CTRL; #p < 0.001 vs. AM1 + AM2 (ANOVA, Bonferroni test). (**B**) HeLa cells were treated as in panel (A). ATF3, ATF4, CHAC1, DDIT3, GDF15 mRNA levels were detected with qRT-PCR. Bars represent the fold change compared to CTRL. Normalized expression values and significance values are provided in Table S5. (**C**) Immunofluorescence pictures of HeLa cells treated as in panel (A). Nuclei were labelled with DAPI (blue) and ATF4 was detected with antibody (red). Representative image galleries of 25 nuclei per condition from three independent experiments are shown. Scale bars: 15 μm. (**D**) Quantification of nuclear ATF4 fluorescence intensity of the same representative experiment as shown in panel (C). Fluorescence intensity is presented in arbitrary units (AU) and represents mean ± SD of three independent experiments. *p < 0.001 vs. CTRL; #p < 0.001 vs. AM1 + AM2 (Welch test followed by Games-Howell test). n (CTRL) = 4968, n(AM1) = 4787, n(AM2) = 4869, n(AM3) = 4721, n(AM1 + AM2) = 3183, n(AM1 + AM3) = 4819, n(AM2 + AM3) = 4774, n(AM16) = 2649.

decreased the level of *HDAC1*, *HDAC3*, and *JDP2* transcripts, which was completely blocked by mIR-3189-3p inhibitor, but not by a negative control miRNA inhibitor. The level of *HDAC5* transcript was significantly increased. The transcript levels of *GSG1* and *PCDH7* were also specifically increased, which further verifies the downregulation of *JDP2*. Moreover, *HDAC3* and *JDP2* were identified as targets of mIR-3189-3p by searching the TargetScan database [36]. These results collectively demonstrate that mIR-3189-3p is induced by treatment with AM16, and suggest that the induced mIR-3189-3p enhances the expression of *ATF3* and *DDIT3* most probably through the down-regulation of *JDP2, HDAC1* and *HDAC3*.

2.9. The AM16 has cytotoxic, anti-proliferative and apoptosis inducing effect

Since neither ISRIB nor the knockdown of *ATF3*, *GDF15*, or mIR-3189-3p was able to completely block the effect of the AM16 we decided to further investigate the mechanism of AM16 induced cell

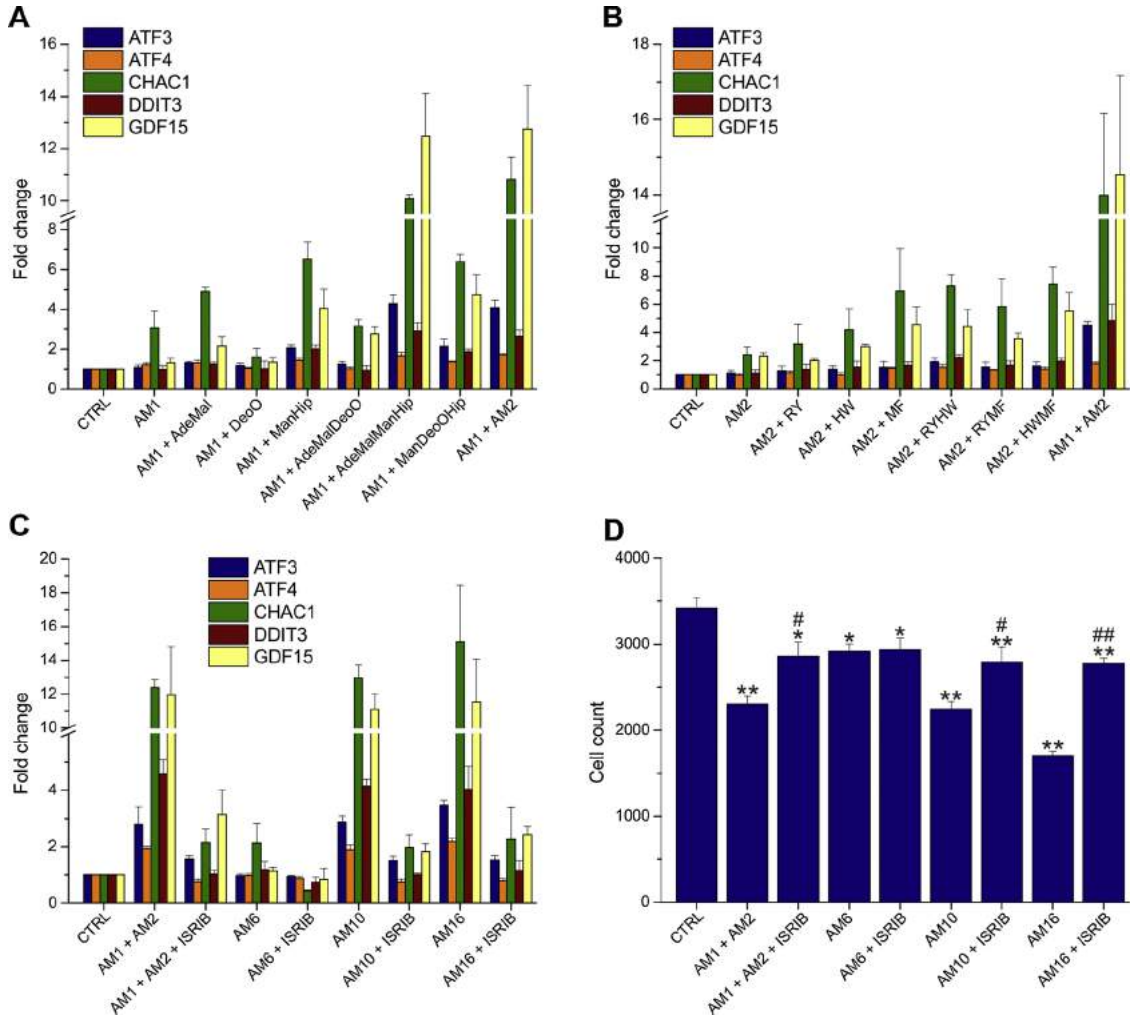

Fig. 6. Ten out of the sixteen AM16 components are sufficient to induce ER stress. (**A**) HeLa cells were treated with AM1, AM1 + AM2, or AM1 and the indicated combinations of adenine (Ade), L-(-)-malic acid (Mal), 2-deoxy-D-ribose (Deo), orotic acid (O), D-(+)-mannose (Man) and hippuric acid (Hip) for 24 h. ATF3, ATF4, CHAC1, DDIT3, GDF15 mRNA levels were detected with qRT-PCR. Bars represent the the fold change compared to CTRL. Normalized expression values and significance values are provided in Table S5. (**B**) HeLa cells were treated with AM2, AM1 + AM2, or AM2 and the indicated combinations of L-arginine (R), L-tyrosine (Y), L-histidine (H), L-tryptophan (W), L-methionine (M), L-phenylalanine (F) for 24 h. ATF3, ATF4, CHAC1, DDIT3, GDF15 mRNA levels were detected with qRT-PCR. Bars represent the average ± standard deviation of two independent experiments. *p < 0.05, **p < 0.001 vs. CTRL; #p < 0.05, ##p < 0.001 vs. AM1 + AM2 (Welch test followed by Games-Howell test). (**C**) HeLa cells were pretreated with vehicle or 500 nM ISRIB for 1 h, followed by co-treatment with AM1 + AM2, AM6, AM10 or AM16 for 24 h. ATF3, ATF4, CHAC1, DDIT3, GDF15 mRNA levels were detected with qRT-PCR. Bars represent the fold change compared to CTRL. Normalized expression values and significance values are provided in Table S5. (**D**) HeLa cells were treated as in panel (C). Bars represent the cell counts per well (average ± standard deviation of three independent experiments). *p < 0.05, **p < 0.001 vs. CTRL; #p < 0.05, ##p < 0.001 vs. the corresponding vehicle treated sample (ANOVA, Bonferroni test).

death and growth inhibition. We investigated whether the effect of the AM16 is mainly due to cytotoxic, growth arresting or apoptosis inducing effects. Treatment of HeLa cells with AM16 caused a significant increase in the number of necrotic/late apoptotic cells as demonstrated by cytocalcein/7-AAD staining (Fig. 10A,B). Cell proliferation measured with EdU incorporation was suppressed upon treatment with AM16 (Fig. 10C,D), which was accompanied by a time dependent decrease of cell number (Fig. 10E). In addition, the AM16 significantly increased the number of apoptotic cells as measured with TUNEL (Fig. 10F,G).

2.10. Inhibitors of apoptosis, but not autophagy, ferroptosis and necroptosis attenuate the effect of the AM16

Next we wanted to investigate the relative contribution of apoptosis, autophagy, ferroptosis and necroptosis to the effect of the AM16 using various inhibitors of these cell death pathways. Since many commonly used inhibitors have antiproliferative effect when applied alone, we used dilution series of the inhibitors and dilution series of the AM16 alone or in combination with the inhibitors and determined the combination index (CI) using cell counting. The CI is the quantitative measure of interaction between the effect of the inhibitors and the AM16 (CI > 1.1 indicates antagonism, CI < 0.9 indicates synergism) [37–39].

First we demonstrated that treatment with AM16, but not with CM causes a dose dependent decrease in the number of HeLa, MCF-7, PC-3, Caco-2, HT-29 and A549 cells, while the number of HRE cells is not affected (Fig. 11A). To select the optimal cell line for investigating the role of ferroptosis we tested the effect of erastin, a known inducer of ferroptosis [40], in conjunction with established inhibitors of ferroptosis: the iron chelator deferoxamine (DFO) and the lipid peroxidation inhibitor ferrostatin-1 (Fer-1) on HeLa, MCF-7, PC-3, Caco-2, HT-29 and A549 cells. Treatment with erastin reduced the cell number in all tested cell lines, however its effect could only be inhibited by DFO and Fer-1 in

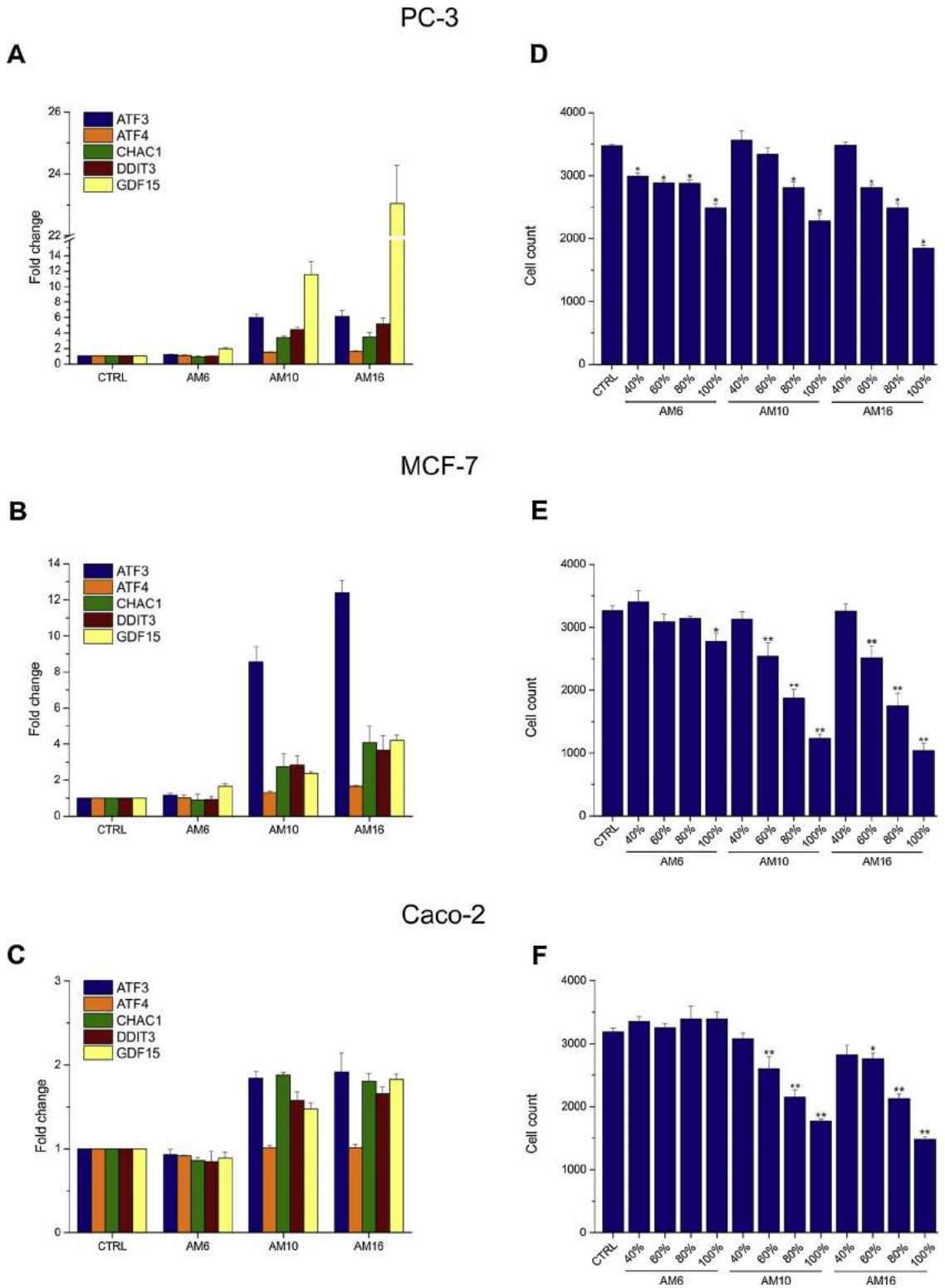

Fig. 7. Ten out of the sixteen AM16 components are sufficient to induce ER stress in PC-3, MCF-7, and Caco-2. (**A-C**) PC-3 (A), MCF-7 (B), Caco-2 (C) cells were treated with AM6, AM10, or AM16 for 24 h. ATF3, ATF4, CHAC1, DDIT3, GDF15 mRNA levels were detected with qRT-PCR. Bars represent the fold change compared to CTRL. Normalized expression values and significance values are provided in Table S5. (**D-F**) PC-3 (D), MCF-7 (E), Caco-2 (F) cells were treated as in panel (A-C). Bars represent the cell counts per well (average ± standard deviation of three independent experiments). *$p < 0.05$, **$p < 0.001$ vs. CTRL (ANOVA, Bonferroni test).

A549 cells (Fig. 11B), indicating that mutant RAS - present only in A549 cells, while HeLa, MCF-7, PC-3, Caco-2, and HT-29 cells have wild-type RAS - which was used in the identification of erastin [41] has an important role in erastin induced ferroptosis. On the basis of these results we have chosen the HeLa and A549 cell lines to test the modulatory effect of ferroptosis inhibitors DFO, Fer-1, the lipophilic antioxidant trolox, the system x_c^- bypassing agent 2-mercaptoethanol and the MEK inhibitor/antioxidant U0126 on the effect of the AM16. As shown in

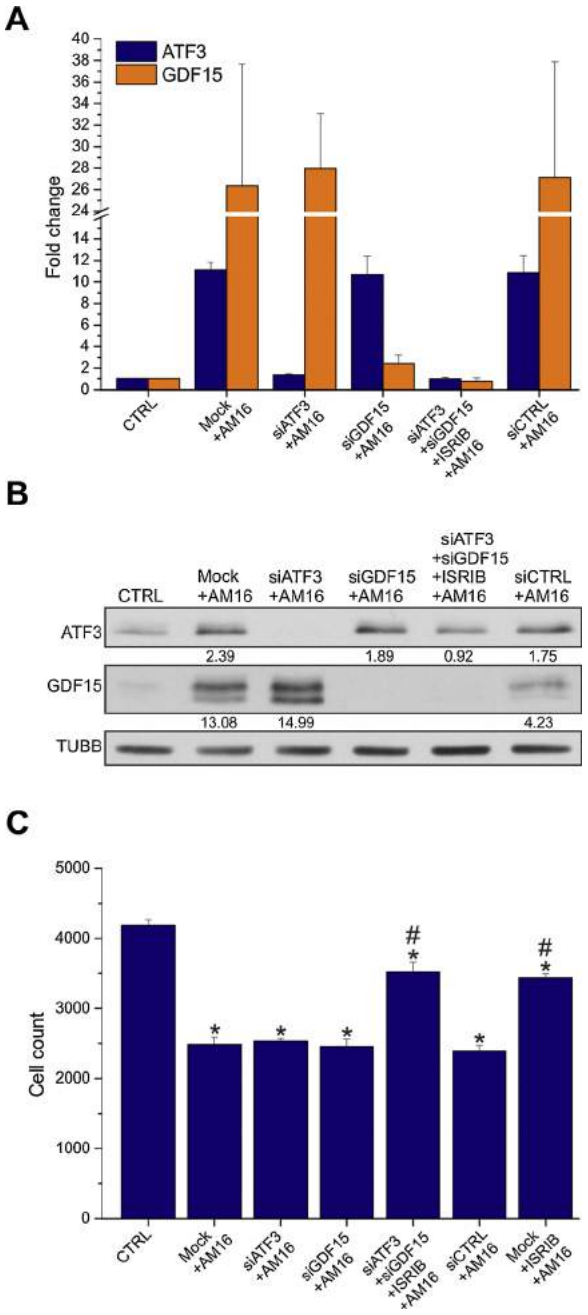

Fig. 8. Knockdown of ATF3 and GDF15 does not attenuate the effect of AM. (**A**) HeLa cells were transfected with 50 nM siRNA against ATF3 (siATF3), 50 nM siRNA against GDF15 (siGDF15), with the combination of 50 nM siATF3 and 50 nM siGDF15, 100 nM siRNA control (siCTRL), or were mock transfected (Mock). 24 h after transfection cells were treated with vehicle or 500 nM ISRIB for 1 h, followed by co-treatment with AM16 for 24 h. ATF3 and GDF15 mRNA levels were detected with qRT-PCR. Bars represent the fold change compared to CTRL. Normalized expression values and significance values are provided in Table S5. (**B**) Representative western-blot for ATF3 and GDF15 in Hela cells transfected and treated as in panel (A). β-tubulin (TUBB) was used as loading control. Full blots are shown in Fig. 9S. (**C**) HeLa cells were transfected and treated as in panel (A). Bars represent the cell counts per well (average ± standard deviation of three independent experiments). *p < 0.001 vs. CTRL; #p < 0.001 vs. Mock (ANOVA, Bonferroni test).

Fig. 11C inhibitors of ferroptosis failed to inhibit the effect of the AM16 in HeLa and A549 cells, while the effect of erastin was antagonized in A549 but not in HeLa cells.

To investigate the possible role of necroptosis in the effect of the AM16 the RIPK1 inhibitor necrostatin-1 and the MLKL inhibitor necrosulfonamide was tested on HT-29 cells since HeLa, PC-3, MCF-7 and Caco-2 cells are missing one or more components of the necroptosis signaling cascade and not responding to the commonly used TNF-α + z-VAD-fmk + Smac mimetic (T + Z + S) necroptosis inducing stimulus [42,43]. We have found that inhibitors of necroptosis failed to inhibit the effect of the AM16 in HT-29 cells, while they effectively blocked the necroptosis induced by T + Z + S (Fig. 11D).

The modulatory effect of inhibitors of caspase, cathepsin or calpain proteases (z-VAD-fmk, E64d, ALLN), cyclophilin D (cyclosporine A), and autophagy/lysosomal function (bafilomycin A1 (BAF), 3-methyladenine (3-MA), and chloroquine) was tested in HeLa, A549, and HT-29 cells. We have found that z-VAD-fmk partially antagonized the effect of the AM16 in A549 and HT-29 (CI: 1.14–1.42), but not in HeLa cells, while E64d, ALLN, cyclosporine A partially antagonized the effect of the AM16 in all three cell lines (CI: 1.2–1.67) (Fig. 11E). We have also tested the combination z-VAD-fmk, E64d, ALLN and cyclosporine A (Z + E + A + C), which also produced a partial and consistent antagonism, however it failed to completely block the effect of the AM16. In addition Z + E + A + C significantly reduced the cell count when applied alone, therefore it was not investigated further. Interestingly, the autophagy inhibitors BAF and 3-MA consistently enhanced the effect of the AM16 in all three cell lines (CI: 0.32-0.86). Taken together these results indicate that ferroptosis and necroptosis are not involved in the mechanism of AM16 induced cell death, while the induction of apoptosis has an important role in the effect of the AM16.

2.11. Combination of ER stress inhibition with knockdown of BBC3 and PMAIP1 completely abrogates the effect of the AM16

As a final point, we wanted to investigate whether the induction of ER stress is responsible for the anti-proliferative and apoptosis inducing effect of the AM16. To this end we treated HeLa cells with AM16 in the presence of ISRIB and determined the number of dead, EdU positive and TUNEL positive cells after 24 h. As shown in Fig. 12A and B ISRIB significantly but not totally inhibited the AM16 induced increase in the number of dead and TUNEL positive cells, while it completely restored the AM16 suppressed cell proliferation.

Since the AM16 induced dead and apoptotic cells were not diminished totally by ISRIB, we continued to search for additional mediators of AM16 induced apoptosis. As *BBC3* and *PMAIP1* were consistently upregulated upon treatment with AM16 in HeLa, MCF-7, PC-3, and Caco-2 cells (Fig. 2D) we tested whether the knockdown of these apoptotic mediators modulates the effect of the AM16. The efficacy of knockdown was verified by qRT-PCR (Fig. 12C), while cell counting demonstrated that both the single-knockdown of *BBC3* or *PMAIP1*, and double-knockdown, and the combination of knockdown and ISRIB significantly inhibited the effect of the AM16 (Fig. 12D). The combination of double knockdown and ISRIB completely inhibited the effect of the AM16.

3. Discussion

In this work, we show that a mixture of amino acids, vitamins and other small molecules present in the serum (AM) selectively induce ER stress and activates the UPR in cancer cells. Our gene expression studies indicate that treatment with AM first induce the expression of ER stress genes (*ATF3*, *ATF4*, *DDIT3*, *PPP1R15A*, *XPB1*), which is followed by the upregulation of genes participating in apoptosis and cell cycle regulation (*BBC3*, *PMAIP1*, *TNFRSF10B*, *CDKN1A*). This, together with the temporally sustained induction of ATF4, ATF3 and DDIT3 proteins, is in agreement with the generally accepted view that long-term and high level activation of UPR signaling promotes cell death instead of restoring ER homeostasis [18,24,25]. The AM elicited induction of *BBC3* and *PMAIP1* is in agreement with our previous report [15], and since these proteins are activated in the late phase of UPR points toward the

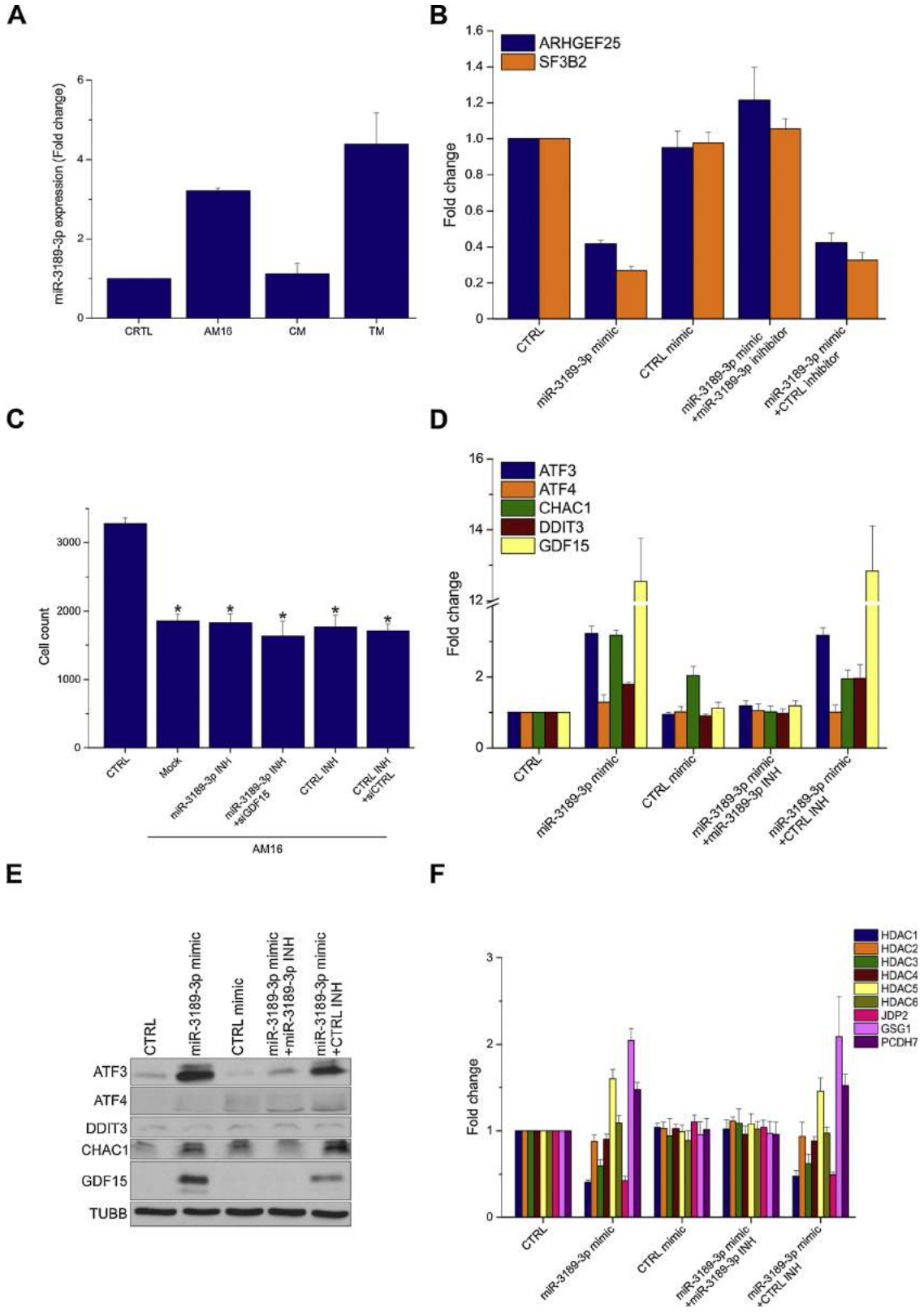

(caption on next page)

Fig. 9. The AM16 induced mIR-3189-3p enhances the expression of ER stress genes. (**A**) HeLa cells were treated for 24 h with AM16, CM or tunicamycin (5 μM, TM). mIR-3189-3p level was detected with qRT-PCR. Bars represent the fold change compared to CTRL. Normalized expression values and significance values are provided in Table S5. (**B**) HeLa cells were transfected with 10 nM miR-3189-3p mimic, 10 nM negative control miRNA mimic (CTRL mimic), with the combination of 10 nM miR-3189-3p mimic and 50 nM miR-3189-3p inhibitor (miR-3189-3p mimic + miR-3189-3p INH), or with the combination of 10 nM miR-3189-3p mimic and 50 nM negative control miRNA inhibitor (miR-3189-3p mimic + CTRL INH) for 24 h. ARHGEF25 and SF3B2 mRNA levels were detected with qRT-PCR after an additional 24 h. Bars represent the fold change compared to CTRL. Normalized expression values and significance values are provided in Table S5. (**C**) HeLa cells were transfected with 50 nM miR-3189-3p inhibitor (miR-3189-3p INH), with the combination of 200 nM miR-3189-3p inhibitor and 100 nM siRNA against GDF15 (miR-3189-3p INH + siGDF15), 50 nM negative control miRNA inhibitor (CTRL INH), or with the combination of 200 nM negative control miRNA inhibitor and 100 nM siRNA control (miR-3189-3p INH + siCTRL), 24 h after transfection cells were treated with AM16 for 24 h. Bars represent the cell counts per well (average ± standard deviation of three independent experiments). *$p < 0.001$ vs. CTRL (ANOVA, Bonferroni test). (**D**) HeLa cells were transfected as in panel (B). ATF3, ATF4, CHAC1, DDIT3, GDF15 mRNA levels were detected with qRT-PCR after an additional 24 h. Bars represent the fold change compared to CTRL. Normalized expression values and significance values are provided in Table S5. (**E**) Representative western-blots for ATF3, ATF4, DDIT3, CHAC1 and GDF15 in Hela cells transfected as in panel (B). β-tubulin (TUBB) was used as loading control. Full blots are shown in Fig. S10. **(F)** HeLa cells were transfected as in panel (B) for 24 h. HDAC1-6, JDP2, GSG1, and PCDH7 mRNA levels were detected with qRT-PCR after an additional 24 h. Bars represent the fold change compared to CTRL. Normalized expression values and significance values are provided in Table S5.

ER stress mediated induction of apoptosis [44].

Detailed analysis of the signaling components revealed that the AM activates all three arms of the UPR (PERK, ATF6, IRE1α), however the results of our inhibition experiments suggest that the activation of PERK and the consequential eIF2α phosphorylation, accompanied by the preferential translation mediated ATF4 induction are the dominant ER stress contributors in the effect of the AM. Our investigations on the mechanism of AM induced cell death revealed that the inhibition of cell proliferation and induction of apoptosis are the two major mechanisms involved in the effect of the AM. Our results link the AM induced ER stress to the inhibition of cell proliferation and to the *BBC3* and *PMAIP1* mediated induction of apoptosis, which is in agreement with the generally accepted role of ER stress in cell fate control [25,27,45]. The fact that the individual inhibition of *ATF3*, *GDF15*, or mIR-3189-3p induction did not influenced the cell number reducing effect of the AM could be attributed to the highly complex and redundant nature of UPR signaling [20,25], and indicate that these components are not essential for the anti-cancer activity of the AM. Interestingly, inhibition of autophagy seemed to enhance the effect of the AM, which could be explained by the highly context dependent outcome of autophagy signaling. It has been shown that under certain circumstances the inhibition of autophagy sensitizes cancer cell to apoptosis [46,47].

The AM and tunicamycin induced increase in the amount of mIR-3189-3p points toward the possible role of this miRNA in the UPR, which is supported by the mIR-3189-3p specific increase in the amounts of *ATF3, DDIT3,* and *GDF15* transcripts. The transcription factor JDP2 has been shown to repress *ATF3* and *DDIT3* transcription [33,34], and various members of the histone deacetylase family (HDACs) were demonstrated to be associated with JDP2 at the promoters of *ATF3* and *DDIT3* [34,35]. Our results demonstrate a specific downregulation of *JDP2*, *HDAC1* and *HDAC3* transcripts by mIR-3189-3p, indicating that these mRNAs are targets of mIR-3189-3p. On the basis of the above we speculate that mIR-3189-3p enhances the expression of *ATF3* and *DDIT3* most probably through the downregulation of *JDP2, HDAC1* and *HDAC3* thereby lifting the repression form the promoters of *ATF3* and *DDIT3*. The increased amount of ATF3 in turn could potentially stimulate the transcription of *GDF15* or stabilize the *GDF15* transcript, thus providing the basis for the mIR-3189-3p feedback loop.

Our investigations on the relative contribution of individual AM components to the activation of the UPR revealed that the amino acid components (L-arginine, L-tyrosine, L-histidine, L-tryptophan, L-methionine, and L-phenylalanine) if applied in conjunction with adenine, L-(-)-malic acid, D-(+)-mannose and hippuric acid are necessary and sufficient to induce ER stress. We emphasize that these molecules are not able to activate the UPR when applied alone, and all of them are necessary to reach the same level of UPR gene induction as produced by the sixteen component mixture AM16. With the exception of L-arginine and D-(+)-mannose to our knowledge there are no reports which would implicate these substances in the activation of the UPR [48–50].

The selectivity of the AM toward cancer cells could be explained in part by the accumulation of its components by cancer cells. Among the amino acid components of the AM L-phenylalanine, L-tyrosine, L-tryptophan and L-methionine are used as tracers in positron emission tomography [5,51,52]. Once inside the cancer cells, components of the AM could selectively activate the UPR, since this signaling pathway is in a heightened state of activation in cancer cells due to the survival benefit which it can provide in the constantly changing and stressful environment of the tumor cell caused by hypoxia or nutritional stress [18,53].

3.1. Conclusions

In summary, we demonstrated that a defined mixture of small molecules selectively induce ER stress and activates the UPR signaling cascade in cancer cells, which leads to the activation of a pro-apoptotic transcription program. In addition we have identified a novel miRNA mediated feedback mechanism of the transcriptional upregulation of certain UPR signaling components. This study provides compelling data to prompt the further evaluation of the AM in cancer therapy alone, or in combination with other ER stress inducing agents.

4. Materials and methods

4.1. Cell lines, chemicals, antibodies, kits, siRNAs, miRNA mimics, gene expression assays, and software

Materials, reagents and software used in this study are listed in Supplementary Table S6.

4.2. Cell culture

Cell lines were obtained from the American Type Culture Collection (ATCC) through LGC Standards GMBH, Germany or from The European Collection of Authenticated Cell Cultures (ECACC) through Sigma-Aldrich. Cell were expanded and early passage stocks were stored under liquid nitrogen. Cell line authentication was performed by Eurofins Medigenomix Forensik GmbH (Ebersberg, Germany). All stocks were tested for mycoplasma with the Mycoplasma Detection Kit both before cryopreservation and after thawing. HeLa (human cervix adenocarcinoma), MCF-7 (human breast adenocarcinoma), PC-3 (human prostate adenocarcinoma), Caco-2 (human colorectal adenocarcinoma, male), A549 (lung adenocarcinoma, male) and HT-29 (human colorectal adenocarcinoma, female) cells were cultured in MEM supplemented with 10 % (v/v) FCS, 100 U/ml penicillin and 0.1 mg/ml streptomycin. HRE (human renal epithelial cells, pooled from donors with different sex) cells were cultured in Renal Epithelial Cell Basal Medium supplemented with hEGF, Hydrocortisone, Epinephrine, Insulin, Triiodothyronine, Transferrin, GA-1000, and 0.5 % FBS. Cells were incubated at 37 °C in a humidified atmosphere at 5 % CO_2.

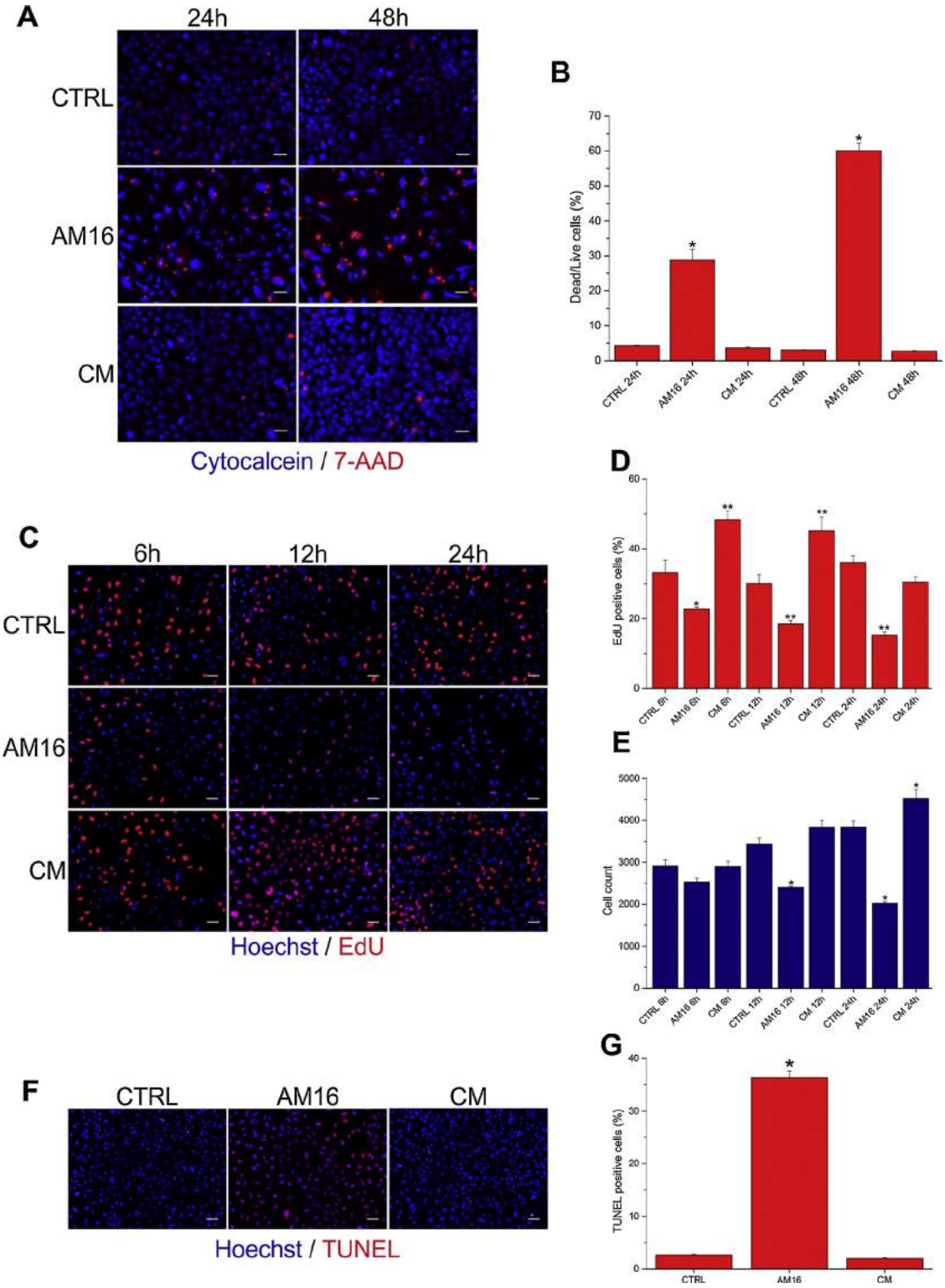

Fig. 10. The AM16 has cytotoxic, anti-proliferative and apoptosis inducing effect. **(A)** Immunofluorescence pictures of HeLa cells treated with AM16 or CM for 24 h and 48 h. Live cells were labeled with cytocalcein violet 450 (blue), and dead cells were detected with 7-AAD (red). **(B)** Quantification of the percentage of dead cells treated as in panel (A). Bars represent the average ± standard deviation of three independent experiments. *$p < 0.05$ vs. the corresponding control sample (Welch test followed by Games-Howell test). **(C)** EdU labelling (red) of HeLa cells treated with AM16 or CM for the indicated periods of time. Nuclei were labelled with Hoechst 33342 (blue). **(D)** Quantification of the percentage of EdU positive HeLa cells treated as in panel (C). Bars represent the average ± standard deviation of three independent experiments. *$p < 0.05$, **$p < 0.001$ vs. the corresponding CTRL (ANOVA, Bonferroni test). **(E)** Quantification of the number of HeLa cells treated as in panel (C). Bars represent the cell counts per well (average ± standard deviation of three independent experiments). *$p < 0.001$ vs. the corresponding CTRL (ANOVA, Bonferroni test). **(F)** TUNEL labelling (red) of HeLa cells treated with AM16 or CM for 24 h. Nuclei were labelled with Hoechst 33342 (blue). **(G)** Quantification of the percentage of TUNEL positive HeLa cells treated as in panel (F). Bars represent the average ± standard deviation of three independent experiments. *$p < 0.001$ vs. CTRL (ANOVA, Bonferroni test). Scale bars: 60 μm.

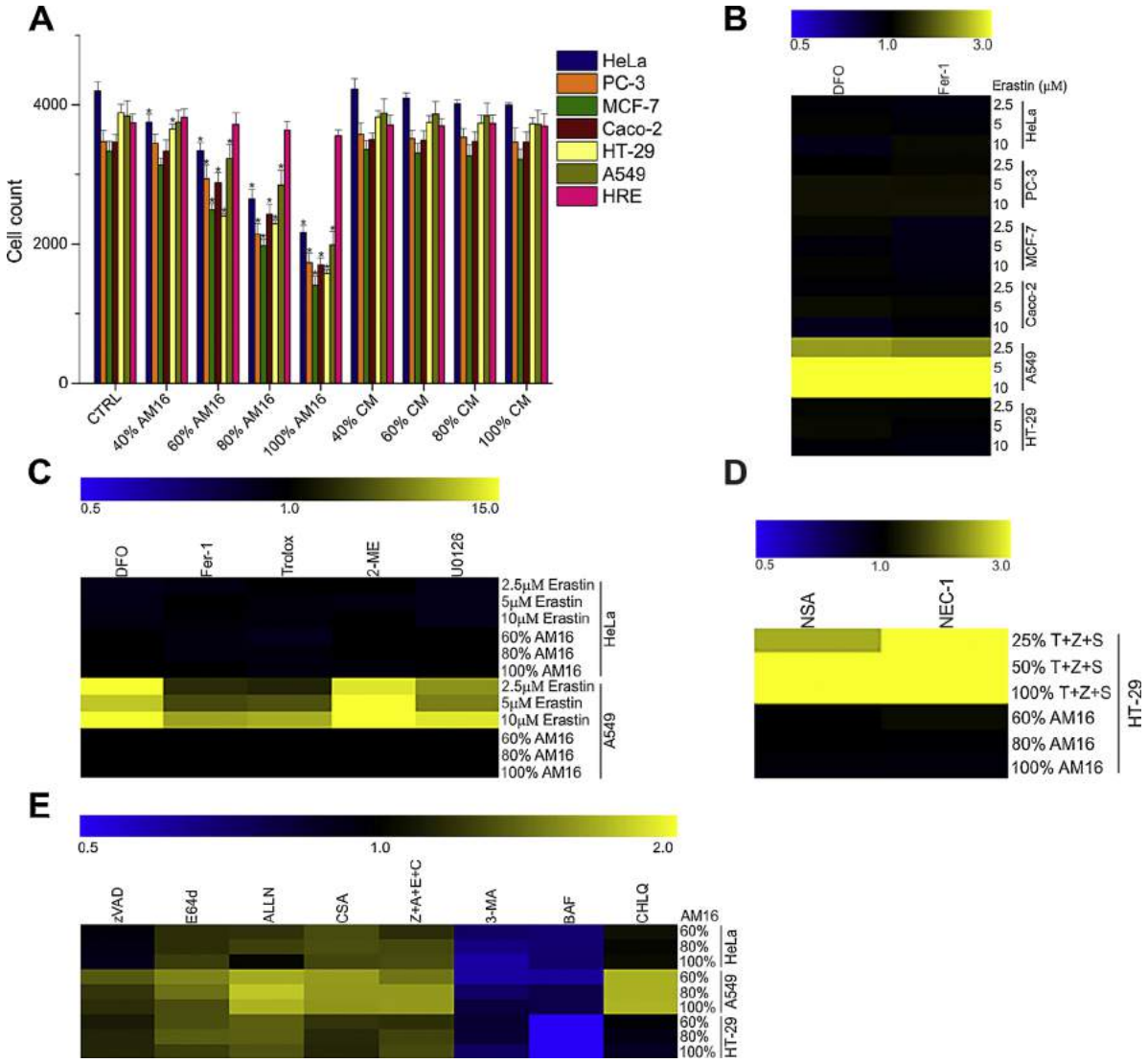

Fig. 11. Inhibitors of apoptosis, but not autophagy, ferroptosis and necroptosis attenuate the effect of the AM16. **(A)** HeLa, PC-3, MCF-7, Caco-2, HT-29, A549 and HRE cells were treated with dilution series of AM16 or CM for 24 h. The dilution of the mixtures is expressed in percentage. Bars represent the cell counts per well (average ± standard deviation of two independent experiments). *$p < 0.001$ vs. the corresponding CTRL (ANOVA, Bonferroni test). **(B)** Heatmap of combination index (CI) values for HeLa, PC-3, MCF-7, Caco-2, HT-29, A549 cells treated with the indicated concentrations of erastin in combination with 100 μM deferoxamine (DFO) or 20 μM ferrostatin-1 (Fer-1) for 24 h. Values represent the average of two independent experiments. **(C)** Heatmap of CI values for HeLa, A549 cells were treated with the indicated concentrations of erastin or AM16 in combination with 100 μM DFO, 20 μM Fer-1, 300 μM trolox, 20 μM 2-mercaptoethanol (2-ME) or 20 μM U0126 for 24 h. Values represent the average of two independent experiments. **(D)** Heatmap of CI values for HT-29 cells treated with the indicated concentrations of TNF-α + z-VAD-fmk + smac mimetic (T + Z + S) or AM16 in combination with 5 μM necrosulfonamide (NSA) or 10 μM necrostatin-1 (Nec-1) for 24 h. 100 % T + Z + S contains 20 ng/ml TNF-α, 20 μM z-VAD-fmk and 0.5 μM BV6 smac mimetic. Values represent the average of two independent experiments. **(E)** Heatmap of CI values for HeLa, A549 and HT-29 cells treated with the indicated concentrations of AM16 in combination with 80 μM z-VAD-fmk, 50 μM E64d, 0.5 μM ALLN, 10 μM cyclosporin A (CSA), 40 μM z-VAD-fmk + 25 μM E64d + 0.25 μM ALLN + 50 μM Cyclosporin A (CSA) (Z + E + A + C), 4 mM 3-methyladenine (3-MA), 1 μM Bafilomycin A1 (BAF) or 50 μM chloroquine (CHLQ) for 24 h. Values represent the average of two independent experiments.

4.3. Active mixture (AM)

The selection of the components of the active mixture 16 (AM16) and the control mixture (CM) has been described previously [10,11]. The composition of the AM16 was the following: 0.2 mM adenine, 0.5 mM L-tryptophan, 0.5 mM pyridoxine hydrochloride, 0.75 mM L-methionine, 0.5 mM biotin, 1 mM orotic acid monohydrate, 2.5 mM 2-deoxy-D-ribose, 2 mM L-tyrosine disodium salt hydrate, 2.5 mM L-histidine, 2.5 mM L-phenylalanine, 2.5 mM L-arginine, 5 mM L-(−)-malic acid, 5 mM sodium hippurate hydrate, 5 mM D-(+)-mannose, 0.0025 mM (−)-riboflavin, 0.15 mM L-ascorbic acid, and 8.95 mM sodium bicarbonate. In some experiments the components of the AM16 were divided into subgroups (AM1, AM2, AM3, AM6, and AM10). The composition of the AM1 was the following: 0.5 mM L-tryptophan, 0.75 mM L-methionine, 2 mM L-tyrosine disodium salt hydrate, 2.5 mM L-histidine, 2.5 mM L-phenylalanine, 2.5 mM L-arginine, and the pH was set to 7.4 with 1 N hydrogen-chloride. The composition of AM2 was the following: 0.2 mM adenine, 1 mM orotic acid monohydrate, 2.5 mM 2-deoxy-D-ribose, 5 mM L-(−)-malic acid, 5 mM sodium hippurate hydrate, 5 mM D-(+)-mannose, and 10.8 mM sodium bicarbonate. The composition of AM3 was the following: 0.5 mM pyridoxine hydrochloride, 0.5 mM biotin, 0.0025 mM (−)-riboflavin, 0.15 mM L-ascorbic acid, and 0.65 mM sodium bicarbonate. The composition of AM6 was the following: 0.5 mM pyridoxine hydrochloride, 0.5 mM biotin, 1 mM orotic acid monohydrate, 2.5 mM 2-deoxy-D-ribose, 0.0025 mM (−)-riboflavin, 0.15 mM L-ascorbic acid, and 1.65 mM sodium

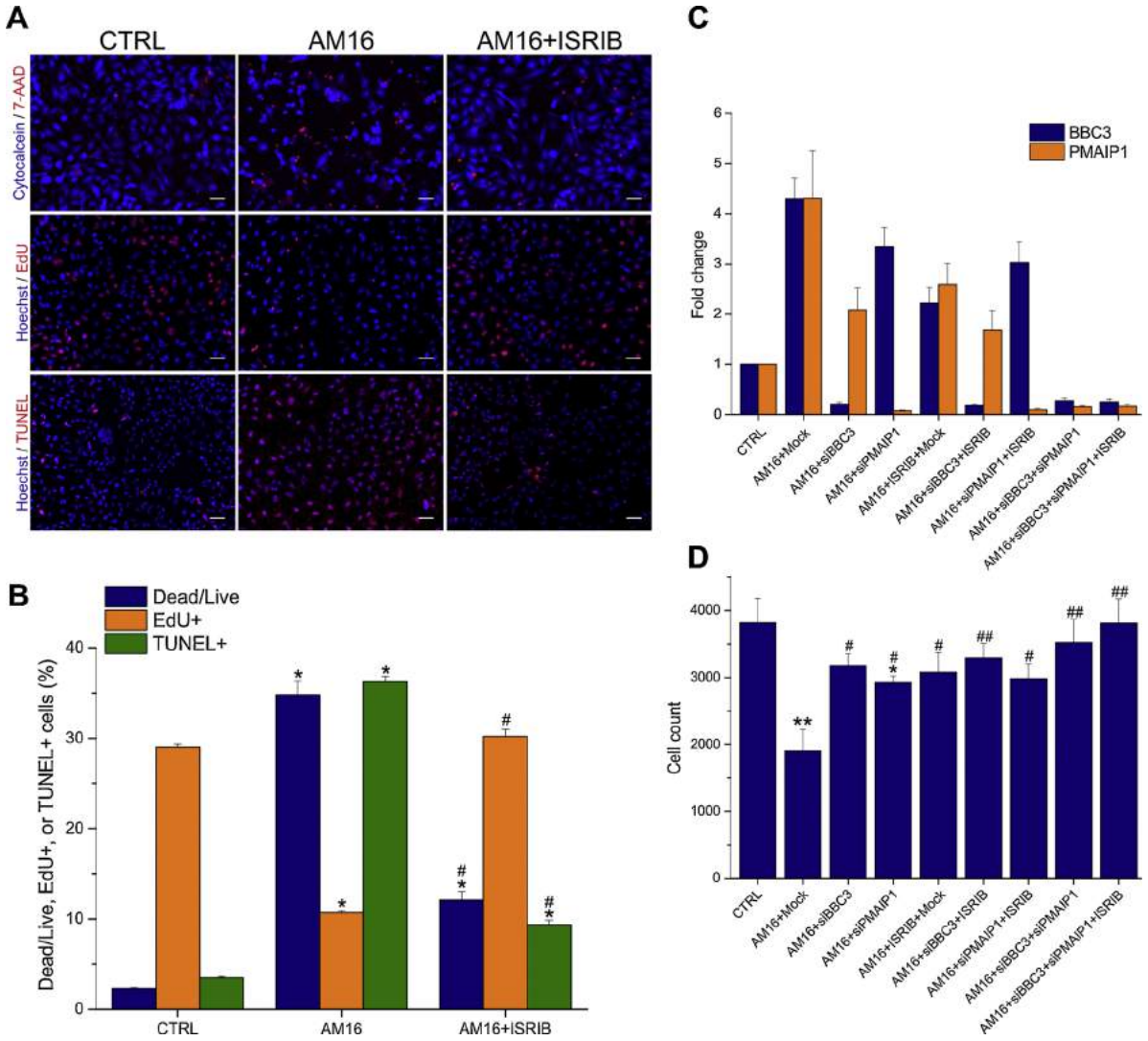

Fig. 12. Combination of ER stress inhibition with knockdown of BBC3 and PMAIP1 completely abrogates the effect of the AM16. **(A)** Immunofluorescence pictures of HeLa cells treated with AM16 or AM16 + 500 nM ISRIB for 24 h. Upper row: live cells were labeled with cytocalcein violet 450 (blue), dead cells were detected with 7-AAD (red). Middle row: EdU labelling (red), Hoechst 33342 (blue). Lower row: TUNEL labelling (red), Hoechst 33342 (blue). Scale bars: 60 μm. **(B)** Quantification of the percentage of dead, EdU positive and TUNEL positive cells treated as in panel (A). Bars represent the average ± standard deviation of three independent experiments. *p < 0.001 vs. CTRL, #p < 0.001 vs. AM16 (ANOVA, Bonferroni test). **(C)** HeLa cells were transfected with 10 nM siRNA against BBC3 (siBBC3), 10 nM siRNA against PMAIP1 (siPMAIP1), with the combination of 10 nM siBBC3 and 10 nM siPMAIP1, or were mock transfected (Mock). 24 h after transfection cells were treated with vehicle or 500 nM ISRIB for 1 h, followed by co-treatment with AM16 for 24 h. BBC3 and PMAIP1 mRNA levels were detected with qRT-PCR. Bars represent the fold change compared to CTRL. Normalized expression values and significance values are provided in Table S5. **(D)** HeLa cells were transfected and treated as in panel (C). Bars represent the cell counts per well (average ± standard deviation of three independent experiments). *p < 0.05 vs. CTRL, **p < 0.001 vs. CTRL, #p < 0.05 vs. AM16, ##p < 0.001 vs. AM16 (ANOVA, Bonferroni test).

bicarbonate. The composition of AM10 was the following: 0.5 mM L-tryptophan, 0.75 mM L-methionine, 2 mM L-tyrosine disodium salt hydrate, 2.5 mM L-histidine, 2.5 mM L-phenylalanine, 2.5 mM L-arginine, 0.2 mM adenine, 5 mM L-(−)-malic acid, 5 mM sodium hippurate hydrate, 5 mM D-(+)-mannose, and 7.3 mM sodium bicarbonate.

4.4. Control mixture (CM)

The CM had the following composition: 0.2 mM hypoxanthine, 0.5 mM L-proline, 0.5 mM nicotinic acid, 0.75 mM glycine, 0.5 mM thiamine hydrochloride, 1 mM uracil, 2.5 mM D-(−)-ribose, 2 mM L-alanine, 2.5 mM L-serine, 2.5 mM L-valine, 2.5 mM L-asparagine, 5 mM sodium succinate dibasic hexahydrate, 5 mM betaine, 5 mM D-(+)-glucose, 0.0025 mM D-pantotenic acid hemicalcium salt, 0.15 mM folic acid.

4.5. Microarray analysis

HeLa cells were treated with AM16 for 3 h, 6 h and 24 h in triplicates. Total RNA was isolated with RNeasy Plus mini kit, RNA quality was assessed with agarose gel electrophoresis. Microarray hybridization and initial data processing were performed by Personmed Ltd. (Turku, Finland) as contract research. In brief, triplicate samples for each time point were converted into biotin-labeled cRNA and were hybridized to a Human HT-12 v.4 Expression BeadChip (Illumina) using standard protocols. Average probe intensities were computed with Genome Studio (Illumina) and analyzed with the following Bioconductor packages: affy, limma, gplots, beadarray, lattice, amap, simpleaffy, xtable, scatterplot3d, ade4 and made4. Data were quantile normalized and differentially expressed genes were identified with 2-sided *t*-test and fold change. Genes with > 1.3 fold change and p value < 0.05 were considered differentially expressed.

4.6. Gene set enrichment analysis

Gene set enrichment analysis (GSEA) was performed with the java GSEA Desktop Application version 2.2.3 [54,55]. The gene ontology biological process gene set collection (GO BP) version 5.2 [56] was used for the enrichment analysis. Upregulated pathways were defined by a normalized enrichment score (NES) > 3, downregulated pathways were identified by a NES < -3. Pathways with a false discovery rate (FDR) p value < 0.25 were considered significantly enriched.

4.7. Quantitative RT-PCR (qRT-PCR)

Total RNA was isolated with PureLink RNA Mini Kit and was treated with DNase I. cDNA was prepared with High Capacity RNA-to-cDNA Kit. PCR primers used for real-time quantitative amplification of the human housekeeping genes *B2M*, *GAPDH*, *HPRT1*, *RPL32*, and *PPIA* were described previously [57,58]. PCR primers for human *APAF1*, *BAX*, *BCL2L1*, *BIRC2*, *BIRC3*, *CASP3*, *CDKN1A*, *CDKN2A*, *IKBKG*, *NFKBIA*, *NFKB1* were also described previously [15]. Total XBP1, spliced XPB1, and unspliced XBP1 transcripts were quantified with primers described previously [59]. All other PCR primers were designed by Primer Express Software, primer sequences are listed in Supplementary Table S7. The expression levels of *BBC3*, *PMAIP1*, *RPL32* were measured with TaqMan gene expression assays. RPL32 was used for normalization. For miRNA analysis, the isolation of small RNA fraction was done with the miRVana miRNA isolation kit. The expression of miR-3189-3p and U6 snRNA were measured using TaqMan microRNA assays following the manufacturer's instructions. U6 snRNA was used for normalization. PCR reactions were run in triplicates using PowerUp SYBR Green Master Mix or Taqman gene expression master mix II, no UNG on an ABI StepOne Real Time PCR System. The stability of the expression level of the housekeeping genes was analyzed in preliminary experiments and RPL32 was chosen for normalization of target gene expression. Fold change values were calculated by dividing the normalized target gene expression measured in the treated samples by that of the untreated control samples [60].

4.8. Western blot

Cells were seeded onto 150 mm Petri dishes at a density of 1.6×10^6 or onto 6-well plates at a density of 1.7×10^5/well. Following the indicated treatments cells were lysed in ice cold 1X RIPA buffer containing Protease and Phosphatase Inhibitor Cocktail. Protein concentrations were measured with the DC protein assay. 30–100 μg proteins were separated on SDS-polyacrylamide gels and transferred to nitrocellulose membranes. Membranes were blocked with 5 % non-fat dry milk (NFDM) or in the case of antibodies against phosphoproteins with 5 % bovine serum albumin (BSA) in Tris-buffered saline (150 mM NaCl, 20 mM Tris-base pH 7.6, 0.1 % Tween 20) (TBS-T) for 1 h at room temperature. Primary antibodies diluted in 5 % NFDM/TBS-T or 5 % BSA/ TBST-T were applied at 4 °C overnight. HRP-conjugated anti-rabbit antibody diluted in 5 % NFDM/TBS-T was applied for 1 h at room temperature. Membranes were developed with LumiGLO chemiluminescent substrate and exposed to x-ray films. Densitometry analysis was performed with the Image Studio Lite software 5.2.5. Densities were normalized to the non-phosphorylated forms or β-tubulin for eIF2α, PERK, IRE1α or ATF6 and BIP, respectively. Full blots are shown in Supplementary Figs. S1-10.

4.9. Reverse transfection

HeLa cells were reverse transfected in 96-well plates at a density of 2.5×10^3cells per well or in 6-well plate at a density of 1.7×10^5 using DharmaFECT 1 according to the manufacturer's instructions. *GDF15*, *ATF3* and negative control siRNAs were used at a final concentration of 50 or 100 nM as indicated. The miRIDIAN microRNA hsa-miR-3189-3p Hairpin Inhibitor, miRIDIAN microRNA Hairpin Inhibitor Negative Control miRNAs were transfected at a final concentration of 50 or 200 nM as indicated. The miRIDIAN microRNA hsa-miR-3189-3p Mimic and miRIDIAN microRNA Mimic Negative Control miRNAs were transfected at a final concentration of 10 nM. The *BBC3* and *PMAIP1* silencer select siRNAs were used at a final concentration of 10 nM. At 24 h post-transfection, the transfection medium was removed and treatment was initiated. At 48 h post-transfection, cells were either fixed and labeled for cell counting or were harvested and analyzed by qRT-PCR.

4.10. Cell counting and immunocytochemistry

HeLa cells were plated and transfected at 2.5×10^3 per well in 96-well black-walled, glass bottom plates (Corning, #CLS4580), then treated as indicated. The cells were fixed with 4 % paraformaldehyde in PBS for 10 min, then were permeabilized with Triton X-100 for 10 min, followed by blocking with 5 % goat serum in PBS for 1 h at room temperature. The antibody against ATF4 diluted in PBS containing 1 % BSA and 0.05 % Triton-X 100 was applied at 4 °C overnight. After washing three times with PBS for 5 min, the cells were incubated with Alexa Fluor 555 Anti-Rabbit IgG diluted as above, in the dark for 1 h at room temperature. Cells were washed once with PBS for 5 min, and then the nuclei were counterstained with DAPI (10 ug/ml in PBS) for 5 min. Cells were imaged using an automated, high-content screening station (Olympus IX83ZDC2 equipped with scanˆR software platform, v2.5.0). In acquisition 25 fields per well and fluorescent channels were imaged using a 10x objective (UPLSAPO; Olympus, numeric aperture: 0.4; refraction: 1.0; correction: 1.0) and a highly sensitive digital CCD camera (C8484-05G02, Hamamatsu) to acquire abundant events for analysis. For the excitation and emission a multiband filter cube (M4DAFIC3C5, Chroma Technology GmbH) was used with a previously adjusted exposure time and other technical parameters. The collected images were analyzed using the Scanˆ R analysis module where nuclei were defined on the basis of DAPI staining with intensity gradient based event recognition and the nuclear intensity of ATF4 was also quantified. For experiments involving only cell counting, the fixation of the cells was directly followed by DAPI staining and imaging.

4.11. Live/dead staining, EdU and TUNEL labeling

HeLa cells were plated at 2.5×10^3 per well in 96-well plates and treated as indicated. For live/dead staining cytocalcein violet 450 and 7-AAD were used from the Apoptosis/Necrosis detection kit following the manufacturer's instructions. For EdU labeling EdU was added at a final concentration of 10 μM at treatment initiation. The incorporated EdU was detected with the Click-iT Plus EdU Alexa Fluor 555 imaging kit following the manufacturer's instructions. TUNEL was performed with the use of Click-iT TUNEL Alexa Fluor 594 imaging kit. For EdU and TUNEL nuclei were labeled with Hoechst 33342 (5 μg/ml). Image acquisition and analysis was performed as described for immunocytochemistry.

4.12. Determination of combination indexes

Cells were plated in 96-well plates and treated with three point, two-fold dilution series of the inhibitors, dilution series of the AM16 alone (40–100%), or with the combination of the two higher concentration of inhibitors and 60 %, 80 %, 100 % AM16 for 24 h. Cells were counted as described for cell counting and the combination indexes were calculated with the Compusyn software [37–39]. The following inhibitors were tested (starting concentration of the dilution series in brackets): deferoxamine (100 μM), ferrostatin-1 (20 μM), trolox (300 μM), 2-mercaptoethanol (20 μM), U0126 (20 μM), necrostatin-1 (10 μM), necrosulfonamide (5 μM), z-VAD-fmk (80 μM), E64d (50 μM), ALLN (500 nM), cyclosporine A (10 μM), 3-methyladenine

(4 mM), bafilomycin A1 (1 μM), chloroquine (50 μM). Erastin was used at 2.5–10 μM concentrations. Necroptosis was induced with 20 ng/ml TNF-α + 20 μM z-VAD-fmk + 500 nM BV6 (Smac mimetic).

4.13. Statistical analysis

Statistical analysis was performed with IBM SPSS Statistics 22 using the statistical tests specified in the figure legends. Normal distribution of the data was evaluated with Shapiro-Wilk test. Homogeneity of variances was assessed with Levene-test. For normally distributed variables with equal variances p values were calculated with one-way analysis of variance (ANOVA) followed by Bonferroni post hoc test. For normally distributed variables with unequal variances p values were calculated with Welch test followed by Games-Howell test. P values less than 0.05 were considered statistically significant. For the quantification of nuclear intensity of ATF4 n represents the number of nuclei analyzed.

Data availability

The microarray data have been deposited in the Gene Expression Omnibus database under accession number GEO: GSE111488. Other datasets generated during the current study are available in the Open Science Framework repository, https://osf.io/m8q9v/; DOI 10.17605/OSF.IO/M8Q9V.

Author contributions

Conceptualization, GY.K., D.S., Z.R., and T.C.; Methodology, GY.K., D.S., B.M., GY.N., M.K.M., Z.R., M.M., and T.C.; Formal analysis, GY.K., D.S. and T.C.; Investigation, GY.K., D.S., B.M., GY.N., M.K.M., Z.R., M.M., and T.C.; Writing – Original Draft, GY.K., D.S., GY.N., Z.R., and T.C.; Supervision, GY.K. and T.C.; Funding Acquisition, GY.K. and T.C.

Databases

Microarray data are available in the GEO databases under the accession number GSE111488.

Declaration of Competing Interest

GY.K.is employee of Culevit Ltd. D.S., GY.N., M.K.M. and T.C. are employees of Soft Flow Hungary Ltd. GY.K. owns a 15 % share in Culevit Ltd.

Acknowledgements

This work has been supported in part by a Ministry for National Economy, Hungary grant GINOP-2.1.1.-15-2015-00046.

Appendix A. Supplementary data

Supplementary material related to this article can be found, in the online version, at doi:https://doi.org/10.1016/j.cellsig.2019.109426.

References

[1] G. Kulcsár, Theoretical and literary evidence for the existence of the passive antitumor defense system, Cancer Biother. Radiopharm. 12 (1997) 281–286.
[2] H. Flodh, S. Ullberg, Accumulation of labelled vitamin B12 in some transplanted tumours, Int. J. Cancer 3 (1968) 694–699.
[3] L. Blomquist, H. Flodh, S. Ullberg, Uptake of 125I-labelled 4-iodophenylalanine in tumours of mice, Br. J. Cancer 23 (1969) 150–152.
[4] E.S. Ong, L. Zou, S. Li, P.Y. Cheah, K.W. Eu, C.N. Ong, Metabolic profiling in colorectal cancer reveals signature metabolic shifts during tumorigenesis, Mol. Cell Proteomics (2010), https://doi.org/10.1074/mcp.M900551-MCP200.
[5] Y. Qi, X. Liu, J. Li, H. Yao, S. Yuan, Fluorine-18 labeled amino acids for tumor PET/CT imaging, Oncotarget 8 (2017) 60581–60588.
[6] C. Giese, S. Lepthien, L. Metzner, M. Brandsch, N. Budisa, H. Lilie, Intracellular uptake and inhibitory activity of aromatic fluorinated amino acids in human breast cancer cells, Chem. Med. Chem. 3 (2008) 1449–1456.
[7] R. Waibel, H. Treichler, N.G. Schaefer, D.R. van Staveren, S. Mundwiler, S. Kunze, M. Küenzi, R. Alberto, J. Nüesch, A. Knuth, H. Moch, R. Schibli, P.A. Schubiger, New derivatives of vitamin B12 show preferential targeting of tumors, Cancer Res. 68 (2008) 2904–2911.
[8] M.G. Vander Heiden, L.C. Cantley, C.B. Thompson, Understanding the Warburg effect: the metabolic requirements of cell proliferation, Science 324 (2009) 1029–1033.
[9] D.R. Green, L. Galluzzi, G. Kroemer, Cell biology. Metabolic control of cell death, Science 345 (2014) 1250256.
[10] G. Kulcsár, Inhibition of the growth of a murine and various human tumor cell lines in culture and in mice by mixture of certain substances of the circulatory system, Cancer Biother. 10 (1995) 157–176.
[11] G. Kulcsár, Synergistic potentiating effect of D(+)-mannose, orotic, and hippuric acid sodium salt on selective toxicity of a mixture of 13 substances of the circulatory system in culture for various tumor cell lines, Cancer Detect. Prev. 24 (2000) 485–495.
[12] G. Kulcsár, Apoptosis of tumor cells induced by substances of the circulatory system, Cancer Biother. Radiopharm. 12 (1997) 19–26.
[13] G. Kulcsár, Experimental evidence for the existence of the passive antitumor defense system formed by the synergistic action of certain small substances of the circulatory system, Cancer Biother. Radiopharm. 18 (2003) 949–963.
[14] G. Kulcsár, Experimental evidence for killing the resistant cells and raising the efficacy and decreasing the toxicity of cytostatics and irradiation by mixtures of the agents of the passive antitumor defense system in the case of various tumor and normal cell lines in vitro, Cancer Biother. Radiopharm. 24 (2009) 67–80.
[15] G. Kulcsár, D. Gaál, P.I. Kulcsár, Á. Schulcz, T. Czömpöly, A mixture of amino acids and other small molecules present in the serum suppresses the growth of murine and human tumors in vivo, Int. J. Cancer 132 (2013) 1213–1221.
[16] L. Bonfili, V. Cecarini, M. Cuccioloni, M. Angeletti, V. Flati, G. Corsetti, E. Pasini, F.S. Dioguardi, A.M. Eleuteri, Essential amino acid mixtures drive cancer cells to apoptosis through proteasome inhibition and autophagy activation, FEBS J. 284 (2017) 1726–1737.
[17] P. Walter, D. Ron, The unfolded protein response: from stress pathway to homeostatic regulation, Science 334 (2011) 1081–1086.
[18] H.J. Clarke, J.E. Chambers, E. Liniker, S.J. Marciniak, Endoplasmic reticulum stress in malignancy, Cancer Cell 25 (2014) 563–573.
[19] S.K. Young, R.C. Wek, Upstream open reading frames differentially regulate gene-specific translation in the integrated stress response, J. Biol. Chem. 291 (2016) 16927–16935.
[20] K. Pakos-Zebrucka, I. Koryga, K. Mnich, M. Ljujic, A. Samali, A.M. Gorman, The integrated stress response, EMBO Rep. 17 (2016) 1374–1395.
[21] D. Acosta-Alvear, Y. Zhou, A. Blais, M. Tsikitis, N.H. Lents, C. Arias, C.J. Lennon, Y. Kluger, B.D. Dynlacht, XBP1 controls diverse cell type- and condition-specific transcriptional regulatory networks, Mol. Cell 27 (2007) 53–66.
[22] J. Hollien, J.S. Weissman, Decay of endoplasmic reticulum-localized mRNAs during the unfolded protein response, Science 313 (2006) 104–107.
[23] K. Yamamoto, T. Sato, T. Matsui, M. Sato, T. Okada, H. Yoshida, A. Harada, K. Mori, Transcriptional induction of mammalian ER quality control proteins is mediated by single or combined action of ATF6alpha and XBP1, Dev. Cell 13 (2007) 365–376.
[24] H. Urra, E. Dufey, F. Lisbona, D. Rojas-Rivera, C. Hetz, When ER stress reaches a dead end, Biochim. Biophys. Acta 1833 (2013) 3507–3517.
[25] C. Hetz, F.R. Papa, The unfolded protein response and cell fate control, Mol. Cell 69 (2018) 169–181.
[26] E. Szegezdi, S. Logue, A.M. Gorman, A. Samali, Mediators of endoplasmic reticulum stress-induced apoptosis, EMBO Rep. 7 (2006) 880–885.
[27] E. Szegezdi, D.C. Macdonald, T. Ní Chonghaile, S. Gupta, A. Samali, Bcl-2 family on guard at the ER, Am. J. Physiol., Cell Physiol. 296 (2009) C941–C953.
[28] C. Sidrauski, J.C. Tsai, M. Kampmann, B.R. Hearn, P. Vedantham, P. Jaishankar, M. Sokabe, A.S. Mendez, B.W. Newton, E.L. Tang, Pharmacological dimerization and activation of the exchange factor eIF2B antagonizes the integrated stress response, Elife 4 (2015) e07314.
[29] M. Boyce, K.F. Bryant, C. Jousse, K. Long, H.P. Harding, D. Scheuner, R.J. Kaufman, D. Ma, D.M. Coen, D. Ron, A selective inhibitor of eIF2alpha dephosphorylation protects cells from ER stress, Science 307 (2005) 935–939.
[30] K. Kubota, Y. Niinuma, M. Kaneko, Y. Okuma, M. Sugai, T. Omura, M. Uesugi, T. Uehara, T. Hosoi, Y. Nomura, Suppressive effects of 4-phenylbutyrate on the aggregation of Pael receptors and endoplasmic reticulum stress, J. Neurochem. 97 (2006) 1259–1268.
[31] M.F. Jones, X.L. Li, M. Subramanian, S.A. Shabalina, T. Hara, Y. Zhu, J. Huang, Y. Yang, L.M. Wakefield, K.V. Prasanth, A. Lal, Growth differentiation factor-15 encodes a novel microRNA 3189 that functions as a potent regulator of cell death, Cell Death Differ. 22 (2015) 1641–1653.
[32] D. Jeansonne, M. DeLuca, L. Marrero, A. Lassak, M. Pacifici, D. Wyczechowska, A. Wilk, K. Reiss, F. Peruzzi, Anti-tumoral effects of miR-3189-3p in glioblastoma, J. Biol. Chem. 290 (2015) 8067–8080.
[33] K. Weidenfeld-Baranboim, T. Hasin, I. Darlyuk, R. Heinrich, O. Elhanani, J. Pan, K.K. Yokoyama, A. Aronheim, The ubiquitously expressed bZIP inhibitor, JDP2, suppresses the transcription of its homologue immediate early gene counterpart, ATF3, Nucleic Acids Res. 37 (2009) 2194–2203.
[34] Y. Chérasse, C. Chaveroux, C. Jousse, A.C. Maurin, V. Carraro, L. Parry, P. Fafournoux, A. Bruhat, Role of the repressor JDP2 in the amino acid-regulated transcription of CHOP, FEBS Lett. 582 (2008) 1537–1541.
[35] I. Darlyuk-Saadon, K. Weidenfeld-Baranboim, K.K. Yokoyama, T. Hai, A. Aronheim,

The bZIP repressor proteins, c-Jun dimerization protein 2 and activating transcription factor 3, recruit multiple HDAC members to the ATF3 promoter, Biochim. Biophys. Acta 1819 (2012) 1142–1153.
[36] V. Agarwal, G.W. Bell, J.W. Nam, D.P. Bartel, Predicting effective microRNA target sites in mammalian mRNAs, Elife 4 (2015) e05005.
[37] T.C. Chou, Theoretical basis, experimental design, and computerized simulation of synergism and antagonism in drug combination studies, Pharmacol. Rev. 58 (2006) 621–681.
[38] T.C. Chou, P. Talalay, Generalized equations for the analysis of inhibitions of Michaelis-Menten and higher-order kinetic systems with two or more mutually exclusive and nonexclusive inhibitors, Eur. J. Biochem. 115 (1981) 207–216.
[39] T.C. Chou, P. Talalay, Quantitative analysis of dose – effect relationships: the combined effects of multiple drugs or enzyme inhibitors, Adv. Enzyme Regul. 22 (1984) 27–55.
[40] S.J. Dixon, K.M. Lemberg, M.R. Lamprecht, R. Skouta, E.M. Zaitsev, C.E. Gleason, D.N. Patel, A.J. Bauer, A.M. Cantley, W.S. Yang, B. Morrison 3rd, B.R. Stockwell, Ferroptosis: an iron-dependent form of nonapoptotic cell death, Cell 149 (2012) 1060–1072.
[41] S. Dolma, S.L. Lessnick, W.C. Hahn, B.R. Stockwell, Identification of genotype-selective antitumor agents using synthetic lethal chemical screening in engineered human tumor cells, Cancer Cell 3 (2003) 285–296.
[42] Z. Su, Z. Yang, L. Xie, J.P. DeWitt, Y. Chen, Cancer therapy in the necroptosis era, Cell Death Differ. 23 (2016) 748–756.
[43] J. Sosna, S. Voigt, S. Mathieu, A. Lange, L. Thon, P. Davarnia, T. Herdegen, A. Linkermann, A. Rittger, F.K. Chan, D. Kabelitz, S. Schütze, D. Adam, TNF-induced necroptosis and PARP-1-mediated necrosis represent distinct routes to programmed necrotic cell death, Cell. Mol. Life Sci. 71 (2014) 331–348.
[44] P. Pihán, A. Carreras-Sureda, C. Hetz, BCL-2 family: integrating stress responses at the ER to control cell demise, Cell Death Differ. 24 (2017) 1478–1487.
[45] M. Corazzari, M. Gagliardi, G.M. Fimia, M. Piacentini, Endoplasmic reticulum stress, unfolded protein response, and cancer cell fate, Front. Oncol. 7 (2017) 78.
[46] P. Boya, R.A. González-Polo, N. Casares, J.L. Perfettini, P. Dessen, N. Larochette, D. Métivier, D. Meley, S. Souquere, T. Yoshimori, G. Pierron, P. Codogno, G. Kroemer, Inhibition of macroautophagy triggers apoptosis, Mol. Cell. Biol. 25 (2005) 1025–1040.
[47] P. Bhat, J. Kriel, B. Shubha Priya, S.N.S. Basappa, B. Loos, Modulating autophagy in cancer therapy: advancements and challenges for cancer cell death sensitization, Biochem. Pharmacol. 147 (2018) 170–182.
[48] C.H. Kubisch, M.D. Sans, T. Arumugam, S.A. Ernst, J.A. Williams, C.D. Logsdon, Early activation of endoplasmic reticulum stress is associated with arginine-induced acute pancreatitis, Am. J. Physiol. Gastrointest. Liver Physiol. 291 (2006) G238–G245.
[49] C. Xu, D.T. Ng, O-mannosylation: the other glycan player of ER quality control, Semin. Cell Dev. Biol. 41 (2015) 129–134.
[50] N. Gao, J. Shang, D. Huynh, V.L. Manthati, C. Arias, H.P. Harding, R.J. Kaufman, I. Mohr, D. Ron, J.R. Falck, M.A. Lehrman, Mannose-6-phosphate regulates destruction of lipid-linked oligosaccharides, Mol. Biol. Cell 22 (2011) 2994–3009.
[51] A.R. Guastella, S.K. Michelhaugh, N.V. Klinger, W.J. Kupsky, L.A. Polin, O. Muzik, C. Juhász, S. Mittal, Tryptophan PET imaging of the kynurenine pathway in patient-derived xenograft models of glioblastoma, Mol. Imaging 15 (2016) 1–11.
[52] Y. Watanabe, H. Kurihara, J. Itami, R. Sasaki, Y. Arai, K. Sugimura, Relationship between the uptake of 18F-borono-L-phenylalanine and L-[methyl-11C] methionine in head and neck tumors and normal organs, Radiat. Oncol. 12 (2017) 17.
[53] C. Hetz, E. Chevet, H.P. Harding, Targeting the unfolded protein response in disease, Nat. Rev. Drug Discov. 12 (2013) 703–719.
[54] A. Subramanian, P. Tamayo, V.K. Mootha, S. Mukherjee, B.L. Ebert, M.A. Gillette, A. Paulovich, S.L. Pomeroy, T.R. Golub, E.S. Lander, J.P. Mesirov, Gene set enrichment analysis: a knowledge-based approach for interpreting genome-wide expression profiles, Proc. Natl. Acad. Sci. U. S. A. 102 (2005) 15545–15550.
[55] V.K. Mootha, C.M. Lindgren, K.F. Eriksson, A. Subramanian, S. Sihag, J. Lehar, P. Puigserver, E. Carlsson, M. Ridderstråle, E. Laurila, PGC-1alpha-responsive genes involved in oxidative phosphorylation are coordinately downregulated in human diabetes, Nat. Genet. 34 (2003) 267–273.
[56] A. Liberzon, A. Subramanian, R. Pinchback, H. Thorvaldsdóttir, P. Tamayo, J.P. Mesirov, Molecular signatures database (MSigDB) 3.0, Bioinformatics 27 (2011) 1739–1740.
[57] A. Colell, J.E. Ricci, S. Tait, S. Milasta, U. Maurer, L. Bouchier-Hayes, P. Fitzgerald, A. Guio-Carrion, N.J. Waterhouse, C.W. Li, GAPDH and autophagy preserve survival after apoptotic cytochrome c release in the absence of caspase activation, Cell 129 (2007) 983–997.
[58] X. Zhang, L. Ding, A.J. Sandford, Selection of reference genes for gene expression studies in human neutrophils by real-time PCR, BMC Mol. Biol. 6 (2005) 4.
[59] C.M. Oslowski, F. Urano, Measuring ER stress and the unfolded protein response using mammalian tissue culture system, Methods Enzymol. 490 (2011) 71–92.
[60] T.D. Schmittgen, K.J. Livak, Analyzing real-time PCR data by the comparative C(T) method, Nat. Protoc. 3 (2008) 1101–1108.